The 5th International Symposium on Adaptive Motion of Animals and Machines (AMAM2011)

– Understanding mechanism for adaptive behavior of animals helps us realizing adaptive behavior of machines, and experimenting on machines to realize adaptive behavior helps us to find new view on biological systems. These two approaches are "two wheels of a cart" to understand the essence of adaptive intelligence. AMAM 2011 is the fifth international symposium dedicated on the interaction among researchers of such interdisciplinary field. They are covering neuromechanics, neurophysiology, biomechanics, robotics, brain science, and other field related to adaptive behavior of animals and machines. Previous symposia were held in Montreal, Canada (2000); Kyoto, Japan (2003); Ilmenau, Germany (2005); and Cleveland, USA (2008).

Oganizing Comittie

- **General Chair**
    – Koichi Osuka (Osaka University)
- **Program Chair**
    – Koh Hosoda (Osaka University)
- **Publication Chair**
    – Akio Ishiguro (Tohoku University)
- **Local Arrangement Chairs**
    – Masahiro Shimizu (Osaka University)
    Shuhei Ikemoto (Osaka University)
    Yasuhiro Sugimoto (Osaka University)
- **Senior Advisory Members**
    – Japan: H. Kimura (Kyoto Institute of Technology)
    Japan: A. Ishiguro (Tohoku Univ.)
    Japan: K. Hosoda(Osaka Univ.)
    Japan: R. Kanzaki(Tokyo Univ.)
    Europe: H. Witte (TU Ilmenau)
    Europe: A. Ijspeert (EPFL)
    North America: A. H. Cohen (Ma ryland Univ.)
    North America: M. Buehler (iRbot)
    North Ameica: R. E. Ritzmann (Case Western Reserve Univ.)
    North America: R. Quinn (Case Western Reserve Univ.)
- **Honorable President:**
    – Japan: K. Tsuchiya (Doshisya Univ.)

Overall Program

- October 11
  - 08:30-09:30 Plenary talk1: Prof. Kaoru Takakusaki
  - 09:40-10:40 Session1-1: Biological System
  - 11:00-12:00 Session1-2: Biped 1
  - 13:30-14:50 Session1-3: Locomotion Mechanism
  - 15:20-16:50 Session1-4: Bioinspired Locomotion
  - 17:30-19:00 Welcome reception

- October 12
  - 08:30-09:30 Plenary talk2: Prof. Andre Seyfarth
  - 09:40-10:40 Session2-1: Biped 2
  - 11:00-12:00 Session2-2: Sensorimotor Coordination
  - 13:30-14:50 Session2-3: Toward Dynamic and Fast Locomotion
  - 15:20-17:30 Poster Session
  - 18:00-20:00 Banquet

- October 13
  - Laboratory bus tour (Osaka Univ. and Kobe Univ.)

- October 14
  - 08:30-09:30 Plenary talk: Prof. Roy Ritzmann
  - 09:40-10:40 Session3-1: Insects and Robots
  - 11:00-12:00 Session3-2: Quadruped Locomotion

October 11 (Day 1)

October 12 (Day 2)

October 14 (Day 4)

Poster Session (October 12, 15:20-)

Plenary Talk

Neurophysiology of gait for understanding basal ganglia motor disorders
- from animal behaviors to the constructive approach -

Kaoru Takakusaki

Research Center for Brain Function and Medical Engineering, Asahikawa Medical University, Asahikawa, Japan
(Tel : +81-166-68-2884; E-mail: kusaki@asahikawa-med.ac.jp)

Abstract: We elucidated substrates for the execution of normal gait and to understand pathophysiological mechanisms of gait failure in basal ganglia dysfunctions. In Parkinson's disease, volitional and emotional expressions of movement processes are seriously affected in addition to the disturbance of automatic movement processes, such as adjustment of postural muscle tone and rhythmic limb movements during walking. These patients also suffer from muscle tone rigidity and postural instability, which may also cause reduced walking capabilities. Neurophysiological and clinical studies have suggested the importance of basal ganglia connections with the cerebral cortex and limbic system in the expression of volitional and emotional behaviors. Here we hypothesize a crucial role played by the basal ganglia-brainstem system in the integrative control of muscle tone and locomotion. The hypothetical model may provide a rational explanation for the role of the basal ganglia in the control of volitional and automatic aspects of movements. It can also be beneficial for understanding pathophysiological mechanisms of basal ganglia movement disorders. A part of this hypothesis has been supported by studies utilizing a constructive simulation engineering technique that clearly shows that an appropriate level of postural muscle tone and proper acquisition and utilization of sensory information are essential to maintain adaptable bodily functions for the full execution of bipedal gait.

Keywords: Basal ganglia-brainstem system, Postural muscle tone, Musculo-skeletal structures, Parkinson's disease

1. BASIC NEURAL STRUCTURES INVOLVED IN THE GAIT CONTROL

1.1 Contribution of forebrain structures

Activation of different areas in the forebrain evokes different types of goal directed behaviors. An important component of these behaviors is the locomotion, which has been considered as an emotional motor behavior that is triggered by signals from the limbic system to the brainstem [1]. However, accurate gait modification requires visuomotor processing in the cerebral cortex so that a precise foot placement can be achieved [2]. Prefrontal and premotor cortices (supplementary motor area and premotor area) are involved in motor planning and programming, respectively [3]. Motor programs at the premotor cortices may include those for postural control and precise limb movement control. Sensory information such as proprioceptive, vestibular and visual sensations is also required for planning and programming in addition to execution of locomotion [1]. The basal ganglia and the cerebellum can assist the above accurate cognitive operations by activating loops with prefrontal (cognitive loop) and premotor/primary motor (motor loop) cortices [4]. Loops involving the basal ganglia and the limbic system (limbic loop) contribute to emotional behavioral expression [1].

1.2 Mechanisms of integrating posture and locomotion by the brainstem and spinal cord

Regardless of whether the locomotion is emotional or volitional, it is accompanied by automatic processes that are controlled by the brainstem and spinal cord [1]. Basic structures involved in the control of locomotion and postural muscle tone are located in the midbrain [1]. One is midbrain locomotor region (MLR), and the other is muscle tone inhibitory region in the pedunculopontine tegmental nucleus (PPN). Signals arising from the MLR

activate "muscle tone excitatory system" and "rhythm generating system". The excitatory system is composed of excitatory reticulospinal tract and monoaminergic pathways such as the coerulospinal and the raphespinal tracts. The excitatory reticulospinal tact and central pattern generators (CPGs), which are composed of spinal interneuronal networks, are major components of the rhythm generating system. Signals from the PPN excite "muscle tone inhibitory system", which is comprised of the pontomedullary reticulospinal tract and spinal inhibitory interneurons. This simultaneously inhibits α- and γ-motoneurons innervating extensor and flexor muscles and interneurons in transmission of reflex pathways (a part of them constitutes CPGs) so that it suppresses postural muscle tone and locomotion [8-10]. There are mutual inhibitory interactions between the excitatory and inhibitory system at the level of the brainstem and spinal cord. These systems contribute to the automatic processes of locomotion such as rhythmic limb movements and adjustment of muscle tone.

1.3 Gait control by the basal ganglia and pathophysiology of gait failure in Parkinson's disease

The brainstem receives excitatory inputs from the cerebral cortex and the limbic system, and inhibitory inputs from the basal ganglia [1]. The MLR/PPN area and the pontomedullary reticular formation receive inputs more preferentially from the premotor cortices rather than the primary motor cortex. Corticospinal system therefore controls precise limb-trunk movements and cortico-brainstem-spinal system may contribute to postural control that accompanies voluntary movement processes. It is established that basal ganglia control the activities of the cerebral cortex and the brainstem via ascending and descending projections. The former contributes to the planning, programming, and gait initiation via thalamocortical loops. The latter may

control gait initiation and modulate locomotor rhythm and postural muscle tone during locomotion.

In Parkinson's disease, loss of dopamine increases GABAergic inhibitory output from the basal ganglia [5]. Excessive inhibition upon thalamocortical loops may reduce cortical activities that enable planning, programming and sensory processing for execution of voluntary movements, resulting in hypokinesia and bradykinesia. An increase in the basal ganglia inhibition together with reduction of cortical excitation upon the MLR and the PPN may result in gait disturbance and hypertonus, respectively [6]. Consequently gait akinesia can be due to reduced activities of the cerebral cortex and the brainstem. Muscular rigidity is also involved in the gait akinesia because hypertonus or co-contraction of extensor and flexor muscles restricts trunk and limb joints' movements.

2. CONSTRUCTIVE APPROACHES TO BIPEDAL GAIT CONTROL

2.1 Design of bipedal simulation based on basal ganglia-brainstem system

Setting the appropriate level of postural muscle tone is necessary for execution of movements depending on environmental conditions [6] Bipedal walking requires alteration of body and leg movements in response to unpredictable perturbations so that stable posture during walking could be maintained. Tomita and Yano [7] proposed a new bipedal control system by modeling the basal ganglia-brainstem system and designed a bipedal robot, according to roles that were clarified by physiological studies [1, 6]. The ranges of motion of each joint are determined according to observed human data. Because adjustment of postural muscle tone is useful to determine body-leg synergies in response to changes in the environment, the robot has a postural muscle tone control system in addition to a locomotor executing system as gait control mechanisms. These two systems are integrated at the level of the spinal cord. During gait the subject receives proprioceptive information through their body and leg, mostly from the plantar foot, which has direct contact with the irregular ground. The ground reactive force exerted on the plantar foot was utilized to alter the level of postural muscle tone of body and leg and to maintain the body equilibrium. Visual sensation was also utilized to maintain postural equilibrium.

2.2 Role of postural muscle tone in the control of bipedal gait modification

Using this technique, examination was made to clear following two points. One was whether appropriate real-time regulation of postural muscle tone enabled the model to execute adaptable bipedal gait. The second was how changes in the operation of muscle tone control system modified bipedal gait. The simulation robot displayed flexible and robust bipedal gait that emerged from appropriate regulation of postural muscle tone in response to real-time alterations of the ground reaction force against various loads without explicit postural control. For example, when the robot was pushed or pulled forward or backward, it immediately adapted to the perturbation so that posture was steadily maintained. It is critically important to note that bipedal gait was greatly modified if postural muscle tone of the simulation robot was increased or decreased. In the case of hypertonus which was achieved by increasing the gain of stretch reflexes, walking speed reduced with a decrease in stride. The robot easily fell down if such perturbations were applied and the robust changes in postural control were ignored. Such gait disturbances are similar to those observed in Parkinsonian patients. Similarly, when postural muscle tone of the robot was reduced, it exhibited unstable bipedal gait characterized by agitation or postural sway of the trunk and a wide stance with postural instability. These characteristics resembled to the ataxic gait often observed in patients with a lesion in the medial cerebellum. Ground reactive force as a sensory feedback was not effectively utilized to control postural equilibrium when the level muscle tone of the model was either high (hypertonus) or low (hypotonus), indicating that the degree of real-time sensory acquisition depends on the level of muscle tone. These findings suggest that fine body structures as well as appropriate mechanisms of controlling muscle tone are essential to maintain stable postural and locomotor synergies in bipedal gait performance.

REFERENCES

[1] K. Takakusaki K, K. Saitoh, H. Harada H, M. Kashiwayanagi. Role of basal ganglia - brainstem pathways in the control of motor behaviors. *Neuroscience Research*, Vol. 50, No.2, pp.137-151, 2004.

[2] Ap.Georgopoulos, S. Grillner, S. Visuomotor coordination in reaching and locomotion. *Science*, 245, pp.1209-1210, 1989.

[3] T. Hanakawa, , Y. Katsumi, H. Fukuyama, M. Honda, T. Hayashi, J. Kimura, H. Shibasaki. Mechanisms underlying gait disturbance in Parkinson's disease: a single photon emission computed tomography study. *Brain*, Vol. 122, Pt. 7, pp. 1271-1282, 1999.

[4] FA. Middleton and PL. Strick PL. Basal ganglia and cerebellar loops: motor and cognitive circuits. *Brain Res. Rev.,* Vol. 31, No. 2-3, pp. 236–250, 2000.

[5] MR. DeLong, T. Wichmann. Circuits and circuit disorders of the basal ganglia. *Archives of Neurology*, Vol. 64, No. 1, pp. 20-24,2007.

[6] K. Takakusaki, N. Tomita, M. Yano. Substrates for normal gait and pathophysiology of gait disturbances with respect to the basal ganglia dysfunction. *Journal of Neurology,* Vol. 255, Suppl 4, pp. 19-29, 2008.

[7] N. Tomita, M. Yano Bipedal robot controlled by the basal ganglia and brainstem systems adjusting to indefinite environment. *Procedings of IEEE/ICME*, pp116-121, 2007.

Stability in walking and running - biomechanical concepts and challenges

Authors: Seyfarth, A
Lauflabor Locomotion Laboratory, Jena University.

In human walking and running, typical patterns of the ground reaction force with two humps in walking and a single hump in running are found. This behavior is widely found in nature and can be well described by assuming spring-like leg function (spring-mass model, Blickhan, 1989, extended to bipedal gaits, Geyer et al., 2006). However, systematic deviations from such a perfectly elastic leg behavior like a telescopic linear spring can be found. One reason for this is that the leg has non-elastic properties (e.g. in materials and muscles Haeufle et al., 2010). Also, the leg is landing at the ground with non-zero contact velocities leading to impact losses (De Wit et al., 2000).

The segmental design of legs with a distal foot segment and almost straight knee configurations could also contribute to deviations in the spring-like leg function (Seyfarth et al., 2001, Maykranz, 2009). In fact, elastic properties at joint level are related to spring-like leg function in a nonlinear fashion (Rummel and Seyfarth, 2008). Furthermore, hip torques joint can redirect the leg force with respect to the center of mass (Maus et al., 2008). By this, the upper body can stay in an upright position guaranteeing postural trunk stability during locomotion. Another example of extending the spring-mass model is to include lateral body movements (Seipel and Holmes, 2005, Peuker and Seyfarth, 2010). Furthermore, extensions to quadrupedal (Gross, 2009) and hexapod (Schmitt and Holmes, 2000) gait models can be considered. Interestingly, all these structural extensions of the model did preserve the previously observed self-stabilizing mechanisms found in the spring mass model (Seyfarth et al, 2001).

With this repertoire of conceptual models it becomes possible to design models of desired complexity, which could inherit features of the underlying template models (Full & Koditschek, 1999). In order to compare the model predictions with experimental data it is important to make sure that the key characteristics of human or animal gait are sufficiently represented in the biomechanical models. So far, there are fundamental differences between the predicted gait pattern and experimental data on human locomotion. For instance, it is not clear which mechanisms cause the observed step-to-step

variability in kinematic and kinetic parameters. This is important as concepts on gait and gait stability often rely on the assumption of a periodic gait pattern. As such steady-state gait patterns are not present in nature, the currently used gait models need to be improved to adequately describe the observations.

References

Blickhan, 1989, J. Biomechanics.
De Wit et al., 2000, J. Biomechanics.
Full and Koditschek, 1999, J Exp. Biol.
Geyer et al., 2006, Proc. Roy. Soc. Lond. B.
Gross et al., 2009, Dynamic Walking.
Haeufle et al., 2010, Bioinspiration & Biomimetics.
Maus et al., 2008, CLAWAR.
Maykranz et al., 2009, Autonome Mobile Systeme.
Peuker and Seyfarth, 2010, WCB.
Rummel and Seyfarth, 2008, IJRR.
Schmitt and Holmes, 2000, Biol. Cybernetics.
Seipel and Holmes, 2005, IJRR.
Seyfarth et al., 2001, Biol. Cybernetics.

AMAM 2011 Plenary Talk

October 14, 2011

Roy E. Ritzmann

Negotiating Complex Terrain: Insect Brains and Behavior and their impact on Robot Design

Abstract

In order to be useful in many dangerous missions, robots should be able to negotiate very complex terrain. Insects move seamlessly through complex environments in a manner that is the envy of any robotic device and, if we can understand how the accomplish this, would provide rich templates for advanced autonomous robot designs. In order to deal with large objects in their path, insects or legged robots must alter leg movements in a precise manner. We employ a range of behavioral and neurobiological techniques to examine how cockroaches perform these tasks. Our behavioral analysis shows how the cockroach evaluates the height and distance of plastic blocks then uses information, mostly from antennal contact, to guide rearing movements that initiate a climb. A shelf creates a choice between climbing over and tunneling. This is again dictated by antennal inputs. If the antennae contact the shelf from above, the cockroach climbs, but contact from below generates tunneling. Ambient light also affects the decision, with more tunneling occurring in the light than under dim light conditions. Likewise, in a T maze, the cockroach typically turns away from the antenna that touches the back wall first, but this "touch-and-turn" rule can be countermanded by stripes moving in the opposite direction. These interactions and others suggest that movements through complex terrain involve multi-sensory interactions that consider many factors in order to change direction of movement in a context dependent fashion. Where in the insect's central nervous system could these interactions merge? We have been examining a group of midline neuropils in the cockroach brain, collectively called the central complex (CC). Electrolytic lesions in specific regions of the CC have precise effects on various locomotory behaviors. Using multi-channel recording, we demonstrated that neurons in CC neuropils respond to antennal and visual stimulation with complex interactions occurring in a decidedly non-linear fashion. More recently, we have been injecting a local anesthetic into the CC to generate reversible changes in the insect's ability to negotiate barriers. In tethered preparations, we find neurons that increase activity in tandem with, and often before, changes in step rate, while stimulation through the same electrodes increase step frequency. Asymmetric activity in the CC precedes turning movement while stimulation in the lateral accessory lobe (a CC output region) regularly evokes turning movement. We are now trying to exam insect behavior in a more realistic environment. Placed in a well-lit arena, cockroaches have a strong tendency to seek out a darkened shelter. Faced with a transparent barrier, the cockroach appears to see the shelter, but its path is blocked. It then must use a combination of visual and tactile cues to get around the barrier and to the shelter. The algorithm that begins to explain how the cockroach solves these problems has been implemented in a wheeled robot that performs remarkably similarly to the insect. We believe that these interdisciplinary studies will lead to greater understanding of how insects negotiate complex terrain as well as robot designs that capture these behaviors.

Research interest

My laboratory examines how insects deal with barriers. We consider behavioral and neurobiological properties of insects facing barriers of various sizes and shape and then work with engineers in Roger Quinn's laboratory to incorporate our findings into robotic designs both for improved control and as hardware models of behavior.

Oral Session

Towards Understanding of Versatility of Animal Behavior:
A Mathematical Model for Ophiuroid Omnidirectional Locomotion

Wataru Watanabe[1], Shota Suzuki[1], Takeshi Kano[1] and Akio Ishiguro[1,2]

[1]Research Institute of Electrical Communication, Tohoku University, Sendai, Japan
(Tel: +81-22-217-5465; E-mail: watanabe@cmplx.riec.tohoku.ac.jp)
[2]Japan Science and Technology Agency CREST
(Tel: +81-22-217-5464; E-mail: ishiguro@riec.tohoku.ac.jp)

Abstract: Our objective is to understand behavioral versatility of animals from the perspective of well-coordinated rhythmic and non-rhythmic movements. To this end, we focus on ophiuroids as simple "best" model living organisms that exhibit spontaneous role assignment of rhythmic and non-rhythmic arm movements, and we model such arm movements by using an active rotator model that can describe both oscillatory and excitatory properties. Simulation results show that the spontaneous role assignment of arm movements is successfully realized by using the proposed model, and the simulated locomotion is qualitatively equivalent to the locomotion of real ophiuroids.

Keywords: Decentralized control, Behavioral versatility, Ophiuroid omnidirectional locomotion, Active rotator model

1. INTRODUCTION

Animals exhibit adaptive and versatile locomotion in real time under unpredictable real world constraints via spatiotemporal coordination of movements of bodily parts. In the field of robotics, a dynamical system approach based on decentralized control mechanisms has been employed to reproduce the ability of animals to perform synergetic movements. In particular, coupled oscillators or distributed neural networks (CPGs) have been widely used for the control systems of robotic agents [1][2]. The core idea underlying these studies is to exploit the intrinsic structural stability of a limit cycle, which induces self-organized behavior of the entire system without any preprogrammed trajectory tracking control.

These studies have provided us with remarkable insights into *adaptability*, which is an important aspect of animal behavior. However, animals well coordinate rhythmic and non-rhythmic movements whereby versatile behavior is generated according to the situation. Such behavioral *versatility*, which is another indispensable aspect, cannot be described solely in terms of limit cycles that exhibit rhythmicity. In order to realize behavioral versatility, we should rethink the limit-cycle-based approach and introduce an extended systematic design scheme that can describe rhythmic and non-rhythmic movements effectively. Accordingly, we focus on *ophiuroid omnidirectional locomotion*, in which the coordination of both rhythmic and non-rhythmic movements is required for achieving efficient locomotion [3].

Thus, our primary objective is to clarify the autonomous decentralized control mechanism that effectively explains ophiuroid omnidirectional locomotion in which the assignment of rhythmic and non-rhythmic movements to the arms can be achieved spontaneously and changed dynamically according to the situation. To this end, we propose a simplified model of ophiuroid robot that is controlled in a fully decentralized manner. As the first step, we carry out simulation experiments, whose results show that the spontaneous role assignment of rhythmic and non-rhythmic arm movements is successfully realized by applying attractant stimuli to the arms.

2. THE MODEL

A schematic illustration of the ophiuroid robot employed in this study is shown in Fig. 1 (a). The robot consists of a *central disk* and five arms. Two motors that can rotate in the vertical (pitch) and horizontal (yaw) direction are implemented in each joint. The joint angle is controlled according to proportional-derivative control.

In order to describe both rhythmic and non-rhythmic arm movements of ophiuroids, we implement distributed control systems based on an *active rotator model* in the joints, as shown in Fig. 1 (b). The time evolution of the phase of the active rotator embedded in the ith arm, ϕ_i, is described as [4]

$$\frac{d\phi_i}{dt} = \omega - a_i \cos \phi_i, \tag{1}$$

where ω is the intrinsic frequency and a_i is a parameter that determines the property of the active rotator.
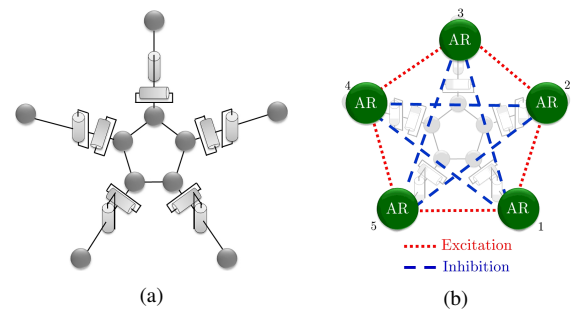
Fig. 1 Schematic illustration of an ophiuroid robot: (a) top view of mechanical system and (b) decentalized control system using active rotators (ARs).

The behavior of the active rotator is divided into three states. When $-\omega < a_i < \omega$, the active rotator exhibits *oscillatory behavior* whereby it rotates along the unit circle with angular velocity $\omega - a_i \cos \phi_i$, resulting in rhythmic movements (*side arm*). On the other hand, when $a_i < -\omega$ and $\omega < a_i$, there exists a pair of equilibrium points at which the condition $\omega - a_i \cos \phi_i = 0$ is satisfied, where one is stable and the other is unstable. In such cases, the active rotator exhibits *excitatory behavior* whereby it converges to the stable equilibrium point when no external force is applied, resulting in non-rhythmic movements (*posterior arm, leading arm*). By modulating the parameter a_i in Eq. (1), we can easily switch between rhythmic and non-rhythmic movements.

In order to dynamically change the role of arm movements, we describe the time evolution of a_i as

$$\tau \frac{da_i}{dt} = \sum_j \varepsilon_{ij} \cos \phi_j + s_i - \varepsilon N_i + \alpha - a_i, \qquad (2)$$

where τ is the time constant and ε_{ij} is a constant that denotes the coupling strength between active rotators. s_i is the sensory input applied to the ith arm and α is a constant. The third term, $-\varepsilon N_i$, is the local sensory feedback term, where ε is a positive constant and N_i is the ground reaction force acting on the ith arm. This local sensory feedback control is employed so that the in-phase rhythmic movements of two arms, which are observed in efficient locomotion of real ophiuroids, are successfully realized.

3. SIMULATION RESULTS

Fig. 2 shows snapshots of the simulated locomotion of the ophiuroid robot. In the interval (i)-(iii), the attractant stimulus was applied to arm 3; it was switched to arm 1 at (iii) and to arm 2 at (v). As observed, the stimulated arm became the leading arm, and the robot moved toward the attractant stimulus with role assignment of the three types of arm movements.

Such spontaneous role assignment is clearly represented by the time evolutions of the parameters a_i and the phases ϕ_i, as shown in Figs. 3 and 4. As shown in
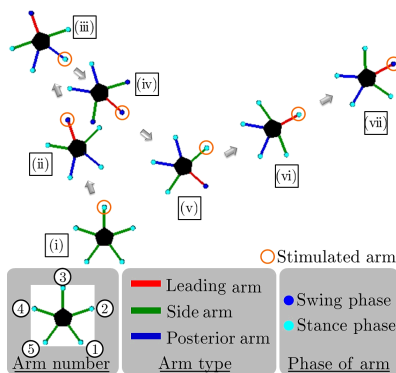
Fig. 2 Snapshots of the simulated locomotion of the ophiuroid robot. These were obtained for every 100,000 time steps, corresponding to the symbols (i)-(vii).
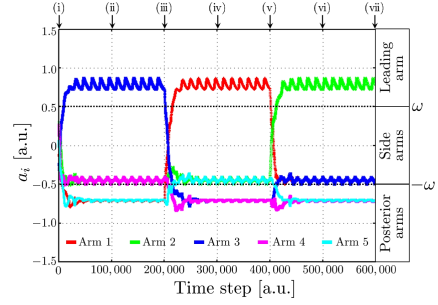
Fig. 3 Time evolution of the parameter a_i.
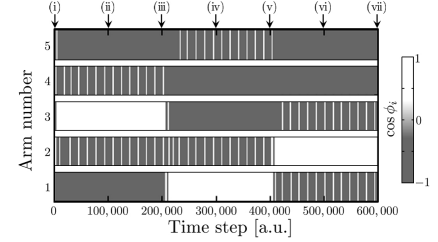
Fig. 4 Time evolution of the phase ϕ_i.

Fig. 3, $a_i > \omega$, $-\omega < a_{i\pm1} < \omega$, and $a_{i\pm2} < -\omega$ are satisfied when the attractant stimulus is applied to the ith arm. In addition, Fig. 4 shows that the phase ϕ_i of the side arms varies periodically, whereas those of the leading arm and posterior arms have a steady state value. These results clearly implies that the role assignment of rhythmic and non-rhythmic movements among the arms is realized spontaneously.

4. CONCLUSION AND FUTURE WORK

In this study, we modeled the ophiuroid omnidirectional locomotion that exhibits well-coordinated rhythmic and non-rhythmic arm movements. Simulation results showed that the proposed model can reproduce the role assignment of such versatile arm movements. In the future work, we plan to extend the model to describe movements of soft and deformable arms, *i.e.,* intra-arm coordination, in addition to inter-arm coordination.

REFERENCES

[1] G. Taga, Y. Yamaguchi and H. Shimizu, "Self-organized control of bipedal locomotion by neural oscillators in unpredictable environment", *Biological Cybernetics*, Vol. 65, pp. 147-159, 1991.

[2] T. Umedachi, K. Takeda, T. Nakagaki, R. Kobayashi and A. Ishiguro, "Fully decentralized control of a soft-bodied robot inspired by true slime mold", *Biological Cybernetics*, Vol. 102, pp. 261-269, 2010.

[3] Y. I. Arshavskii, S. M. Kashin, N. M. Litvinova, G. N. Orlovskii and A. G. Fel'dman, "Coordination of arm movement during locomotion in ophiurans", *Neurophysiology*, Vol. 8, No. 5, pp. 404-410, 1976.

[4] S. Shinomoto and Y. Kuramoto, "Phase Transitions in Active Rotator Systems", *Progress of Theoretical Physics*, Vol. 75, No. 5, pp. 1105-1110, 1986.

Method for obtaining quantitative change in muscle activities by difference in sensory inputs about human posture control

Hiroaki Ogawa[1], Ryosuke Chiba[2], Kaoru Takakusaki[3], Hajime Asama[1], Jun Ota[1]

[1]Department of Precision Engineering, The University of Tokyo, Tokyo, Japan
[2]Graduate School of System Design, Tokyo Metropolitan University, Tokyo, Japan
[3]Research Center for Brain Function and Medical Engineering, Asahikawa Medical University, Asahikawa, Japan

Abstract: Human posture control is a very complicated mechanism integrating multi-inputs and outputting correct motion. In this research, we propose a method to obtain quantitative changes in muscular activity caused by changing sensory inputs assuming that muscle activity is divided into external force elements and modality elements, and we propose that the this method is a viable means for determining the validity of this idea and calculating quantitative changes in muscular activity.

Keywords: mobiligence, human posture control, standing posture, muscle activity

1. INTRODUCTION

Humans control their posture by controlling the muscle activity of the whole body with the cranial nervous system using multi-sensory inputs. The construction of sensory inputs and muscular activity model has a significant meaning medically and biologically because this model more clearly elucidates the brain functions. Thus, examining the relationship between senses and muscular activity is important as the first step in constructing this model.

In former studies, the human posture control was researched by Nashner[1] and Bottaro[2]. In these studies, however, changes in muscular activity that resulted from changing sensory inputs were an unknown. Therefore, this paper proposes a method to obtain quantitative changes in muscular activity caused by changing sensory inputs.

To achieve this purpose two challenging points exist: i)the method of changing sensory inputs and ii)the quantification of changes in muscular activity by sensory inputs. Regarding the method, we propose a method of changing sensory inputs by inhibiting or stimulating three sensory systems (visual, vestibular and somatosensory) which are considered closely related to posture control. Regarding the quantification, muscle activity changes seem to occur when an external force is applied to the body causing posture changes. Thus, we propose a method to estimate changes in muscular activity by external force and exclude them.

In this study, maintaining a standing posture is targeted due to measuring changes in muscular activity by sensory inputs because it is a simple movement limited to changes in muscular activity. In addition, physically-healthy persons are targeted because how the brain functions may differ from those of physically-challenged.

2. PROPOSED METHODS

It is assumed that the muscular activity of posture control is expressed in elements changed by external forces and elements as indicated by the sensory inputs, making the following formula applicable:

$$A_{ctivity\_i} = f_i(\boldsymbol{F_{orce}}) + g_i(\boldsymbol{M_{odality}})$$
$$i = 1, 2, \cdots, n$$

$A_{ctivity\_i}$ is scalar of the ith muscular activity. $\boldsymbol{F_{orce}}$ is a vector meaning the external force applied to the body.

$\boldsymbol{M_{odality}}$ is a vector meaning the sensory inputs condition.

The method for obtaining $g_i(\boldsymbol{M_{odality}})$ is described. $f_i(\boldsymbol{F_{orce}})$ is calculated from the model constructed by measuring electromyogram (EMG) of subject's muscles in various postures. $A_{ctivity\_i}$ is obtained by measuring EMG of subject's muscles when subject's senses are inhibited or stimulated. $g_i(\boldsymbol{M_{odality}})$ is calculated as the difference between $A_{ctivity\_i}$ and $f_i(\boldsymbol{F_{orce}})$. Figure 1 shows the outline of this method.
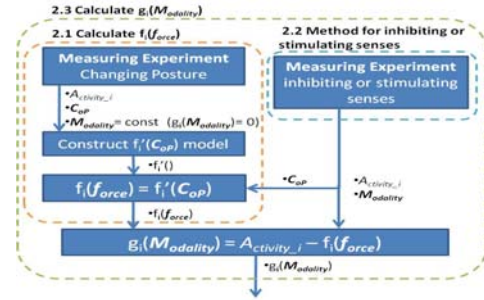
Fig. 1   Method Outline

2.1   Calculate $f_i(\boldsymbol{F_{orce}})$

In maintaining a standing posture, posture and external forces are assumed to be unique provided the Center of Pressure (CoP) position is uniquely decided. In this study, $\boldsymbol{C_{oP}}$ is defined as a vector meaning CoP position and $f_i(\boldsymbol{F_{orce}})$ is considered equal to $f_i'(\boldsymbol{C_{oP}})$ for easily understanding changes in muscular activity by external force. Thus, $f_i(\boldsymbol{F_{orce}})$ is calculated from $f_i'()$ and $\boldsymbol{C_{oP}}$.

Experiments are performed to measure $\boldsymbol{C_{oP}}$ and $A_{ctivity\_i}$ when a subject's senses are uninhibited or not stimulated and subject leans to the front or back, to the left or right, and any combination thereof. The weight shift values using four scales are used to determine $\boldsymbol{C_{oP}}$. The EMG of each muscle are used to determine $A_{ctivity\_i}$. Three-dimensional models of $f_i'()$ are constructed with planes calculated from all three points composing measured $\boldsymbol{C_{oP}}$ and $A_{ctivity\_i}$. $f_i(\boldsymbol{F_{orce}})$ in arbitrary posture can then be calculated.

2.2   Method for inhibiting or stimulating senses

Sensory inputs from visual, vestibular, and somatosensory systems are considered: the visual sense is inhibited by closed eyes, the vestibular sense is

inhibited by a caloric test that upset the vestibular system by pouring cold water into the ear cavity, and the somatosensory sense is stimulated by touching a part of the body. If these senses are inhibited or stimulated, subjects tend to change their posture.

- If only the vestibular sense is inhibited, subject can maintain the standing posture (Fig. 2A).
- If both visual and vestibular senses are inhibited simultaneously, subject leans (Fig. 2B).
- If both visual and vestibular senses are inhibited and somatosensory sense is stimulated, subject recovers its standing posture (Fig. 2C).
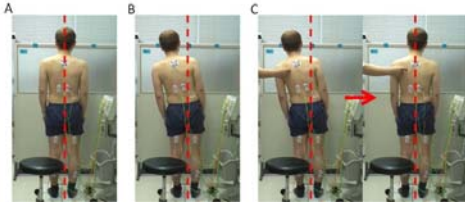
Fig. 2   Posture Change

2.3   Calculate $g_i(M_{odality})$

Experiments easure C_{oP} and $A_{ctivity\_i}$ and $M_{odality}$ when subject's senses are inhibited or stimulated by the method described inm paragraph 2.2. $M_{odality}$ is recorded for the eight combinations of the three sensory systems. Then $f_i(F_{orce})$ is calculated from C_{oP} by the method described in paragraph 2.1. $g_i(M_{odality})$ can be calculated as the difference between $A_{ctivity\_i}$ and calculated $f_i(F_{orce})$.

3.   EXPERIMENT

3.1   Experiment Conditions

Subject is one male in his twenties. Figure 3 shows muscles measured in experiments.
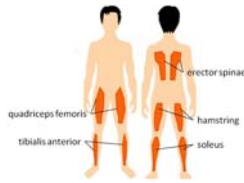
Fig. 3   Measured Muscles

3.2   Results

Figure 4 shows calculated $f_i'()$ of each muscle. The x-y plane means C_{oP}. $g_i(M_{odality})$ were calculated and investigated by an analysis of variance (ANOVA) to evaluate contribution ratio of each element of Modality in $g_i(M_{odality})$ as shown in Table 1. A is visual factor; B is vestibular factor; C is somatosensory factor; and A×B, A×C, and B×C are interactions with each factor. The value is the variance ratio. A higher value means that $g_i(M_{odality})$ is more affected by that factor. If there is 0.05 or 0.01 level of statistical significance in the factor, probability $p<0.05$ (*) or $p<0.01$ (**) is added. The item of the sign ○ shows variance ratio is 1.0 or less, within the range of error.

3.3   Discussion

The existence of threshold is considered from Figure 4, especially in y of tibialis anterior. Three-dimensional models of $f_i'()$ constructed with planes composed partially is considered more precise than with the plane composed of the whole.

Concerning the validity of the assumption about the muscular activity, if $f_i(F_{orce})$ and $g_i(M_{odality})$ are changed by F_{orce} and $M_{odality}$, then elements of the muscular activity are considered valid. Figure 4 shows that $f_i'(C_{oP})$ is not constant but changes according to C_{oP}. This means that $f_i(F_{orce})$ changes when F_{orce} changes. Moreover, significant differences can be found in Table 1. This means that $g_i(M_{odality})$ changes by $M_{odality}$. Therefore, we believe that this assumption is valid. The changes in muscle activity are obtained as $f_i(F_{orce})$ and $g_i(M_{odality})$ when the proposed method is used.

Table 1 shows that the factors affecting $g_i(M_{odality})$ differ respectively, which also indicates that some muscles are influenced by one sense, two or more senses, and even the interaction of senses.
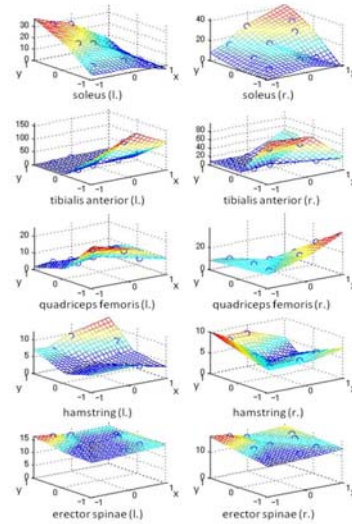
Fig. 4   Calculated $f_i'(C_{oP})$ for Each Muscle

Table 1   ANOVA Results

F value	A	B	C	A×B	A×C	B×C
soleus (l.)	1.85	123.26**	○	○	1.46	15.64**
soleus (r.)	12.94**	211.73**	10.62**	○	1.97	8.77*
tibialis anterior (l.)	○	154.45**	5.22*	○	7.42*	○
tibialis anterior (r.)	○	43.75**	○	○	4.66	1.41
quadriceps femoris (l.)	○	36.71**	○	○	○	3.09
quadriceps femoris (r.)	1.91	88.65**	1.57	1.50	5.58*	○
hamstring (l.)	2.93	○	1.72	○	○	○
hamstring (r.)	○	3.10*	1.86	9.19*	○	○
erector spinae (l.)	5.76*	172.53**	6.26*	6.77*	15.00**	9.38*
erector spinae (r.)	○	73.02**	2.79	4.61*	9.42*	3.73

A: visual, B: vestibular, C: somatosensory
* : $p<0.05$, ** : $p<0.001$, ○: pooling into error term

4.   CONCLUSIONS

This paper proposes a method for obtaining quantitative change in muscle activity caused by changes in sensory input conditions. This method was founded on the assumption that muscular activities were divided into external force elements and modality elements. Results of investigating whether this assumption was valid proved that this assumption was actually valid, and this method was a viable means for obtaining quantitative changes in muscular activity.

REFERENCES
[1] Nashner LM, et al. "The organization of human postural movements : A formal basis and experimental synthesis." *The Behavioral and Brain Sciences 8*: 135-172, 1985.
[2] Bottaro A, Yasutake Y, Nomura T et al. "Bounded stability of the quiet standing posture: an intermittent control model." *Human Movement Science 27*, 473-495, 2008.

Brain Freedom from Body :
Neuronal Activity during Goal-Approach by Behavior and Goal-Operation by BMI in the Rat

Yoshio Sakurai[1] and Susumu Takahashi[2,3]

[1]Department of Psychology, Kyoto University, Kyoto, Japan
(Tel:+81-75-753-2848; E-mail:ysakurai@bun.kyoto-u.ac.jp)
[2]Khoyama Center for Neuroscience, Kyoto Sangyo University, Kyoto, Japan
(Tel:81-075-705-1508; E-mail:tsusumu@cse.kyoto-su.ac.jp)
[3]PRESTO, Japan Science and Technology Agency, Kawaguchi, Japan

Abstract: The present study focuses on brain-body interaction and reports how neuronal activity is involved in and limited by body movements. The core method is a high-performance brain–machine interface (BMI) system, which uses long-term stable recording of multiple neuronal activity and real-time spike-sorting with combination of independent component analysis and newly developed multi-electrodes. The system detects in real time precise firing frequency and synchrony of neighboring individual neurons of behaving animals. The tasks we employed are goal-approach and goal-operation tasks for rats. In the former task, the rats are required to approach a wall (goal) to get reward. In the latter task, they have to operate the wall by their neuronal activity with the BMI and draw it to get reward. We present here that firings of the hippocampal neuronal populations were remarkably enhanced when they were working to operate the external goal. This result suggests that the hippocampal neuronal activity can directly operate devices in external environments and it can be highly active when the brain is released from restraint by body movements.

Keywords: Brain-body interaction, Brain-machine interface, Hippocampus, Neuron.

1. INTRODUCTION

Although great progress has been made in analyses of electrophysiological data from behaving animals, it still remains unclear how really dynamic activity of individual neurons and their functional connectivity are in the working brains. One of the main reasons for that lack of clarity might be that physical limitations of body movements generating behaviors often restrain the freedom of neuronal dynamics. Indeed, as a great psychologist J. J. Gibson has indicated [1], coding of external information is dependent on and modulated by behaviors operating external environments. Neuronal activity to code external valid information, therefore, must be based on brain-body interaction for behavior and affected and restrained by body movements. In this study, we specifically focuses on the interaction between neural activity and body movements. We investigate real neuronal dynamics underlying recognition of and intention to a goal by comparing neuronal activity when the animals approach the goal by behavior with their body movements and when they operate and draw the goal by their neuronal activity with a brain-machine interface (BMI).

We have developed a high-performance BMI system to detect actual dynamics of neuronal populations of the working brains. Using the BMI system, neuronal codes, i.e., firing frequency and synchrony of neurons, in the brain of the behaving animal can directly control external devices in real time instead of the animal's behavior. The keys to constructing the BMI system are recording multineuronal activities from behaving animals for long periods, detecting firing frequencies of individual neurons and firing synchrony among many neighboring neurons, making neuronal codes to control external devices, and showing dynamic and flexible changes of the neuronal codes in the working brain.

2. METHODS

2.1 Animals and apparatus

Male Wistar albino rats were used. The rats were trained in an operant chamber of $22(H) \times 49(W) \times 46(D)$ cm. One wall of the chamber has illuminated sensor holes to detect the nose-poke behavior of rats. A food dispenser behind the wall delivered 25-mg food pellets to a magazine located at the center of the wall. All experimental procedures accorded with NIH and Kyoto University guidelines for Animal Research.

2.2 Long-term recording of multineuronal activity

Approximately one week after surgery for electrode implantation, the multi-electrodes (dodecatrodes) [2] were lowered into the brain using the microdrive [3]. The activity detected from the dodecatrodes was judged to be multineuronal if its peak amplitude was more than two times greater than the noise, i.e. the signal-to-noise ratio was greater than 2.0. When multineuronal activity was detected, the rat was returned to its home cage. If activity remained present after one or more days, then the data were judged to be stable and suitable for long-term recording [3].

2.3 Real-time spike sorting with ICA

We have developed a system for real-time automatic sorting of multineuronal activity with independent component analysis (ICA) and call it RASICA [2]. The ICA used is a powerful method of solving both the

spike-overlapping and nonstationary waveform problems [4,5] and can compensate the electrode drift to render the spike-sorting stable with very little computational expense.

2.4 Neuronal codes to control tasks and devices

With the RASICA, we select any of the recorded individual neurons to detect specific patterns of frequency or synchrony of their firings. The detected patterns of firing frequency and synchrony are respectively defined as *frequency code* and *synchrony code*. When the system detects these neuronal codes, it transmits TTL signals to a computer that controls the tasks and the reward dispenser.

2.5 Tasks by behavior and neuronal codes

We have constructed goal-approach and goal-operation tasks, conducted by behavior with body movements and neuronal codes with BMI respectively. Fig.1 is a rat performing both of the tasks. Fig.2 is a schematic drawing of the goal-operation task.
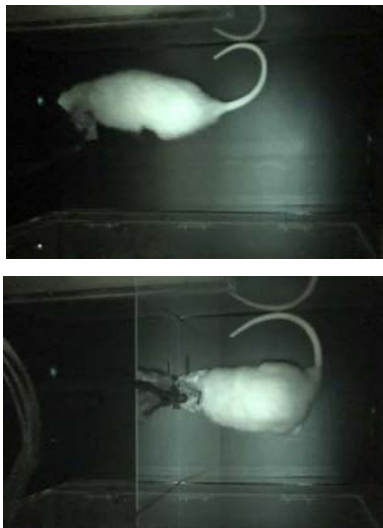
Fig. 1 Upper photo: A rat performing the goal-approach task. It moves from the right-side wall to the left-side one and conduct a nose-poke to the illuminated hole to get reward of pellets. Lower photo: The same rat performing the goal-operation task with BMI. The goal (the hole on the left wall) is being operated and drawn to the rat by neuronal codes.
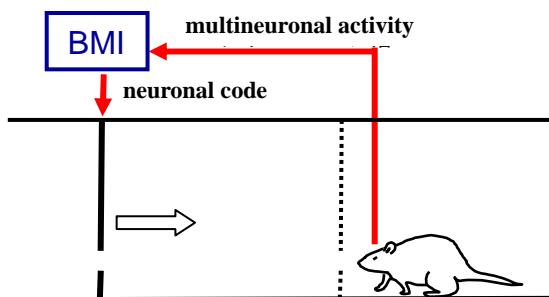
Fig. 2 Schematic drawing of the goal-operation task. The goal (the hole on the left wall) is being operated and drawn to the rat by neuronal codes with BMI.

3. RESULTS AND DISCUSSION

We analyzed activity of hippocampal CA1 neurons when the rat was performing the goal-approach task and the goal-operation task. In the former task, neuronal activity was just recorded during movements to the goal. In the latter task, the frequency code from the hippocampal neurons drew the left wall to the rat. Fig. 3 is an example of data showing changes of firing frequencies of the neurons during the 2 days of training of the tasks. The result shows that hippocampal neuronal activity can be used to control external devices and be remarkably enhanced when the animals use not their body movements but their neuronal firing to reach goals.

The present study suggests that neuronal activity can be highly active when the brain is released from restraint by body movements. This fact possibly contributes to development of high-performance brain-machine interfaces in the near future.
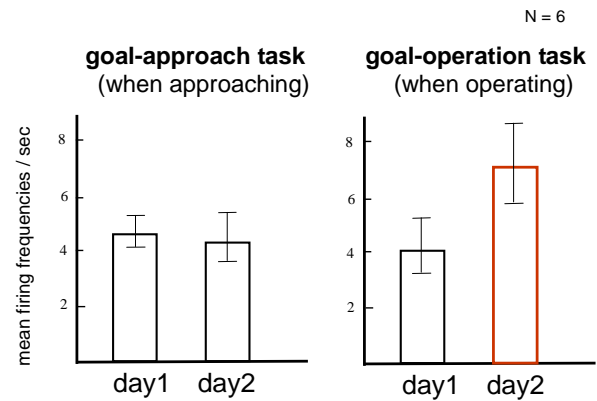
Fig. 3 Mean firing frequencies of the hippocampal CA1 neurons during 2 days of training of the goal-approach and goal-operation task.

REFERENCES

[1] Gibson, J.J. (1979). *The ecological approach to visual perception*. Hillsdale, Lawrence Erlbaum.

[2] Takahashi, S., Sakurai, Y. (2005). Real-time and automatic sorting of multineuronal activity for sub-millisecond interactions in vivo. *Neuroscience*, 134, 301-315.

[3] Sakurai, Y., Takahashi, S. (2006). Dynamic synchrony of firing in the monkey prefrontal cortex during working memory tasks. *Journal of Neuroscience*, 26, 10141-10153.

[4] Takahashi, S., Anzai, Y., Sakurai, Y. (2003). Automatic sorting for multineuronal activity recorded with tetrodes in the presence of overlapping spikes. *Journal of Neurophysiology*, 89, 2245-2258.

[5] Takahashi, S., Sakurai, Y.（2009）Sub-millisecond firing synchrony of closely neighboring pyramidal neurons in hippocampal CA1 of rats during delayed non-matching to sample task. *Frontiers in Neural Circuits,* 3(9), 1-18.

Anchoring the SLIP template: The effect of leg mass on running stability

Frank Peuker[*1], Sten Grimmer[1], Soha Pouya[2], Rico Moeckel[2], Auke Ijspeert[2] and André Seyfarth[1]

[*]Corresponding author: frank.peuker@uni-jena.de

[1]Lauflabor Locomotion Laboratory, Friedrich-Schiller Universität Jena, Dornburger Str. 23, Jena, Germany

[2]Biorobotics Laboratory, Institute of Bioengineering, École Polytechnique Fédérale Lausanne (EPFL), Switzerland

Abstract: Spring-like leg behavior was found in the global dynamics of human and animal running in sagittal plane. The corresponding template model, the conservative spring-loaded inverted pendulum (SLIP), shows stability for a large range of speeds and is, therefore, a promising concept for the design of legged robots. However, an anchoring of this template is needed in order to provide functions of biological structures (e.g., mass distribution, leg design) and engineers' details for construction. We extend the SLIP template model towards two new models that we call M-SLIP and BM-SLIP by adding considerable leg masses to investigate the influence of leg rotation on running stability. Our study clearly reveals that the spring-loaded inverted pendulum can be anchored in a leg mass model. This supports model- and simulation-driven engineering towards robotic behavior inspired from biological systems.

Keywords: anchor; template; legged locomotion; stability; leg swing control; leg swing dynamics

1. INTRODUCTION

The biomechanical description of human and animal locomotion relies on so called *template models* [1]. A template model is the simplest model and has the least number of parameters, which is able to describe the basic behavior of the considered gait. The most common template model for human locomotion is the spring-loaded inverted pendulum (SLIP, [2]). By abstracting the leg to a massless linear spring with stiffness k and the body to a point mass m, the SLIP resembles the global dynamics of running in sagittal plane [2]. Furthermore, gait patterns from the SLIP model show self-stability if the leg stiffness k and the angle of attack α (landing angle of spring) is adjusted properly [3]. That means, that despite its great simplicity, the SLIP model can recover from small perturbations (e.g. drop height or initial velocity) without any control, neither feed-forward nor feedback. Therefore, the SLIP model is a promising underlying concept for the design of legged robots that combine both, energy-efficiency and dynamic stability.

However, the transfer of the SLIP to a technical device needs an anchoring in more elaborate structures. Due to its template character, the SLIP is missing important structures from a higher level of detail like, for instance, trunk, segmented leg, foot, friction, slipping or leg inertia. Following the concept of *templates and anchors* [1], a piecewise adding of details to the SLIP model can reveal the mechanisms or the functions of biological structures, and thus, guide engineers towards nature-driven robotics.

In the present paper, we extend the SLIP model by adding leg mass (M-SLIP and BM-SLIP model, see Fig. 1). About one third of the human mass is covered by both legs [4, 5] with a leg CoM located at 40% of leg length with respect to the hip joint. This gives rise to high rotational inertia and a significant influence on the overall dynamics can be expected. Effects emerging from adding leg mass include swing leg dynamics and impact forces. Further, the leg behavior in a SLIP model is represented by one spring. Since running has clear single contact and flight phases, this procedure is appropriate. However, in humans, running is characterized by an alternating stance and flight phase of legs. These coupled legs interact in each phase. For SLIP running, it was shown that running stability is largely influenced by the swing leg dynamics [6]. The effect of swing leg dynamics on mass-attached legs is yet unclear.
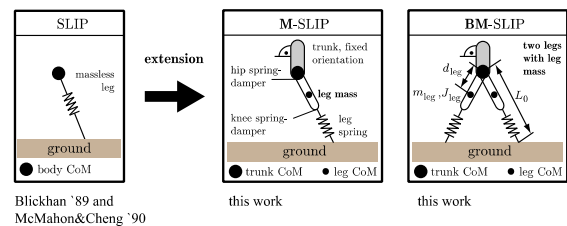
Fig. 1 We extend the SLIP model (a template model for describing human and animal running) by adding leg mass (m_{leg}) and leg moment of inertia (J_{leg}) at a particular distance from the trunk CoM (d_{leg}). We include a hip spring-damper (parallel combination of a linear spring and viscous damper) to control the leg during swing phase to a certain position. We distinguish a monopedal version (M-SLIP) and a bipedal version (BM-SLIP) to describe single-legged running (like kangaroos) and bipedal running (like humans). The knee spring-damper accounts for the alignment of rigid leg and massless spring, thus modeling a telescopic mass-attached leg. For the sake of simplicity and to disregard the problem of trunk stabilization, we fix trunk orientation.

In a first approach, we aim at investigating the influence of leg mass on gait stability and test the hypothesis that SLIP solutions can be inherited to the M-SLIP model. If so, the curse of dimensionality [7] could be broken because model designers can follow the low-dimensional SLIP path of stability within the higher-dimensional M-SLIP model when searching for stable gait patterns. Here, we vary two parameters (leg stiffness k and angle of attack α) and keep the initial velocity fixed to search for stable running patterns. The corresponding domain of stable running patterns, i.e. the combination of leg stiffness k and angle of attack α, is known from SLIP simulations as J-shaped area [3]. Here, we investigate how this domain is transformed in the M-SLIP model. In a second approach, we extend the M-SLIP model by adding a second leg (BM-SLIP) to

investigate the influence of swing leg inertia on gait stability.

2. RESULTS AND DISCUSSION

We use the steps-to-fall map to determine stable running patterns. Thereby, we record the number of steps until the model falls over. We limit the maximum number of steps to 50. If the model achieves this number, we classify the solution as stable. We vary leg stiffness k and angle of attack α on an equidistant grid (64 x 64) and record corresponding domains of stable running patterns for the SLIP, the M-SLIP and the BM-SLIP model (see Fig. 2).
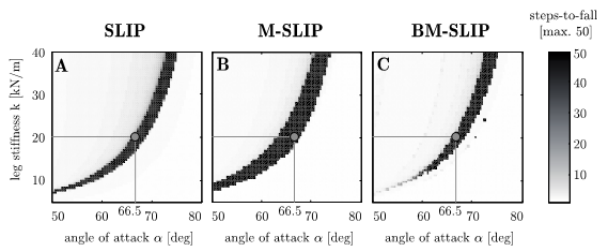
Fig. 2 Steps-to-fall maps by varying leg stiffness k and angle of attack α. The domain of stable SLIP running patterns is inherited to the M-SLIP and BM-SLIP model. The stable domain enlarges in single-legged running (M-SLIP), and slightly shrinks in bipedal running (BM-SLIP). Physiological leg data from humans are applied. Hip stiffness (1.5 kNm/rad) and knee stiffness (50 kNm/rad) are chosen to guarantee appropriate landing condition.

Steps-to-fall maps of the SLIP (running with massless legs), M-SLIP (single-legged running or forward hopping respectively) and BM-SLIP (bipedal running) show the characteristic J-shape. The domain of stability enlarges in single-legged running: For any angle of attack α, the range of leg stiffness k that yields to stable running is increased. In bipedal running, the stability domain is thinned out slightly: Stable running patterns of flat angles of attack ($\alpha = 50$ deg $- 60$ deg) disappear, while those of steeper angles of attack ($\alpha = 65$ deg $- 75$ deg) are kept completely.
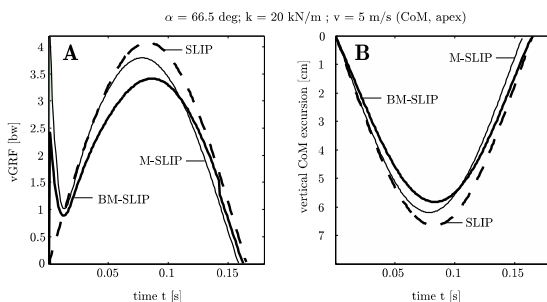
Fig. 3 **A.** Vertical ground reaction force (vGRF) in bodyweights (bw) of all three investigated models: SLIP (dashed line), M-SLIP (single-legged running, medium line) and BM-SLIP model (bipedal running, bold line). Leg rotation causes a strong impact peak at the instant of touch-down (t = 0) which smoothly decays within the first 20 ms. **B.** Vertical excursion of the body CoM during stance phase of all three investigated models (SLIP – dashed line; M-SLIP – solid line; BM-SLIP – bold line). The body CoM excursion is calculated with respect to the touch-down height (0 cm). The maximum body CoM excursion decreases in leg mass models (M-SLIP and BM-SLIP).

We select one pair of leg stiffness k and angle of attack α (demarked in Fig. 2: k = 20 kN/m, $\alpha = 66.5°$) to record vertical ground reaction force (vGRF) and CoM excursion of all three models (see Fig. 3). While the vGRF of the massless SLIP does show a smooth single hump, the vGRF of M-SLIP and BM-SLIP show a large impact peak at the instant of touch-down (t = 0 s), which smoothly decreases within 20 ms. Shortly after the impact peak (t > 20 ms), the M-SLIP model follows the vGRF shape of the SLIP but then increases bending before achieving peak vGRF of the SLIP. The vGRF of the BM-SLIP is even lower than in the M-SLIP model. Comparing peak values of vGRF, the SLIP model takes the highest value ($\sim 4\ bw$), followed by M-SLIP ($\sim 3.75\ bw$) and BM-SLIP model ($\sim 3.5\ bw$).

3. CONCLUSION

In this work, we extended the SLIP model by adding leg masses, which yield to the M-SLIP (modeling single-legged running) and BM-SLIP (modeling bipedal running). Both models were able to inherit self-stability by coordinating additional degrees of freedom to SLIP behavior (e.g., hip control) and adjusting additional parameters to biological data (e.g., human mass distribution). Furthermore, both models allow a more realistic transfer to control and design of real legged robots and, as a novel feature, leg swing dynamics can now be predicted. We are presenting simulation results comparing the three models.

4. ACKNOWLEDGMENT

REFERENCES

[1] R. J. Full and D. E. Koditschek, "Templates and anchors: neuromechanical hypotheses of legged locomotion on land," *The Journal of experimental biology,* vol. 202, pp. 3325-32, Dec 1999.

[2] R. Blickhan, "The spring-mass model for running and hopping," *Journal of biomechanics,* vol. 22, pp. 1217-27, 1989.

[3] A. Seyfarth, H. Geyer, M. Günther, and R. Blickhan, "A movement criterion for running," *Journal of biomechanics,* vol. 35, pp. 649-55, May 2002.

[4] C. Clauser, J. McConville, and J. Young, "Weight, volume, and center of mass of segments of the human body," *AMRL-TR,* vol. 69, p. 70, 1969.

[5] C. Clauser, J. McConville, and J. Young, "Weight, Volume, and Center of Mass Segments of the Human Body," *Journal of Occupational and Environmental Medicine,* vol. 13, p. 270, 1971.

[6] H. Knuesel, H. Geyer, and A. Seyfarth, "Influence of swing leg movement on running stability," *Human movement science,* vol. 24, pp. 532-43, Aug 2005.

[7] R. Bellman, "Adaptive control processes: a guided tour," ed: Princeton University Press, 1961.

Running Motion in a Musculoskeletal Bipedal Robot using Muscle Activation Pattern Control Based on a Human Electromyogram

Satoshi Nishikawa[1], Ryuma Niiyama[2] and Yasuo Kuniyoshi[3]

[1]Graduate School of Interdisciplinary Information Studies, The University of Tokyo, Tokyo, Japan
(Tel: +81-3-5841-6339; E-mail: nisikawa@isi.imi.i.u-tokyo.ac.jp)
[2]CSAIL, Massachusetts Institute of Technology, Cambridge, MA, USA (ryuma@csail.mit.edu)
[3]Department of Mechano-Informatics, The University of Tokyo, Tokyo, Japan (kuniyosh@isi.imi.i.u-tokyo.ac.jp)

Abstract: Some robots driven by muscle-type actuators have been studied based on a bio-inspired approach. However, a method of motion generation for them has not been established. We propose a control method based on a human electromyogram (EMG) for a musculoskeletal robot with mono- and bi-articular muscles. The simulation results show that the method is more effective than non-EMG-based method. In a dynamic simulator, we demonstrate that the method can generate feasible motor command for bipedal running with complex musculoskeletal system.

Keywords: Running, Bipedal Robot, Musculoskeletal System, Electromyogram, Muscle Activation Pattern

1. INTRODUCTION

In order to improve a physical ability of legged robot, musculoskeletal structure of animal is the useful reference. A musculoskeletal system has many interesting characteristics, such as the free control of stiffness through antagonistic actuation and bi-articular muscles contributes to the isotropy of the force distribution.

On the other hand, because running is acknowledged to be an especially challenging task, many robots have been developed that can run. Despite having this ability, these robots have not used the findings of animals enough. Therefore, musculoskeletal robots have been developed. Lucy [1] has pneumatic muscles and is capable of planar walking. However, with only mono-articular muscles and control similar to angle control, this robot cannot make the best use of the characteristics of the musculoskeletal system. Although musculoskeletal robots with bi-articular pneumatic muscles are able to run [2], this is manually tuned. Briefly, the control method of musculoskeletal robot has not been established.

Thus, we propose a bio-inspired control method. We demonstrate the bipedal running with musculoskeletal robot with bi-articular muscles in a dynamic simulator.

2. ATHLETE ROBOT

We used a model of the Athlete Robot [2](Fig. 1), which weighs about 10 kg and has a body height, thigh length, and shank length of 1.2 m, 0.3 m, and 0.36 m, respectively. This robot is driven with pneumatic artificial muscles. We used OpenHRP3 [3] as the dynamic simulator. The kinetic data for the robot were taken from 3D-CAD data. We used the theoretical equation of tension of the pneumatic muscle shown in (1) [4].

$$F = p\{A(1 - \epsilon)^2 - B\}, \tag{1}$$

where F, p, and ϵ denote the contraction force, inner pressure, and contracting ratio, respectively, and A and B are constants.

3. CONTROL

In the legged locomotion, contact force control is more important than angle control. Contact force distribution is determined according to which combination of muscles is chosen. Therefore, an appropriate control of muscle activation strength is required. In deciding muscle activation strength, it is valid to use electromyogram (EMG), corresponding to muscle activation strength of humans.

Thus, we propose muscle activation pattern control based on a human EMG. This control consists of muscle activation patterns using a simple step function as the basis function and the learning thereof. To make learning efficient, we use a human EMG data (Fig. 2). In addition, we estimate the switching time since timing is especially important for dynamic movement.

We divide a period of running into two phases because of the difference of dynamics, namely, the thrust phase and the swing phase. Setting the threshold to half the maximum strength of the EMG, we can divide the swing phase into two phases, namely the recovery swing phase and the foot descent phase, and determine simplified patterns (an example of IL is shown in Fig. 2). Details of the muscle activation patterns for each phase and certain parameters concerning switching time are decided by a combination of constrained random sampling and hill-

Fig. 1 Athlete Robot with layouts of its muscles.
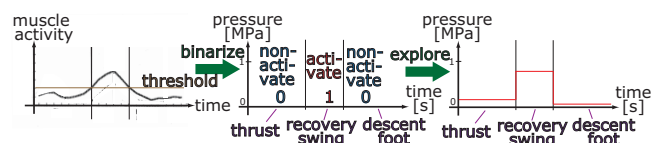
Fig. 2 EMG [5] and muscle activation pattern.

climbing optimization. In constrained random sampling, we fix the pressure of decided non-activation muscles to zero, and randomly explore the pressures of decided activation muscles and a few parameters for switching time. In hill-climbung optimization, we optimize all the parameters. Additionally, we decide the switching time of the next cycle using information from the previous cycle and the prediction at liftoff time. The duration of each phase is decided at the moment of liftoff.

4. SIMULATION EXPERIMENTS

4.1 Experimental Settings

We performed a bipedal running in a simulator. To make the robot learn a steady running motion, we provided an initial velocity. To begin, we issued the initial commands for 3.7 s to bring the robot to its starting posture. Next, we applied force from behind for 0.3 s to give the robot an initial velocity of 2.0 m/s. The evaluation metric used is the distance before falling down. The parameters of the control are the muscle activation strength of seven muscles shown in Fig. 1 in the three phases, the ending time of the initial posture (t_{init}), and the ratio of the foot descent phase to the whole swing phase (τ).

4.2 Comparison between EMG-based Sampling and Non EMG-based Sampling

We conducted constrained random sampling based on a human EMG to determine general parameters of the control. The numbers of learning parameters were 11 or 12 (excluding Gmin and ADD of all phases and non-activated muscles decided by a human EMG). Having conducted 300 trials by four ways (using EMG of [5] or [6] or [7] with IL of [5] or [7] with IL of [6]), respectively, we obtained several combinations of parameters that realized several steps of running.

We also experimented with non EMG-based sampling to verify the effect of EMG-based sampling. The numbers of learning parameters were 10 or 11 or 12 (excluding Gmin, ADD, and 5 or 6 or 7 randomly-selected parameters). We have conducted 300 trials by four different parameters, respectively. From the results, the average distances were 2.24 m and 1.99 m, with variances of 1.38 and 0.07, for the experiments with EMG-based sampling and non EMG-based method, respectively (Fig. 3). Thus, EMG-based sampling is more advantageous to find general parameters of the running motion.

4.3 Optimization of Running Motion

We conducted hill-climbing optimization of five high ranking parameters obtained from each constrained random samplings. The number of learning parameters is 23 (all the parameters). Based on the results of 150 trials, the evaluation metric increased greatly and the robot successfully realized a running motion from EMG-based samplings (Fig. 3). Thus, EMG-based sampling is effective to achieve a running motion. The optimal parameters are shown in Fig. 4. The mean velocity of the robot was 2.1 m/s, and it took 13 steps in 12.5 m (Fig. 4). As can be seen from the graph, the running pace is steady.
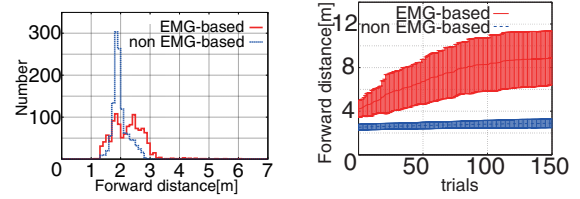
Fig. 3 Distribution of evaluation metric for random sampling (left) and the mean learning curve with standard deviation for hill-climbing optimization (right).
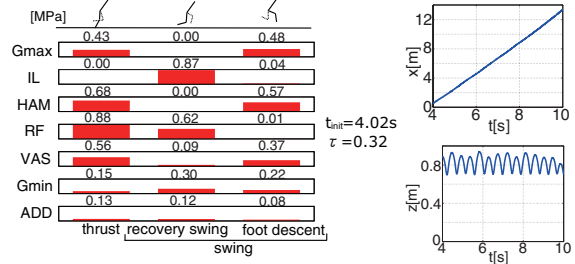
Fig. 4 Optimal parameters (left) and displacement of the robot during running (right).

5. CONCLUSION

In this study, we proposed a method to implement running in a musculoskeletal bipedal robot, and examined the running motion of a robot in a dynamic simulator. We used muscle activation pattern control in the learning based on a human EMG. Using hill-climbing optimization after EMG-based constrained random sampling, the robot model achieved 13 steps running. The mean distance before falling down in EMG-based method is about three times greater than that in non-EMG-based method. This result shows that an EMG-based search is efficient for finding appropriate patterns. Future works include the use of posture feedback for infinite running and application of this method to a real robot.

REFERENCES

[1] B. Verrelst et al., "The pneumatic biped "Lucy" actuated with pleated pneumatic artificial muscles", Autonomous Robots, vol. 18, no. 2, pp. 201-213, 2005.

[2] R. Niiyama et al., "Athlete robot with applied human muscle activation patterns for bipedal running," in Proc. Humanoids, pp. 498-503, 2010.

[3] S. Nakaoka et al., "Constraint-based dynamics simulator for humanoid robots with shock absorbing mechanisms", in Proc. IROS, pp. 3641-3647, 2007.

[4] H. Schulte et al., "Characteristics of the braided fluid actuator", Dept. Phys. Med. Rehabil., No.5, 1961.

[5] W. Montgomery et al., "Electromyographic analysis of hip and knee musculature during runnning", Am J Sports Med, vol. 22, no. 2, pp. 272-278, 1994.

[6] G. Cappellini et al., "Motor patterns in human walking and running", J Neurophysiol, vol. 95, pp. 3426-3437, 2006.

[7] S. Swanson et al., "An integrated biomechanical analysis of high speed incline and level treadmill running", Med Sci Sports Exerc, vol. 32, no. 6, pp. 1146-1155, 2000.

Avian bipedal locomotion

John A. Nyakatura[1], Emanuel Andrada[2], Reinhard Blickhan[2] and Martin S. Fischer[1]

[1]Institut für Spezielle Zoologie und Evolutionsbiologie, Friedrich-Schiller-Universität, Jena, Germany
(Tel : +49-3641-949183; E-mail: john.nyakatura@uni-jena.de)
[2]Motion Science, Institut für Sportwissenschaften, Friedrich-Schiller-Universität, Jena, Germany
(Tel : +49-3641-94710; E-mail: emanuel.andrada@uni-jena.de)

Abstract: Birds represent the vast majority of bipedal species. The avian bipedal locomotion project aims to characterize the functional morphology and biomechanics of small birds in order to distinguish common principles of avian bipedalism in contrast to 'the other bipedal species' (humans). The paper introduces the project and ongoing experiments.

Keywords: Locomotion, birds, x-ray motion analysis, force plate, biomechanics, inverse dynamics analysis

1. INTRODUCTION

Not only humans are able to move bipedally. Most of the approximately 10.000 species of bird are able to efficiently locomote on the ground by their hindlimbs. They do so although the hindlimbs display a surprisingly variable array of specializations. These include highly variant limb element proportions, and the presence or absence of swimming, climbing or cursorial specializations to differing habitats. Moreover, birds vary from less than 10g to 150.000g in body weight. Therefore, birds represent an ideal testbed to study the morphological and biomechanical characteristics of bipedal terrestrial locomotion.

However, some obvious differences to the bipedal gait of humans exist. Due to a cranially shifted center of mass (CoM), the thigh is oriented sub-horizontally to position the feet beneath the CoM [1]. Evolutionary changes of the distal hindlimb likely related to the adoption of active flight have lead to further modifications of the hindlimb elements. The hindlimb of modern birds comprises of the thigh, tibiotarsus (TT), tarsometatarsus (TMT), and the phalanges. In contrast to humans, the heel and middle foot, i.e., the TMT, do not contact the ground during locomotion. The knee acts as the main fulcrum of limb retraction [2]. In birds, movements in the knee contribute to progression more than the hip [3]. Whereas the ankle joint contributes to step length in humans, it is doing so only at very high speeds in birds [3]. Moreover, in humans the transition from walking to running is reflected by a change of the kinetics of the CoM and the footfall pattern [4]. In contrast, birds transition from kinetic walking to running without a change of the footfall pattern [5]. Only at very high speeds an aerial phase is adopted [3]. Thus, three basic avian gaits can be defined: (i) walking, (ii) grounded running with a double support phase, and (iii) running without a double support phase.

Data for avian bipedalism is limited to ground dwelling, terrestrially adapted birds. Therefore the high variability of the group and especially smaller, less terrestrial species are chronically underrepresented.

In the avian bipedal locomotion project we aim to characterize the terrestrial locomotion of small birds from the perspectives of functional morphology and biomechanics in a comparative approach. We designed experiments that will help us to scrutinize body-mass and hindlimb proportions related effects on the characteristics of avian terrestrial locomotion to better reflect the variability of birds. Moreover, we study aspects of the movements of the CoM and self-stability. Additionally, we plan to conduct perturbation experiments in order to gain an understanding of the adaptability of avian bipedal locomotion.

2. APPROACH AND METHODS

In birds, proximal hindlimb elements are covered by feathers, wings, and musculature (Fig. 1). Therefore, we use x-ray motion analysis for a detailed three-dimensional (3D) kinematic description *via* direct observation of bone movements *in vivo*. To this end, we record synchronized high-speed x-ray movies in the latero-lateral and ventro-dorsal projections in two experimental situations: (i) during steady-state locomotion on a treadmill that allows us to record a great range of speeds, and (ii) while traversing two custom-built force plates positioned in front of the image intensifiers (Fig. 1). The latter setup allows us to simultaneously record six degrees of freedom (6dof) substrate reaction forces (SRFs) and torques produced by individual limbs. The dataset will subsequently be used to analyze 3D inverse dynamics and aspects of self stability. In the experiments both x-ray projections are 3D calibrated to assess x-, y-, z- coordinates of skeletal landmarks. Coordinates of the skeletal landmarks are used to obtain kinematic data of hindlimb elements and joints.

To establish our experimental setup and protocol we chose to use a well studied, easily available and terrestrially adapted small bird: the quail. Subsequently, a broad range of small bird species will be acquired from private breeders and trained to perform in our experiments.
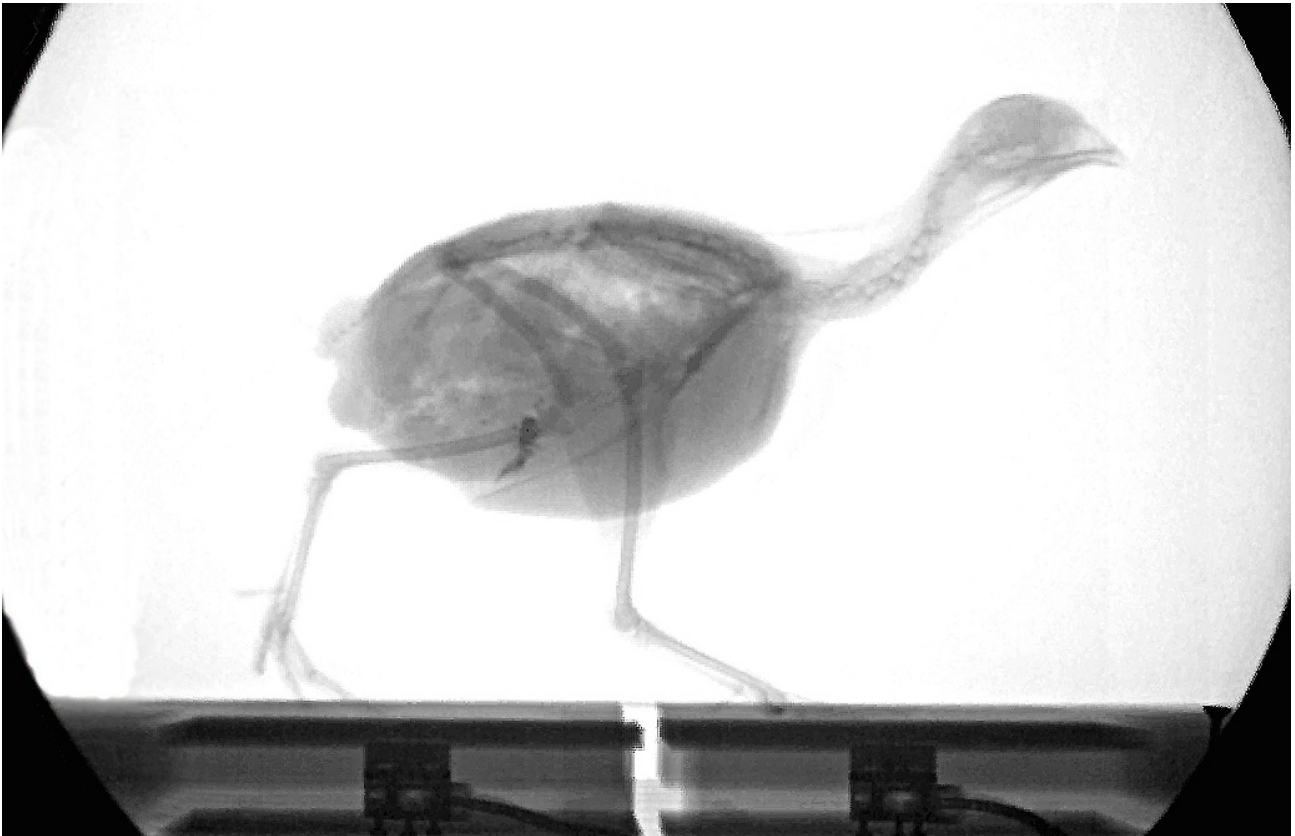
Fig. 1: Latero-lateral x-ray projection of a quail traversing two custom-built force plates. The experiment integrates kinematic and kinetic data.

Body-mass related effects are studied using a 'domestic scaling system' – different breeds of chicken. Chicken can be considered as geometrically similar. At the same time, the smallest breeds weigh 10 times less than the heaviest. Thus, in a comparative study the effects of body-mass can be studied while minimizing other influences.

The effects of differing hindlimb proportions are studied within waders which exhibit extremely variant hindlimb proportions, despite close phylogenetic relationship as well as similar body size and weight. We already started experiments with relatively long-limbed Northern lapwing. In contrast, we will also study oyster catchers that have a relatively short TMT and stilts that have an extremely elongated TMT.

3. EARLY RESULTS AND OUTLOOK

The need for the usage of x-ray motion analysis is illustrated by the recording of considerable movements of the thigh during our experiments. On the treadmill a tenfold speed range is easily achieved in all species tested so far. The combination of SRF measurement and kinematics allows us to reconstruct center of pressure paths beneath the feet and movements of the CoM. These data are currently used for a three-dimensional inverse dynamics analysis. Moreover, the effect of speed-dependent head movements ("head-bopping") on the movement of the CoM is determined.

The comparative approach will help to formulate common principles of bird bipedalism and lead to a better understanding of functional and biomechanical differences and similarities between birds and humans. Future experiments will include perturbations to provoke compensating movements in order to gain an understanding of the adaptivity of avian bipedalism.

REFERENCES

[1] J.R. Hutchinson, V. Allen, "The evolutionary continuum of limb function from early theropods to birds", *Naturwissenschaften*, Vol. 96, No. 4, pp. 23-448, 2009.
[2] S.M. Gatesy, "Guineafowl hind limb function. I: cineradiographic analysis and speed effects", *Journal of Morphology*, Vol. 240, No. 2, pp. 115-125, 1999.
[3] S.M. Gatesy, AA Biewener, "Bipedal locomotion: effects of speed, size and limb posture in birds and humans", *Journal of Zoology,* Vol. 224, No. 1, pp. 127-147, 1991.
[4] G.A. Cavagna, H. Thys, A. Zamboni, "The sources of external work in level walking and running", J*ournal of Physiology*, Vol. 262, pp. 639-657, 1976.
[5] J.A. Hancock, N.J. Stevens, A.R. Biknevicius, "Whole-body mechanics and kinematics of terrestrial locomotion in the Elegent-crested Tinamou *Eudromia elegans*", *Ibis*, Vol. 149, No. 3, pp. 605-614, 2007.

MaTBot: A Magneto-adhesive Track roBot for the inspection of artificial smooth substrates

Max Fremerey[1], Stanislav Gorb[2], Lars Heepe[2], Dominik Kasper[1], Hartmut Witte[1]

[1]Department of Biomechatronics, University of Technology, Ilmenau, Germany
(Tel : +49-03677 691803; E-mail: {maximilian-otto.fremerey; dominik.kasper; hartmut.witte}@tu-ilmenau.de)
[2]Department of Functional Morphology and Biomechanics, University of Kiel, Germany
(Tel : +49-431 8804513; E-mail: {sgorb; lheepe}@zoologie.uni-kiel.de)

Abstract: This paper introduces the small sized tracked climbing robot *MaTBot*. Due to the combination of different adhesion principles, a bio-inspired micropatterned adhesive tape and a permanent magnet, we designed the robot capable of climbing up smooth (flat) artificial substrates. For the purpose of the novel contact mechanism, a laminated track was manufactured. The robot can climb up; the angles of slope are below 60° on glass substrates solely using the adhesive tape and up to 90° on ferromagnetic substrates by additional employing the magnetic adhesion principle. The robot has a size of 60 mm · 60 mm · 16 mm, its weight is less than 60 g. The maximum of velocity averages 6.9 cm/s. Due to the used passive adhesion principles, a rather long period of application is achieved.

Keywords: Bio-inspired adhesion principle, magnetic adhesion principle, small sized climbing robots

1. INTRODUCTION

The miniaturization of climbing robots and the resulting decrease of their weights enables the implementation and investigation of various adhesion principles and their combination. Mainly derived from the results of biological research on adhesion mechanisms the small-sized climbing robot *MaTBot* is designed. In addition to the latest state of the art concerning small sized climbing robots with passive adhesion principles [1, 5, 7, 9, 10], *MaTBot* employs a combination of two adhesion principles: 1) a bio-inspired dry adhesion principle using a new generation of a micropatterned dry adhesive tape and 2) a magnetic principle utilizing effect of permanent magnetization.

Possible areas of application are inspection and maintenance of smooth artificial structures e.g. surfaces of solar cells, glass facades, ship hulls, pipes, tanks, etc.

2. ADHESION PRINCIPLES

Inspired by the functional morphology of tarsal hairs of male Chrysomelidae beetles [3, 6] a bio-inspired micropatterned elastomer tape with enhanced adhesion compared to a smooth control made of the same material is employed to produce dry adhesion.
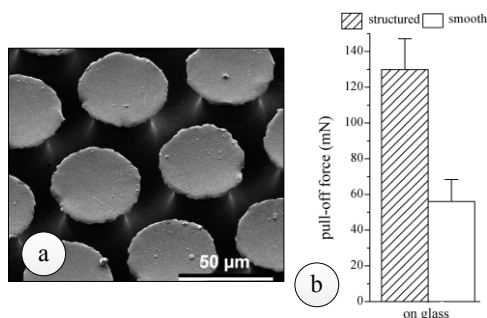
Fig. 1: a) SEM micrograph showing bio-inspired micropatterned adhesive tape with an about twice higher adhesion compared to a smooth control of the same material (b) measured in a flat-on-flat contact scheme [3, 6].

Enhanced adhesive capability of this tape was shown to be a combination of intermolecular Van der Waals forces and particular mushroom-like crack-trapping geometry. Adhesion in normal direction of about 4.1 N/cm^2 was previously reported [3, 6].

The magnetic adhesion principle relies on tiny NdFeB permanent magnets having dimensions of 2.85 mm · 2.85 mm · 0.5 mm. The force of a single magnet averages 0.78 N. Both adhesion principles enable to maintain contact without the consumption of energy.

3. DESIGN OF MATBOT

3.1 Design and manufacturing of the robot

The design of *MaTBot* follows the guideline for mechatronic development VDI 2206. The required torque for locomotion is generated by two servo drives (BMS-Bluebird 303, torque of about 70 Nmm at 4.8 V). With respect to the low center of mass, a self-made drive gear is used. Therewith a secure transmission of the driving torque from servo drives to tracks was obtained.
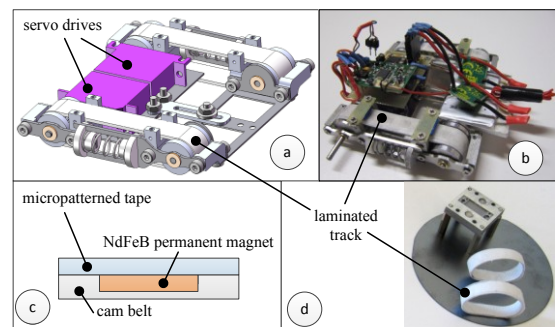
Fig. 2: a) CAD drawing and b) prototype of *MaTBot*, c, d) principle (c) and prototype (d) of the laminated track, respectively

The base frame of *MaTBot* is made of 0.5 mm stainless steel. It also carries the energy supply and the control unit. *MaTBot* is an open-loop remote controlled device at 35.030 MHz.

3.2 Design and manufacturing of the laminated track

Figure 2c, d) displays the structure of the laminated track of *MaTBot*. The first layer resembles a cam belt. It enables force transmission between drive gear and track. The NdFeB permanent magnets compose the second layer, whereas the third layer consists of the micropatterned tape.

Manufacturing process has three steps: 1) molding the cam belt using silicone elastomer WM 372 (Weißmetall Inc., Wuppertal, Germany) 2) insertion of NdFeB permanent magnets into the belt 3) bonding of the micropatterned tape to the belt using two-component silicone elastomer. Due to this bonding process, magnets are completely embedded inside the track. However, apparent contact area between substrate and tracks averages 6.40 cm^2.

4. EXPERIMENTS

4.1 Preparation and experiments

In order to evaluate the performance of *MaTBot* on various inclines of flat glass and ferromagnetic substrates, experiments include the measurement of speed and the period of application. For reproducible and consistent conditions during experiments a purpose-built testing area was designed. It enables the setting of the slope angle of the substrate.

4.2 Results

Current experimental results are summarized in table 1 and 2.

Table 1: The *MaTBot* performance

investigated feature	experimental results
climbing abilities	presently 0-60° (common window glass) and 0-90° (ferromagnetic material)
maneuverability	Good due to separately controlled tracks

Table 2: Climbing abilities of *MaTBot* on common window glass. (*) = result is mean value out of five measurements. Cleaning of substrate and tracks was performed before each run, temperature during measurement: 24 °C, humidity 30 %
(++) = Tracks are equipped without micropatterned tape due to tiny angle of slope

Mean value of	angle of slope			
	0° (*) (++)	20° (*) (++)	40° (*)	60° (*)
speed (cm/s)	6.9	5.8	5.5	4.9
period of application (min.sec)	28.16	27.47	23.40	no long-time measurement due to failure of power amplifiers
max. travelled distance (in m)	≈ 117	≈ 97	≈ 78	

The experiments demonstrated the general advantage of the use of the laminated track. The achieved slope angle was about 60° just due to the contribution of dry adhesion. During all experiments *MaTBot* has demonstrated a very good maneuverability. The period of application averaged between 28 and 24 minutes travelled distance during this time ranged between 117 and 78 meter (line movement, length of the robot: 0.06 meter).

Novel modifications of bio-inspired silicone foils will improve the robot performance in the future: Possible constructional modifications of the robot, such as implementation of wider tracks or a tail like structure, might additionally contribute to stronger adhesion on smooth glass.

5. CONCLUSIONS

The combination of two adhesion principles was implemented into the small-sized climbing robot *MaTBot*. Equipped with laminated tracks, the robot is capable of moving over smooth inclined substrates made of different materials. Experiments have also illustrated long travelling distances of the robot together with the good maneuverability and fast locomotion speed.

REFERENCES

[1] Daltorio, K., Gorb, S., Peressadko, A., Horchler, A. R. & Quinn, R. (2005), A robot that climbs walls using micro-structured polymer feet, *CLAWAR 05* , pp. 131-138

[2] Fremerey, M., Gorb, S. N., Mämpel, J. & Witte, H. (2010), Towards an adhesive gripping module for handling tasks and small-sized climbing robots, *CLAWAR 10*, pp. 133-141

[3] Gorb, S. N., Varenberg, M., Peressadko, A. & Tuma, J. (2007), Biomimetic mushroom-shaped fibrillar adhesive microstructure, *J. Roy Soc. Interface*, vol. 4, no. 13, pp. 271-275

[4] Gorb, S. N., Sinha, M., Peressadko, A., Daltorio, K. & Quinn, R., Insects did it first: A micropatterned adhesive tape for robotic applications, *Bioinspiration & Biomimetics*, vol. 2, pp. 117-125

[5] Greuter, M., Shah, G., Caprari, G., Tâche, F., Siegwart, R. & Sitti, M. (2005), Toward micro wall-climbing robots using biomimetic fibrillar adhesives, 3rd Int. Symp. Autonomous Minirobots for Research and Edutainment (AMiRE), pp. 39-46

[6] Heepe, L., Varenberg, M., Itovich, Y & Gorb, S.N. (2011), Suction component in adhesion of mushroom-shaped microstructure, *J. Roy Soc. Interface,* vol. 57 , pp. 585-589

[7] Kim, S., Spenko, M., Trujillo, S., Heynman, B., Mattoli, V. & Cutkosky, M. R. (2007), Whole body adhesion: Hierarchical, directional and distributed control of adhesive forces for a climbing robot, *Proc. 2007 IEEE Int. Conf. Robotics and Automation,* Roma, Italy, pp. 1268-1273

[8] Rochat, F., Schoeneich, P., Truong-Dat Ngyen, O. & Mondada, F. (2009), Tripillar: Miniature magnetic caterpillar climbing robot with plane transition ability, *CLAWAR 09*, vol. 1, pp. 343-350,

[9] Unver, O., Murphy, M. P. & Sitti, M. (2005), Geckobot and waalbot: Small-scale wall climbing robots, *AIAA 5th Aviation, Technology, Integration and Operations Conf.*

[10] Unver, O. & Sitti, M. (2009), Tankbot: A miniature, peeling based climber on rough and smooth surfaces, *IEEE Int. Conf. on Robotics and Automation, Kobe*, pp. 2282-2287

Variable Impedance Actuation to Increase the Behavioural Diversity of Legged Robots

Derek Leach, Nandan Maheshwari, Fabian Günther and Fumiya Iida

Biologically Inspired Robotics Lab, Swiss Federal Institute of Technology Zurich, Switzerland
(E-mail: [derek.leach, nandan.maheshwari, fumiya.iida]@mavt.ethz.ch)

Abstract: A single leg hopping robot has been constructed which includes a clutch in series with the hip motor and a prototype Linear Multi-Modal Actuator (LMMA) at the knee. The single leg will be used to test how the different actuation methods can improve the behavioural diversity of the robot.

Keywords: Multi-Modal Actuator, clutch, brake, Variable Impedance Actuator, dynamic legged locomotion, behavioural diversity

1. INTRODUCTION

The desire to develop fully autonomous, deliberative, mobile robots that can competently sense and interact with their environment (human or hostile), manipulate objects and traverse challenging terrain, fuels much of the research in the robotics field.

For operating in diverse environments and over difficult terrain, legs are the best means for locomotion, however conventional legged robot locomotion has a very high energetic cost of transport [1]. Furthermore, intrinsic to a robot's autonomy is its ability to ambulate whilst supplying its own power, current power supply technology and energy storage greatly constrict the performance of the robot in this regard.

Consequently much of the focus in legged robot locomotion research has concentrated on using passive elements to make legged locomotion as efficient as possible [2, 3] and using compliance to allow legged robots to traverse rough terrain whilst reducing control effort and improving stability [4, 5]. The robots that have been designed to operate most efficiently can often only do so in a single mode and a narrow performance range. Hosoda et al [6] showed how variable compliance allowed for many more modes, however their pneumatic actuation is not conducive to a robot's autonomy.

In this paper we introduce a new actuator and actuation method that we hope will go some way to increasing the behavioural diversity of the robot whilst maintaining efficient locomotion. The power will be supplied electrically so that these methods can eventually be implemented in autonomous robots.

Goal Our goal is to implement actuation into a robot leg such that there are several different modes of operation. It will be able to travel efficiently and stably in steady state locomotion at a range of speeds and it will be able to switch to fully controllable actuated mode for precise leg movements.

Challenge Each of these operational modes requires a different set of mechanisms. Efficient and stable locomotion requires springs to store the energy and free swinging movement of the leg, whilst position output will require precise control of the leg and so high impedance. A mechanism is needed to change the impedance to suit the required task.

Solution We present a new means of actuating a robot leg utilizing brakes and clutches which will provide many different modes of operation.

2. THE ROBOT

To validate our actuation methods, they will be tested on a two segment hopping leg robot attached to a boom. This configuration has successfully been able to test leg performance and dynamic locomotion [7] and so will provide our first means of evaluation.

2.1 The Leg

We have designed a 2 segment leg, with a thigh and a shank each 60 cm long. The leg can be seen in Fig. 1.

Fig. 1 Two segment hopping leg robot attached to a test rig with a passive spring in place of the actuator.

The hip has one rotary degree of freedom actuated by a Maxon RE65 DC motor with 25:1 planetary gear reduction. The motor is connected in series with a magnetic clutch to the leg. With the clutch engaged the motor has full positive drive of the leg, with the clutch disengaged the leg swings freely.

The knee joint also has one rotary degree of freedom and will be powered by the Linear Multi-Modal Actuator (LMMA), mounted to the thigh at one end and the shank at the other.

2.2 The Linear Multi-Modal Actuator (LMMA)

Fig. 2 shows the prototype Linear Multi-Modal Actuator (LMMA), the actuator is 670 mm long, has a range of 120 mm and weighs 4.5 kg. The actuator's frame consists of two guide rails along which three blocks can slide. Each block has a brake mechanism that can fix it to brake rails—which run parallel to the guide rails—and prevent it from sliding. From Fig. 2, the Spring and Middle-Block are connected by a spring and the Middle and Motor-Block are connected by a ball screw driven by a DC motor.
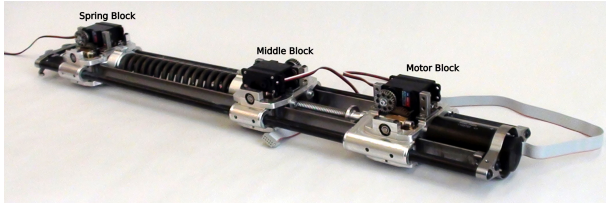
Fig. 2 Linear Multi-Modal Actuator.

To reduce the number of components and simplify the mechanism, early prototypes used the guide rails as the brake rails, however this did not provide sufficient braking force so in this prototype we have included dedicated flat brake rails to maximize the braking area.

2.3 Modes of the LMMA

Applying the correct brake configurations allows the actuator output to: slide freely; become completely rigid; provide direct position control from the motor; or become a series elastic actuator. Furthermore the spring can be charged by the DC motor and discharged. With a charged spring, an instantaneous power output can be supplied greater than the motor alone can provide.

When used to power a leg joint, these modes will allow for different behaviours. For dynamic hopping and running the LMMA can be used in the series elastic configuration to exploit the compliance in the spring for efficiency. Direct actuation removes the bandwidth limit of the spring and allows high impedance and accurate position control of the joint.

For the single hopping leg, applying the brakes of the LMMA during push off can arrest the release of the spring and so produce a short hop. Whilst in the flight phase, the stored energy in the spring can be dissipated, kept or charged more for a higher hop. In this way different hopping patterns can be produced for traversing obstacles.

Just as humans lock their knee joint when standing, this actuator will be able to use its rigid mode to fix the length of the leg. Furthermore the brake mechanism in each block is not back drivable, so once applied no extra energy is consumed.

3. CONTROL OF DYNAMIC LOCOMOTION

Actuating passive dynamic walkers so that they overcome energetic losses can provide for very efficient locomotion, Kuo [8] showed how hip actuation and toe-off provide different performance characteristics for this gait. We similarly aim to actuate the leg to return it to a stable passive forward hopping state using the hip and knee actuators.

Our hopping robot will be developed in stages. Currently a passive spring is connected to the knee joint in place of the LMMA (Fig. 1) and the hip is directly connected to the motor. With this configuration open loop hopping control is possible with a sinusoid position input at the hip. Next we will include the hip clutch to explore how this can improve the energy efficiency of the leg. Once the hip actuation has been developed the LMMA will be mounted in place of the passive spring at the knee and its modes will be explored. At first the series elastic mode will be utilized to improve the dynamic performance of the hopping gait with just the passive knee.

For both the hip and knee actuator a control architecture will be developed to cope with and exploit their discrete nature.

REFERENCES

[1] A. D. Kuo, "Choosing Your Steps Carefully" *Robotics and Automation Magazine, IEEE*, Vol. 14, No. 2, pp. 18–29, 2007.

[2] M. Ahmadi and M. Buehler, "Stable Control of a Simulated One-Legged Running Robot with Hip and Leg Compliance", *IEEE Transactions on Robotics and Automation*, Vol. 13, No. 1, pp. 96–104, 1997.

[3] R. McN. Alexander, "Three uses for springs in legged locomotion", *International Journal of Robotics Research*, Vol. 9, No. 2, pp. 53–61, 1990.

[4] G.A. Pratt, "Low impedance walking robots", *Integrative and Comparative Biology*, Vol. 42, No. 1, pp. 174–181, 2002.

[5] R. Blickhan, A. Seyfarth, H. Geyer, S. Grimmer, H. Wagner and M. Guenther, "Intelligence by Mechanics", *Philosophical Transactions of the Royal Society A: Mathematical, Physical and Engineering Sciences*, Vol. 365, No. 1850, pp. 199–220, 2007.

[6] K. Hosoda, T. Takuma, A. Nakamoto and S. Hayashi, "Biped robot design powered by antagonistic pneumatic actuators for multi-modal locomtion", *Robotics and Autonomous Systems*, Vol. 56, No. 1, pp. 46-53, 2008.

[7] A. Sayyad, B. Seth and P. Seshu, "Single-legged hopping robotics research—A review", *Robotica*, Vol. 25, No. 5, pp. 587–613, 2007.

[8] A. Kuo, "Energetics of Actively Powered Locomotion Using the Simplest Walking Model", *Journal of Biomechanical Engineering*, Vol. 124, No. 1, pp. 113–120, 2002.

ROLV – A Hybrid Wheel Robot Using Compliant Mechanisms for Locomotion

Jörg Mämpel[1,*], Sebastian Köhring[1], Robert Koopmann[1], Kristian Langguth[1], Roy Lichtenfeld[1], and Hartmut Witte[1]

[1]Department of Biomechatronics, Ilmenau University of Technology, Ilmenau, Germany
(*Tel : +49-3677-694689; E-mail: joerg.maempel@tu-ilmenau.de)

Abstract: This work describes the design of a hexapod robot with hybrid wheels. The integration of compliant mechanisms in a mobile robot was a main focus during the design process. Compliant mechanisms are integrated in the trunk and in the coupling between the trunk and the drives for damping, and thus for reduction of internal mechanical stress. Three types of effectors are available: A wheel, a stiff hybrid wheel and an elastic hybrid wheel. The elastic effectors are designed for using resonance effects for locomotion.

Keywords: legged wheel; robot locomotion, climbing

1. INTRODUCTION

Agile locomotion in various terrains is still a challenge relative to the mechanical design of robots. On flat terrain, wheeled locomotion is still the best choice under the focus of ground impact forces, velocity and power effort. For the locomotion in difficult terrains like stairs, scree or even natural ground special legged systems (walking robots) have been developed with often a complex mechatronic design. Additionally there are some biologically inspired robots [1] using hybrid wheels for locomotion e.g. the WHEGS® robots [2], RHex robots [3] and ASGUARD ROBOT [4]. The effectors of these robots are mostly constructed in a very stiff way; they are not designed for using resonance effects for locomotion.
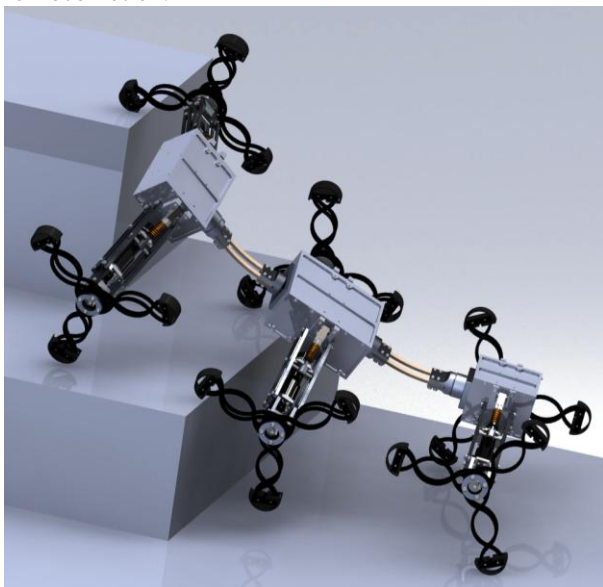
Fig. 1 RoLV robot is designed for the locomotion on different terrain. The robot is parted into three subsystems connected by compliant joints. The 'legs' are designed with a damping behavior

In this paper the design of a hexapod robot called RoLV (**Ro**lling **L**eg **V**ehicle) is introduced. It's an experimental hexapod platform; different effectors can be mounted at the robot in order to compare the different types of locomotion.

2. DESIGN

2.1 Robot platform

The RoLV robot (fig. 1) is designed for agile locomotion on flat and structured terrain. Its mass is about 11.5 kg. The size is about 1 m (length) x 0.6 m (width) x 0.3 m (height). The robot is design as an autark mobile system with onboard energy supply (22.2 V, 3.4 Ah, Lithium-polymer accumulator) and wireless communication. The robot's 'trunk' consists of three parts, which are connected by compliant mechanics. The robot has six DC motors, each driving one effector. The drives are integrated in a chassis frame designed as a double wishbone axle.

2.2 Robust locomotion by a compliant trunk

The parts of the trunk and the chassis are rigid body constructions connected by compliant elements. The connectors between the parts of the trunk have two different main functions. Two parts of the trunk are connected with a DOF (degree of freedom) = 2 and hence they can relatively rotate in two axes (cf. fig. 2 right). The first degree of freedom (rotation α) is realized by the two bending rods (3) arranged in parallel orientation. The second DOF (rotation β) is realized by a revolute joint (4) with integrated viscoelastic elements (rubber) and thus elastic and damping properties.
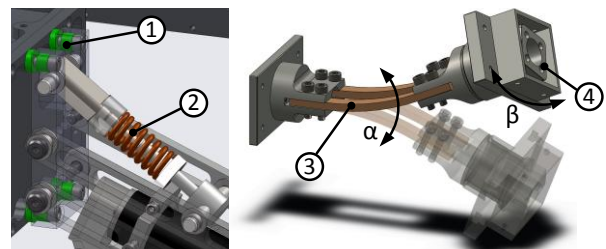
Fig. 2 Left: Compliant connection between the trunk and the chassis (elements (1)) and the suspension element for vertical shock-like motion (2). Right: Compliant connection between the trunk elements consisting of two parallel arranged bending rods (3) and a revolute joint with rubber elements

The connections between the trunk and the chassis are designed to have a shock-absorbing behavior (fig. 2 left). Rubber elements (1) are located between the trunk

element and the mounting plate of the chassis construction. Additionally a suspension element damps vertical motions and allows a better adaption to unstructured terrain. The damping factor of this spring-damper-system is high, thus only damping and no swinging behavior could be observed. The high DOF of the robot leads to high ability for adaptation to the shaped ground. Actually, three different types of effectors are available: 1. wheels, 2. stiff hybrid-wheels, and 3. elastic hybrid-wheels.

2.3 Classic effectors

The wheel effector is designed for locomotion on flat and lightly structured terrain. The power needed for locomotion is very low, because of the low resistance of rolling. The movability in structured environment is limited, e.g. stairs and scree slopes are difficult.

The stiff hybrid wheel has three spoke-like elements made of POM plastic (polyoxymethylene). The material is very robust and can resist high mechanical loads without any brittle fractures. At the end of each spoke-like element, there is a buffer made of rubber. Those buffers damp the mechanical impact load and increase the traction. The movability on stairs and scree is very good. But on flat terrain, the mechanical impact on the effectors and thus the chassis as well as the gearbox and the DC drives is very high.

Fig. 3 Left: Different classic effectors are available for ROLV robot with a diameter of about 0.32 m. Left: Wheel effector. Right: Stiff hybrid wheel effector with three spoke-like elements

2.4 Elastic hybrid wheels

The elastic hybrid wheel combines the advantage of a high movability in structured terrain with a reduced mechanical load in comparison with a stiff hybrid wheel. During fast locomotion, the resonance effects are used for locomotion for reduction of the power effort. Therefore the spring factor of the hybrid wheel is adjusted to the mass of the robot.

The eigenfrequency f_{eig} of a mass spring system is calculated as follows

$$f_{eig} = \frac{1}{2\pi} \sqrt{\frac{c_{Robot}}{m_{Robot}}} \qquad (1)$$

Using formula (1) and aiming eigenfrequency $f_{eig} = 4.1$ Hz, a robot stiffness is calculated with an amount of $c_{Rob} = 7.63$ Nmm^{-1}. In tripod gate, the spring factor for one spoke-like effector is $c_{Eff} = 2.54$ Nmm^{-1}.

The elastic effector is modeled like shown in fig. 4

left as a serial configuration of two spring-damper-systems – one acting in radial direction, one in tangential direction. The dimensioning of the effector is done in several steps: analytic calculation of the dimension, optimization by FEM (finite elements method), and designing suitable for production.

The elastic hybrid wheel consists of four identical plates made of POM (cf. fig 4 right), which a stacked in a special opposite way. At the end of the effectors, rubber buffers are assembled like at the stiff hybrid wheel.
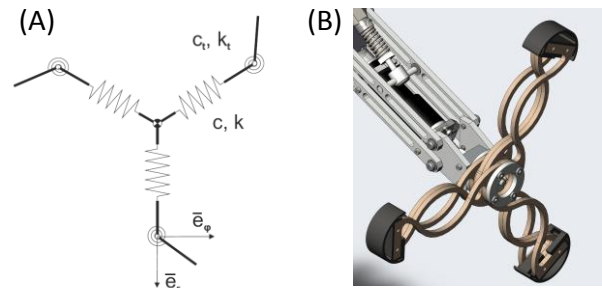
Fig. 4 Left: Spring-damper model of the elastic hybrid wheel, right: designed elastic hybrid wheel

The experimentally measured elasticity of the effectors is nearly equivalent to the aimed elasticity. In experiments, mechanical resonance was observed during locomotion at a determinate velocity of the robot. Further experiments will be done soon to quantify parameters and to make some energy balance analyses.

3 CONCLUSIONS

An elastic hybrid wheel was developed for a hexapod robot using resonance during locomotion. It could be observed, that the mechanical load is reduced during the impact of the elements of a hybrid wheel and that a resonance appears at a determinate velocity of the robot. Whether a reduction of the power is achieved, has to be verified in further experiments.

REFERENCES

[1] T. Allen, R. Quinn, R. Bachmann, and R. Ritzmann (2003):"Abstracted biological principles applied with reduced actuation improve mobility of legged vehicles," in *Proceedings IROS 2003:* pp. 1370–1375.

[2] A. Boxerbaum, J. Oro, G. Peterson, and R. Quinn (2008): "The latest generation Whegs™ robot features a passive-compliant body joint," in *IROS 2008*, pp. 1636–1641.

[3] U. Saranli, (2001): "RHex: A Simple and Highly Mobile Hexapod Robot," *The International Journal of Robotics Research*, vol. 20, no. 7, pp. 616–631,

[4] M. Eich, F. Grimminger, S. Bosse, D. Spenneberg, and F. Kirchner (2008): "Asguard: A Hybrid-Wheel Security and SAR-Robot Using Bio-Inspired Locomotion for Rough Terrain," in *Proceedings ROBIO 2008,* pp. 774–779.

LocoKit - A Construction Kit for Exploration of Morphology of Legged Robots

Jørgen Christian Larsen and Kasper Stoy

The Maersk Mc-Kinny Moller Institute
University of Southern Denmark
{jcla , kaspers}@mmmi.sdu.dk

Abstract: Producing steady stable and energy efficient locomotion in legged robots with the ability to walk in unknown terrain is a big challenge in robotics. In addressing this challenge, it is often desirable to experiment with different morphologies and see how they influence on the way the robot walks. This is however not always easy, since robots are often built as a fixed system with a limited possibility of changing the morphology without redesign a significant part of the robot. This work is focusing on the creation of a robotic construction kit specifically aimed at easing the process of constructing legged robots. This is accomplished by giving the creator the possibility to easily do morphological changes to the robot even after it have been build, to see how it effects the robot's ability to walk in unknown terrain.

Keywords: LocoKit, Quadruped, Robot, Modular Robot, Walking

1. INTRODUCTION

For decades, scientists have tried to build legged robots with the ability to walk in unknown terrain, in order to make them more useful for real-world tasks. Often, mobile robots are using wheels for transportation, mostly because they provide a number of advantages in terms of stability, controllability, efficiency and speed. Even though wheels have been used for decades, not only on mobile robotic platforms but also on cars, trucks, farming equipment etc. they still have certain disadvantages that legs does not have, of which the biggest might be the ability to handle unknown terrain. When constructing robots, one often tends to build a robots as a whole, meaning that the robot is a fixed structure with limited possibility to change mechanical parameters on the robot after it has been build. Since the morphology of the robot is of vital importance to its performance, it is important to have a system that allows for changing the morphology of the robot in order to explore how different morphologies effects its walking abilities. This is the main reason why we feel that the conventional way of building walking robots may not be the best scientific way of exploring walking abilities in robots. In trying to come up with a solution, we have introduced the modular robotic construction kit, called LocoKit, created by Larsen et. al [3]. In this paper we demonstrate that by extending principles from modular robots, LocoKit gives the opportunity to study different morphological questions, by enabling the constructor to build legged robots from LocoKit and then afterwards start adjusting mechanical parameters on the robot, which again changes the morphology of the robot. Modular robots have been a field of research for the past 25 years and have shown us, that modular robots are able to form a number of different morphologies, all able to perform locomotion, either on legs, crawling or as a loop robots, [2][4][5].

2. MOTIVATION

When looking at animals and the morphological richness between different species, it is obvious that it is a good place to start looking when we want to get inspiration on how to create legged robots. Animals like dogs, monkeys and lizards, are all extremely good at doing legged locomotion in an elegant, efficient and lithe way. It seems like the whole body is part of their walk. When looking at the walking style of these three different classes of animals, it is obvious that their walking style is quite different from one another. They have a different morphology. While all being very good at legged locomotion, their individual morphology gives each of them certain advantages. A dog is for instance good at running fast, but a monkey is a much better climber and a lizard can move almost unseen given its flat posture. It is clear the the morphology is of vital importance to each animals ability to move. Legged robots are often created so that they look like an animal, for instance a dog. The process of modelling a dog as a robot is easily done by using a stiff frame as the body of the robot, onto which four legs are attached. The robot is also often symmetrical, which gives the robot a centre of mass placed conveniently in the centre of the robot, making it easier to make the robot stable during walk. However, building a robot by only having it look like an animal, might not always be good enough. It requires fine tuning of the morphology of the robot to get comparable walking performance to animals. I order to contribute with a new approach to designing walking robots, we are designing a robotic construction kit called LocoKit. The goal with LocoKit is to create a robotic construction kit focused on building dynamically walking robots. Since the morphology of the robots might play a big role in the walking performance, LocoKit have been created in a way that allows the constructor to adjust the morphology of the robot, even after the robot has been assembled. These adjustment could be length, width, height, centre of mass, compliance, different spines etc.

3. EXPERIMENTS

To test the construction kit, experiments have been conducted with two very different robots - *see Figure 1.*
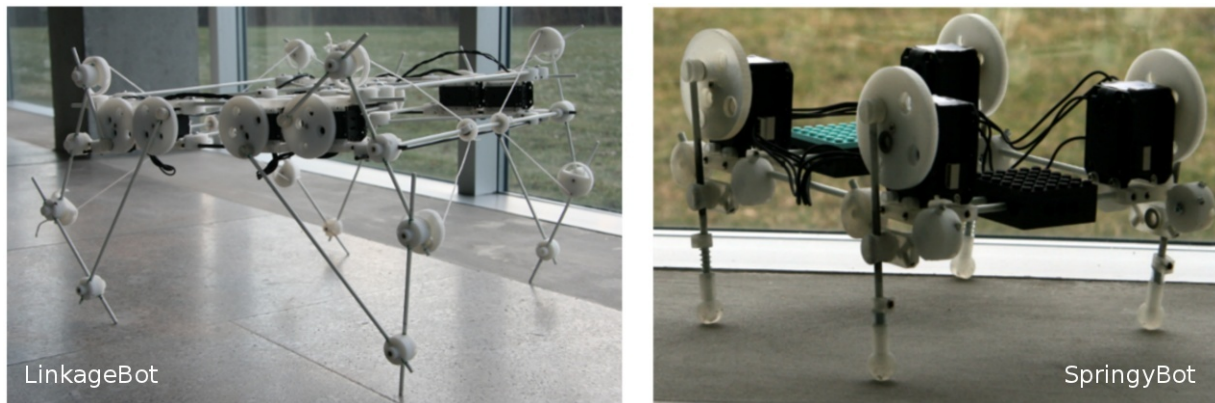
Fig. 1 Two robots build from LocoKit. On the left is the LinkageBot with a weight of 1600 g, W55 D43.5 H30 (cm) and on the right is SpringyBot with a weight of 650 g, W25 D20 H18 (cm).

The purpose of these two example experiments is to illustrate how the construction kit can be used to answer questions related to morphology.

3.1 Experiments on linkage-bar systems

The robot, LinkageBot, have been inspired by the Strandbeest robots by Jansen et. al [1]. The robot is constructed with two motors per leg, making it possible to control the trajectory of the foot from the controller - *see Figure 1*. With this robot we wanted to see if it would be possible to build a linkage-bar mechanism with LocoKit and also to see how much freedom we would have afterwards to adjust the morphology of the robot. On this robot, it was of great benefit to have the opportunity to adjust the lengths of the individual components in the legs. This made it possible in an easy way to study how different reachable spaces of the foot affected the walking abilities of the robot.

3.2 Experiments on compliance, weight and energy efficiency

The second robot, SpringyBot, with only one actuator per leg, giving the legs a fixed trajectory - *see Figure 1* have also been designed. With this robot we wanted to see how simple a robot we could build, and still gain a benefit from the adaptability of LocoKit. Firstly on this robot we started to add different levels of compliance to the legs to see how this would effect the walking ability. Secondly, we tries increasing the weight of the robot to see how this would effect the energy efficiency of the robot. These experiments show how the energy efficiency increases together with the weight. These results are similar to what is seen in animals.

4. CONCLUSIONS

The robotic construction kit, LocoKit, have been developed to make it easier to build and explore different morphologies on walking robots with the ability of doing efficient and dynamic locomotion in unknown terrain. The kit supports opportunities for changing parameters in the construction, even after the robot has been assembled. These are for now parameters like length, width, height and centre of mass. In the current state of the system,

it have been used in several experiments, showing that the system is able to form legged robots with very different morphology - *see Figure 1*. The robots build from LocoKit have been tested in both flat terrain as well as in unknown terrain. Experiments show that the LocoKit system still needs some optimisation in order to perform stable legged locomotion in unknown terrain, however for walking on flat terrain the robots shows stable forward locomotion.

In future work the LocoKit system will be enhanced with better opportunities for adding compliance in the structures, as well as the possibility of doing online morphosis, that is, changing the morphology of the robot.

5. ACKNOWLEDGMENTS

REFERENCES

[1] T. Jansen. *Theo Jansen: The Great Pretender*. OIO Publishers, 2007.

[2] H Kurokawa, E Yoshida, K Tomita, a Kamimura, S Murata, and S Kokaji. Self-reconfigurable M-TRAN structures and walker generation. *Robotics and Autonomous Systems*, 54(2):142–149, February 2006.

[3] J.C. Larsen, R.F.M. Garcia, and K. Stoy. Increased versatility of modular robots through layered heterogeneity. In *Proceedings of the ICRA Workshop on Modular Robots, State of the Art*, pages 24–29, Anchorage, Alaska, May 2010.

[4] J. Sastra, S. Chitta, and M. Yim. Dynamic Rolling for a Modular Loop Robot. *The International Journal of Robotics Research*, 28(6):758–773, May 2009.

[5] Wei-Min Shen, Maks Krivokon, Harris Chiu, Jacob Everist, Michael Rubenstein, and Jagadesh Venkatesh. Multimode locomotion via SuperBot reconfigurable robots. *Autonomous Robots*, 20(2):165–177, April 2006.

Combining Bio-inspired Sensing with Bio-inspired Locomotion

Danish Shaikh[1][§], John Hallam[1][†], Jakob Christensen-Dalsgaard[2], Auke J. Ijspeert[3]

[1]Mærsk Mc-Kinney Møller Institute, University of Southern Denmark, Odense, Denmark
(E-mail: {[§]danish,[†]john}@mmmi.sdu.dk)
[2]Department of Biology, University of Southern Denmark, Odense, Denmark
(E-mail: jcd@biology.sdu.dk)
[3]Biorobotics Laboratory, École Polytechnique Fédérale de Lausanne (EPFL), Lausanne, Switzerland
(E-mail: auke.ijspeert@epfl.ch)

Abstract: In this paper we present a preliminary Braitenberg vehicle–like approach to combine bio-inspired audition with bio-inspired quadruped locomotion in simulation. Locomotion gaits of the salamander–like robot *Salamandra robotica* are modified by a lizard's peripheral auditory system model that modulates the parameters of the locomotor central pattern generators. We present phonotactic performance results of the simulated lizard-salamander hybrid robot.

Keywords: bio-inspired robotics, audition, locomotion, central pattern generators

1. INTRODUCTION

Lizards have an amazingly directional peripheral auditory system [2] given its simplicity in design. Moreover, it is reported to have the highest directionality among all vertebrates [3]. The system has been extensively studied, modelled and applied as a controller for wheeled robots in phonotaxis tasks. We apply the same to a salamander–like quadruped robot *Salamandra robotica* designed and built in the Biorobotics Laboratory at EPFL. The notable feature of this robot is its undulatory locomotion, mimicking tetrapods such as salamanders and lizards that exhibit lateral bending of the trunk during locomotion. These animals stabilize their heads such that it is always oriented towards the direction of motion, possibly to minimize the oscillation of the head-centered reference frame for auditory spatial information which would otherwise oscillate along with the head, resulting in oscillating auditory cues. In order to observe the effect of such oscillating cues on the robot's sound localization ability, we integrate the auditory system model into the robot and evaluate its phonotactic performance in simulation.

2. THEORETICAL BACKGROUND

2.1 The Lizard Peripheral Auditory System

The auditory system (Fig. 1(a)) is composed of a tympanum (TM) on each side of the head, connected via wide internal Eustachian tubes (ET). Since the sound wavelengths to which it responds to (170–340 mm) are larger than the head size ($\sim$13 mm), the incident sound waves diffract around the animal's head, creating essentially equal sound pressures at the two tympani. The acoustical coupling formed by sound transmission through the ET translates small phase differences between sound waves arriving at either tympanum, whose magnitude depends on the relative direction from which the sound appears to originate, into relatively larger differences in perceived sound amplitude at either tympanum. The directionality can be visualized (Fig. 2) via an equivalent electrical model [4] (Fig. 1(b)) and given mathematically as
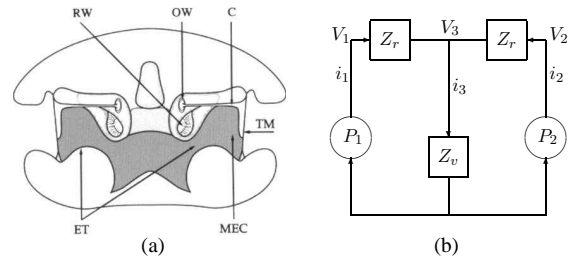
Fig. 1: (a) Lizard ear structure and (b) electrical model.
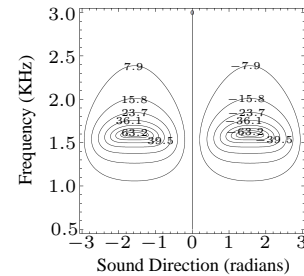
Fig. 2: Amplitude difference (i_{ratio}) between either side.

$$
\begin{aligned}
\left| \frac{i_1}{i_2} \right| &= \left| \frac{G_\mathrm{I} \cdot V_1 + G_\mathrm{C} \cdot V_2}{G_\mathrm{C} \cdot V_1 + G_\mathrm{I} \cdot V_2} \right| \text{ or} \\
i_{\mathrm{ratio}} &= 20 \left(\log |i_1| - \log |i_2| \right) \mathrm{dB},
\end{aligned}
\tag{1}
$$

where i_1 and i_2 model left and right tympanal vibrations respectively and G_I and G_C are ipsilateral and contralateral frequency-dependent (1000–2200 Hz) gains.

2.2 *Salamandra robotica*

Salamandra robotica (Fig. 3) is designed to be a tool for neuroscientific studies in the role of spinal central pattern generators in producing various locomotion gaits in salamanders [1]. It exhibits locomotion patterns that match those of a real salamander. The neuronal model used to generate different locomotion gaits is based on central pattern generator (CPG) circuits in the spinal cord of the salamander. Since lizards exhibit terrestrial locomotion patterns similar to salamanders, it makes sense to combine the former's auditory sensing model and the latter's neuromotor model. Furthermore, an accurate model of the robot in a realistic physics-based simulation environment (Webots[TM]) is readily available (Fig. 3(b)).

(a) CPG model (figure by A. Ijspeert, courtesy Biorobotics Laboratory, EPFL).

(b) Webots™ model.
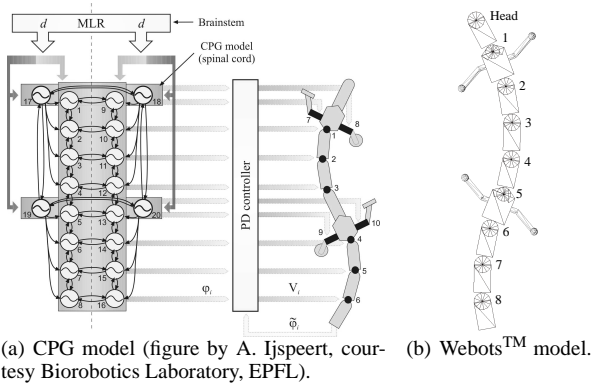
Fig. 3: *Salamandra robotica*

2.3 Sensory Guidance of Locomotion

Braitenberg vehicles conceptually describe the generation of different behaviours as a consequence of varying the structure of the sensorimotor couplings. We model the coupling between the ear model and the locomotor CPGs as a cross connection (Eq. (2)), with the *left* sensory output (i.e. the left tympanal vibration i_l) modulating the body CPGs to the *right* side and vice versa. The modulated parameters are the amplitudes μ_l and μ_r of the left and right body CPG oscillations respectively. Decreasing μ decreases bending of the trunk, attenuates the head oscillations and thus the auditory cue oscillations. In order to observe the effect of change in the amplitude of auditory cue oscillations on sound localization ability, we define a gain parameter α which governs the extent to which μ is modified. Since the variation in the response of the auditory system model varies for different frequencies, the sensory outputs are normalized to generalize the sensorimotor coupling over the relevant frequency range of 1000–2200 Hz, making α frequency-independent.

$$
\begin{aligned}
\mu_l &= \operatorname{sgn}(i_r - i_l) \cdot (1 + \alpha \cdot \operatorname{sgn}(i_r - i_l)) \\
\mu_r &= \operatorname{sgn}(i_l - i_r) \cdot (1 + \alpha \cdot \operatorname{sgn}(i_l - i_r))
\end{aligned}
\tag{2}
$$

3. EXPERIMENTS AND RESULTS

The goal the robot in the phonotaxis tasks was to localize and locomote towards a simulated sound source of given frequency and angular displacement with respect to its head, placed 5 m away from the robot. The angular displacement was varied over the frontal $\left[-\frac{\pi}{2}, +\frac{\pi}{2}\right]$ region in 5° steps, resulting in 37 trials. The frequency was randomly chosen to be 1900 Hz from the 1000–2200 Hz range and kept constant over all the trials. For each trial, the robot's trajectory and CPG outputs were logged. The heading errors (Fig. 4) were determined by first dividing the trajectory into 10 parts and computing the heading vector for each part. These were then averaged and the absolute difference between the average heading and the ideal heading, which is a straight line from the robot to the source, was computed. Figure 5 depicts sample body CPG outputs during a right turn from one of the trials.

4. CONCLUSIONS AND FUTURE WORK

We have integrated a lizard's peripheral auditory system model into a salamander–like quadruped robot and
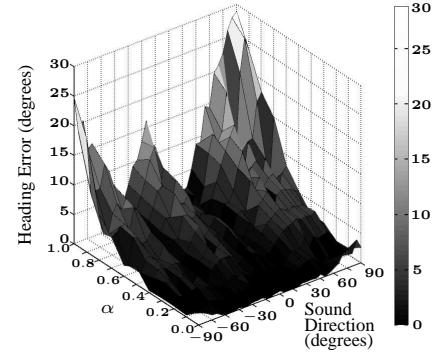
Fig. 4: Absolute angular error in heading.
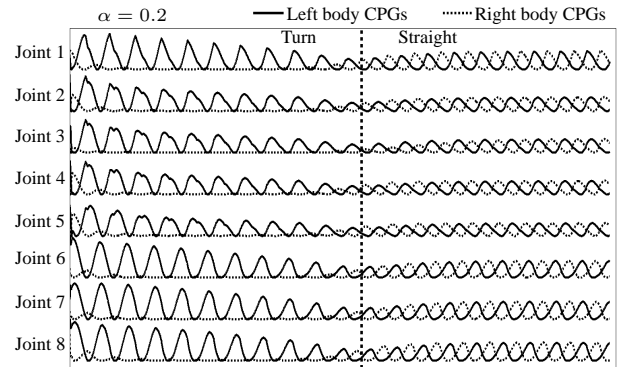
Fig. 5: CPG outputs while turning. Sound source at +75°.

evaluated the phonotactic performance of the lizard-salamander hybrid in simulation. In spite of the head oscillations typical in undulatory locomotion, the robot successfully localizes the sound source. Decreasing α increases contralateral inhibition and ipsilateral excitation, respectively reducing and amplifying μ of the body CPGs on either side, attenuating the head oscillations and consequently the auditory cue oscillations, resulting in tighter turns towards the sound source. However, the error surface is flat at $-45° \pm 10°$ and $+25° \pm 10°$. This is due to the initial conditions of the CPGs which swing the head roughly 25° to the right and then 45° to the left. This "bias" can be eliminated by allowing the oscillations to settle down before sensory modulation. In the future, real-world trials will be conducted for comparison.

REFERENCES

[1] A. J. Ijspeert, A. Crespi, D. Ryczko, and J. M. Cabelguen, "From Swimming to Walking with a Salamander Robot Driven by a Spinal Cord Model", *Science*, Vol. 315. No. 5817, pp. 1416–1420, 2007.

[2] J. Christensen-Dalsgaard, "Directional Hearing in Nonmammalian Tetrapods", *Sound Source Localization*, Springer Handbook of Auditory Research, Vol. 25, pp. 67–123, 2005.

[3] J. Christensen-Dalsgaard and G. A. Manley, "Directionality of the Lizard Ear", *Journal of Experimental Biology*, Vol. 208, No. 6, pp. 1209–1217, 2005.

[4] N. H. Fletcher and S. Thwaites, "Physical Models for the Analysis of Acoustical Systems in Biology", *Quarterly Reviews of Biophysics*, Vol. 12, No. 1, pp. 25–65, 1979.

A Neural Network Model for Burrow Surveilance of Fiddler Crabs

Seung-Eun Yu and DaeEun Kim

Biological Cybernetics Lab,
School of Electrical and Electronic Engineering,
Yonsei University, Seoul, Korea
(E-mail: daeeun@yonsei.ac.kr)

Abstract: Fiddler crabs demonstrate burrow surveliance behavior. They defend their burrow against their intruders when the intruders approach their burrow. It seems that crabs can estimate the distance between an intruder and the burrow. In this paper, we analyze the geometry relations among the crab itself, its burrow and an intruder, and derive the trigonometric equation. The retinal position of an intruder, the azimuth and elevation angle depending on the crab-burrow distance can determine the intruder-burrow distance in principle. In this paper, we show a neural network with multilayer perceptrons for the mapping function to determine the intruder-burrow distance. However, our experiments reveal that the distance estimation may be difficult when an intruder approaches the burrow from the opposite side. We suggest that additional information of the intruder image size will be helpful for the distance estimation, or crabs simply determine whether or not the intruder is close to the burrow within some distance rather than estimate the distance accurately.

Keywords: distance estimation, vision, fiddler crab, distance neuron, retinal position

1. INTRODUCTION

Animals use their own sensory systems in various tasks effectively. Foraging insects like bees and desert ants use landmark-based information to return to a target location [2]. The sand scorpions use their tactile senses on their legs to detect insect prey at night without any additional visual or auditory senses [1]. Fiddler crabs are wary of approaching predators or colleagues, and dash back to the burrows in order to protect their nests [9].

It seems that the fiddler crabs can estimate the intruder-burrow distance to a certain extent. The retinal elevation and azimuth angle of the point which a target object contacts with the ground is uniquely determined by the distance between the object and the crab observer [11]. Reversely, the observer can determine the distance of the object. For the burrow surveillance of fiddler crabs, [5], it appears that the fiddler crabs *Uma vomeris* use retinal position information of an intruder to measure the distance between an intruder and the burrow, and respond to protect the nest if the intruder approaches the burrow within some distance.

There have been many neural models involved with distance estimation in animal behaviors, for example, motion detection neurons [4], feature detecting neurons [3], and small moving targets detection neurons [7]. Fiddler crabs might also use neurons with similar characteristics. In this paper, we first analyze the geometric relations with the crab, burrow and an intruder to determine the burrow-intruder distance. A trigonometric equation can be represented with a neural network with multilayer perceptrons. We investigate the role of image size of the intruder for the distance estimation. Instead of estimating the distance accurately, fiddler crabs could respond depending on whether or not the intruder reaches the defense zone of the burrow.

2. DISTANCE ESTIMATION WITH RETINAL POSITION

We first analyze the intruder-burrow distance estimation of the fiddler crabs using the retinal position to defend their nests against an intruder. From the previous works, the fiddler crabs use path integration for the distance L and direction to the burrow [9, 10]. In addition, the crabs align their body axis toward the homing direction [9]. From the alignment, the fiddler crabs can estimate the direction α between the burrow and an intruder, using the retinal azimuth angle. Let d_t be the distance between the crab and the intruder. Then with the cosine law, the distance between an intruder and the burrow can be obtained with Eq. (1).

$$d = \sqrt{d_t{}^2 + L^2 - 2d_t L cos(\alpha)} \tag{1}$$

If the retinal position of an intruder is available, the crab can determine the intruder-burrow distance, using simple geometrical computation shown in Equation (2).

$$(x, y) = (h\frac{\sin(\alpha)}{\tan(-\beta)}, h\frac{\cos(\alpha)}{\tan(-\beta)} - L) \tag{2}$$

where L indicates the crab-burrow distance obtained from the path-integration information, h is the height of the crab's eyes from the ground, and for the retinal position, the azimuth and elevation angle of the intruder, are represented as α and β, respectively, and (x, y) is the position of the intruder with respect to the burrow.

The intruder-burrow distance d is the important factor to determine the defense zone for whether the crab will respond or not to run into the burrow for protection. The distance d and the approaching direction ϕ can be obtained with the location given in Eq. (2), which are given below:

$$(d, \phi) = (\sqrt{x^2 + y^2}, \tan^{-1}(\frac{y}{x})) \tag{3}$$

3. SIMULATION AND RESULTS

In this paper, we first compose a visual space inspired by the visual field of the crab. For compound eyes of the fiddler crab [6, 8], the number of optic receptors varies depending on the eye regions. In order to observe a target object or an intruder in the flat field efficiently and accurately, the visual space around the horizon has a larger number of visual receptors than the other regions. It means visual information of an intruder with the retinal position can directly map the burrow-intruder distance [5]. We showed that the distance estimation can be obtained by the computation with geometry and trigonometric equations, but the crabs would employ a comparatively simple neuronal network to estimate the distance. Thus, we built a mapping function with multi-layered perceptrons and we used backpropagation learning method for the distance estimation with the retinal view of a target object. Initially, the input parameters are the azimuth and elevation angle of the target as well as the crab-burrow distance. Later, we added the image size information of the intruder for the input parameter. We assume that the crab-burrow distance is estimated with path integration by the crab itself.

The error is smaller when the intruder is approaching from the observer side than the opposite side. If the intruder is at the far region, it is hard to estimate the distance accurately. The burrow surveilance is thus influenced by the approach direction. In the neural network training without the image size information of an intruder, the performance much degrades as seen in in Fig. 1(b). The apparent size information can be helpful to determine the burrow-intruder distance. However, biological experiments [5] show that the burrow surveilance behavior is not influenced by the apparent size of the intruder and it seems the performance does not depend on the approach direction. Possibly the fiddler crabs do not estimate the burrow-intruder distance accurately, but instead they may only check if the intruder is inside the defense zone. It would be an easier task for the fiddler crabs. The above simple approach for navigation can be applied to biomimetic robots modeling the surveilance behavior of fiddler crabs.

Acknowledgments.

Fig. 1 Error bar representing the amount of error in estimating the distance for each direction when the observer is 30cm away from the burrow (a) image size information is used (b) image size information is not used

REFERENCES

[1] P.H. Brownell. Prey detection by the sand scorpion. *Scientific American*, 1984.

[2] BA Cartwright and TS Collett. Landmark learning in bees. *Journal of Comparative Physiology A: Neuroethology, Sensory, Neural, and Behavioral Physiology*, 151(4):521–543, 1983.

[3] MA Frye and RM Olberg. Visual receptive field properties of feature detecting neurons in the dragonfly. *Journal of Comparative Physiology A: Neuroethology, Sensory, Neural, and Behavioral Physiology*, 177(5):569–576, 1995.

[4] C. Gilbert and N.J. Strausfeld. The functional organization of male-specific visual neurons in flies. *Journal of Comparative Physiology A: Neuroethology, Sensory, Neural, and Behavioral Physiology*, 169(4):395–411, 1991.

[5] J.M. Hemmi and J. Zeil. Burrow surveillance in fiddler crabs. II. The sensory cues. *The Journal of experimental biology*, 206(Pt 22):3951, 2003.

[6] M. Land and J. Layne. The visual control of behaviour in fiddler crabs. *Journal of Comparative Physiology A: Neuroethology, Sensory, Neural, and Behavioral Physiology*, 177(1):91–103, 1995.

[7] K. Nordström and D.C. O'Carroll. Small object detection neurons in female hoverflies. *Proceedings of the Royal Society B: Biological Sciences*, 273(1591):1211, 2006.

Bio-Inspired Heterogeneous Step Sizes for a Six-Legged Walking Robot

Arne Roennau, Georg Heppner and Ruediger Dillmann

Interactive Diagnosis- and Servicesystems (IDS), FZI Research Center for Information Technology, Karlsruhe, Germany
(E-mail: {roennau, heppner, dillmann}@fzi.de)

Abstract: The stick insect *Carausius morosus* uses non identical step sizes while walking with its six legs. As a consequence, the step size differences create a systematic mechanical tension between these legs during the stance phase. In this work, we implemented a step size adaptation for the walking robot LAURON, which allows us to create heterogeneous step sizes. Experiments with different step size configurations show the effects of this systematic mechanical tension on the walking performance of a six-legged walking robot.

Keywords: bio-inspired robotics, stick insect, step size, hexapod, six-legged walking robot

1. INTRODUCTION

Biologically-inspired robots with a natural appearance are fascinating and usually come along with a big public interest. On the one hand, following the design and control rules of Nature increases the acceptance by the public and on the other hand these design principles can help to develop energy efficient, fast, robust and reliable robots. Especially, walking robots are typical examples for bio-inspired robots. The six-legged walking robot LAURON was inspired by the stick insect. In a recently published work we focused on the creation of a biologically-inspired free gait walking pattern [1]. Although this work concentrated on gait generation and coordination of the legs we noticed that the step sizes of our stick insects varied significantly from one leg to the other.

Our extraction of the stick insect's step sizes is based on video analysis and was carried out by hand, which makes this method very time consuming. We could see a trend in our data to different step sizes for certain leg groups, but the data basis was too small.

In literature, we found several works, which include more reliable data on the step sizes of the stick insect. The step sizes for the left and right leg are equal in most cases. Therefore, the step sizes are only distinguished for the front, middle and rear leg. In this work we will focus on the relative differences between the step sizes. The step size of the middle leg will be used as reference value. All ratios have the form (front:middle:rear). In the work of Holk Cruse the step sizes of the stick insect *Carausius morosus* are equal on a narrow path (1.0 : 1.0 : 1.0), but are unequal when walking on a flat terrain (0.8 : 1.0 : 1.1) [2]. Straight walking stick insects also have different step sizes in the work of M. Gruhn [3]. Here, we found a ratio of (1.4 : 1.0 : 1.1). Baessler does not give exact values for the AEP and PEP, but gives ranges for these two values. These ranges do not allow us to determine an exact ratio. However, the published ranges show non identical step sizes for the front, middle and rear legs [4]. Another example verifying our observations can be found in the work of B. Diederich [5]. In this work detailed experiments have shown that the sick insect adapts its step sizes when climbing uphill (1.1 : 1.0 : 0.96) or downhill (0.8 : 1.0 : 0.8).

Fig. 1 LAURON IVc: Fourth generation of the bio-inspired (stick insect) walking robot LAURON.

Similar to previous observations, the step sizes on a flat terrain are different for the front, middle and rear legs (0.94 : 1.0 : 0.96). With non identical step sizes, the stick insect creates a systematic mechanical tension between its legs. A possible explanation for this behaviour is the improvement of its walking capabilities and the adaptation to certain situations.

In this work, we will investigate the effects of non identical step sizes on the walking process of a six-legged walking robot. We do not know of any six-legged robot trying to use non identical step sizes. But these bio-inspired heterogeneous step sizes might create a more biological locomotion with a reduced energy consumption and an increased stability based on systematic mechanical tension. We will discuss and demonstrate the effects of heterogeneous step sizes based on the results of real experiments with LAURON IVc (see Fig. 1).

2. APPROACH

Our approach is evaluated with the fourth generation of the six-legged robot LAURON. Its kinematic structure is a simplified version of the morphology of the stick insect *Carausius morosus*. Each leg has three degrees of freedom and is equipped with many sensor systems.

LAURON is controlled by a behaviour-based control system. Due to the modular structure of this control system the step size adaptation only needed to be imple-

mented in a single behaviour. The steering behaviour creates the AEP and PEP for each leg. Then the corresponding trajectories are created by the independent swing and stance behaviours. In this work we use the step size of the two middle legs as reference value. The step sizes of the front and rear legs can be varied as a ratio of the middle legs' step size and independently from each other. The swing, stance period and the duty factor (ratio of these two values to each other) are dependant on the desired walking velocity and the current gait. All legs have the same swing and stance time. Therefore, an increased step size of one leg pair will result in a slower stance velocity and create a mechanical tension between this leg pair and the others. In contrast, a smaller step size creates a faster stance movement, which induces an opposite mechanical tension. The adaptation of the step size ratios between the front, rear and middle legs enables us to create many different mechanical tension configurations. Now, we are able to transfer the observations made with the stick insects to the walking robot LAURON IVc.

3. RESULTS AND EXPERIMENTS

After implementing the step size adaptation, we conducted several experiments with different step size ratios between the front, middle and rear legs. The first effects were not as visible as expected. But, walking with certain ratios made a more stable and smoother impression than with others. These subjective and personal impressions were analysed with the help of the joint torques, number of step cycles and energy consumption.
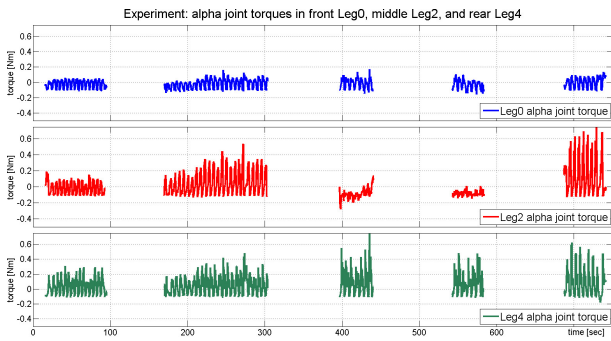
Fig. 2 Experiment: heterogeneous step sizes with effects on joint torques, chronology: R_1, R_7, R_8, R_8, R_9.

All experiments were conducted under the same conditions. LAURON walked a fixed distance with a fixed velocity in its tripod gait. Only the step size ratio and the step size of the middle legs was changed from one experiment to the other. In Fig. 2 we have illustrated the alpha joint torques of the front (top), middle (middle) and rear leg (bottom). The used step size ratios in these five experiments were as follows: R1, R7, R8, R8 and R9 (see Table 1). In the last experiment the step size of the middle legs was increased from 100mm to 200mm. The data shows that the torque distribution changes together with the ratio. With ratio R8 the joint torques in the middle leg are the smallest. The walking performance during this experiment was very good and even made a better

impression than with identical step sizes (R1).

More experiments can be found in Table 1. The tested ratios were inspired by the natural ratios of the stick insect found in literature. The number of cycles shows how effective each ratio was (lower value = better). Although R8 and R9 almost have the same number of step cycles the consumed energy is significantly higher with R9. It is very difficult to evaluate all effects of the heterogeneous step sizes on the walking process. But our experiments show clearly that a systematic mechanical tension can have a positive effect on the walking process of a six-legged walking robot.

exp. no.	ratio	width	cycles	energy
R_1	1.0 : 1 : 1.0	100	15	6249
R_2	0.8 : 1 : 1.1	100	12.5	6390
R_3	1.4 : 1 : 1.1	100	7.5	3257
R_4	1.1 : 1 : 1.4	100	7.5	4131
R_5	1.0 : 1 : 1.0	140	6.5	3312
R_6	0.9 : 1 : 0.9	100	12	5508
R_7	0.5 : 1 : 0.5	100	23.5	12411
R_8	1.5 : 1 : 1.5	100	7	3151
R_9	0.5 : 1 : 0.5	200	8	4884

Table 1 Experiments showing the effects of different step size ratios: width := step size of middle legs [mm], cycles := step cycles, energy := needed energy [J].

4. CONCLUSION AND FUTURE WORK

We were able to show that the joint torques, walking velocity and walking efficiency can be influenced in a positive way by using non identical step sizes while walking with a six-legged robot. In this ongoing work we are currently verifying this positive effect and investigating the effects of a systematic mechanical tension for walking up slopes. In the future, we want to improve LAURON's walking capabilities by using specialised step size ratios for different scenarios.

REFERENCES

[1] A. Roennau, G. Heppner, T. Kerscher, R. Dillmann, "Behaviour-based Free Gait Inspired by Walking Stick Insect", *Proceedings of CLAWAR2010, 13th International Conference on Climbing and Walking Robots*, Nagoya, Japan.

[2] H. Cruse, "The function of the legs in the free walking stick insect,Carausius morosus", *Journal of Comparative Physiology A*, Vol. 112, pp. 235-262, 1976.

[3] M. Gruhn et al., "Straight walking and turning on a slippery surface", *Journal of Experimental Biology*, Vol. 212, pp. 194-209, 2009.

[4] U. Baessler, "Zur Beeinflussung der Bewegungsweise eines Beines von Carausius morosus durch Amputation anderer Beine", *Kybernetik 10*, 1972.

[5] B. Diederich et al., "Stick Insects Walking Along Inclined Surfaces", *Integrative and Comparative Biology*, Vol. 42, Number 1, pp. 165-173, 2002.

Dynamic leg function of the BioBiped humanoid robot

C. Maufroy[1], H.-M. Maus[1], K. Radkhah[2], D. Scholz[2], O. von Stryk[2], A. Seyfarth[1]

[1]Friedrich-Schiller-University Jena, Lauflabor Locomotion Laboratory, Jena, Germany
[2]Technische Universität Darmstadt, Department of Computer Science, Darmstadt, Germany
{christophe.maufroy, moritz.maus, andre.seyfarth}@uni-jena.de ; {radkhah, scholz, stryk}@sim.tu-darmstadt.de

Abstract: This contribution presents the concept and design of the first robot of the BioBiped series, aiming to transfer biomechanical insights regarding the mechanics and control of human walking and running to bipedal robot design and actuation. These are supported by preliminary experiments with the robot, where synchronous and alternate hopping motions could be successfully realized. This demonstrates that the robot design has the potential to develop dynamic gait patterns such as walking and running.

Keywords: Humanoid robot, bipedal walking and running, compliant segmented legs.

1. INTRODUCTION

Hopping, walking and running appear as natural and quite easy tasks for a healthy adult, yet for todays robots they impose big challenges. There are various problems for robots to perform these kinds of motion, including but not limited to mechanical robustness due to high joint torques, constraint forces and shocks from impacts, a high peak power demand especially in hopping and running, and, of course, postural stability of the robot.

Biomechanists have tried to point out mechanisms how these problems might be solved in human and animal locomotion [1-6]. We follow this approach by developing the lower body of the humanoid robot BioBiped1, the first prototype of a robot series aiming to transfer biomechanical insights regarding the mechanics and control of human locomotion to a novel bipedal robot design. With such platform, we hope to achieve human-like locomotion with various gaits (hopping, running and walking) with a single robot design. We aim at first to realize bouncing gaits like hopping and running, a central locomotor capability missing in most state-of-the art humanoid robots but surprisingly well described by simple template models [2]. This contribution describes the robot design philosophy and presents the results of preliminary experiments towards that goal.

2. ROBOT DESIGN CONCEPTS

The BioBiped1 robot (BB1, shown in Fig.1-right) is designed and realized in a way that allows to mimic important properties of the human locomotor system. One of them is segmentation: the robot leg is composed of three rotational joints in the sagittal plane (hip, knee and ankle) with segments sized according to human morphology. Another characteristic of the robot is the use of compliance at the joint level, which distinguishes it from conventional humanoid robots. This is achieved by series elastic, mono- and biarticular actuation of joints (represented in Fig.1-left) representing the main human muscle groups. Following biomechanical knowledge that power generation is mainly achieved by monoarticular muscles, while biarticular muscles mostly contribute to trans-
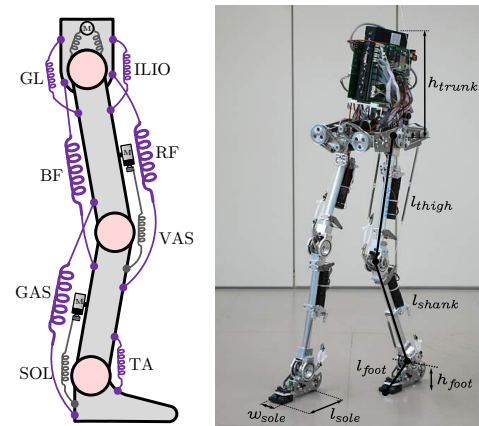
Dimensions and mass					
h_{trunk}	269	mm	l_{thigh}	330	mm
l_{shank}	330	mm	l_{foot}	122	mm
h_{foot}	67	mm	l_{sole}	168	mm
w_{sole}	40	mm	total mass	9.2	kg

Fig. 1 BB1 robot. (Left) actuation concept: the monoarticular anti-gravity muscles Vastus (VAS) and Soleus (SOL) are active. The other muscles (biarticular: Rectus Femoris (RF), Biceps Femoris (BF), Gastrocnemius (GAS); monoarticular: Gluteus Maximus (GL), Iliopsoas (ILIO), Tibialis Anterior (TA)) are passive. The hip joint is actuated by extended series elastic actuators. (Right) Picture of the prototype and main dimensions (Down).

fer this power between joints [6], monoarticular muscles (VAS and SOL) are active (i.e. with a motor in series to a spring, mimicking the muscle-tendon complex of extensor muscles) while the antagonist and biarticular structures are passive.

3. RESULTS AND DISCUSSION

As preliminary steps towards the realization of running, vertical hopping motions with synchronous or alternate motion of the legs (resp. synchronous hopping (Fig.2) and alternate hopping) were considered. The knee and ankle motors were controlled to follow reference po-

| Max. Compression | Stretching | Lift-Off | Apex | Flexion | Touch-Down | Max. Compression |
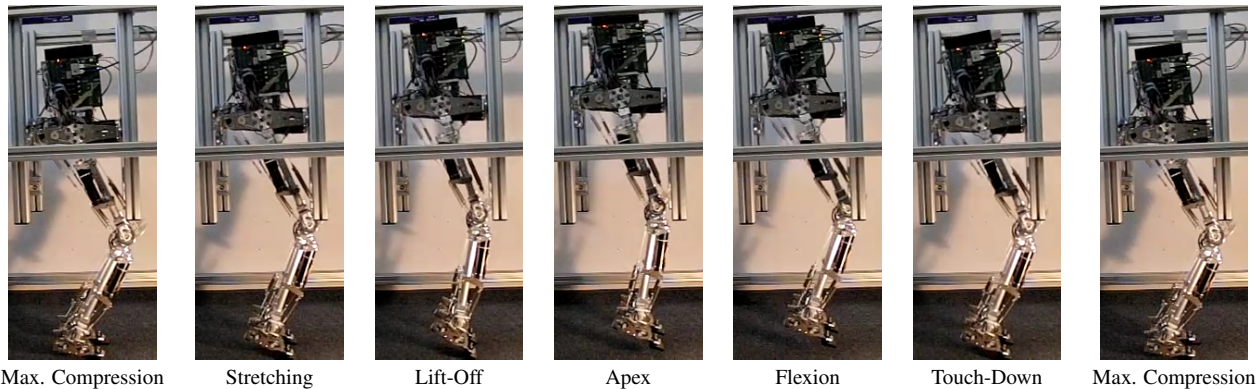
Fig. 2 Snapshots of one cycle of synchronous hopping motion. The robot pelvis motion is constrained to a 1D vertical translational degree of freedom by the surrounding frame.

sitions switched periodically between two set points, corresponding to configurations with retracted and extended legs, for synchronous hopping (Fig.3(a)). The same strategy was used for alternate hopping, with the addition of a third set point corresponding to an intermediate position in preparation for touchdown (Fig.3(b)). The hip pitch motor was controlled to result in a "free motion" (no torque applied) of the hip pitch joint. Additional springs were used to stabilize the leg configuration during aerial phase (a pair at the hip and one antagonist to the knee and ankle extensors). With this approach, hopping motions could be achieved in both cases with performances matching those of human for similar tasks (flight phase duration up to 200 ms leading to an average duty factor $\simeq 0.5$ (Fig.3) and ground clearance of up to 5 cm). The corresponding videos are available here: [7].

These preliminary results validate the robot design, as they demonstrate its ability to support high forces and impacts during the landing and to produce the required power to initiate and sustain hopping motions, a prerequisite for the realization of running. Further investigations will address intraleg coordination (for example, the influence of biarticular structures and the role of sensory feedback) to enhance leg operation and the realization of running by introducing fore and back swinging of the leg. In the latter case, the upper body, that will be enhanced in future versions of the robot, is likely to play an important role in counteracting the motion of the legs.

REFERENCES

[1] R. Alexander, Mechanics of bipedal locomotion, in *Perspectives in experimental biology*, (Oxford, UK: Pergamon Press, 1976), pp. 493-504.

[2] R. Blickhan, "The spring-mass model for running and hopping", *J Biomech*, 22(11-12):1217-1227, 1989.

[3] M. Fischer and R. Blickhan, "The tri-segmented limbs of therian mammals: kinematics, dynamics, and self-stabilization–a review.", *J Exp Zool A Comp Exp Biol*, 305(11):935–52, 2006.

[4] H. Geyer et al., "Compliant leg behaviour explains basic dynamics of walking and running", *Proc Roy Soc B*, 273(1603):2861-2867, 2006.
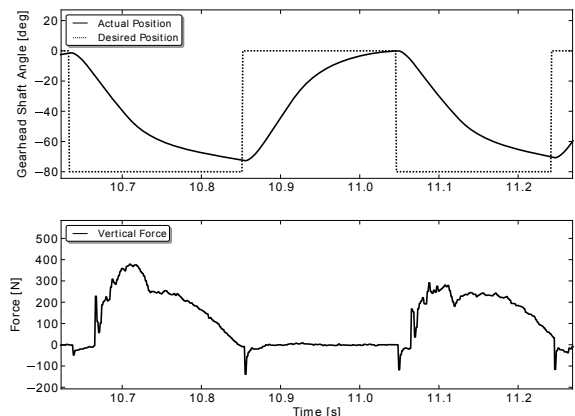
(a) synchronous hopping motion
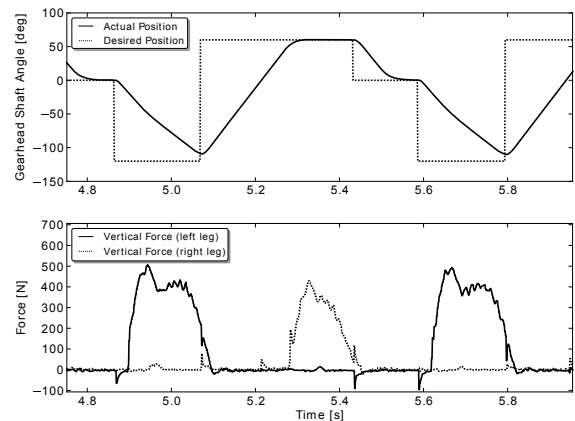
(b) alternate hopping motion

Fig. 3 For each type of hopping motion: (Up) Set points (dotted line) and actual position (solid line) of the knee motor. (Down) Force measured by the forefoot force sensors with axis perpendicular to the foot sole.

[5] H.-M. Maus et al., "Upright human gait did not provide a major mechanical challenge for our ancestors", *Nat Commun*, 1(6):1-6, 2010.

[6] G. J. van Ingen Schenau et al., "The unique action of biarticular muscles in complex movements", *J Anat*, 155:1-5, 1987.

[7] BB1 videos: "http://www.biobiped.de/videos.html"

Isochron of human walking derived from the perturbation of floor

Tetsuro Funato[1], Tetsuro Hosokawa[2], Shinya Aoi[13], Nozomi Tomita[3] and Kazuo Tsuchiya[23]

[1] Kyoto University, Kyoto, Japan. (Tel. & Fax: +81-774-65-6489; E-mail: funato@me.kyoto-u.ac.jp)
[2] Doshisha University, Kyoto, Japan. [3] CREST, JST, Japan.

Abstract: The rhythm of human walking is controlled for maintaining the stability. The stable motion composes limit cycle and the stabilization property is determined by the phase condition neighbor to the limit cycle described as isochron. This paper draws the isochron by analyzing the stabilization process after frontal perturbation. The isochron contained discontinuous flow around the hopping phase, considered to reflect the tuning of the phase control at hopping.

Keywords: Human walking, Isochron, Limit cycle.

1. INTRODUCTION

Walking is a cyclic motion actuated by the rhythm generated by the central pattern generator. The rhythm attracts the walking motion into stable cycle, which enables the walking with limited feedback control. Animals are considered to improve the stability by controlling the rhythm itself, such as resetting the rhythm by the timing of hopping and landing [1]. The motion slightly departed from the limit cycle returns by the effect of the attractor and the active tuning of the rhythm control. The process of the stabilization is described by isochron that is the contour of the phase over the whole area in phase space [2]. The property of the rhythm control for walking is entirely described by the isochron, thus the control mechanism by the rhythm can be described by the isochron.

Human body contains large number of segments including left and right limbs and trunk, and this high degree of freedom (DOF) has complicated the discussion of the limit cycle. Whereas, researches has shown the limbs and their segments moves rather coordinately and substantial DOF for walking has shown to be no more than two or three, thanks to the coordination. We have shown the limit cycle of the walking can be drawn in the three dimensional space spanned by the principle components using singular value decomposition (SVD)[3].

The aim of this research is to depict the isochron of human walking in the three dimensional phase space and to discuss the property of the walking rhythm reflecting the rhythm control. The experiment applying perturbation on human during walking is performed, and the returning process to the limit cycle is analyzed.

2. MATERIALS AND METHODS

Experimental device and procedure

Treadmill is set on the floor that can move horizontally by the equipped motor (Fig.1), and the perturbation is applied on the subject walking on the treadmill. The velocity of the treadmill is 4.0 [km/h] and the trial continues for 40 [s]. The floor moves from behind to front (arrowed direction) once in one trial. The amplitude of the perturbation is 30 [mm] and the velocity is 270 [mm/s].

Subjects are 3 healthy males. They are required to look at a small circle which locates far front of the subjects and the motions of their joints were measured with

Fig. 1 Experimental device. Treadmill horizontally moves with servo motor equipped on the floor of the treadmill. Subjects walk on the treadmill suffering pulsed perturbation in arrowed direction once for one trial.

a motion capturing system. Reflective markers were attached to the subjects' skin overlying the following body landmarks of both hemibodies: ear tragus, upper limit of the acromion, greater trochanter, lateral condyle of the knee, lateral malleolus, second metatarsal head, and heel. The markers are also attached at treadmill and floor for measuring the translation of floor. The sampling rate is 500[Hz]. Subjects gave informed consent prior to data collection according to the procedures of the Ethics Committee of Doshisha University.

Calculation of limit cycle by SVD

The elevation angles of 8 segments (head, trunk, thigh(right,left), shank(right,left), foot(right,left)) referred as $\theta_{\mathrm{segment}}$ are calculated. The motion of these 8 segments is mutually coordinated and the coordinate pattern of segments and that of time can be derived by SVD.

$$\Theta = \Theta_0 + \sum_i \boldsymbol{z}_i \left(\lambda_i \, \boldsymbol{v}_i \right)^{\mathrm{T}},$$

here Θ is a matrix whose column composed by the time series of $\theta_{\mathrm{segment}}$ ($\Theta = [\theta_{\mathrm{head}}, \theta_{\mathrm{trunk}}, \ldots]$). Θ_0 is the matrix of the same size with Θ, which the temporal average of Θ is iteratively arrayed. z_i, v_i, λ_i are left singular vector, right singular vector and singular value of $\Theta - \Theta_0$ for each.

The level of singular values of walking has indicated that over 99% of the motion during 1 step is composed by 3 components, and the whole motion is constructed by the activation of time independent pattern z_i by $\lambda_i v_i$ as activation pattern. The orbit of $\lambda_i v_i$ draws a stable cycle in the space spanned by z_i as the coordination, and this stable cycle can be considered as a limit cycle of whole body motion [3].
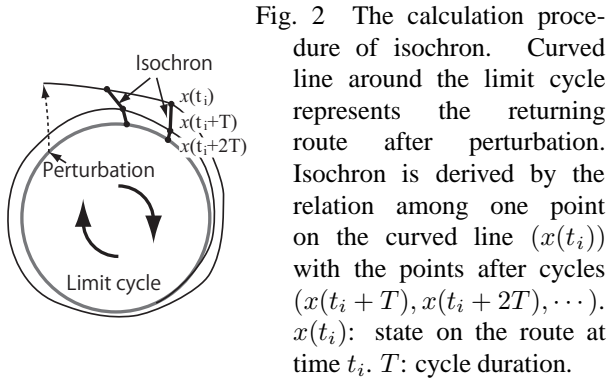
Fig. 2 The calculation procedure of isochron. Curved line around the limit cycle represents the returning route after perturbation. Isochron is derived by the relation among one point on the curved line ($x(t_i)$) with the points after cycles ($x(t_i + T), x(t_i + 2T), \cdots$). $x(t_i)$: state on the route at time t_i. T: cycle duration.
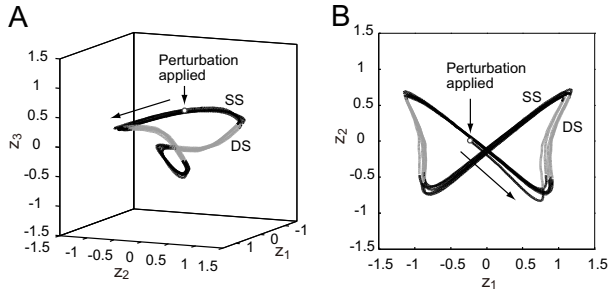
Fig. 3 Limit Cycle depicted on the z_1-z_2-z_3 space. The circle labeled by 'perturbation applied' represents the perturbation phase and the the orbit is drawn for 3 cycles after the perturbation. The part drawn by black line is single support phase (SS) and that drawn by gray line is double support phase (DS). Both figures A and B are the result of the same trial drawn from different viewpoints.

Derivation of isochron

Isochron is a contour of the phase spanned entire area in the phase space, where points on the same isochron has same phase with corresponding points on limit cycle. After the motion has slightly flied out from the limit cycle, the state returns with the orbit characterized by the isochron (fig.2 as image). The point $x(t_i)$ at time t_i and the points n cycle after that point ($x(t_i + nT)$) exists on the same isochron with different place. Thus the part of isochron can be calculated by connecting $x(t_i)$, $x(t_i+T)$, $x(t_i + 2T)$, $\cdots$.

In this paper, the lines for isochron is calculated for 100 points on the returning route of 1 trial. The experiment is duplicated for 75 times, thus the resulting isochron is depicted by 7500 lines.

3. RESULTS AND DISCUSSIONS

Limit cycle and the cycle of perturbation

Limit cycle of the whole body motion can be depicted in the 3 dimensional space of z_i. Before drawing the limit cycle in 3 dimensional space of z_i, we have confirmed whether the coordination of the cycle with perturbation z_i^{pert} is identical to that of cycle without perturbation z_i^{stable}. For this purpose the correlation between z_i^{pert} and z_i^{stable} is calculated. Then the correlation $z_i^{\text{pert}} \cdot z_i^{\text{stable}}$ was higher than 0.9 for every trial. This result indicated the perturbed cycle can be depicted in the same space.

Then, the orbit of whole body motion is drawn in the
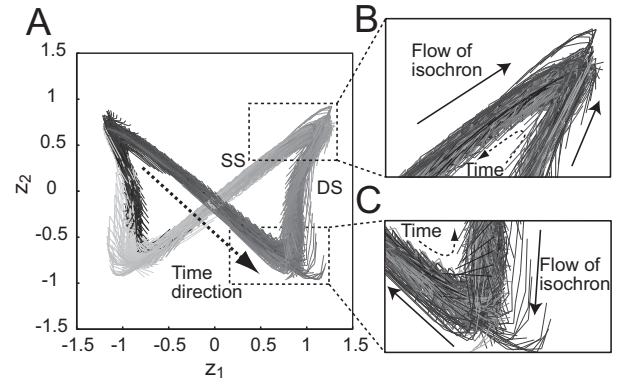
Fig. 4 The calculated isochron from the experiment. The colors on the figure A represents the phase of the isochron. A: the isochron with the same viewpoint with Fig.3B. Fig.B is the closeup of the Fig.A around hopping phase, and Fig.C is that around landing phase. The direction of isochron around hopping phase (Fig.B) changes discontinuously and not around landing phase (Fig.C).

space spanned by z_1-z_2-z_3 as shown in Fig.3. The figure shows the orbit for three cycles starting from the perturbation labeled as 'perturbation applied'. Double support phase(DS) and single support phases(SS) was distinguished by their colors, both Figs. A and B displayed same one trial where the perturbation is applied during SS. As shown in figure B, the orbit gradually approaches the limit cycle after perturbation tracking different route among first cycle and two cycles after that.

Isochron

Fig. 4 shows the calculated isochron by connecting the points on orbit from 1st to 5th cycle after the perturbation. Isochron exists as surrounding the limit cycle and the direction of the flow of isochron heads opposite the flow of motion without the part of DS. In DS, the direction of flow of isochron changes at the center of DS, and the flow of isochron concentrated at the connection of DS and SS, i.e. hopping time (Fig.4B). This discontinuous of the flow cannot be observed around landing time(Fig.4C). This result indicates the phase is tuned by the hopping event against frontal perturbation.

4. CONCLUSION

Isochron of the human walking was depicted by the experiment with frontal perturbation. The derived isochron showed disconnection at hopping considered to be the effect of rhythm tuning.

REFERENCES

[1] S.Yakovenko, et. al., *Biol Cyber*, Vol. 90, No. 2, pp. 146–155, 2004.

[2] Y. Kuramoto. Chemical Oscillations, waves, and Turbulence. Springer-Verlag, 1984.

[3] T.Funato, et. al., *Exp Brain Res*, Vol. 205, No. 4, pp. 497–511, 2010.

Only the Groucho number ensures dynamic similarity during walking

Emanuel Andrada and Reinhard Blickhan

Science of Motion, Institute of Sport Science, Friedrich-Schiller-Universität, Jena, Germany
(Tel : +49-3641-94710; E-mail: emanuel.andrada@uni-jena.de)

Abstract: In this paper, we present a method to assess dynamical similarity in bipedal walking based on a dimensionless bipedal spring-mass model (BSMM). We first introduce a new formulation of the BSMM based on the Groucho number. We discuss, afterwards, how to experimentally measure the necessary parameters. The use of the dimensionless bipedal spring-mass model permits to evaluate whether two systems operate dynamically similar, and to judge whether these systems walk in a self-stable region.

Keywords: bipedal spring-mass model, dynamic similarity, bipedal locomotion, Groucho number.

1. INTRODUCTION

Not only Humans are able to walk bipedally. Also many avian species are successful as semi or complete terrestrial animals. Interestingly, the evolutionary constrains imposed by the avian body plan leads to a different geometrical construction of avian legs compared with those in humans. Based on theropod hindlimb configuration, that of birds was highly modified during evolution. The femur was shifted to a more horizontal orientation and relatively shorted. Bones of the distal limb segments have been fused and modified, leading to the tibiotarsus and tarsometatarsus. Overall changes in hindlimbs geometry are understood as adaptations to cursorial locomotion, to leap from the substrate during takeoff, and to absorb the shock of landing [1, 2]. Finally, birds do not walk with the soles of their feet, like humans do, but on their toes (digitigrade locomotion).

Different patterns in limb proportions and orientation may reflect different segment usages and loadings, and thus different local kinematics and dynamics. On the other hand, that fact does not exclude that global locomotion during walking used by humans and birds could not be dynamically similar. We think, this question was not adequately addressed so far.

Specially since popularized by Alexander [3], the Froude number (Fr) $Fr = u^2/gh$ has been used so far to compare bipedal and quadrupedal locomotion. Here, u is the cursorial velocity, h is the leg length, and g is gravity. The Froude number is directly related to the inverted pendulum, as it actually reflects the ratio between inertial and gravitational forces during walking or running. The inverted pendulum template, however, cannot adequately reflect the dynamics of walking.

The simplest model, which is able to reproduce bipedal gait dynamics, i.e. motions of the centre of mass (CoM) and ground reaction forces (GRF), is the bipedal spring-mass model (BSMM) [4]. Although human legs are complex in structure and control, it seems that they can generate a spring like behavior during walking at moderate speeds [6]. Until now, the BSMM was formulated only dimensional. Results were afterwards converted to dimensionless description using the Fr for speed. But, as stated before, Fr may not be an adequate quantity to characterize dynamic similarity of compliant systems. In that case, dynamic similarity can only be ensured, if both systems have the same Groucho number (Gr), $Gr = u\omega_0/g$. here, u is the cursorial velocity, ω_0 is the natural frequency of the system, and g is gravity [5]. In this paper, we present a method to assess dynamic similarity in bipedal walking based on a dimensionless BSMM. We first introduce a new formulation of the BSMM based on the Gr. We discuss, afterwards, how to measure experimentally the necessary parameters. Finally we demonstrate how we can use this formulation to compare the dynamics of two systems and whether these two systems walk in a self-stable region.

2. METHODS

2.1 Dimensionless bipedal spring-mass model

The template for this study is a dimensionless BSSM. This describes the action of the stance leg(s) by a (two) dimensionless linear spring(s) of leg stiffness $\hat{k} = kl_0/mg$. Note that the dimensionless rest length $\hat{l}_o$ is equal to $\hat{k}$. The dimensionless equations of motion restricted to the sagittal plane are:

$$\ddot{\hat{x}} = -\hat{k} \sum_{i=1}^{a} \left(\frac{\hat{x}_{FPi}}{\hat{l}_i} - \frac{\hat{x}_{FPi}}{\hat{l}_0} \right) + \hat{x} \sum_{i=1}^{a} \left(\frac{\hat{l}_0}{\hat{l}_i} - 1 \right) \qquad (1)$$

$$\ddot{\hat{y}} = -1 + \hat{y} \sum_{i=1}^{a} \left(\frac{\hat{l}_0}{\hat{l}_i} - 1 \right) \qquad (2)$$

where $a = 1$ for the single (SSPh) and 2 for the double support phase (DSPh). All following quantities are dimensionless: $\ddot{\hat{x}}, \ddot{\hat{y}}, \hat{x}, \hat{y}$ are the accelerations, and positions of the CoM. $\hat{x}_{FPi}$ is the horizontal distance between CoM and foot (feet) position(s), and $\hat{l}_i$ is the leg length of the stance leg(s). A dimensionless model is characterized by a minimal set of parameters. In our case we chose the dimensionless stiffness $\hat{k}$, the angle of attack α_0, the leg compression λ, and the Groucho velocity Gr.

2.2 Simulation

Simulations start when the supporting leg is oriented vertically ($\hat{x} = \hat{x}_{FPi} = 0$), initial height $\hat{y}_0 = \hat{l}_0 - \lambda$, and horizontal velocity equal to the Gr. The model switches to the DSPh when for leg 2 the condition $\hat{y} = \hat{l}_0 \sin \alpha_0$ is met. Then it returns to SSPh when for leg 1 $\hat{l}_1 = \hat{l}_0$. We exploit the convergence to fixed points to find steady-state locomotion. We map the space (Gr, $\hat{k}$, α) for different λ. If any of these states lies in the basis of attraction of a fixed point, the model converges to steady-state trajectories. We accept a fix point as stable if the simulation reaches 100 steps.

2.3 Experimental Parameters

In order to compare different systems such as humans or animals, four parameters have to be experimentally determined: $\hat{k}$, α_0, Gr, and λ. As leg length in our model is symmetric related to touch down (TD) and take off (TO) events,   some assumptions have to be made, in order to determine k (for both humans and birds leg length is longer at TO compared with TD). So we compute k as $k = GRF_{midstance}/\Delta l$, where $\Delta l = ((l_{leg(TD)} + l_{leg(TO)}) / 2) - l_{leg(midstance)}$. α_0 represents leg orientation with respect to the ground at TD. Gr is the cursorial velocity, and λ can be obtained as $\lambda = GRF_{midstance}/BW$.

3. RESULTS, DISCUSSION & FURTHER WORK

Depending on the chosen parameters, the model converges or not to steady-state locomotion. As we fix λ, we can also investigate whether the fixed points are shifted to lower or higher values of λ compared to its starting value (basin of attraction). As an example Fig. 1 displays fixed points for simulations started at a λ = 0.9. Six stable walking sub-domains are revealed.

At lower Gr velocities, the number of peaks in the vertical GRF increases up to seven. In Fig. 1, the fix points are presented divided into three clusters, depending on the final λ value (black $0.8 \leq \lambda \leq 0.95$, magenta $\lambda < 0.8$ and blue $\lambda > 0.95$). As expected, stable solutions do not exist for $\lambda > 1$ in the M-shape sub-domain. Furthermore, only a discrete set of start parameters result in stable operation at λ values close to 0.9. Our results show that for an even number of peaks, λ should be lower as 1, while for uneven number of peaks, it should be higher than 1. This can be explained mostly by means of the symmetry of the GRF. On the other hand, it seems that λ never reaches the value of 2. Using data from the literature [6] and the method explained in section 2.3 we had been able to locate a point which represents human walking at 1.15 m/s. Normal values of λ at those speeds seem to oscillate about ~ 0.85 [6].
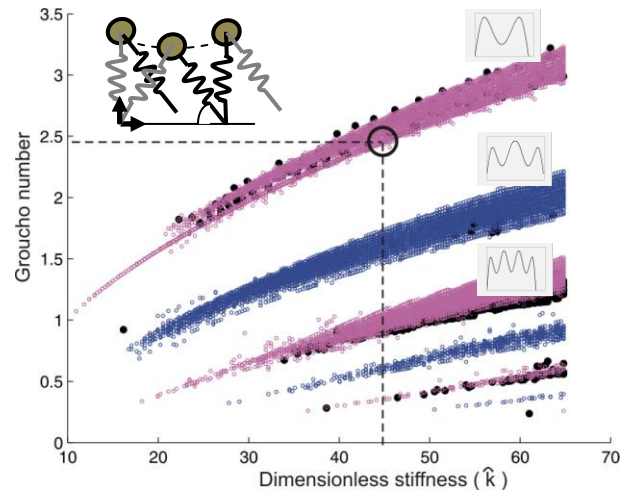
Fig. 1 Dimensionless stable walking sub-domains using leg compression λ = 0.9 as start parameter.

The point computed is located inside the stable region between fix points of λ values close to 0.9 and below 0.8 (Fig.1). Lower values of λ increase the width of the M-shape sub-domain, and diminish that of the multi-peak sub-domains. Lower values of λ increase also the vertical excursion of the CoM, which may lead to an increase in the cost of transport. Therefore, it seems that humans use rather self-stable walking regions, which minimize energy consumption (system parameters optimized for "endurance walking").

Also the analysis of the influences of body-size (child, adult), or leg-stiffness (young, old) on walking dynamics must be based on an adequate dimensionless formulation.

We are now performing, in cooperation with the Inst. of Systematic and Evolutionary Zoology of the University of Jena, kinematic and dynamic studies on small birds like quails using high-speed x-ray motion analysis and custom designed force plates. Results of these experiments will be examined with respect to dynamic similarities or differences.

REFERENCES

[1] R.J. Raikow, Locomotor system. *in Form and Function in Birds*,   Academic Press, London, 1985.
[2] S.M. Gatesy, "Hind Limb Scaling in Birds and other Theropods: Implications for Terrestrial Locomotion", *J. Morph.*,   No. 209, pp. 83-96, 1991.
[3] R.M. Alexander, "Estimates of Speeds of Dinosaurs" *Nature* No. 261, pp. 129-130, 1975.
[4] H. Geyer et al., "Compliant Leg Behavior Explains Basic Dynamics of Walking and Running " *Proc. R. Soc. B,* No. 273, pp. 2861-67, 2006.
[5] T.A. McMahon et al., "Groucho Runing",   *J. Appl. Physiol.,* Vol. 62, No. 6, pp. 2326-37, 1987.
[6] S.W. Lipfert, *Kinematic and Dynamic Similarities between Walking and Running*, Verlag Dr Kovac, Hamburg, 2010.

Perception, motor learning, and speed adaptation exploiting body dynamics: case studies in a quadruped robot

Matej Hoffmann[1], Nico Schmidt[1], Kohei Nakajima[1], Fumiya Iida[2], and Rolf Pfeifer[1]

[1]Artificial Intelligence Laboratory, Department of Informatics, University of Zurich, Switzerland
E-mail: {hoffmann, nschmidt, nakajima, pfeifer}@ifi.uzh.ch
[2]Institute of Robotics and Intelligent Systems, Swiss Federal Institute of Technology Zurich, Switzerland
E-mail: fumiya.iida@mavt.ethz.ch

Abstract: Animals and humans are constantly faced with a highly dimensional stream of incoming sensory information. At the same time, they have to command their highly complex and multidimensional bodies. Yet, they seamlessly cope with this situation and successfully perform various tasks. For autonomous robots, this poses a challenge: robots performing in the real world are often faced with the curse of dimensionality. In other words, the size of the sensory as well as motor spaces becomes too large for the robot to efficiently cope with them in real time. In this paper, we demonstrate how the curse of dimensionality can be tamed by exploiting the robot's morphology and interaction with the environment, or the robot's embodiment (see e.g., [1]). We present three case studies with underactuated quadrupedal robots. In the first case study, we look at terrain detection. While running on different surfaces, the robot generates structured multimodal sensory information that can be used to detect different terrain types. In the second case study, we shift our attention to the motor space: the robot is learning different gaits. The online learning procedure capitalizes on the fact that the robot is underactuated and on a "soft" control policy. In the third case study, we move one level higher and demonstrate how - given an appropriate gait - a speed adaptation task can be greatly simplified and learned online.

Keywords: legged robot, terrain detection, locomotion learning, speed adaptation, body dynamics
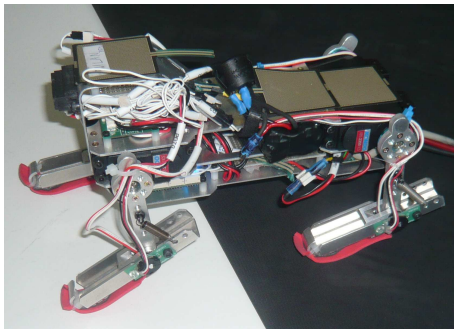
Fig. 1 **Quadruped robot used in case studies 1, 2.** A total of 12 sensors from 4 modalities (4 pressure sensors on feet, 4 angular sensors in passive knee joints, 3 acceleration sensors, and 1 infrared sensor) were used.

1. EXPERIMENTAL SETUP

We have used two underactuated quadrupedal robots in our case studies. They had four identical legs driven by position-controlled servomotors in the hips. The 'knees' were passive and had springs attached. The mechanical design (the weight distribution, proportions, springs used etc.) is a result of our previous research [2]. The robot used in the first two case studies can be seen in Fig. 1.

2. CASE STUDY 1: TERRAIN DETECTION

The first case study dealt with perception, in particular terrain classification. In mobile wheeled robots, this problem is typically solved through fusion of several several distal, i.e. non-contact, sensors (e.g., cameras, laser range finders), followed by supervised classification into traversable vs. non-traversable terrain. Sensing using non-contact sensors has the obvious advantage that information is available ahead of time. On the other hand, such sensors deliver information relevant for traversability in a very indirect manner. Therefore, we have decided to follow an alternative strategy: we want to profit from a full-fledged interaction of the robot with the ground. Following the approach of Lungarella and Sporns [3], who studied how active generation of multimodal sensory stimulation delivers structured sensory information, we have employed information-theoretic methods (mutual information and transfer entropy) that explicitly compare not only sensory but sensory-motor information structure generated by the robot running on different grounds.

3. CASE STUDY 2: LEARNING GAITS

In case study two, we have shifted our attention to the problem of motor learning. The state of the art in robotics can be characterized by two different streams. The first, "traditional", stream employs control laws that prescribe trajectories to the robot's body and the legs and then enforce them using stiff, high-power, actuation. A model of the robot's forward and inverse kinematics and/or dynamics is required. The robot is then capable of precisely executing arbitrary trajectories, picking specific footholds for instance. A good example is the Little Dog [4]. The second "stream" draws inspiration from biology, following the observation by Marc Raibert that the brain does not control the body, but makes suggestions only. The goal is not to override the complex dynamics of the body

in the environment but rather exploit it and channel it in particular directions. This strategy results in simplification of central control and greater energy efficiency. Pfeifer et al. [1] provide an overview. We have also conducted studies in a similar vein [2] that gave rise to the quadruped platforms used in this study. Nevertheless, the robots coming out of these studies still lack the versatility of the robots that follow the "strong control" paradigm - they are often restricted to a single gait (an extreme example being the passive dynamic walkers).

In this case study we have conducted preliminary experiments in online learning of different gaits in our underactuated quadruped platform. We use online optimization (simulated annealing - SA) to acquire signals for four active joints of the robot. By taking advantage of the symmetries of the body, we managed to reduce the dimension of the parameter space to mere 7 parameters - to our knowledge, this is extremely low - for instance, Chernova and Veloso [5] faced 54 dimensions in the AIBO robot. We have successfully learned gaits for different speeds and also some turning gaits. Typically, tens of iterations of the SA algorithm (with 30 seconds per iteration, for instance) were required to learn a gait. Videos of the gaits will be shown at the conference.

This case study demonstrates that learning is possible in real time. This follows from the underactuated nature of the robot and the "soft" control policy. It is not only the number of actuated degrees of freedom that is responsible for the shrinking dimensionality; it is also the control "philosophy". Whereas in the AIBO or Little Dog the trajectory of the legs as well as the body is parametrized, in our case, we prescribe signals to the actuators only - everything else (e.g. COM trajectory) is emergent from the interplay of the actuators, the body, and the environment.

4. CASE STUDY 3: SPEED ADAPTATION

In our third case study, we closed the perception-action loop and studied a feedback control scenario. The robot equipped with an ultrasonic distance sensor should keep a fixed distance from the treadmill end and respond to changes of speed of the running belt and to changes of the target distance. The difficulty of the task largely depends on the complexity of speed modulation in the robot. We have developed a bounding gait in which the speed can easily be controlled with a single paramater - frequency of all legs. Moreover, the relationship between the frequency and the resulting speed of the robot was linear and the gait covered a big range of speeds, from 4 to 28 cm/s (or 0.25 to 1.7 of robot's length). The task could then be accomplished with a simple proportional-derivative (PD) control of a single parameter: frequency. The controller was tuned by an online parameter search for the P and D gains using the simulated annealing algorithm. A sample of the performance is depicted in Fig. 2.

We have shown how the speed adaptation task in a legged robot can be simplified to the maximum and hence learned online. Let us analyze the components that are responsible for this behavior. First, the characteristics of
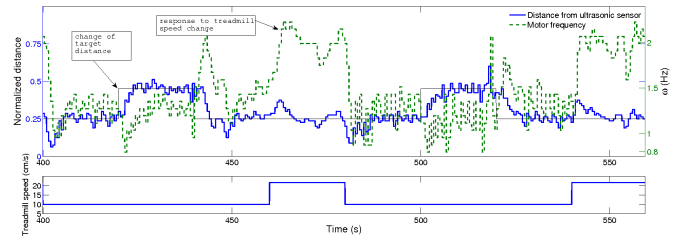
Fig. 2 **Speed adaptation performance.** The top graph shows the target (target distance - black line) tracking performance by the robot (actual distance measured by sensor in blue; distance had a range 10-90 cm and was normalized). When the target moves, the robot needs to respond with an appropriate change in frequency (green dotted line). The same applies when the treadmill speed (bottom graph) changes.

the gait - linear relationship of frequency to speed plays a key part. Second, the optimization algorithm has come up with a high gain controller, which allows for quicker responses and better tracking performance. However, it also results in oscillations of the control parameter (cf. Fig. 2, top). Interestingly, the system could absorb the large perturbations. We hypothesize that this was possible due to mechanical self-stabilization of our system [2]. Third, the fact that a new control parameter can be introduced at any time further simplifies the situation and allows for quicker responses.

5. ACKNOWLEDGMENTS

REFERENCES

[1] R. Pfeifer, M. Lungarella, and F. Iida, "Self-organization, embodiment, and biologically inspired robotics," *Science*, vol. 318, pp. 1088–1093, 2007.

[2] F. Iida, G. Gómez, and R. Pfeifer, "Exploiting body dynamics for controlling a running quadruped robot," in *Proc. Int. Conf. Advanced Robotics (ICAR05)*, Seattle, U.S.A., 2005, pp. 229–235.

[3] M. Lungarella and O. Sporns, "Mapping information flow in sensorimotor networks," *PLoS Comput Biol*, vol. 2, pp. 1301–12, 2006.

[4] J. Buchli, M. Kalakrishnan, M. Mistry, P. Pastor, and S. Schaal, "Compliant quadruped locomotion over rough terrain," in *Proc. IEEE/RSJ Int. Conf. Intelligent Robots and Systems*, 2009, pp. 814–820.

[5] S. Chernova and M. Veloso, "An evolutionary approach to gait learning for four-legged robots," in *Proc. IEEE/RSJ Int. Conf. Intelligent Robots and Systems*, 2004, pp. 2562 – 2567 vol.3.

Dynamic Self-organizations of motor-proteins under non-equilibrium condition

Akira Kakugo[1,2], JianPing Gong[1]

[1]Division of Life Science, Faculty of Science, Hokkaido University Sapporo 060-0810, Japan.
[2]PRESTO, Japan Science and Technology Agency, 4-1-8 Honcho Kawaguchi, Saitama 332-0012, Japan
(Tel : +81-11-706-3474; E-mail: kakugo@sci.hokudai.ac.jp)

Abstract: In this study, we show that the energy-dissipative active self-assembly of microtubules (MTs) via a kinesin-based motility system produces various MT assemblies such as bundle-, network-, and ring-shaped structures depending on the initial conditions. Structural polymorphism of the MT assembly is depicted through phase diagrams, and morphogenesis of the MT assembly is discussed based on the following factors; binding force between MTs and motility-driving force from kinesins. This study provides new insights into the energy-dissipative dynamic self-organization of biological systems.

Keywords: Microtubules; active self-assembly; bottom-up approach

1. INTRODUCTION

Cytoskeletal proteins such as actins and microtubules and their motor proteins, *i.e.* myosins and kinesins, are known to play important roles in the formation of cellular shapes.[1–4] It has been demonstrated that isolated actins and microtubules can be self-organized into structures with specific patterns such as asters, networks, rings, and so on, associating with their motor proteins.[5–9] Other efforts have been also made to integrate cytoskeletal proteins into an ordered structure to exploit more complex functions in vitro, as observed in nature.[10, 11] Recently, to quest more complex assemblies, a method to integrate MTs into a bundle structure on a kinesin-coated surface has been developed by employing a streptavidin (St)-biotin (Bt) interaction during the sliding motion of MTs in the presence of ATP.[6] This ATP-driven, energy-dissipative self-assembly process was termed as an active self-assembly (AcSA) process and AcSA is different from a conventional self-assembly process that occurs towards the thermodynamic equilibrium without any external energy supply. Therefore, we termed the latter as a passive self-assembly (PaSA) process.[12] Indeed, AcSA process has been widely and intensively studied to obtain new insights into emergent properties found in living cells.[13, 14] Thus, AcSA has great potential to facilitate various motor protein assemblies in terms of the sizes, shapes, and properties of motion. In this study, we systematically studied the effects of initial conditions such as the Bt to tubulin (Tub) ratio, St/Bt ratio, and Tub concentration (C_{Tub}) that may strongly influence the morphology of the MT assembly produced through the AcSA process.

2. RESULTS AND DISCUSSION

Effect of St/Bt modification on motility of MT

The AcSA process requires the motility of the MTs. Because it was considered that the high molecular weight of St might prevent MTs from binding to kinesins because of steric hindrance, we first investigated the effect of the modification ratio of St / Bt on the motility of individual MTs keeping the Bt/Tub at 1/1. Consequently, the velocity of the MTs were obtained as 0.129, 0.059, 0.054 and 0.045 μm/s for the St/Bt ratio of 0, 1/64, 1/16 and 1 respectively. Thus, MT velocity was slightly decreased with the increase of the St/Bt ratio and this suggested that the total driving force exerted on MTs should be decreased due to the reduced interaction of MTs with kinesins. Fixing the St/Bt ratio at 1/2, we also investigated the effect of Bt/Tub on the motility of MTs. On changing the Bt/Tub ratio from 1/64 to 1/1, MTs velocity was found to lie in the range of 0.03~0.05 μm/s, without showing any regular change.
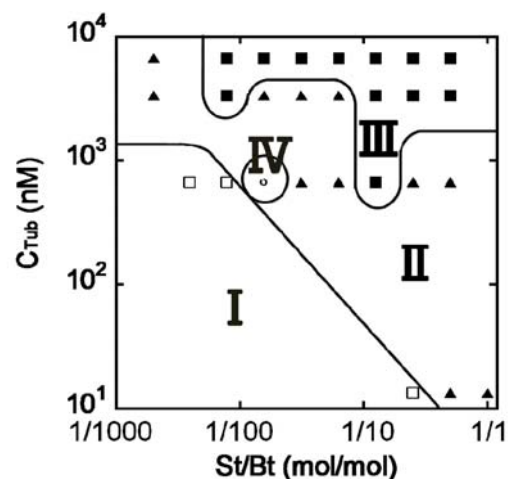
Figure 1. Phase diagram for the morphology of MTs assemblies, in which the phase behavior is summarized as a function of the St/Bt ratio and C_{Tub} for constant a molar ratio of Bt/Tub = 1/1; □: single MT phase (I); ▲: bundle phase (II); ■: network phase (III); ○: ring shaped assemblies dominant (IV).

Effect of C_{Tub} and the St/Bt ratio on the structural morphology of MT assemblies

Next, we investigated the effect of C_{Tub} and the St/Bt ratio on the morphology of MT assemblies. Based on the result in the Bt/Tub ratio study, the Bt/Tub ratio was fixed at 1/1 to allow the MTs to form assemblies effectively. To study the structural variety of the MT assemblies, C_{Tub} and the St/Bt ratio were widely varied from 13.4 nM to 6720 nM and from 1/256 to 1/1, respectively. Under the experimental conditions stated above, the morphology of MTs was observed under the fluorescent microscope after 4 h of the AcSA process. The C_{Tub} and St/Bt phase diagram is shown in

Figure 1.   When C_{Tub} was in a lower range as 13.4 – 672 nM, the MTs existed as single filaments in the lower St/Bt region (I) and were in the bundled state in the high St/Bt region (II).   When C_{Tub} was in a higher range as 3360 – 6720 nM, networks of MT assemblies were observed in the high St/Bt region (III).   However, the boundary between phase II and III in the C_{Tub} and St/Bt phase diagram was complicated. A singular point (IV) where ring-shaped MTs assemblies were preferentially observed was found as shown in Figure 1.   The point IV emerged in close vicinity to the complex boundary of phase II and III (C_{Tub} ~ 672 nM, St/Bt ~ 1/64).   The diameters of the ring-shaped MT assemblies observed in this region were widely distributed (1.1 μm~13.2 μm), and the preferential rotation of those assemblies in a CCW was still preserved (CCW/clockwise (CW) = 33/7).   These results agree well with those reported in a previous paper.[15, 16]

Discussion of the polymorphism of MT assembly

It was considered that the factors such as binding force between MTs, driving force, and sticking that disturb the sliding motion, are responsible for the polymorphism of MT assembly.   The binding force between MTs was expected to increase with increasing St/Bt ratios up to a certain optimum ratio.   Meanwhile, the driving force exerted on MTs may decrease by increasing St/Bt ratios because of the steric hindrance of Sts and may reach a plateau after Sts fully covers the Bts on MTs.   Motility of sliding MTs could be disturbed by increasing the St/Bt ratio, which results in an increased steric hindrance, being diminishing the chance of interaction among kinesins and MTs.   Here, we focus again on the C_{Tub} of 672 nM.   When the St/Bt ratio was smaller than 1/128, single MTs were observed.   This can be attributed to the low binding force between MTs and the high driving force for dissociating the cross-linked MTs.   Under such conditions, ring or bundle formation may be difficult to achieve.   The ring-shaped MT assemblies observed in the bundle phase appeared between the single and network phase.   In this region, large amounts of single MTs were observed at the beginning of the AcSA process.   This suggests that the relatively large driving forces and moderate binding forces suppress the formation of bundle-shaped assemblies but facilitate the formation of ring-shaped assemblies, in which a configuration with intrafilament interactions is favorable. With further increases in the St/Bt ratio, the binding force increases, and the driving force simultaneously decreases. This may facilitate the interfilament cross-linking needed to form MT bundles.   The bundled MTs may also suppress the formation of a ring-shaped assembly because of the increased rigidity.   At the optimum St/Bt ratio, the highest cross-linking efficiency will be a trade-off between the binding and driving forces.   Under optimum condition, MTs will be cross-linked even if there are not many cross-linking points.   Therefore, cluster-like aggregations may appear in this phase (III).   The optimum St/Bt ratio for network formation was determined to be approximately 1/8, which was not the stoichiometric ratio that we expected.   Thus, the polymorphism of the MT assembly may result from the close coupling of these factors.

Conclusions

In this study, we showed that MTs were self-organized into various structures (linear, bundles, network, and rings) in response to initial conditions of C_{Tub}, St/Bt ratio, and Bt/Tub ratio through AcSA.   We also showed that the ring-shaped assemblies were preferentially formed under a specific condition.   These results indicated that not only the density of the MTs but also other factors such as driving force, binding force, and steric hindrance were responsible for the polymorphism of MT assembly.   We expect that the present study will provide new insights into the energy-dissipative dynamic self-organization processes of biological systems. In future, the knowledge in dynamic self-organization process may also widen the range of potential applications of motor proteins in biodevices and biomachines.

REFERENCES

[1] D. J. Sharp, G. C. Rogers, J. M. Scholey, *Nature*, 2000, **407**, 41-47.

[2] T. Pollard, *Nature*, 2003, **422**, 741-745.

[3] M. L. Gardel, K. E. Kasza, C. P. Brangwynne, J. Liu, D. A. Weitz, *Methods Cell Biol.*, 2008, **89**, 487-519.

[4] J. Stricker, T. Falzone, M. L. Gardel, *J. Biomech.*, 2010, **43**, 9-14.

[5] F. J. Nédélec, T. Surrey, A. C. Maggs, S. Leibler, *Nature*, 1997, **389**, 305-308.

[6] H. Hess, J. Clemmens, C. Brunner, R. Doot, S. Luna, K. H. Ernst, V. Vogel, *Nano Lett.*, 2005, **5**, 629-633.

[7] P. Kraikivski, R. Lipowsky, J. Kierfeld, *Phys. Rev. Lett.*, 2006, **96**, 258103.

[8] V. Schaller, C. Weber, C. Semmrich, E. Frey, A. R. Bausch, *Nature*, 2010, **467**, 73-77.

[9] R. Kawamura, A. Kakugo, Y. Osada, J. P. Gong, *Nanotechnology*, 2010, **21**, 145603.

[10] T. B. Brown, W. O. Hancock, *Nano. Lett.*, 2002, **2**, 1131.

[11] W. Roos, A. Roth, E. Sackmann, J. P. Spatz, *Chem. Phys. Chem.*, 2003, **4**, 872.

[12] G. M. Whitesides, B. Grzybowski, *Science*, 2002, **295**, 2418-2421.

[13] V. Schaller, C. Weber, C. Semmrich, E. Frey, A. R. Bausch, *Nature*, 2010, **467**, 73-77.

[14] P. Kraikivski, R. Lipowsky, J. Kierfeld, *Phys. Rev. Lett.*, 2006, **96**, 258103.

[15] R. Kawamura, A. Kakugo, K. Shikinaka, Y. Osada, J. P. Gong, *Biomacromol.*, 2008, **9**, 2277-2282.

[16] H. Liu, E. D. Spoerke, M. Bachand, S. J. Koch, B. C. Bunker, G. D. Bachand, *Adv. Mater.*, 2008, **20**, 4476-4481.

Robot Head Stabilization During Periodic Locomotion Using Adaptive Dynamical Systems

Sébastien Gay[1−2] Auke Ijspeert[1] and José Santos-Victor[2]

[1]Swiss Federal Institute of Technology, Switzerland - [2] Instituto Superior Técnico, Portugal

Abstract: We present a gaze stabilization system using only visual information as feedback for a self tuning dynamical system. We describe how the dynamical system tunes its internal parameters to those of the optical flow information to generate compensatory commands. We show that the system can be applied to head stabilization during periodic locomotion, but also to tracking periodically moving objects.

Keywords: gaze stabilization, adaptive frequency oscillators, dynamical systems, optical flow, vision, locomotion.

1. INTRODUCTION

Robot head stabilization is usually achieved by using a fast vestibular sensor in the head of the robot as main sensory input and applying a gain function to the rotational information it provides to generate compensatory commands for the head. These gains are usually modulated by computing the remaining retinal slip in the camera image, typically using optical flow ([5], [2], [3]). These approach reach good performance but require the presence of both a camera and a vestibular sensor in the head of the robot. Furthermore they usually can handle only rotations of the head. Typically, during locomotion, the motion of the head of the robot is a combination of rotations and translations.

In this paper, we investigate how well the head can be stabilized by using visual information alone. This may seem like a big restriction due to the relative slowness of the camera sensors, but since our main target is gaze stabilization during locomotion, we can make some simplifications. Assuming that the motion of the head of the robot during locomotion around each axis to stabilize is periodic and close to a sine wave, we use adaptive dynamical systems to learn the frequency and phase shift of the optical flow and generate compensatory signals with the proper amplitude to reduce the optical flow to a minimum. The commands are generated at a much higher rate than that of the optical flow, and are, at convergence, perfectly phase locked with the visual feedback. The system then becomes mostly feedforward and tries to predict the parameters of the compensatory signals before the feedback arrives. We show that this system can be used during periodic locomotion and for object tracking similarly.

2. THE DYNAMICAL SYSTEM

Our head stabilization simply uses one oscillator per degree of freedom to stabilize, getting feedback from the optical flow and outputting commands for that degree of freedom. Our oscillator is based on Adaptive Frequency Oscillators (AFOs, [1], [4]), dynamical systems generating sine shaped oscillations and capable of tuning their internal frequency to that of an external forcing signal. The equations of our system are given next:

$$\dot{r} = \gamma(1 - r^2)r \tag{1}$$
$$\dot{\phi_1} = \omega - \sin\phi_1 \epsilon F \tag{2}$$
$$\dot{\phi_2} = \omega - \sin\phi_2 \beta F \tag{3}$$
$$\dot{\omega} = -\sin\phi_1 \kappa F \tag{4}$$
$$x = r\cos\phi_2 \tag{5}$$
$$\dot{\alpha} = -\eta x F \tag{6}$$
$$\theta = \alpha x + O \tag{7}$$

where r is the radius of the limit cycle of the oscillator (i.e. the amplitude of its oscillations), ϕ its phase, ω its frequency and θ its output here used to control the position of the head actuator. α here directly defines the amplitude of the oscillations and O their offset. F is an external forcing signal (here the opposite of the mean optical flow). κ, β, ϵ and η are scaling factors for the forcing signal. This oscillator is equivalent to a standard AFO merged with a Hopf oscillator and sharing its radius and frequency (Equations 1, 2 and 4 define an AFO while Equations 1 and 3 define a Hopf). This oscillator allows us to control the speed of convergence of the frequency, the amplitude and the phase locking of the output oscillations with the forcing signal independently, by setting the corresponding scaling factors.

The amplitude α is initially set to zero. When the oscillator is synchronized with the forcing signal, the correlation between x and F becomes positive on average and the amplitude of the compensatory oscillations α starts increasing. This leads to the optical flow decreasing until it reaches a minimum, causing frequency, amplitude and phase shift to stop evolving. Perturbations in the parameters of the forcing signal are tracked and damped out by the system.

3. THE VISUAL FEEDBACK

The oscillator described before generates sine shaped oscillations but outputs nothing in open loop since the amplitude α is initially set to 0. To bring the system to generate compensatory signals, it has to be excited by a properly chosen signal. It is necessary and sufficient that the chosen feedback satisfies the following conditions: it should have zero mean, have the same frequency and

phase as the motion of the head of the robot and decrease monotonically to zero when the head is stabilized around the considered axis. Note that the signal can come from any sensor and does not need to be an estimate of the head rotation. In this paper we use optical flow since it does not require any extra sensor, is very easy to compute and by default satisfies the conditions given earlier.

To stabilize the gaze of the robot using three axis in the head we typically use three instances of our oscillator with as forcing signals F the y component of the mean optical flow vector for the pitch axis, its x component for the yaw, and for the roll the y component of the difference between the mean vectors computed in the left and right quarter of the camera image. Note that the forcing for the roll axis assumes that the actuator rotates the camera around the center of the image, which is not always true. In particular, for robots having two eyes distributed around the actuator axis, this forcing may be adapted using the left quarter of the left image and the right quarter of the right one.

4. RESULTS

We applied our system in simulation on the Hoap2 humanoid robot walking and the salamander shaped robot *Salamandra Robotica* swimming, with qualitatively similar results (check the video[1]) Figure 1 shows the evolution of the important quantities of the system when the salamander robot is swimming. *Salamandra Robotica* is a modular 12 DoF robot controlled by Central Pattern Generators (CPG) allowing it to swim by generating a traveling wave along its body. For our experiment, the frequency of the swimming wave is initially set to 1Hz and switched to 1.5Hz at $t = 30s$. The frequency converges to that of the forcing signal for each axis. Note that the frequency of the motion around the pitch axis is twice that of the other axis. This is specific to this gait and environment and is discovered automatically by the system. When the change of frequency occurs at $t = 30s$, the system tracks it and converges to the new values. The compensatory commands generated cause the optical flow to be reduced to less than 5 pixels/frame, almost half of which is due to the forward motion of the robot.

As said earlier, we use only visual information, optical flow, to stabilize the head of the robot. In addition to the aforementioned pros of doing that, using visual feedback has the advantage of giving movement information independently whether the robot is moving or an external object is moving in front of the robot. Thus the system can be applied without any modification (except for rescaling of the flow amplitude) to object tracking. When using optical flow, this assumes that only the object provides optical flow information (i.e. the rest of the scene is uniform). Instead, simple blob detection or object segmentation may be used. We successfully applied the system on the real Hoap3 robot tracking an apple attached to a spring allowing it to oscillate in front of the robot with different frequencies for the vertical and horizontal axis.

(a) pitch axis   (b) roll axis

(c) yaw axis   (d) optical flow
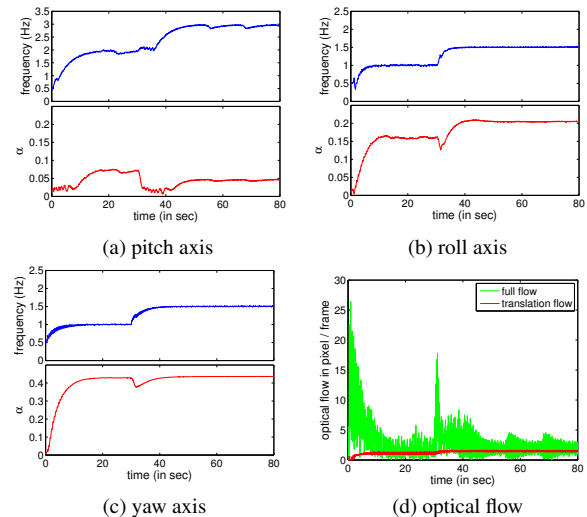
Fig. 1: Evolution of the frequency and the amplitude (α) of the oscillator when the salamander robot swimming. The frequency of swimming is initially 1Hz and at t = 30s the frequency is switched to 1.5Hz. Figure 1d shows the evolution of the mean optical flow magnitude over time as well as the flow due to the forward motion of the robot

5. CONCLUSION

We presented a method for stabilizing the gaze of the robot using an adaptive dynamical system excited by the optical flow information from the camera image. We showed that the system can be applied for periodic locomotion or for tracking periodically moving objects. At the moment, the main limitation of the system is the assumption of a nearly sine shaped motion of the head. In cases where the head motion is not sine like, the performance of the decreases. Future work will include ways to overcome this limitation, notably by embedding adaptive shape filters in the current dynamical system.

REFERENCES

[1] Jonas Buchli and AJ Ijspeert. Self-organized adaptive legged locomotion in a compliant quadruped robot. *Autonomous Robots*, pages 331–347, 2008.

[2] A Lenz, T Balakrishnan, A G Pipe, and C Melhuish. An adaptive gaze stabilization controller inspired by the vestibulo-ocular reflex. *Bioinspiration & Biomimetics*, 3(3):035001, September 2008.

[3] F Panerai, G Metta, and G Sandini. Learning visual stabilization reflexes in robots with moving eyes. *Neurocomputing*, 48(1-4):323–337, October 2002.

[4] L Righetti, J Buchli, and a Ijspeert. Dynamic Hebbian learning in adaptive frequency oscillators. *Physica D: Nonlinear Phenomena*, 216(2):269–281, April 2006.

[5] T Shibata and S Schaal. Biomimetic gaze stabilization based on feedback-error-learning with nonparametric regression networks. *Science And Technology*, 14:201–216, 2001.

---

[1]http://www.youtube.com/watch?v=GWG8RVWL_fo

Actively-compliant Leg for Dynamic Locomotion

Thiago Boaventura, Claudio Semini, Jonas Buchli, Darwin G. Caldwell

Department of Advanced Robotics, Italian Institute of Technology (IIT)
Email: {thiago.boaventura, claudio.semini, jonas.buchli, darwin.caldwell}@iit.it

Abstract: Dynamic legged locomotion of animals and humans is often described and studied by models, such as spring-mass or muscle models. To experimentally verify a wide range of such models, machines with torque-controlled joints are required. To this end, we present a torque-controlled robotic leg with high control performance that allows for example to implement virtual components such as exponential springs and dampers. A series of hopping experiments with different spring stiffness profiles demonstrates the versatility and advantages of this approach.

Keywords: Variable compliance, Spring mass model, Virtual components, Torque control.

1. INTRODUCTION

The use of legs for mobile robots is mainly motivated by the legs' superior ability to locomote in challenging terrains. The versatility needed to move in uneven environments usually limits the applicability of wheeled robots in scenarios such as construction sites, disaster recovery areas, and the field of service robotics.

To achieve the locomotion performance that is required for this kind of applications, a robot with torque controlled joints is needed. Torque control permits, for example, the control of the end-effector contact forces and impedance [1]. Moreover, Jacobian transpose force control (e.g. virtual model control [2]) and model based control techniques, such as inverse dynamics control, gravity compensation, and operational space control can be implemented straightforwardly. Having these control capabilities is not only desirable but mandatory for robust performance of robots in unstructured and partially unknown environments [3].

Furthermore, torque-controlled articulated robots can be exploited also for investigating hypotheses from other fields, such as biological motor control [4] and biomechanics. In these areas, systems-theoretical hypotheses on the control systems and the role of the mechanical structure of animals and humans are frequently formulated (e.g. [5]), but notoriously hard to validate. Moreover, theories about leg stiffness variations for different surfaces [6] and reasons for gait transitions and selection in running quadrupeds [7, 8] for instance can be experimentally validated.

In this contribution we will show that hydraulic actuation provides both robustness for handling large impact forces, and also high bandwidth for actively emulating passive elements. In dynamic locomotion, having virtual components instead of real ones represents a great advantage since it is possible to emulate elements that are hard to physically realize (e.g. nonlinear springs or muscle models). Furthermore, they permit to set parameters such as stiffness and damping for adapting to a specific task or terrain on the fly. This allows for instance to imitate the adaptation that constantly happens in Nature during dynamic locomotion. Legged animals, for example, adjust their leg stiffness according to the performed motion. With the actuation technology and control approach we present here, this natural behavior can be mimicked.

2. HYQ: A LOCOMOTION PLATFORM

The results we present here are part of the HyQ project [9]. HyQ is a quadruped robot that allows the study of highly dynamic, all-terrain locomotion, Fig. 1. It has 12 active degrees of freedom. The hip and knee flexion/extension joints are driven by hydraulic cylinders. The naturally very stiff hydraulic actuation has very peculiar characteristics that make it a good choice for highly dynamic articulated robots, such as its high power-to-weight ratio, fast response, robustness, and high force capabilities.
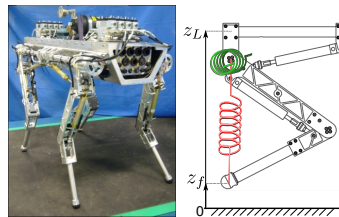
Fig. 1 HyQ robot (left) and leg virtual elements (right).

We implemented a high performance force-based impedance control for the HyQ leg. In a gait cycle, this controller is able to offer both fast movements during the flight phase and accurate force tracking during the stance phase.

3. EXPERIMENTS AND RESULTS

Spring mass models are generally known as good abstractions to describe the spring-like leg behavior found in human and animal walking and running [10]. To mimic this behavior, a Jacobian transpose based force control was used to emulate virtual systems on the articulated HyQ leg. The hip joint uses a rotational spring-damper. The knee instead employs a linear spring-damper, which is placed between the foot and the hip joint, Fig. 1. These virtual components are used to parametrize the desired compliance, e.g as needed for walking. We experimentally tested different stiffness profiles among them linear and exponential springs.

To implement hopping in place, we fixed the leg to a vertical slider that constrains it to perform only vertical movements. The length of the virtual linear spring ($l = 0.55\ m$) is then varied sinusoidally ($\delta l = 0.04\ m$) at a constant frequency of $1.6\ Hz$. Moreover, its stiffness is linearly changed from $800\ N/m$ to $3000\ N/m$.
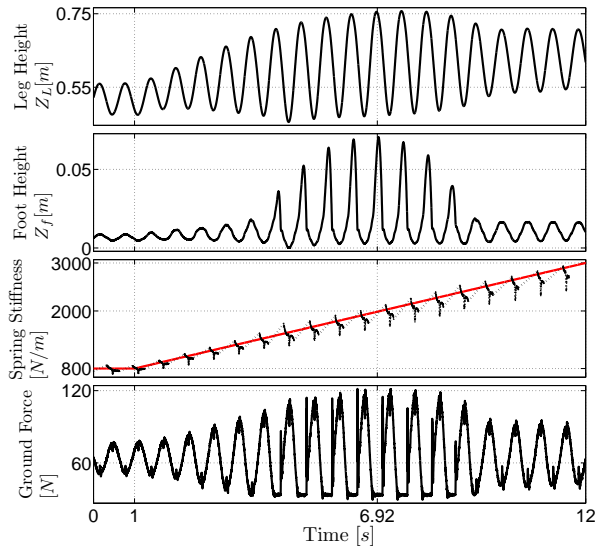
Fig. 2 Variably compliant system: keeping a sinusoidal excitation for the virtual spring length, the stiffness is linearly increased at a rate of $200\ N/ms$. This changing in stiffness alters the resonance frequency of the leg (spring-mass system) and for a certain range of stiffness it resonates and starts to hop.

As we can see in Fig. 2, during the first second the leg height Z_L is oscillating with a constant amplitude due to the sinusoidal variation in the length of the virtual linear spring. After $1\ s$, the spring stiffness starts to increase and, consequently, the amplitude of the leg height oscillation grows due to resonant effects. When the stiffness and thus the natural frequency of the spring mass system resonates with the sinusoidal spring length excitation, the leg starts to hop, as can be seen in the foot height (Z_f) plot. The resonance peak occurs at $6.92\ s$, when the stiffness is about $2000\ N/m$. The ground contact forces were measured by a force plate and, during the hopping, they reach a peak value of $120\ N$. The stiffness created by the virtual linear spring was plotted only for the stance phase and interpolated during the flight phase (dashed black line).
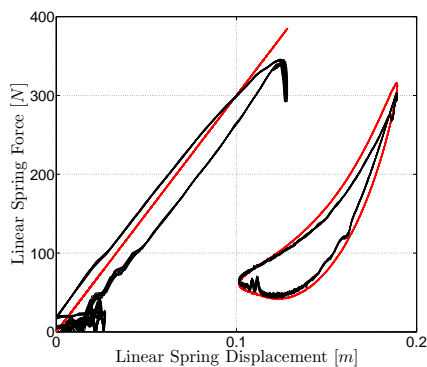

Fig. 3 Implementation of two different compliance profiles: a linear spring and an exponential spring-damper. The plot shows the reference profile created by the virtual component (red) and the real profile obtained (black).

The versatility of employing virtual components goes beyond the capability of dynamically changing parameters such as stiffness. They permit also to emulate muscle based actuation models of different complexities, ranging from simple springs to more complex models as shown in [11]. To demonstrate this ability, we present two different virtual components: a linear spring, and an exponential spring with constant damping coefficient. As it can be seen in Fig. 3, the stiffness tracking for both systems is limited by nonlinear phenomenas such as hysteresis and static friction. However, we consider the stiffness tracking satisfactory for most locomotion tasks.

4. CONCLUSIONS

Virtual components can, by using a high-performance force control, actively create a variable compliance actuation system without the insertion of any additional mechanical component. In our case, this compliance is entirely virtual (actively controlled), since hydraulic actuation is intrinsically very stiff. To demonstrate the versatility and dynamic motion capability of the HyQ leg, we implemented a virtual spring-damper system between the foot and the hip. Using this virtual system, as en example, we successfully implemented a hopping task by changing the leg stiffness on the fly.

The high-performance system we present opens new possibilities for investigating multidisciplinary aspects. Consequently, it represents a potential way to expand the current boundaries for dynamic locomotion in robotics.

REFERENCES

[1] N. Hogan, "Impedance control - an approach to manipulation. parts I, II, III," *ASME J. Dyn. Syst. Meas. Control*, vol. 107, pp. 1–24, 1985.

[2] J. Pratt, C. Chew, A. Torres, P. Dilworth, and G. Pratt, "Virtual model control: An intuitive approach for bipedal locomotion," *Int. J. Robot. Res.*, vol. 20, no. 2, pp. 129–143, 2001.

[3] J. Buchli, M. Kalakrishnan, M. Mistry, P. Pastor, and S. Schaal, "Compliant quadruped locomotion over rough terrain," in *IROS*, 2009, pp. 814–820.

[4] L. Selen, D. Franklin, and D. Wolpert, "Impedance control reduces instability that arises from motor noise," *J Neurosci*, vol. 29, no. 40, pp. 12 606–12 616, 2009.

[5] H. Geyer and H. Herr, "A muscle-reflex model that encodes principles of legged mechanics produces human walking dynamics and muscle activities," *IEEE Trans Neural Syst Rehabil Eng*, vol. 18, no. 3, pp. 263–273, 2010.

[6] D. P. Ferris, M. Louie, and C. T. Farley, "Running in the real world: adjusting leg stiffness for different surfaces," *Proc. R. Soc. Lond. B*, vol. 265, pp. 989–994, 1998.

[7] D. Hoyt and R. Taylor, "Gait and the energetics of locomotion in horses," *Nature*, vol. 292, pp. 239–240, 1981.

[8] C. Farley and C. Taylor, "A mechanical trigger for the trot-gallop transition in horses," *Science*, vol. 253, pp. 306–308, 1991.

[9] C. Semini, N. G. Tsagarakis, E. Guglielmino, M. Focchi, F. Cannella, and D. G. Caldwell, "Design of HyQ - a hydraulically and electrically actuated quadruped robot," *IMechE Part I: J. Sys Cont Eng*, 2011, (in print).

[10] R. Blickhan, "The spring-mass model for running and hopping," *J. Biomechanics*, vol. 22, no. 11–12, pp. 1217–1227, 1989.

[11] H. Geyer, A. Seyfarth, and R. Blickhan, "Compliant leg behaviour explains basic dynamics of walking and running," *Proc. Roy. Soc. Lond. B*, vol. 273, no. 1603, pp. 2861–2867, 2006.

Slip-Model-Compatible and Bio-Inspired Robotic Leg with Reconfigurable Length

Farrukh Iqbal Sheikh[1], Helmut Hauser, Lijin Aryananda, Hung Vu Quy, and Rolf Pfeifer

[1]Artificial Intelligence Laboratory, Department of Informatics, University of Zurich, Switzerland
(Tel : +41-79-3747186; E-mail: fsheikh, hhauser, lijin, vqhung, pfeifer@ifi.uzh.ch)

Abstract: We present a novel robotic leg design with reconfigurable length. The design combines key features from bio-mechanical principles into a novel robotic leg with only two actuated degrees of freedom (DOF). The leg configuration with one rotary hip joint and one prismatic knee joint makes it compatible to the Spring Loaded Inverted Pendulum (SLIP) model and will therefore potentially allow direct transfer of suitable control parameters obtained by the simulation of the SLIP model [3]. We have implemented the first prototype and conducted preliminary hopping experiments based on energy-efficient hopping at optimal frequency in human experiment [1]. We measured the ground reaction force and electrical power consumption of the module over a range of hopping frequencies. Our results suggest that the leg driven at its optimal frequency is more dynamic and energy efficient. The externally measured ground reaction forces are very consistent with the results obtained in [1].

Keywords: Legged robots, energy efficiency, spring-mass model.

1. INTRODUCTION

Legged robot locomotion has been progressing over recent years supported by the fact that legged robots have the potential to traverse more efficiently rough terrain than the wheeled robots [2]. Inspiration for these designs mainly comes from nature as animal running, hopping and jumping yet present the most efficient and astonishing solution towards energy-efficient legged locomotion. The mechanics of legged animals are composed of many complex components. Some of the core properties of these mechanics can be captured by a simple spring-mass model (SLIP) [3], which makes this model is a promising solution towards building and controlling better legged robots.

Pioneering work has been demonstrated by Marc Raibert in his single legged planar hopper [2]. It uses two actuated DOFs, one rotary to control the forward and the backward motion and a second pneumatically powered telescopic leg for restoring energy and ground interaction. The SCOUT II quadruped robot is able to locomote in fast and dynamic gaits, with only one active rotary DOF and passive linear compliance [4]. Nevertheless, the use of one DOF limits its performance on rough terrain. In contrast, the Tekken robot utilizes three active DOFs per leg and is potentially capable to handle rough terrain up to certain extent [5]. However, with the accumulated motors weights, dynamically fast gaits are difficult to achieve.

In this paper, we present a novel robotic leg design with reconfigurable length using two actuated DOFs, which combines the strengths of the SCOUT II and Tekken robot, namely the lower DOF and the high motion flexibility. The design is based on a number of specifications, some of which are derived from bio-mechanical studies: light-weight, compact, high-speed and back-drivable vertical DOF with the ability to inject and regulate the required energy into the system, linear compliance that allows easy force measurement needed for impedance control, large range of joint motion, and variable-height ground clearance.

In the next section, we describe the design and implementation details of the leg prototype. We have performed some preliminary experiments with a single leg setup and report on our measurement results based on the electrical power consumption and ground reaction forces at varying hopping frequencies.

2. DESIGN AND IMPLEMENTATION

Based on the specifications listed above, we have designed and implemented the first leg prototype. As shown in Fig.1, The physical prototype uses two actuated DOFs, one rotary (the hip) to oscillate the leg within the range of 180^0 and a second (the knee) which is defined as a prismatic joint to alter and adjust the module length within the range of 100 mm. Both joints can be directly operated from the trunk segment. Thus, the weight of the leg segment can be considerably reduced.
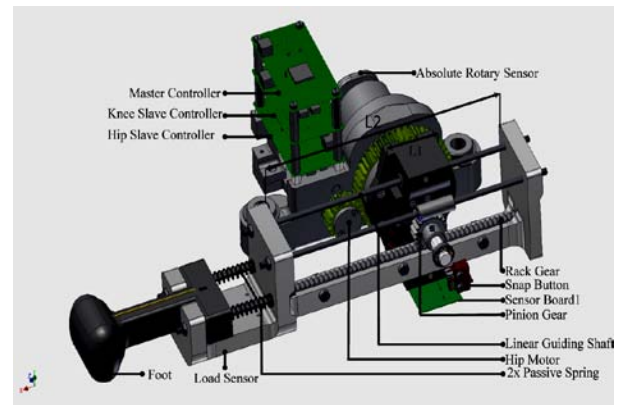
Fig. 1 Leg prototype; overall dimension (LxWxH: 80x123x240mm); weight: 0.75Kg; K per spring: 0.98 N/mm}; Translational speed (knee): 136.4 mm/s.

The prismatic knee motion is implemented by using a pinion and rack gear mechanism. We have also inserted two compression springs to introduce linear compliance in series with the leg segment. The combination of the prismatic knee joint and linear compliance provide the following capabilities: (i) The leg can inject and regulate the amount of energy needed for effective and efficient ground interaction during locomotion, (ii) It allows variable-height ground clearance, (iii) When integrated in a multi-legged robot, it provides the possibility for the robot to adapt its morphological parameters (leg length and center of mass), according to

the current environment or task, (iv) The linear spring allows energy storage through passive compliance and provides easy force measurement for impedance control, which can add active compliance to the system.

In addition to these capabilities, the leg configuration with one rotary hip joint and one prismatic knee joint makes it compatible to the Spring Loaded Inverted Pendulum (SLIP) model. This would allow direct transfer of suitable control parameters obtained by the SLIP model and significantly reduces the search space of optimal control parameters in the future. The current leg design is modular. Thus, the complete Quadruped robot can be realized by combining four such modules together with the trunk module.

3. EXPERIMENTAL RESULTS

The performance of the leg was tested in a sagittal plane against the gravity on a force plate. The hopping gait was selected to systematically perform experiment based on the measurements of optimal frequency in [1]. During the experiment, the straight posture of the module was maintained by actuating the hip motor at a constant angle and in-place hopping was carried out by operating the knee motor at different control frequencies. At each frequency, the total power consumption and the vertical ground reaction force (GRF) were measured.
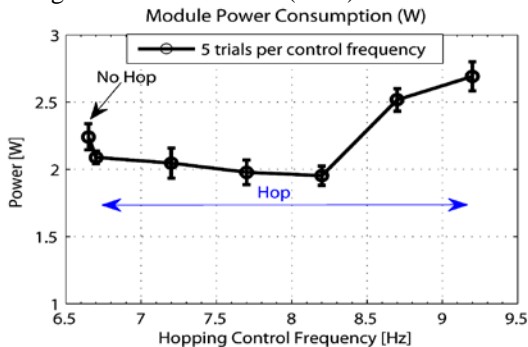

Fig. 2 Determining the optimal frequency by investigating the effect of different frequencies on the module power consumption while hopping.

Fig.2 shows the power consumption at different control frequencies (averaged over 5 trials per frequency). At 6.65 Hz, no hopping was observed and the average electrical power consumption of the module was about 2.242 ±0.096 W. When the control frequency was increased to 6.7 Hz, the module started to hop and the amount of power consumption dropped. When we increased the frequency further, the consumption decreased further until it reached a minimum at 8.2 Hz. At higher frequencies, the electrical power consumption increased again significantly. Thus, we concluded that 8.2 Hz is the optimal frequency of the leg module.

Fig. 3 (a) shows the vertical force exerted on the ground by the system during the ground contact phase, measured using a force plate, which is consistent with results obtained in human hopping in (b). According to [1], the time window, when the reaction force exceeded one body weight during landing and take-off is equivalent to half of the resonant period, i.e., T/2.
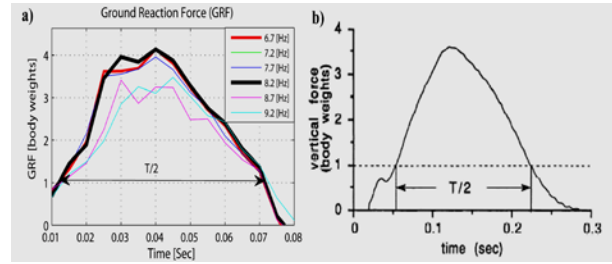
Fig. 3 (a) GRF measured in hopping of the leg prototype, each line is the mean GRF of five successive hops per control frequency; b) GRF measured in human hopping, taken from [1]

We obtained this time window by using the data shown in Fig.3 (a) 59.6 ±0.001 ms. Hence, the optimal frequency was $f\_res = 1/T = 8.39 ±0.087$ Hz. Further, the effective stiffness of our robotic leg was computed by using the equation $k = m\omega^2 = 2084.74 ±43.31$ N/m, where m=0.75 kg is the mass of the module. Fig.4 shows a sequence of the hopping at the optimal frequency. About 20 mm ground clearance was observed.
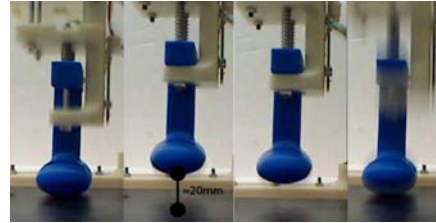
Fig. 4 Hopping frame sequence, starting from mid-stance touch-down to take-off and from take-off to landing.

4. CONCLUSION

We present a novel biologically inspired two-DOF leg with reconfigurable length, which is compatible to the SLIP model. We evaluated the preliminary performance of the leg module on the hopping gait based on the concept of energy-efficient hoping at optimal frequency [1]. We plan to further develop and investigate the dynamical properties and performance of the presented leg design in walking and running, and to validate the results in comparison to simulations based on the SLIP model.

5. ACKNOWLEDGMENT

6. REFERENCES

[1] Claire T. Farley et al., "Hopping Frequency in Humans: a test of how springs set stride frequency in bouncing gaits", *The American Physiological Society,* 1991, pp 2127-2132.

[2] Marc H. Raibert, "Legged Robots that Balance", *MIT press,* ISBN 0-262-681196.

[3] R. Blickhan, "THE SPRING-MASS MODEL FOR RUNNING AND HOPPING", *Journal of Biomechanics,* Vol. 22, No. 11/12, 1989, pp 1217-1227.

[4] Ioannis Poulakakis, "On the Stability of the Passive Dynamics of Quadrupedal Running with a Bounding Gait", *The international Journal of Robotics Research*, 2006, pp 669-687.

[5] Hiroshi Kimura et al., "Biologically inspired adaptive walking of a quadruped robot", *Phil. Trans. R.Soc, 2007*, pp. 153-170.

Cheetah-inspired robot: design of a high speed galloping quadruped

Sangbae Kim

Department of Mechanical Engineering, Massachusetts Institute of Technology
(Tel: +1-617-452-2711; E-mail: sangbae@mit.edu)

Abstract: Legged robotics has drawn much attention from robotic researchers due to its versatility over wheeled systems in non-smooth terrain. Despite recent advances in a range of technologies, the realization of agile dynamic locomotion remains as a difficult challenge. High power requirement and control of fast dynamics attributes the difficulties. The multidisciplinary nature of the design task, in addition, compounds the difficulties. We present the cheetah robot project and address three major challenges associated with developing a high-speed running quadruped. The challenges include high torque density actuator development, lightweight, robust structure fabrication, and hierarchical control architecture. We extensively observe fast running animals to obtain insights and guidelines in various aspects ranging from the body level dynamics to the foot structure details. From the observation of cheetahs, we hypothesize the influence of active body articulation in high speed running. Another hypothesis drawn from cheetahs is that active tail not only helps to reject disturbances in steady state running but also improves agility in changing direction.

Keywords: Selected keywords relevant to the subject.
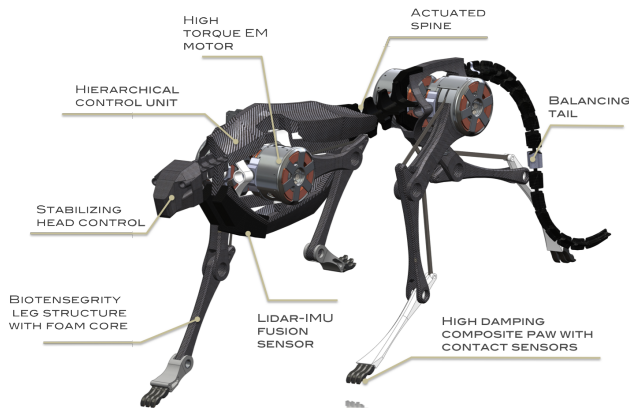
Fig. 1 The solid model of the cheetah-inspired running platform under construction.

1. APPROACHES

The presentation addresses three major challenges and corresponding strategies in developing a high speed running robot.

1.1 High torque density actuators

The actuators often limit the performance of legged robots since torque/force density of conventional actuators are substantially lower than biological muscles, while electromagnetic motors and internal combustion engines achieve high power density at high speed. These high speed actuators require high gear reduction to generate high torque at the joint of the leg. The high gear reduction increases the weight of the robot and the high reflected inertia from the high gear reduction prevents high bandwidth impedance control. This is a typical case found in many legged robots.

This problem can be mitigated by carefully selecting a motor size. A large radius motor has a high rotational inertia but requires less gear reduction due to its high torque density; torque density is proportional to the ra-

dius of the gap between the stator and the rotor. Another aspect of motor characteristics considered is the thermal mass. Unlike factory robots, the duty factor of the motor usage is much lower in legged robots. A momentary recovery action may requires high current yet only for a short period of time not in a regular fashion. In order to utilize the maximum capability of the motor preventing from thermal failure, utilizing temperature information of the coil is essential. Also, higher thermal mass of the motor lengthen the time of high torque operation and slows the thermal dynamics for safety.

1.2 Lightweight and robust structure

For a highly dynamic platform, the properties of the structure can play an important role in running performance. High speed running requires high ground reaction forces as duty factor, the ratio of the ground phase to the airborne phase and high acceleration of the leg. This entails difficulties in structure design of the leg. Since the weight of the robot determines stresses upon impacts caused by regular locomotion or failures, lightweight structure is critical as well as the compliant structure. We employ a bio-inspired design principle called 'biotensegrity' which allows lightweight and robust structure combined with compliances. As an implementation of this principle, we introduce a new rapid prototyping technique that allows foam-core-hard-shell structure combined with embedded tendon materials.

1.3 Hierarchical control architecture

The third challenge is to develop a hierarchical control architecture. The primary control strategies are as follows:

• Decoupled plenary dynamics: unlike bipeds, the stance quadruped running stance is narrow and long. With an assumption that the sagittal plane dynamics can be mostly decoupled from frontal one in straight running, we can develop each control algorithms independently and merge them.

49

- Hierarchical controller development: the body level controller and leg level controller will be developed in parallel to reduce the complexity of the dynamics in high level planning. The model will be divided at the shoulder joints as force ports. The body level controller will perform a 'gait planning' assuming that each leg can deliver a 'commanded' force profile. Port force mapping tool: the tool will be developed to provide a force generation capability of the leg in space at given running speed, including the leg dynamics, the friction cone constraint, and the actuator torque limit. This tool will guide the design of the controller providing the estimation of the force profile to the body level controller.

The Effect of Morphology on the Spinal Engine Driven Locomotion in a Quadruped Robot

Qian Zhao, Hidenobu Sumioka, and Rolf Pfeifer

Artificial Intelligence Laboratory
Department of Informatics, University of Zurich
Andreasstrasse 15, CH-8050 Zurich, Switzerland
E-mail: (zhao, sumioka, pfeifer)@ifi.uzh.ch

Abstract: The biological hypothesis of spinal engine states that the locomotion is mainly achieved by the spine, while legs only serve as assistance. Inspired by this spinal engine hypothesis, a compliant, multi-DOF, biologically inspired spine has been developed and embedded into a quadruped robot without actuation on legs. The experimental results support this spinal engine hypothesis and reveal that this kind of robot can achieve rapid, stable, and even dynamical locomotion by appropriately tuning the spine's morphological parameters, e.g., rearranging the silicone blocks.

Keywords: Spinal engine, Locomotion, Quadruped robot

1. INTRODUCTION

Over the past decades, it has been widely accepted that locomotion is generally achieved by the coordination of the legs and the spine is only considered to be carried along in a more or less passive way [1]. This popular hypothesis has been accepted by most of robotics researchers as well as biologists. A considerable amount of research has been conducted on legged robots with little consideration on their spines [2]. However, Gracovetsky has proposed an alternative hypothesis with an emphasis on the spinal engine in human locomotion, i.e., locomotion is firstly achieved by the motion of the spine; the limbs came after, as an improvement but not a substitute [3]. Then, he extended this hypothesis to quadruped animals featuring flexion-extension spinal movement [4]. This implies that the spine is the key structure in locomotion. Recently, some robotics researchers came to realize the importance of the spine, but most of them still consider the spine as an assistant element to enhance the capability of locomotion [5], [6].

In this paper, we proposed a biologically inspired spine model and its application to a real quadruped robot to investigate its role in locomotion. Preliminary experimental results support the hypothesis of spinal engine and reveal that rapid and dynamical locomotion can be achieved only by actuating the biologically inspired tendon-driven actuated spine, without taking the actuation of the legs into account. More morphologies of the spine are explored and the results suggest that the locomotion behavior can be changed by tuning the morphology of the spine.

2. BIOLOGICALLY INSPIRED SPINE MODEL

Fig.1 (a) shows an artificial spine endowed with biological characteristics. It consists of cross-shaped rigid vertebrae made of ABS plastic, silicon blocks and cables driven by motors. The vertebrae are separated by the silicon blocks, which work as intervertebral discs.

They are connected by a cable through themselves and the silicon blocks. The four driven cables are pulled respectively by four RC motors, which can control the stiffness and movement of the spine. In this design, multiple socket-ball joints (Fig.1 (b)) are taken to produce a more versatile posture and a wider motion space. The resulted spine can be bent in all directions within a certain predefined angle and form asymmetrical complex configuration by rearranging the silicone blocks in between.
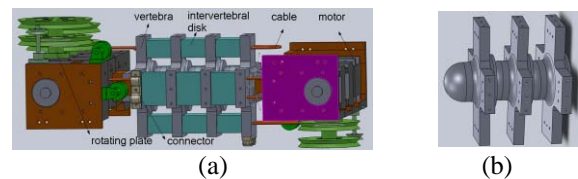
Fig. 1 The whole spine structure (a) and its socket-ball joints (b).

3. DESIGN OF THE QUADRUPED ROBOT

The developed artificial spine is embedded into a quadruped robot (29 cm wide, 23 or 25 cm long, 20 cm high and 1.1 kg). There are 3 linear springs in each stick-shaped leg to cushion shock from the ground. The legs are fixed to the body. The bottom of foot is glued with asymmetrical friction material to control the walking direction. Sine waves with tunable parameters are taken as control signals for 4 motors to generate the spinal movement.

4. EXPERIMENTAL RESULTS

To better understand the role of spine in locomotion and the correlation between its morphological property and locomotion behavior, a series of experiments were conducted under the condition of different spinal structures which differ in the shape and the stiffness distribution. During the experiments, several control parameter sets were tested for 5 trials and the best one was chosen. Fig.2 shows two robots equipped with symmetrical rectangle and rhombus shaped spines.

(a)   (b)

Fig.2 Robots equipped with rectangle (a) and rhombus (b) shaped tendon-driven actuated spine.

4.1 Moving forward

Table.1 shows that the robot is able to walk forward rapidly with stable and reproducible performance. We have also observed the shape of the spine does not affect much on its speed. Fig.3 exhibits the symmetrical, periodical flexion-extension spinal movements generating power to locomotion. However, its feet slide on the ground due to the lack of ground clearance.

Table. 1 Results of the moving forward performance

Symmetrical spine shape	Rectangle	Rhombus
Ave speed (cm/s)	14.5	11.7
Std speed	0.3	0.3

(a)

(b)
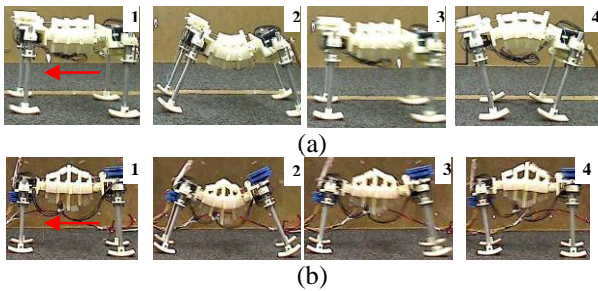
Fig.3 Sequential pictures of the robot's locomotion with the rectangle (a) and rhombus (b) shaped spine under the same control set. The red arrows represent the walking direction.

4. 2 Turning left/right

Table.2 shows the robot is able to turn right or left stably with the symmetrical rectangle shaped spine by introducing the lateral movement in addition to the flexion-extension movements. The speeds slightly differ due to the manufacture and assembly error.

Table. 2 Results of turning performance

Rectangle-shaped spine	Turing Right	Turing Left
Ave angular speed (°/s)	6.2	5.1
Std angular speed	1.0	0.5

4. 3 Dynamical movement

In this experiments, the asymmetrical spine morphologies are introduced where the silicones in the fore part of the spine were partially taken out in the above two morphologies. Fig.4 exhibits more dynamical lifting up movement based on these two new morphologies due to the asymmetrical arrangement of the silicone blocks. However, the rhombus shaped spine can lift up not only the fore legs, but the rear legs, which might be explained by the more asymmetrical stiffness

distribution formed by this shape.

(a)

(b)
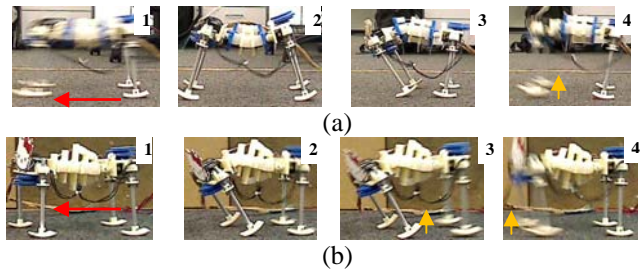
Fig.4 Sequential pictures of the robot's locomotion with the asymmetrical rectangle (a) and rhombus (b) shaped spine under the same control set. The yellow arrows represent the movement of lifting up.

5. CONCLUSIONS

A novel highly-compliant, multi-joint artificial spine inspired by biology has been developed and applied to a quadruped robot to test the biological hypothesis of spinal engine. Preliminary experimental results showed that the rapid and stable forward moving can be achieved when the silicon blocks are distributed symmetrically in the spine, whereas more dynamical movement can be observed by taking asymmetrical distribution of silicon blocks. This phenomenon has been observed in the cases of both the rectangle and rhombus morphologies, but the robot equipped with rhombus-shaped spine can lift up rear legs, which might be interpreted by its spine's ability to generate more complex asymmetrical configuration. The sensitive turning performance in the rectangle case has been observed to further support the spinal engine hypothesis.

All the results emphasized the concept of spinal engine and demonstrated the possibility for a robot to achieve different locomotion modes by appropriately tuning the morphological parameters of the spine without taking the actuation of the legs into account.

REFERENCES

[1] R.M. Alexander, "Principles of Animal Locomotion", *Princeton University Press*, Princeton NJ, 2003.

[2] M. H. Raibert, "Legged robots", *Communications of the ACM*, 29(6):pp.499-514, 1986.

[3] S. A. Gracovetsky, "An hypothesis for the role of the spine in human locomotion: a challenge to current thinking", *J Biomed Eng*, 7(3): pp. 205–216, 1985.

[4] S. A. Gracovetsky, "Energy transfers in the spinal engine", *J Biomed Eng*, 9(2): pp. 99–114, 1987.

[5] T. Takuma, "Facilitating Multi-modal Locomotion in a Quadruped Robot utilizing Passive Oscillation of the Spine Structure", *2010 IEEE/RSJ International Conference on Intelligent Robots and Systems*, ThBT5, 2010.

[6] K. Tsujita, "Gait Transition by Tuning Muscle Tones using Pneumatic Actuators in Quadruped Locomotion" , *Proc. of IEEE/RSJ IROS2008*, Vol. 1-3, pp. 2453-2458, 2008.

On Control of Flapping Flight of Butterfly with Experimental Observation

Kei Senda[1], Naoto Yokoyama[1], Masafumi Matsusaka[1], Norio Hirai[2], and Makoto Iima[3]

[1]Department of Aeronautics and Astronautics, Kyoto University, Kyoto, Japan
(Tel : +81-774-38-3960; E-mail: senda@kuaero.kyoto-u.ac.jp)
[2]Department of Environmental Sciences and Technology, Osaka Prefecture University, Osaka, Japan
[3]Department of Mathematical and Life Sciences, Hiroshima University, Hiroshima, Japan

Abstract: This study discusses controls of flapping flights of butterflies. Free-flying motions of butterflies are measured in a low-speed wind tunnel of an experimental system. A numerical model realizes a free flight by repeating of a joint motion, whereas the flapping flight is unstable. A feedback control is designed and it successfully stabilizes the free-flying motion of the butterfly model. The control of a living butterfly is analyzed by comparison between an experimental observation and a numerical simulation.

Keywords: Flapping flight, Butterfly, Control, Experimental observation

1. INTRODUCTION

Flapping flights of butterflies seem unstable, but in reality they are stable. Butterflies can maintain stable flapping flights robustly against environmental uncertainties and variations. References [1, 2] have shown that free vortices in wakes generated by flapping provide a type of passive stabilization effects, but they cannot make butterflies' flights sufficiently stable. Therefore, the objective of this study is to clarify active controls of butterflies. The approach is as follows. At first, motions of living butterflies are experimentally observed in order to understand their controls. Secondly, an artificial feedback control is designed and implemented to an existing numerical simulator [1, 2]. Finally, similarities and differences of two controls are analyzed by comparison between an experimental observation and a numerical simulation.

2. EXPERIMENTAL OBSERVATION

An experimental system with a low-speed wind tunnel (Fig. 1) has been constructed. A free-flying butterfly is put into the wind tunnel, and the flapping-of-wings motion in the flow is captured by three high-speed cameras. The joint angles of the butterfly are calculated from the measured positions of typical points on the body in video images. The variables that represent kinematics are defined in Fig. 2. The states of the thorax are represented by $[x, z, \theta_t]^T$ and the joint angles of the abdomen and wings are represented by $[\theta_a, \beta, \eta, \theta]^T$.

3. ARTIFICIAL FEEDBACK CONTROL

Eq. (1) is the perturbation equation that is a linear sampled-data system where sampling is taken every flapping period T [s] from the numerical simulator and linearized:

$$\delta \boldsymbol{x}(t_{k+1}) = \boldsymbol{A}\delta\boldsymbol{x}(t_k) + \boldsymbol{B}\delta\boldsymbol{u}(t_k), \qquad (1)$$

where $t_{k+1} = t_k + T$, $\boldsymbol{x} = [x, z, \theta_t, \dot{x}, \dot{z}, \dot{\theta}_t]^T$ the controlled-variable vector, $\boldsymbol{u}$ the manipulated-variable vector, and δ perturbation. Based on the optimal regu-
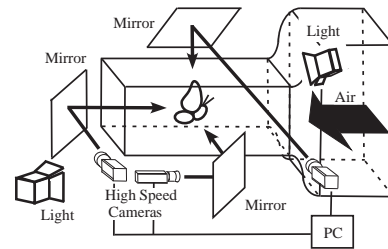
Fig. 1 Experimental setup.
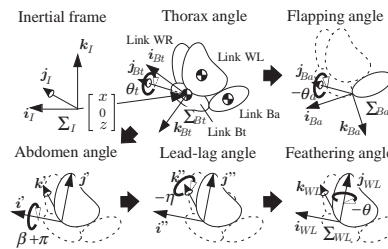
Fig. 2 Definition of the parameters on kinematics.

lator theory, a feedback-controller is designed as:

$$\delta\boldsymbol{u}(t_k) = -\boldsymbol{K}\delta\boldsymbol{x}(t_k), \qquad (2)$$

where $\boldsymbol{K}$ is a feedback gain.

The poles of the autonomous system are

$$\begin{aligned} &0.891,\ 0.597,\ 0.520,\ -0.0559, \\ &-2.60 \times 10^{-5},\ 1.27 \times 10^{-4}, \end{aligned} \qquad (3)$$

where the controller is implemented to the nominal plant. On the other hand, the corresponding values of the original nonlinear simulator implemented by the controller are

$$0.957,\ 0.934,\ 0.915,\ 0.881,\ 0.797,\ 0.751. \qquad (4)$$

The magnitude of the value is the expansion rate of the corresponding mode. Each controlled system is stable because the all values are less than one and any perturbation reduces. However, the control performance is decreased because the controller is designed for the reduced-order and linearized plant and implemented to the original nonlinear model.

53
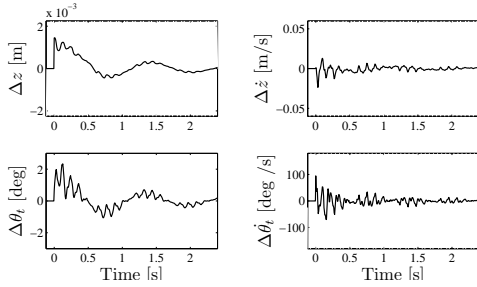
Fig. 3 Response of perturbations for 20 periods of simulator.

4. COMPARISON

A living butterfly repeats almost same periodic motion when it maintains steady flapping flight. But, each motion is slightly different from others. The standard trajectory is the most typical trajectory that is selected from the experimental data of an individual under the same condition. A perturbed trajectory is in a slightly different state at the beginning of downstroke, but it tends to approach the standard trajectory. For the simulator, the standard trajectory is when it maintains steady flapping flight, and a perturbed trajectory has one fifth of the initial perturbation of the experimental perturbed trajectory.

The response of a perturbation for 20 periods is shown in Fig. 3, where the initial perturbation is applied at the beginning of downstroke, time $t = 0$ [s]. The perturbation is reducing, and the control is stable.

Fig. 4 shows the first 3 periods of Fig. 3. Fig. 5 shows the response to the same initial perturbation observed in experiments that corresponds to the simulator. In this case, there are relatively large initial perturbations in $\dot{z}$ and $\dot{\theta}_t$. The former is negative and the latter is positive. Both controllers in the living butterfly and the simulator tend to suppresses increasing of the thorax angle and the descending speed. They are regarded as corresponding controllers because their transient response of the controlled variables are similar to each other.

Between the living butterfly and the simulator, their transient responses of the manipulated variables are compared. In case of the living butterfly, $\Delta(\theta + \theta_t)$ is kept almost 0 whereas $\Delta\theta$ is almost always negative value. If positive perturbation of $\Delta\theta_t$ is generated by an initial perturbation, the leading edge is twisted down, i.e. $\Delta\theta$ becomes negative, and $\Delta(\theta + \theta_t)$ is kept 0. Negative moment of force is applied to the thorax because of this wing torsion. The similar behavior is observed in the simulator.

On the other hand, there are differences to realize the $\Delta\theta$. The θ may be indirectly controlled by manipulating η because the butterfly seems difficult to drive θ directly. On the other hand, the simulator is modeled such that it can directly manipulate both η and θ independently. Therefore, the way to manipulate η is different from the living butterfly.
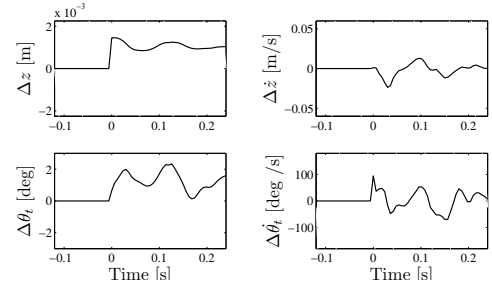
Fig. 4 Response of perturbations for 3 periods of simulator.
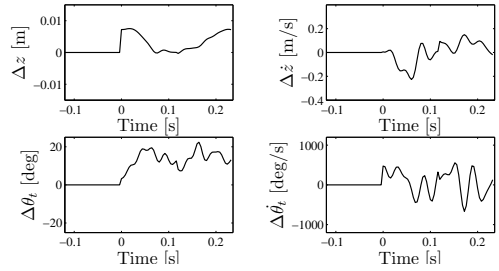
Fig. 5 Response of perturbations for 20 periods of living butterfly.
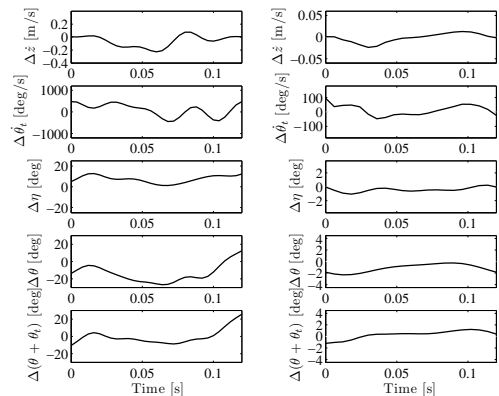
Fig. 6 Response of perturbations, left: experiment, right: simulator.

5. CONCLUSION

Comparison between the living butterfly and simulator has provided following results. Both control systems have been stabilized. Their transient responses of the controlled variables against the same perturbations have been similar, but those of the manipulated variables different. It might be because the simulator has not modeled some mechanical structures of living butterflies. Therefore, to design controllers considering the properties of living butterflies will help us to understand their control.

REFERENCES

[1] Senda, K. et al., "Stabilization of Flapping-of-Wing Flight of Butterfly, Considering Wakes," in *Bio-mechanisms of Swimming and Flying*, Springer, 2007, pp. 193-204.

[2] Senda, K. et al., "On Flight Mechanics of Flapping Butterfly," *IEEE International Conference on Robotics and Automation* Kobe, Japan, May 12-17, 2009, pp. 17-22.

Study of adaptability of an insect using the brain-machine hybrid system: Sensory feedback in odor searching behavior

Ryo Minegishi[1], Atsushi Takashima[2], Daisuke Kurabayashi[3], Ryohei Kanzaki[4]

[1]Department of Advanced Interdisciplinary Studies, The University of Tokyo, Tokyo, Japan
(Tel : +81-3-5452-5197; E-mail: minegishi@brain.imi.i.u-tokyo.ac.jp)
[2]Collaborative Research Division, Art, Science, and Technology Center for Cooperative Research, Kyushu University, Japan
(Tel : +81-92-807-4563; E-mail: takashima@astec.kyushu-u.ac.jp)
[3]Department of Control and System Engineering, Tokyo Institute of Technology, Japan
(Tel : +81-3-5734-2548; E-mail: dkura@irs.ctrl.titech.ac.jp)
[4]RCAST, The University of Tokyo, Japan
(Tel : +81-3-5452-5195; E-mail: kanzaki@rcast.u-tokyo.ac.jp)

Abstract: We developed the brain-machine hybrid system as a new approach to investigate adaptability of insects. In this system, the mobile robot as a body was controlled according to the steering signals from the moth's brain. By changing the conversion rule from signals to robot behavior, we can intervene with the relationship between brains and environments. From the experiments, we observed that the moths on the robot responded correctively to forcibly given movement both while the robot was immobile and mobile in command signals. We also tested biased motor gain condition and compensative responses were also observed in these conditions.

Keywords: adaptability, brain-machine hybrid system, sensory feedback, insect, chemical plume tracking, cyborg.

1. INTRODUCTION

Insects can react appropriately to changing environmental conditions using their comparatively small brains. We call this ability as adaptability.

Male silkworm moths, *Bombyx mori*, orient toward conspecific females displaying a programmed behavioral pattern (straight-line walking, zigzagging turns and looping) upon detection of sex pheromone by their antennae. This behavioral pattern is repeated each time a pheromone plume is encountered resulting in localization of the goal.

In a previous study, it has been reported that the silkworm moth could compensate for motor asymmetry and show adaptive behavior in the orientation behavior to a pheromone source [1]. In that study, an insect-controlled two-wheeled robot was built to examine the adaptability. The robot moved based on the locomotion of the silkworm moth on a sphere mounted on the robot. Using the robot, artificial changes of motor gain could produce unintentional movements for the silkworm moth, and under these conditions, the silkworm moth could adapt to the new circumstances. Moreover, it was suggested that the silkworm moth used visual cues under these conditions.

Recently in the interdisciplinary field of neuroscience and robotics, closed-loop experimental systems that connect a brain with a robot have been developed [2]. We have suggested a new closed-loop experimental system, a brain-machine hybrid system that mounts a moth head on a robot as sensors and a controller. We constructed a brain-machine hybrid system using motor signals related to the steering behavior of the male silkworm moth for controlling a two-wheeled mobile robot. Using this system, we can acquire knowledge about adaptive processing in the brain by controlling the motor output of the robot.

2. BRAIN-MACHINE HYBRID SYSTEM

2.1 Selection of command signals

We recorded steering signals from neck motor neurons, 2nd cervical nerve b (2nd CNb). These neurons convey signals to regulate head swing [3]. Head swing angle and walking angular velocity are correlated [3].

We recorded the signals by sucking the cut end of the left and right 2nd CNbs into the glass microelectrodes by using syringes and acquired neural activities by using amplifiers. Signals from 2nd CNb contain five units that have different spike amplitudes. We chose units corresponding to the optic flow stimuli that induced head swing.

2.2 Setting a spike-behavior conversion rule

We set a spike-behavior conversion rule as we have already reported [4]. We assumed a two-wheeled mobile robot in a two-dimensional coordinate system. The forward velocities of the left and right wheels were calculated proportionally to the right and left spiking rate per 0.1 second. As a result, the angular velocities of the robot were calculated as the difference of right and left spike rate per 0.1 second.
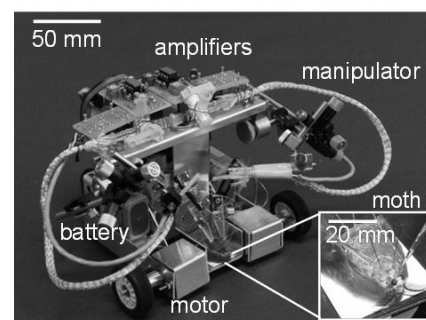

Fig. 1 Brain-machine hybrid system

2.3 Characteristics of the amplifiers

To amplify small signals recorded from nerves for use by the micro controller on a mobile robot (e-puck, EPFL), we made instrumentation amplifiers. We designed our instrumentation amplifiers with an input resistance of 100 MΩ, a gain of 80 dB (variable), a frequency bandwidth of 150 Hz – 3.2 kHz.

2.4 Experiments in a wind tunnel

To test the behavioral pattern and odor source orientation behavior of the hybrid system, we used an experimental wind tunnel (flow speed 0.7 m/s). The wind tunnel provided enough space (W 840 mm x H 300 mm x L 1800 mm) for the hybrid system (W 140 mm x H 60 mm x L 130 mm). In the wind tunnel, air puffs were regulated by electric valves operated by LabVIEW program.

Using the hybrid system, we observed the programmed behavioral pattern of a male moth following a single pheromone stimulus (bombykol 100 ng absorbed in a filter paper, 500 ms stimulus duration). By plotting angles formed between pheromone source direction from the hybrid system's start point and the longitudinal axis of the hybrid system, elements of the moth's programmed behavioral patterns (straight-line walking, zigzagging turns, and loop) were observed. Average angular velocity for 5 seconds was 9.57 degrees/s (before the stimulus) and 35.8 degrees/s (after the stimulus). Similar results were observed in 7 examples in 3 individuals.

We tested whether the hybrid system could orient and reach a pheromone source (bombykol 1000 ng) in the wind tunnel. We set the goal line 100 mm from the pheromone source. As a result, 10 successful examples in 7 individuals (in 24 trials) were observed.

3. RESPONSES ABOUT ADAPTABILITY

3.1 Responses to disturbances

As the initial step toward understanding the adaptability, we examined whether the activities of 2nd CNb changed responding to given disturbances. We gave disturbances as angular velocity and forward velocity, and the activities of 2nd CNb only responded to the angular velocity.
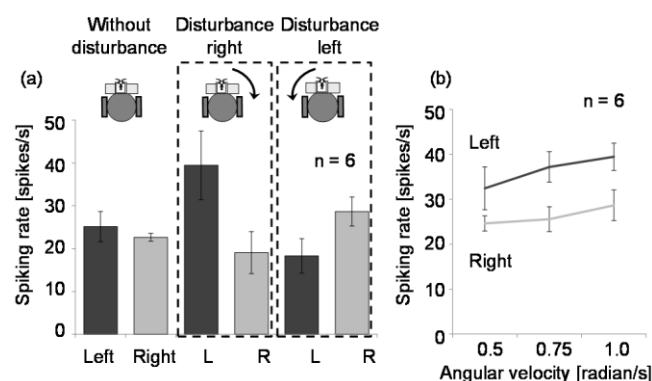

Fig. 2 Responses to angular velocity disturbances

They show compensative responses to keep the position of the hybrid system. Average spiking rates without the disturbances were 22.7 spikes/s (right) and 25.2 spikes/s (left). Average spiking rates of the contralateral 2nd CNb during the 1.0 radian/s disturbances were 28.7 spikes/s (right) and 39.5 spikes/s (left) (Fig. 2 (a)). These responses increased proportionally to the angular velocity (Fig. 2 (b)).

3.2 Biased motor gain conditions

We changed a conversion rule of the hybrid system to examine adaptability to the new conditions. We biased left and right motor by doubling the velocity. In those conditions, activities of the contralateral 2nd CNbs to the biased side excited and the activities of ipsilateral 2nd CNbs were inhibited, and in several examples the hybrid system still could reach the pheromone source.

4. CONCLUSION

We developed the brain-machine hybrid system. Using the selected command signals on the hybrid system, we reconstructed the programmed behavioral pattern and orientation behavior of a male silkworm moth. Moreover, we examined adaptability of a moth by giving disturbances and changing the spike-behavior conversion rule to make biased conditions. In these experiments, moths on the hybrid system showed compensatory responses to keep their position.

5. ACKNOWLEDGEMENT

REFERENCES

[1] S. Emoto, N. Ando, H. Takahashi, R. Kanzaki, "Insect controlled robot -evaluation of adaptation ability-", J. Robotics and Mechatronics. Vol. 19, No. 4, pp. 436-443, 2007.

[2] B. D. Reger, K. M. Fleming, V. Sanguineti, S. Alford, F. A. Mussa-Ivaldi, "Connecting brains to robots: An artificial body for studying the computational properties of neural tissues", Artif. Life. Vol. 6, pp. 307-324, 2000.

[3] T. Mishima, R. Kanzaki, "Coordination of flipflopping neural signals and head turning during pheromone-mediated walking in a male silkworm moth *Bombyx mori*", J. Comp. Physiol. A. Vol. 183, pp. 273-282, 1998.

[4] R. Minegishi, A. Takashima, D. Kurabayashi, R. Kanzaki, "Construction of a brain-machine hybrid system to evaluate adaptability of an insect", Rob. Auton. Syst, (in press).

Molecular aspects of the serotonergic system in the cricket CNS: implication in the adaptive modulation of behavior

Takayuki Watanabe[1] and Hitoshi Aonuma[2]

[1]Research Institute for Electronic Science, Hokkaido University, Sapporo, Japan
(Tel : +81-11-706-3832; E-mail: taka226@ncp8.es.hokudai.ac.jp)
[2]Research Institute for Electronic Science, Hokkaido University, Sapporo, Japan
(Tel : +81-11-706-3832; E-mail: aon@es.hokudai.ac.jp)

Abstract: Serotonin (5-HT) modulates various aspects of behaviors in animals. We use the field cricket *Gryllus bimaculatus* as a model animal to study the neural basis of the adaptive modulation of behavior in the insect microbrain system. In this paper, we examined genes involved in 5-HT synthesis and transduction in the cricket central nervous system (CNS). As a result, three genes involved in 5-HT synthesis and four 5-HT receptor genes were identified. Expression analysis of the 5-HT related genes revealed that the 5-HT system is widely distributed in the cricket.

Keywords: Serotonin, *TRH*, *TPH*, *AADC*, 5-HT receptors, *Gryllus bimaculatus*

1. INTRODUCTION

5-HT functions as a neurotransmitter/modulator, or as a neurohormone that modulates various principal behaviors, such as feeding, circadian behavior, sleep, sexual behavior, and social behavior. We focus on the serotonergic modulation of aggressive and escape behaviors in the field cricket *Gryllus bimaculatus* to understand the neural basis of the adaptive modulation of behavior. Although physiological and behavioral aspects of the cricket serotonergic system have been extensively studied [2, 3, 4], its molecular basis has not been investigated yet. In this paper, we identified genes involved in synthesis and transduction of 5-HT in the cricket.

2. MOLECULAR ASPECTS OF 5-HT SYSTEM IN INSECTS

2.1 5-HT synthesis pathway

5-HT is synthesized by a two step reaction process. The first step of 5-HT synthesis is catalyzed by tryptophan hydroxylase, which encoded by two distinct genes (*TRH* and *TPH*) in insects [5]. The second step of 5-HT synthesis is catalyzed by AADC (Fig. 1).
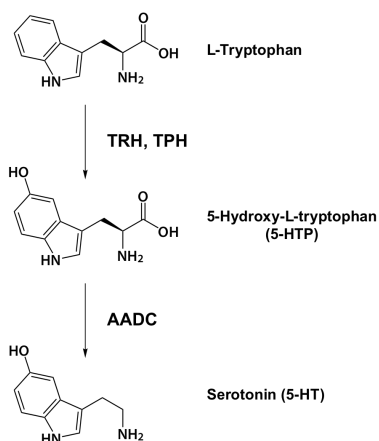
Fig. 1   5-HT synthesis pathway in the cricket.

2.2 5-HT receptors

All of the insect 5-HT receptors belong to the G-protein-coupled receptor (GPCR) superfamily, and are classified into three subtypes (5-HT_1, 5-HT_7, and 5-HT_2) which are coupled with subtype-specific signal transduction mechanisms (Fig. 2, Table 1) [6].

Table 1   Insect 5-HT receptors.

Family	Subtype	Down-stream signal transduction	
5-HT_1	5-HT_{1A}	G_i -coupled	Decrease in cAMP
	5-HT_{1B}		Increase in IP_3
5-HT_2	$5\text{-HT}_{2\alpha}$	G_q-coupled	Increase in IP_3 (?)
	$5\text{-HT}_{2\beta}$	?	?
5-HT_7		G_s-coupled	Increase in cAMP

3. MATERIALS AND METHODS

In the present study, we identified *TRH*, *TPH*, *AADC*, *5-HT_{1A}*, *5-HT_{1B}*, *5-HT_{2a}*, and *5-HT_7* in *G. bimaculatus*.

To obtain the partial cDNA fragment of the target genes, we searched EST clones corresponding to the target genes on the GenBank database, otherwise we designed degenerate primers to amplify the partial cDNA fragment of the target genes. 5' and 3' RACEs were performed to extend partial cDNA clones by amplifying the 5′ and 3' sequences of the corresponding mRNAs. Tissue-specific expression patterns were examined by RT-PCR.
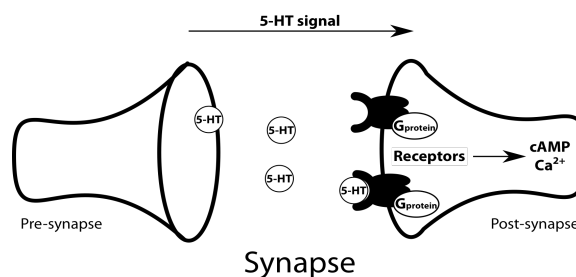

Fig. 2   5-HT signaling.

4. RESULTS AND DISCUSSION

4.1 *TRH*, *TPH*, *AADC* genes and their distribution in the cricket (Fig. 3).

We identified three genes involved in 5-HT synthesis in the cricket CNS. We found two transcript variants of *TRH* gene in the central brain. Two tryptophan hydroxylase genes (*TRH* and *TPH*), which are selectively expressed in the neuronal and peripheral tissues, respectively in the fruitfully [7], were co-expressed in the neuronal tissues in the cricket. This data suggests that TRH- and TPH-mediated 5-HT biosynthesis pathways are not compartmentalized into neuronal and peripheral tissues in the cricket, and the cricket CNS has two distinct mechanisms of the regulation of 5-HT synthesis.

AADC gene, which is involved not only in 5-HT biosynthesis but also in biosynthesis of dopamine and melanin, was ubiquitously expressed in the cricket. Dopamine functions as a neurotransmitter or neuromodulator, and melanin plays essential roles in cuticular tanning/sclerotization and the immune response in insects. Ubiquitous expression of *AADC* might reflect its functional importance in various biochemical pathways.
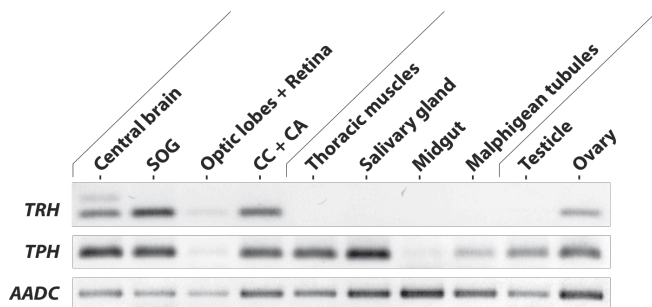

Fig. 3 Expression patterns of the 5-HT synthesis pathway-related genes.

4.2 Four 5-HT receptor genes and their distribution in the cricket (Fig. 4).

We identified four 5-HT receptor genes (*5-HT$_{1A}$*, *5-HT$_{1B}$*, *5-HT$_{2\alpha}$*, and *5-HT$_7$*) expressed in the cricket CNS. The 5-HT system is involved in modulating various behaviors in the insect CNS, and in the peripheral tissue, 5-HT controls various physiological phenomena such as heart beat, salivary gland secretion, diuresis in the Malpighian tubules. Tissue-specific expression patterns of four 5-HT receptor genes showed that the 5-HT system is widely distributed in the cricket, and that the 5-HT system might regulate various aspects of physiological phenomena via distinct 5-HT receptor pathways.
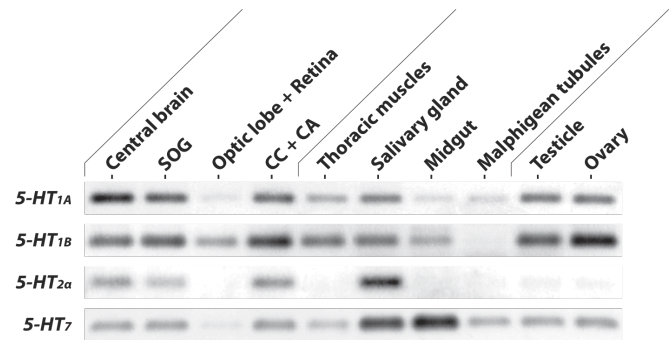
Fig. 4 Expression patterns of four 5-HT receptors.

5. CONCLUSION

To elucidate molecular basis of the cricket 5-HT system, we identified seven genes essential for the synthesis and transduction of 5-HT in the cricket *G. bimaculatus*. Our data suggest that two distinct 5-HT synthesis pathways co-exist in the cricket CNS. The four of 5-HT receptor genes were expressed in various tissues at differential expression levels, suggesting that the 5-HT system is widely distributed in the cricket. Functional analysis of each 5-HT receptor will reveal the differential involvement of specific 5-HT receptor subtypes to behavior in the cricket.

REFERENCES

[1] T. Watanabe, H. Sarasota, H. Aonuma, "Identification and expression analysis of the genes involved in serotonin biosynthesis and transduction in the field cricket *Gryllus bimaculatus*." *Insect Molecular Biology*. Revised.

[2] AS. Saifullah, K. Tomioka, "Serotonin sets the day state in the neurons that control coupling between the optic lobe circadian pacemakers in the cricket *Gryllus bimaculatus*" *J Exp Biol*, Vol. 205, pp. 1305–1314, 2002.

[3] PA. Stevenson, HA. Hofmann, K. Schoch, K. Schildberger, "The fight and flight responses of crickets depleted of biogenic amines" *J Neurobiol*, Vol. 43, pp. 107–120, 2000.

[4] T. Nagao, T. Tanimura, T. Shimozawa, "Neurohormonal control of the mating interval in the male cricket, *Gryllus bimaculatus* DeGeer" *J Comp Physiol*, Vol. 168, pp. 159–164, 1991.

[5] CM. Coleman, WS. Neckameyer, "Serotonin synthesis by two distinct enzymes in *Drosophila melanogaster*" *Arch Insect Biochem Physiol*, Vol. 59, pp. 12–31, 2005.

[6] AJ. Tierney, "Structure and function of invertebrate 5-HT receptors: a review" *Comp Biochem Physiol A Mol Integr Physiol*, Vol. 128, pp. 791–804, 2001.

[7] WS. Neckameyer, CM. Coleman, S. Eadie, SF. Goodwin, "Compartmentalization of neuronal and peripheral serotonin synthesis in *Drosophila melanogaster*", *Genes Brain Behav*, Vol. 6, pp. 756–769, 2007.

Gait Versatility Through Morphological Changes in a New Quadruped Robot

Hung Vu Quy, Gilles Ramstein, Flurin Casanova, Lijin Aryananda, Matej Hoffmann, Farrukh Iqbal Sheikh
and Helmut Hauser

Artificial Intelligence Laboratory, University of Zurich, Zurich, Switzerland
Tel: +41 44 635 4592; E-mail: (vqhung, casanova, lijin, hoffmann, fsheikh, hhauser) at @ifi.uzh.ch and
gilles187@hotmail.com

Abstract: In dynamic locomotion, robots' morphology and the ability to adapt it online play an important role for energy efficiency and coping with the highly unpredictable perturbations from the environment. In this paper, we present the design and implementation of a quadruped robot, whose morphology is particularly targeted toward energy-efficient dynamic locomotion. We propose a combination of mechanisms, which allows for gait versatility, energy-efficient actuation and ground clearance through adaptation of morphology (i.e., morphosis). We report on a series of experiments to validate the robot's performance in different locomotion conditions.

Keywords: robot design, legged locomotion, morphological computation, gait versatility, energy efficiency, morphosis

1. INTRODUCTION

Biological systems show amazing locomotion capabilities. The combination of their morphology (musculoskeletal structure, body shape, etc.) and sensory-motor control allows them to traverse diverse terrains and to switch among gaits to maintain varying levels of speed at optimized energy efficiency. With the goal to match these impressive capabilities, roboticists have put vast efforts to derive inspiration from biology and transfer it into the design of robots' morphology [1]. We have identified the following key factors that need to be addressed in a dynamic legged robot:

- **Power:** In dynamical running, the robot has to deliver a large amount of energy within a fraction of a second in order to jump off.
- **Compliance:** For energy storage and instant adaptation to external forces, compliant structures have to be integrated into the robot's legs.
- **Ground clearance.** When legs are propagated forward during a swing phase, they need to clear the ground.
- **Gait versatility:** Legged animals are able to locomote in different gaits, mostly, in order to adapt to new terrain or to change speed, at minimized cost of transport [2]. Therefore, it is crucial for an agile robot to be able to exhibit different gaits.

To integrate all these, sometimes competing requirements, into a single design is a challenge. For instance, high power-to-weight ratio conflicts with controllability and gait versatility. Specifically used as inspirations in our work are the iSprawl [3] and Scout II [4] robots. The iSprawl robot demonstrates fast and robust dynamic hexapedal locomotion, due to carefully designed compliant properties and the fast and efficient prismatic joint actuations. The Scout II quadruped robot shows several fast and robust running gaits (i.e., trot, bound, and gallop), but only with one rotational degree-of-freedom per leg and linear compliance.

We present a novel solution to address the previous listed key factors: the quadruped robot UZH1 (Fig. 1). High power-to-weight ratio was achieved by using only one motor for locomotion per leg. The motors were placed towards the center of mass in order to minimize counter-forces and inertial moments. In addition, the motors rotate continuously providing energy-efficient output since they do not "fight" against their own inertia (which is the case as oscillating). The oscillatory movement of the leg is then achieved through a crank-slider mechanism.

The additional design requirements were fulfilled in the following manner: First, compliance was introduced by incorporating springs within the leg structure. Second, ground clearance was already incorporated into the crank-slider mechanism, obtaining an oval foot trajectory. With this adopted mechanism, while we gain a two-dimensional foot trajectory with only one motor per leg, these trajectories are fixed and not controllable. Therefore, third and last, we introduced the missing flexibility that is needed for different gaits through mechanisms that allow the robot to change its leg configuration - which we call *morphosis.* The ground clearance profile (GCP) can be adjusted online (through additional lightweight "morphosis motors") and offline. With the morphosis capabilities our work goes beyond that of K. Iida[5].
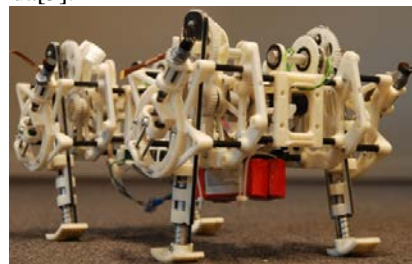
Fig.1 UZH1 Robot Prototype; overall dimension: (LxWxH: 350, 250x200 [mm]); weight: 2.25kg.

The paper is organized as follows, we begin by presenting the design concept and implementation details of the UZH1 robot. We then describe a series of experiments designed to evaluate the robot's performance.

2. DESIGN AND IMPLEMENTATION

As shown in Fig.2, each leg of the UZH1 robot has two degree of freedoms: a prismatic and a rotary joint. The first one is a passive compliant joint allowing for energy storage and impact absorption. The second one is controlled by the continuous rotation of a crank disk

mounted at the end point of the leg. The leg is constrained by one end point mounted on the crank disk and the slider rotating about the fix point. As a result, the foot produces a GCP as shown in Fig.2 (d).
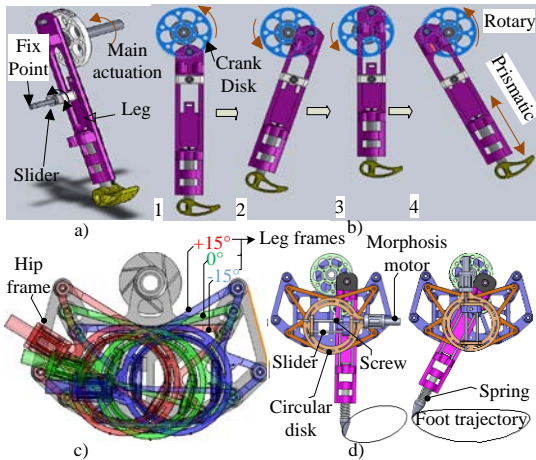
Fig.2 Operational principle of the robot's leg design; (a) main components of the robot leg; (b) from (1)-(4): leg movement in one working cycle; (c-d) online and offline morphosis possibilities influencing the foot trajectory.

In order to provide diverse locomotion capabilities, we introduce two levels of morphosis: online and offline. In the online morphosis, we vary the fix point position in order to provide possibilities to change leg configuration. As shown in Fig.2, the position of the fix point determines the trajectory of the end point of the robot's foot. By moving the fix point along with the screw via the morphosis motor, the foot trajectory, which depends on the offset angle and the oscillating amplitude, can be varied. The influence of the fix point movement on the changing ratio between the offset angle and the oscillating amplitude also depends on the orientation of the screw, shown in Fig. 2 (d).

In the offline morphosis, the circular disk, at which the screw is mounted on, can be rotated in a full circle with resolution of 5° on the leg frame allowing to vary the foot trajectory. Additionally, one can rotate the whole leg frame by 15° to either side. As a result, this creates a larger change of the offset angle, shown in Fig. 2 (c).

3. EXPERIMENT: GAIT VERSATILITY

We investigated the robot's capabilities using a simple CPG architecture [6] without any sensory feedback. The main goal of the presented experiments is to gain insights to the abilities of the compliant, morphological structure of UZH1 in combination with this simple open-loop control.
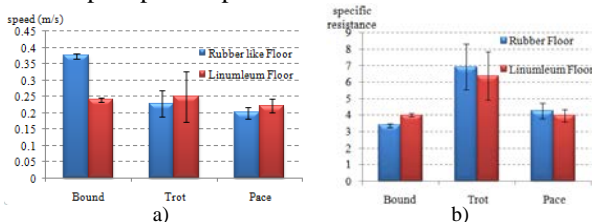

Fig.3 The robot speeds and specific resistances in different gaits on different floor materials.

In a series of experiments, we have jointly explored the space of control (speed, duty factor, phase difference), morphological parameters (slider orientations and fix point positions) and different terrains. These resulted in three different gaits, namely bound, trot, and pace. The highest speeds and the specific resistances are shown in Fig.3.

As a result, the morphological parameters such as the combination of different slider orientations and the fix points at the best speeds were thoroughly investigated through number of experiments as shown in the Fig.4.
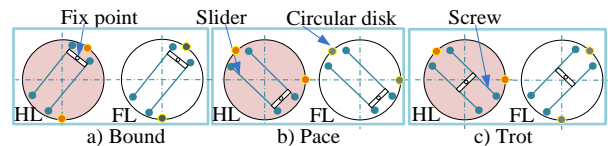

Fig.4 The different slider combinations in different gaits for the best speed; FL: front leg; HL: hind leg.

4. DISCUSSION, CONCLUSION, FUTURE WORK

We presented a novel robot design that aims at dynamic, energy-efficient, yet versatile locomotion. The missing active degrees of freedoms that were sacrificed for the sake of higher power-to-weight ratio were compensated by mechanisms that manipulate the robot's morphology. We have successfully demonstrated the robot's performance in multiple gaits and multiple grounds, with a simple feed-forward controller. We speculate that the robustness that we observed was due to self-stabilization properties of the compliant mechanical structure.

The current level of the energy-efficiency is shown in Fig.3b. We plan to investigate how to improve it with closed-loop control using touch sensors at the feet in order to achieve proper footfalls. In addition, we will compare rotary with oscillatory movement regarding energy consumption of the main actuators as future work.

5. ACKNOWLEDGEMENT

6. REFERENCES

[1] R. Pfeifer, M. Lungarella, and F. Iida, "Self-Organization, Embodiment, and Biologically Inspired Robotics", *Science* 16, 318 (5853), 1088-1093, 2007.

[2] D.F. Hoyt, and C. R. Taylor. "Gait and the energetics of locomotion in horses." *Nature* 292(5820): 239-240, 1981.

[3] S. Kim, J. Clark and M. Cutkosky, "iSprawl: Autonomy, and the Effects of Power Transmission", *Climbing and Walking Robots,* Part VII, pp. 859-867, 2005.

[4] I. Poulakakis, J. A. Smith, and M. Buehler, "Modeling and experiments of untethered quadrupedal running with a bounding gait: The Scout II Robot". *International Journal of Robotics Research*, vol. 24, no. 4, pp. 239-256, April 2005.

[5] K. Iida, Y. Hayami, T. Hira, T. Yasuno, T. Kamano, "Evolutionary Acquisition for Moving Performance of Reduced D.O.F's Quadruped Robot," *SICE-ICASE, 2006 International Joint Conference* , pp. 3005-3010, 2006.

[6] S. Pouya, J. Van den Kieboom, A. Sproewitz, and A.J. Ijspeert, Automatic Gait Generation in Modular Robots: to Oscillate or to Rotate? that is the question", *in Proceedings of IROS 2010.*

Stable Dynamic Walking of a Quadruped Robot "Kotetsu" against Perturbations on Posture and Rhythmic Motion

Christophe Maufroy[1] and Hiroshi Kimura[2]

[1]Locomotion Lab., University of Jena, Jena, Germany
(Tel: +49-3641-9-45743; E-mail: christophe.maufroy@uni-jena.de)
[2]Division of Mechanical and System Engineering, Kyoto Institute of Technology, Kyoto, Japan
(Tel: +81-75-724-7352; E-mail: kimura61@kit.ac.jp)

Abstract: We are developing a general quadrupedal locomotion controller by using a neural model involving a CPG (Central Pattern Generator) utilizing normal ground reaction force (leg loading) sensory feedback for both rolling motion (posture) and gait (rhythmic motion) control. In this abstract, we report the results of experiments using a quadruped robot "Kotetsu" in order to verify the results of our previous simulation study. Movies and detailed specifications of the robot can be seen at: *http://robotics.mech.kit.ac.jp/kotetsu/*.

Keywords: Quadruped Robot, Leg Unloading, Phase Modulation, CPG, Lateral Perturbation

1. INTRODUCTION

It is known about the stance-to-swing transition in animals that the transition is initiated by hip extension in decerebrate cats[1]. It is also known that the stance phase is indeterminately prolongated as long as the leg loading is over a given threshold[2]. Being motivated by the study[3], we showed in simulations that rhythmic motion of each leg is achieved as a result of the phase modulations based on leg unloading and leg coordination (gait) emerges allowing to realize dynamic walking in the low- to medium-speed range[4]. In addition, we reported the result of first experiments using a quadruped robot "Kotetsu" while comparing to the result of simulations[5]. Recently, we considered perturbations to rhythmic motion such as split-belt treadmill walking and obtained primitive results[6] combining leg unloading and hip extension for the stance-to-swing phase transition referring to[3]. In this abstract, we report on integration of posture and rhythmic motion control based on leg unloading and show experimental results using Kotetsu against perturbations to posture (rolling motion).

2. PHASE MODULATIONS BASED ON LEG UNLOADING

2.1 Single Leg Controller

Each leg is actuated by a control unit called the Leg Controller (LC). Each LC is associated with a simple oscillator with a constant and unitary amplitude and a variable phase ϕ^i, where i is the leg index[1]. The desired trajectories are calculated using the oscillator phase ϕ^i. The positions of the foot at the swing-to-stance and stance-to-swing transition are named as AEP (anterior extreme position) and PEP (posterior extreme position). We consider dynamics of an oscillator phase ϕ^i, where $\dot{\phi}^i = \hat{\omega} + \omega_{mod}$ (ω_{mod}=0 in the stance phase).

Resetting of ϕ^i is employed so that $\phi^i = \hat{\phi}_{AEP}$ and $\phi^i = \hat{\phi}_{PEP}$ at the onset of stance and swing phases, respectively. The phase transition is initiated by using normal ground reaction force: f_n^i (leg loading) and force thresholds[3]. That is, [swing-to-stance transition:] $f_n^i > \hat{\chi}_{TD} \; \& \; \phi^i > \hat{\phi}_{AEP}/2$ and [stance-to-swing transition:] $f_n^i < \chi_{LO}^i$. The force threshold: χ_{LO}^i of hind legs is expressed as follows[2]:

$$\chi_{LO}^{\{LH,RH\}} = \begin{cases} -5(N) & \text{if } \phi^i \leq \phi_{AEP} + \pi/2 \\ \hat{\chi}_{LO} & \text{otherwise} \end{cases} \quad (1)$$

χ_{LO}^i of forelegs is described in the next section as ACM.

Rolling motion (lateral posture) can be stabilized by using such leg phase modulations based on leg unloading.

2.2 Ascending Coordination Mechanism (ACM)

In our previous simulation study[4], it was shown that the lateral perturbation preventing alternation of leg loading between contralateral legs caused a conflict between the control of the rhythmic pitching motions of the legs and the posture control in the frontal plane when we employed no explicit inter-leg coordination among LCs. Therefore, we employed the two-fold ACM in order to solve such conflict and confirmed its effectiveness in simulations.

When we implemented such ACM in the control system of Kotetsu, we found in the experiments that a foreleg sometimes caused the stance-to-swing phase transition before the ipsilateral hind leg and the gait shifted to the pace. As the reason of such disorder of phase transitions, we noticed the following:

- Since CoM of the body of Kotetsu is slightly backward than the kinematical center of the body, the leg loading of a foreleg becomes smaller than that of the ipsilateral hind leg.

In order to solve such disorder of phase transitions, we slightly modified the first part of ACM in simulations, which modulates force threshold of the foreleg.

---

[1]Respectively, LH and RH mean for the left and right hind legs, and LF and RF mean for the left and right forelegs. The hat ^ symbol is used to represent the nominal value of a single variable.

[2]The value: -5 is not important and it works as far as the value is negative.

Consequently, we implemented the following ACM. In eq.(2), firstly the force threshold of the foreleg χ_{LO}^{sF} (where s stands for either R or L) is linearly increased from 0 to $\hat{\chi}_{LO}$ as the phase of the ipsilateral hind leg: ϕ^{sH} increases in order to delay (or inhibit) the stance-to-swing transition of the foreleg (ACM_{inh}) and prevent disorder of the phase transition above described. Secondly, χ_{LO}^{sF} is linearly increased from χ_{LO}^{sF} to $\chi_{LO}^{sF} + \hat{\chi}_{ampl}$ as ϕ^{sH} increases to promote (or excite) the stance-to-swing transition of the ipsilateral foreleg (ACM_{exc}) and keep alternation of leg loading between contralateral legs against the lateral perturbation. Thirdly, the stance-to-swing transition of the foreleg is inhibited during the stance phase of the ipsilateral hind leg.

$$\chi_{LO}^{sF} = \begin{cases} \tau_{acm} \cdot \hat{\chi}_{LO} & \text{if } \phi^{sH} < \hat{\phi}_{acm} \\ \hat{\chi}_{LO} + \chi_{mod} & \text{if } \phi^{sH} \in [\hat{\phi}_{acm}; \hat{\phi}_{AEP}] \\ -5(N) & \text{if } \phi^{sH} > \hat{\phi}_{AEP} \end{cases} \quad (2)$$

$$\chi_{mod} = \tau_{mod}(\phi^{sH}) \cdot \hat{\chi}_{ampl}$$

where $\hat{\phi}_{acm} = 0.5 \cdot \hat{\phi}_{AEP}$, $\tau_{acm} = \phi^{sH}/\hat{\phi}_{acm}$ and

$$\tau_{mod}(\phi) = (\phi - \hat{\phi}_{acm})/(\hat{\phi}_{AEP} - \hat{\phi}_{acm}).$$

In eq.(3), ϕ_{LO}^{sH} is the LC phase of the hind leg at the moment when the foreleg transits to the swing phase. If ϕ_{LO}^{sH} is greater than $\hat{\phi}_{acm}$, it means that the transition to the swing phase of the foreleg is delayed. Therefore, we make the swing motion of the foreleg become faster in order to compensate such delay of the transition (ACM_{ω}).

$$\omega^{sF} = \hat{\omega} + \omega_{mod}^{sF} \quad (3)$$

$$\omega_{mod}^{sF} = \begin{cases} 0.5 \cdot \tau_{mod}(\phi_{LO}^{sH}) \cdot \hat{\omega} & \text{if } \phi_{LO}^{sH} \in [\hat{\phi}_{acm}; \hat{\phi}_{AEP}] \\ 0 & \text{otherwise} \end{cases}$$

3. RESULTS OF EXPERIMENTS

As the lateral perturbation disturbing ordinary rolling motion, an impulse of 0.56 (Kgm/s), that pushed the center of the body to the right was applied at the timing where left fore and hind legs are in the swing phase. The results of experiments are shown in Fig. 1 and Fig. 2, where ACM_{inh} was employed in both cases. In both figures, the gait (solid lines mean the stance phase), leg loading of RF and body roll angle (rotation to the right is positive) are shown. We can see the effectiveness of ACM_{exc}, and can not see the effectiveness of ACM_{ω} in Fig. 2. But ACM_{ω} contributed to make RF land on the correct position and prevent the robot from falling down by stumbling of RF. As a result, we confirmed the validity of our simulation study[4] even though we used a little different ACM to cope with disturbances by the different position of CoM and noise of force sensor output in Kotetsu.

REFERENCES

[1] Hiebert, G., et al. (1996) Contribution of hind limb flexor muscle afferents to the timing of phase transitions in the cat step cycle, *J. of Neurophys.*, 75, 1126-1137.
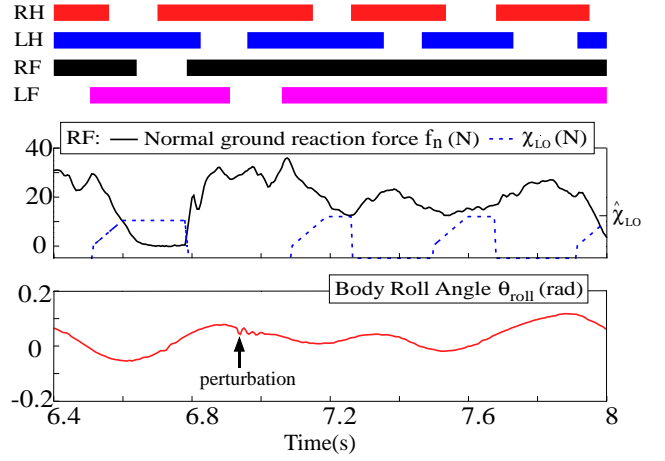
Fig. 1 Results of an experiment against the lateral perturbation without ACM_{exc} and ACM_{ω}. Alternation of leg loading between contralateral legs was prevented, and leg loading of RF was kept high. Since max value of χ_{LO} was constant, the stance-to-swing phase transition of RF was not initiated. Consequently Kotetsu fell down to the right side.
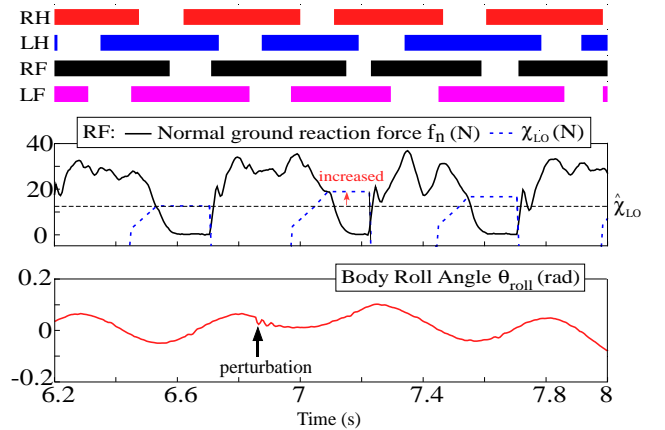
Fig. 2 Results of an experiment against the lateral perturbations with ACM_{exc} and ACM_{ω}. Although leg loading of RF was kept high, the stance-to-swing phase transition of RF was initiated because max value of χ_{LO} was increased by ACM_{exc}. Consequently the gait was stabilized and Kotetsu kept walking.

[2] Duysens, J. & Pearson, K.G. (1980). Inhibition of flexor burst generation by loading ankle extensor muscles in walking cats. *Brain Res.*, 187, 321-32.

[3] Ekeberg, O. & Pearson, K. (2005). Computer simulation of stepping in the hind legs of the cat: an examination of mechanisms regulating the stance-to-swing transition. *J. of Neurophysiology*, 94(6), 4256-68.

[4] Maufroy, C., Kimura, H. & Takase, K. (2010). Integration of Posture and Rhythmic Motion Controls in Quadrupedal Dynamic Walking using Phase Modulations based on Leg Loading/Unloading, *Autonomous Robots* 28(3), 331-353.

[5] Maufroy, C., Nishikawa, T. & Kimura, H. (2009). Stable dynamic walking of a quadruped Robot "Kotetsu" using phase modulations based on leg loading/unloading. *Proc. of ICRA 2010*, 5225-5230.

[6] Imaoka, D., Higashi, Y. & Kimura, H. (2011) Gait adaptation of a quadruped robot in split-belt treadmill walking using leg phase adjustment. *Proc. of 38th SICE Symp. on Intelligent Sys.*, 349-354.

Oncilla Robot—A Light-weight Bio-inspired Quadruped Robot for Fast Locomotion in Rough Terrain

Alexander Sproewitz[1], Lorenz Kuechler[1], Alexandre Tuleu[1], Mostafa Ajallooeian[1], Michiel D'Haene[2], Rico Moeckel[1], Auke Jan Ijspeert[1]

[1]Biorobotics Laboratory, EPFL, Lausanne, Switzerland
(Tel: +41-21 693 26 44; E-mail: alexander.sproewitz@epfl.ch)
[2]Reservoir Laboratory, Ghent University, Ghent, Belgium

Abstract: On the hardware level, we are proposing and testing a bio-inspired quadruped robot design (*Oncilla robot*), based on light-weight, compliant, and three-segmented legs. Our choice of placing the compliance such that it is spanning two joints enforces a non-linear spring stiffness. Based on the SLIP-model assumption, we compare progressive and degressive stiffness profiles against a linear-leg stiffness. To facilitate fast and throughout testing also of control approaches we have created a robot model of *Oncilla robot* in simulation (in Webots [1], a physics-based simulation environment). Here we are presenting new simulation results based on open-loop-central pattern generator (CPG) control and PSO-optimization of the CPG parameters. Our quadruped robot is equipped with passive compliant elements in its legs, and we apply two different strategies to make use of the legs' compliance during stance phase. This enables us to find stable trot gait patterns propelling the robot up to 1 m/s (more than four times the robot's leg length), depending on the applied stance phase leg-strategy. Different trot gait patterns emerge, and resulting trot gaits are variable in stability (tested as robustness against external perturbations) and speed.

Keywords: Quadruped robot, compliant three-segmented leg design, bio-inspired, fast locomotion, stability, CPG.

1. MOTIVATION AND HARDWARE

By designing, building and testing a robust, compliant, light-weight and versatile quadruped robot we want to provide a bio-inspired platform for development and testing of different approaches to motion control (e.g. locomotion and reaching, or stepping). Hence we are developing a new version of our previous robot *Cheetah* [2]. Both the physics-based simulated version and the in-construction version of *Oncilla robot* (named after a small-sized feline animal from South-America) are based on a mammalian animal, of approximate size and weight of a house cat *(Felis catus)*. *Oncilla robot* features three segmented legs both for its front and hind limbs, similar to our previous quadruped robot *Cheetah*, Fig. 1(a). Quadruped, mammalian animals have a distinct three segmented limb construction both for their front and hind limbs (front limb: if the scapula is included [3-6]). As it has been suggested by [7], Oncilla robot's limbs are panthographic. Hence proximal and distal limb segment are connected with a parallel mechanism, see Fig. 1(a). This keeps e.g. thigh and foot segment of the hind limbs parallel at all times, and resembles the animals leg segment behaviour for most of a step cycle. The robot's pantographic legs are equipped with a passive spring mechanism. The orientation and the type of springs used (extension springs) classifies the robot's leg as a passively extending, gravity loaded, compliant leg. Each of *Oncilla robot*'s legs is equipped with three actuators. The proximal actuator is responsible for leg protraction and retraction. The second actuator is flexing the two mid-joints by a cable mechanism. Extension of mid-limb joints is only possible by the passive, linear spring. The third actuator will be responsible for the ablation DOF. For some more details please refer to [2].

2. THREE-SEGMENTED LEG DESIGN

The combination of a three-segmented leg design and a two-joint spanning compliance produces a non-linear leg force behavior for *Oncilla robot's* legs. We checked the self-stability regions of different leg segmentation ratios for our leg design (λ from 0.1 to 0.5, where λ is the segmentation ratio of the mid segment to the leg length). We found that we can shift the leg force characteristics from a progressive leg force, over a mostly linear leg force, into a degressive leg force profile (Fig. 2). A SLIP-model [8] of a single three segmented leg with the corresponding *altered* stiffness profile is checked for *self-stability* (Fig. 2). Please note that the original SLIP model is assuming only linear leg forces, i.e. this would correspond to a prismatic leg design. Black areas in Fig. 2 indicates stable solutions for the pantograph leg, for comparison the stable area for the linear SLIP model is plotted in grey. The second row of Fig. 2 shows the leg force for a relevant range of the virtual leg. For $\lambda = 0.1$ (progressive leg force profile) the stable area is decreased. For $\lambda = 0.3$ the area of stability is mostly unchanged as the leg force profile practically shows a linear shape. For $\lambda = 0.5$ the stability region is slightly bent upwards for low angles of attack and low leg stiffness. This is desirable as for a given leg stiffness stable running is possible in a larger range of angles of attack. As one result of our SLIP model based simulation we will use a degressive leg force behavior in our future hardware implementation of *Oncilla robot*.

(a)　　　　　　　　(b)

(c)　　　　　　　　(d)
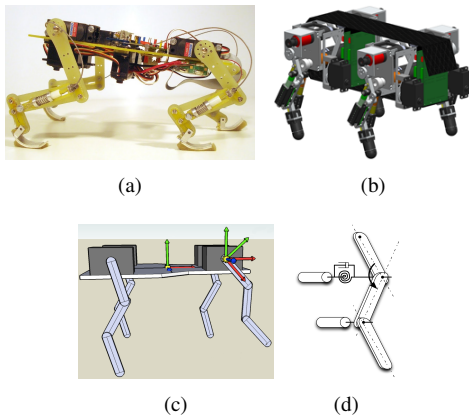
Fig. 1 *(a)* Our previous quadruped robot *Cheetah* (head is to the right)—basis for the robot used in the experiments applying open-loop-CPG. The robot's leg design is three-segmented, and pantographic. Its midleg joints are actuated through a cable mechanism. *(b)* Our new *Oncilla robot*, CAD design. New features are optimized gearbox and motor, brushless motor drivers, sensors, and additional compliant units per leg. Knee joints are actuated by an efficient cable mechanism. *(c)* Simulated robot model (simulation environment Webots). *(d)* The panthographic behaviour is hard-coded by a dedicated joint controller. This keeps proximal and distal leg segment parallel at all times. Compliance is introduced by serial elasticity in the proximal knee joint.

3. OPEN-LOOP-CPG CONTROL

To fast and throughout test both the design of hardware and controller we are using a Webots-based, simulated model of *Oncilla robot*. It is controlled with an open-loop-CPG [2], all open CPG parameters are optimized with a PSO-based optimization algorithm. Interesting results indicate a strong dependency of hip amplitude and speed of the robot (Fig. 3). We use the 500 best solutions from each optimization run (repeated several times for the same fixed frequency), plotted are the average robot speed and the robot's hip amplitude. Maximum speed reached is $1\,\mathrm{m/s}$.[1]

ACKNOWLEDGEMENTS

REFERENCES

[1] O. Michel, "Webots 5, fast prototyping and simulation of mobile robots," 2008.
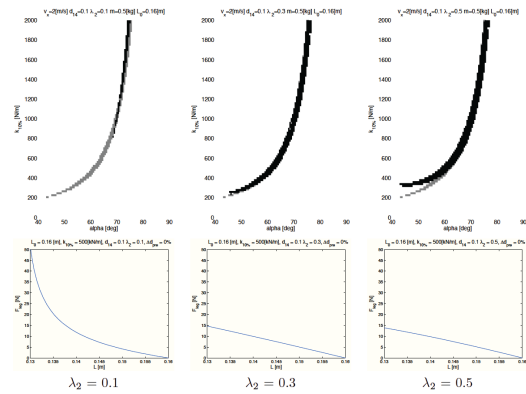
Fig. 2 The first row shows the stability plots for $\lambda = 0.1$, $\lambda = 0.3$ and $\lambda = 0.5$ tested with the apex return map on the SLIP model. The second row shows the corresponding leg force profile (progressive, linear and degressive).
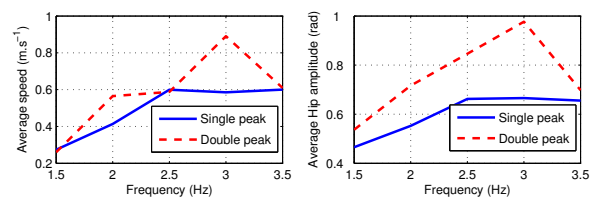
Fig. 3 Amplitude and speed average comparison for two different knee joint control strategies.

[2] S. Rutishauser, A. Sproewitz, L. Righetti, and A. J. Ijspeert, "Passive compliant quadruped robot using central pattern generators for locomotion control," in *2008 Proc BIOROB*, 2008.

[3] J. Halbertsma, "The stride cycle of the cat: the modelling of locomotion by computerized analysis of automatic recordings.," *Acta Physiologica Scandinavica, Supplement*, vol. 521, pp. 1–75, 1983.

[4] H. Witte, J. Biltzinger, R. Hackert, N. Schilling, M. Schmidt, C. Reich, and M. Fischer, "Torque patterns of the limbs of small therian mammals during locomotion on flat ground," *J Exp Biol*, vol. 205, pp. 1339–1353, May 2002.

[5] M. Fischer and R. Blickhan, "The tri-segmented limbs of therian mammals: kinematics, dynamics, and self-stabilization–a review," *Journal of Experimental Zoology. Part A, Comparative Experimental Biology*, vol. 305, pp. 935–952, Nov. 2006.

[6] M. Schmidt and M. Fischer, "Morphological integration in mammalian limb proportions: Dissociation between function and development," *Evolution*, vol. 63, no. 3, pp. 749–766, 2009.

[7] H. Witte, R. Hackert, W. Ilg, J. Biltzinger, N. Schillinger, F. Biedermann, M. Jergas, H. Preuschoft, and M. Fischer, "Quadrupedal mammals as paragons for walking machines," in *Proc AMAM*, pp. TuA–II–2.1 – TuA–II–2.4, 2003.

[8] J. Rummel, F. Iida, J. Smith, and A. Seyfarth, "Enlarging regions of stable running with segmented legs," pp. 367–372, 2008.

Poster Session

A Fluid-filled Deformable Robot That Exhibits Spontaneous Switching among Versatile Spatio-temporal Oscillatory Patterns Inspired by True Slime Mold

Takuya Umedachi[1,3], Ryo Idei[2] and Akio Ishiguro[2,4]

[1]Department of Mathematical and Life Sciences, Hiroshima University, Higashi Hiroshima, Japan
(Tel: +81-82-424-7336; E-mail: takuya.umedachi@gmail.com)
[2]Research Institute of Electrical Communication, Tohoku University, Sendai, Japan
(Tel: +81-22-217-5465; E-mail: idei@cmplx.riec.tohoku.ac.jp, ishiguro@riec.tohoku.ac.jp)
[3]Research Fellow of the Japan Society for the Promotion of Science
[4]Japan Science and Technology Agency, CREST, Tokyo, Japan

Abstract: This paper presents a fluid-filled modular robot inspired by a living coupled oscillator system constructed by plasmodium of true slime mold. The robot consists of homogeneous modules which are physically coupled with fluid-filled tubes. Exploiting this physical long distant interaction, the robot is capable to induce versatile oscillatory patterns and transitions between the rich oscillatory patterns in a fully decentralized manner. The simulation results obtained are expected to shed new light on design scheme of life-like robots to reproduce astoundingly versatile and adaptive behaviors.

Keywords: Morphological computation, fluid-driven robot, modular robot, autonomous decentralized control

1. INTRODUCTION

Animals exhibit qualitatively-different versatile behaviors and switch these behaviors according to the situation encountered. This versatility of the behaviors enables animals to reproduce astoundingly adaptive motions in unexpected complex environments. In contrast to this, most robots fail to negotiate with unexpected complex environments as quickly and smoothly as their biological counterparts. One goals of the research described here is to understand how animals generate versatile behaviors and to use these findings to build life-like robots that reproduce truly versatile and adaptive behaviors.

To this end, we have employed a so-called "back-to-basics" approach. More specifically, we have focused on plasmodium of true slime mold. The plasmodium is of interest to biologists as well as roboticists for the following reasons. First, the plasmodium exhibits versatile spatio-temporal oscillatory patterns[1], which is driven by interacting homogeneous elements of the plasmodium in the absence of a central nervous system or specialized organs. Second, and more surprisingly, transitions between the versatile oscillatory patterns occur autonomously[1]. Exploiting this versatility, the plasmodium is thought to be capable to induce adaptive locomotions. Hence, the plasmodium is thought to have archetypal structure to induce the behavioral intelligence, and therefore it is one of the best-simple models to investigate essential for the behavioral intelligence of animals.

One factor that helps the plasmodium exhibit such oscillatory patterns is its reliance on physical communication (morphological computation) stemming from the protoplasmic streaming. The plasmodium employs purely decentralized control mechanisms based on coupled biochemical oscillators similar to CPG, which is physically coupled with tubes filled with the protoplasm. By producing protoplasmic streaming through the tubes, physical long-distance interaction is induced between the

oscillators, which is akin to that observed in waterbeds. This physical interaction leads to phase modification on each oscillator based on its pressure from the protoplasm[2]. In light of these facts, the physical interaction stemming from the protoplasmic streaming plays an essential role in creating and switching the versatile oscillatory patterns. Therefore, the purpose of this study is to build such autonomous decentralized system that induce rich oscillatory patterns and to understand archetypal structure to induce such intelligence.

Based on the above considerations, we introduce a fluid-filled modular robot inspired by a living coupled oscillator system constructed by plasmodium of true slime mold. Each module of the robot has a deformable outer skin, stemming from Real-time Tunable Springs (RTSs), filled with fluid. The robot consists of these homogeneous modules which are physically coupled with fluid-filled tubes. Exploiting this physical long distant interaction, the robot is capable to induce surprisingly versatile oscillatory patterns and transitions between them in a fully decentralized manner.

2. THE MODEL

2.1 Mechanical system

The fluid-filled modular robot consists of several modules that are physically connected with tubes (Fig. 1). Each module of the robot is composed of its control system (*i.e.*, decoupled oscillators), a deformable outer skin, and fluid as protoplasm inside the outer skin. The outer skin consists of 4 mass particles and 2 pairs of RTSs that are able to actively alter their resting lengths (*i.e.*, unstretched length of the elastic element). By altering the resting length of each RTS, the protoplasm are pushed and pulled competitively. This physical interaction is simulated by potential constraint on area surrounded by the mass particles on each module. Here, module i contains two de-coupled phase oscillators. According to the
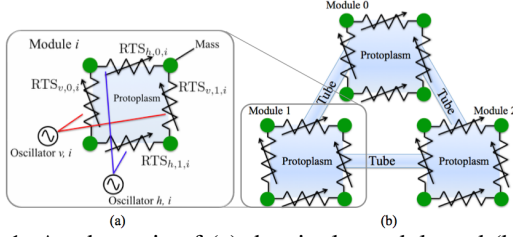
Fig. 1 A schematic of (a) the single module and (b) the robot composed of three modules.

phase, $\theta_{n,i}(n = v, h)$, resting lengths of one pair of $\text{RTS}_{n,m,i}(m = 0, 1)$ are controlled (see Fig. 1 (a)).

2.1.1 RTS

The resting length of $\text{RTS}_{n,m,i}$, $l_{n,i}^{RTS}(\theta_{n,i})$, alters according to $\theta_{n,i}$, and is given by

$$l_{n,i}^{RTS}(\theta_{n,i}) = \bar{l}_{n,i}(1 - a\cos\theta_{n,i}), \quad (1)$$

where a is a constant in space and time and $\bar{l}_{n,i}$ represents the mean length. Depending on its resting length, spring constant $k_{n,i}^{RTS}(\theta_{n,i})$ of $\text{RTS}_{n,m,i}$ varies as follows:

$$k_{n,i}^{RTS}(\theta_{n,i}) = \frac{\alpha_i}{l_{n,i}^{RTS}(\theta_{n,i})}, \quad (2)$$

where α_i is a constant given by the material and geometric properties of the elastic material.

The tension on $\text{RTS}_{n,m,i}$, $T_{n,m,i}$, can be measured by a force sensor, and then the actual length, $l_{n,m,i}$, can be calculated from the following equation:

$$T_{n,m,i} = k_{n,i}^{RTS}(\theta_{n,i})(l_{n,m,i} - l_{n,i}^{RTS}(\theta_{n,i})). \quad (3)$$

RTS is indispensable for this system in terms of the active-passive mechanical feature: by sensing the tension, force from the other RTSs through the protoplasm can be detected as "discrepancy" between the controlled value, $l_{n,i}^{RTS}$, and the actual value, $l_{n,m,i}$.

2.1.2 Protoplasmic streaming

In order to simulate protoplasmic streaming between the modules, area S_i on module i is expressed as

$$\frac{dS_i}{dt} = \sum_j D_{i,j}\{p_j(t) - p_i(t)\}, \quad (4)$$

$$p_i(t) = \lambda \sum_{m=0}^{1}\left(\frac{T_{v,m,i}}{l_{h,m,i}} + \frac{T_{h,m,i}}{l_{v,m,i}}\right), \quad (5)$$

where p_i, p_j are pressure on module i, j respectively, which are connected with the tube, and $D_{i,j}$ is constant that defines fluid conductance of the tube. p_i is calculated based on tension on RTSs. Eqs. (4), (5) express protoplasmic streaming between module i and module j via the tube based on the pressure difference and fluid conductance.

2.2 Control system

Here, we introduce the dynamics of the oscillator model to be implemented in each pair of RTSs. The equation of the oscillator is expressed as

$$\frac{d\theta_{n,i}}{dt} = \omega - \frac{\partial}{\partial\theta_{n,i}}\left(\frac{\sigma}{2}\sum_{m=0}^{1}T_{n,m,i}^2\right) + \xi_{n,i}(t), \quad (6)$$
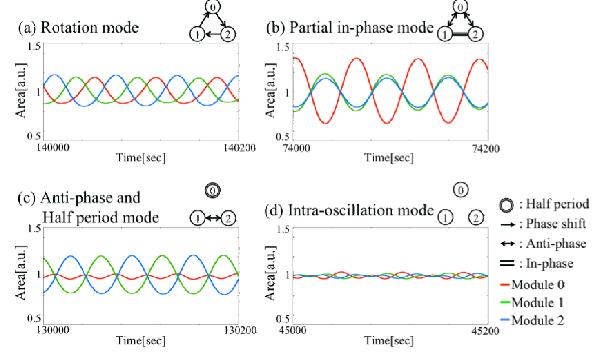

Fig. 2 Oscillatory patterns in three modules. Schematic diagrams of phase relations among three oscillators are indicated at upper right of the plots. A double circle shows that the corresponding module has double frequency. Relationships between two modules are indicated by $=$: in phase; $\rightarrow$: $\frac{2\pi}{3}$ phase shift; $\leftrightarrow$: anti phase.
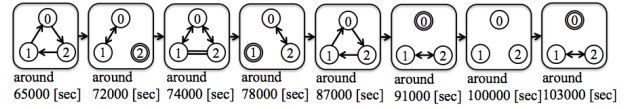

Fig. 3 Transitions between the several oscillation modes.

where ω is the intrinsic frequency of the oscillators, the second term is local sensory feedback so as to reduce the discrepancy (*i.e.*, tension on RTS) [2], and the third term is faint noise.

3. SIMULATION RESULTS

In order to confirm the validity of the model, we conducted simulation experiment on 3 modules[1] (see Fig. 2 and Fig. 3). As can be seen in Fig. 2, we confirmed 4 oscillatory patterns: (a) Rotation mode, (b) Partial in-phase mode, (c) Anti-phase and Half period mode, (d) Intra-oscillation mode[2]. More surprisingly, we confirmed transition between them as shown in Fig. 3.

4. CONCLUSION

A fluid-filled modular robot which exhibits versatile oscillatory patterns and transition between them without the need of any hierarchical structure were presented.

REFERENCES

[1] A. Takamatsu, "Spontaneous Switching among Multiple Spatio-temporal Patterns in Three-oscillator Systems Constructed with Oscillatory Cells of Slime Mold Å h, *Physica D*, Vol.223, pp.180-188, 2006.

[2] T. Umedachi, K. Takeda, T. Nakagaki, R. Kobayashi and A. Ishiguro, Å gFully Decentralized Control of a Soft-bodied Robot Inspired by True Slime Mold Å h, *Biological Cybernetics*, Vol.102, pp.261-269, 2010.

---

[1]The parameters of the robot are as follows: $\alpha_0 = 10.0$ [a.u.]; $\alpha_1 = 10.0$ [a.u.]; $\alpha_2 = 11.0$ [a.u.]; $\sigma = 0.003$ [a.u.]; $\theta_{n,0}(t = 0) = \pi/4$ [rad]; $\theta_{n,1}(t = 0) = 0.0$ [rad]; $\theta_{n,2}(t = 0) = \pi/4$ [rad]; $D_{i,j} = 0.01$ [a.u.].
[2]The names of the oscillatory patterns (a), (b), and (c) were determined by reference to Takamatsu's work [1].

Decentralized Control of an Earthworm-like Robot That Fully Exploits Mechanical Interaction

Kazuyuki Yaegashi[1], Takeshi Kano[1], Ryo Kobayashi[2,3], and Akio Ishiguro[1,3]

[1]Research Institute of Electrical Communication, Tohoku University, Sendai, Japan
(Tel: +81-22-217-5465; E-mail: yaegashi@cmplx.riec.tohoku.ac.jp)
[2]Department of Mathematical and Life Sciences, Hiroshima University, Higashi Hiroshima, Japan
(Tel: +81-82-424-7335; E-mail: ryo@math.sci.hiroshima-u.ac.jp)
[3]Japan Science and Technology Agency, CREST, Tokyo, Japan

Abstract: To clarify the mechanism of mechanical interaction between individual components of a body, which contributes to the emergence of animal behavior, we focus on the locomotion of an earthworm. We theoretically analyze the locomotion of earthworms on the basis of a continuum model, and we derive the optimal force distribution that enables efficient locomotion. We propose a decentralized control scheme on the basis of the optimal force distribution, and we verify its validity through simulations.

Keywords: Autonomous decentralized control, Earthworm, Continuum model

1. INTRODUCTION

Animals exhibit adaptive and efficient locomotion in real time under unpredictable real-world constraints. A key mechanism underlying such functionality of animals is autonomous decentralized control, whereby nontrivial macroscopic behavior or functionality emerges through coordination between simple individual components. Thus, autonomous decentralized control is expected to be employed as a useful tool for designing robots that are as intelligent as animals.

The design of the interaction between individual components is an important issue for the development of robots based on autonomous decentralized control. The interaction can be designed in two forms: informational (neural) interaction and mechanical interaction. The former has been systematically studied on the basis of coupled-oscillator systems [1], whereas the latter has been designed on an ad-hoc and tailor-made basis for specific applications, although this approach can lead to the emergence of highly adaptive and efficient behavior as a consequence of interaction between the body and the environment [2]. Thus, we need to establish a systematic method for designing the mechanical interaction on the basis of a suitable model of a living organism.

To address this issue, we focus on an earthworm, which locomotes by propagating waves of bodily contractions from the head to the tail. Because this wave propagation is significantly slower than neuronal signal propagation, the mechanical interaction in an earthworm is expected to be governed by an inherent autonomous decentralized control mechanism. In this study, we analyze the locomotion of earthworms on the basis of a continuum model that was previously developed for snake locomotion [3], and we derive the optimal force distribution for efficient locomotion. We propose an autonomous decentralized control scheme on the basis of this result, and we verify its validity through simulations.
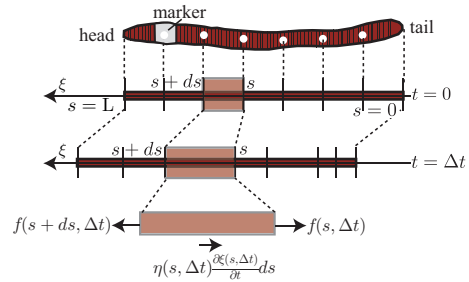
Fig. 1 Schematic illustration of continuum model of an earthworm.

2. CONTROL SCHEME BASED ON THEORETICAL ANALYSES

The adopted model is shown in Fig. 1. The body consists of a continuous line of length L. Forces of compression and tension can be actively generated in each section of the body; according to these forces and ground frictional forces, which we will describe later, each section of the body contracts or extends. Here, we disregard the viscoelasticity of the body for simplicity. The body is parameterized by the arc length s, which is defined as the distance of a point from the tail end when the body does not contract or extend. $\xi(s,t)$ denotes the absolute coordinate of the point expressed by the arc length s at time t. The actively generated forces of compression and tension are denoted by $f(s,t)$, where the tensional force is taken as positive. The ground friction is modeled by the viscous friction; the coefficient of the viscous friction, $\eta(s,t)$, is assumed to vary depending on the rate of expansion and contraction as follows:

$$\eta(s,t) = \frac{1}{au(s,t) - b}, \qquad (1)$$

where a and b are positive constants, and $u(s,t)$ is the ratio of expansion to contraction.

Under the assumption that the inertia of the body is negligible, the force-balance equation in each section of the body is expressed as follows:

$$\eta(s,t)\frac{\partial \xi(s,t)}{\partial t} = \frac{\partial f(s,t)}{\partial s}. \qquad (2)$$

From Eqs. (1) and (2), the velocity of the center of mass v_g is given as follows:

$$
\begin{aligned}
v_g &= \frac{1}{L}\int_0^L \frac{\partial \xi(s,t)}{\partial t}ds, \\
&= \frac{1}{L}\int_0^L (au(s,t)-b)\frac{\partial f(s,t)}{\partial s}ds. \quad (3)
\end{aligned}
$$

When we assume that the body does not generate forces at the head and tail ends, *i.e.*, $f(0,t)=f(L,t)=0$, Eq. (3) can be rewritten as

$$
v_g = -\frac{a}{L}\int_0^L \frac{\partial u(s,t)}{\partial s}f(s,t)ds. \quad (4)
$$

Now, we derive the optimal force distribution for efficient locomotion of an earthworm. It can be obtained by deriving the functional form of $f(s,t)$ that maximizes v_g under the following isoperimetric condition:

$$
\int_0^L f^2(s,t)ds = c_1^2, \quad (5)
$$

where c_1 is a positive constant. Using the Lagrange multiplier method, we obtain

$$
f(s,t) = -\frac{c_1}{\sqrt{\int_0^L \left(\frac{\partial u(s,t)}{\partial s}\right)^2 ds}}\frac{\partial u(s,t)}{\partial s}. \quad (6)
$$

Thus, to maximize v_g, $f(s,t)$ needs to be proportional to $\partial u(s,t)/\partial s$. This result would suggest that an earthworm locomotes efficiently when it generates a force proportional to the derivative of the ratio of expansion to contraction.

Next, we propose an autonomous decentralized control scheme that would enable an earthworm-like robot to realize efficient locomotion. The body of the robot consists of N links concatenated one-dimensionally. Each link can actively generate forces of compression and tension, through which it contracts and extends. The frictional coefficient of each link decreases as it extends. Except for the link at the head end whose length can be manipulated by the robot controller, the force generated by the ith link from the head end, f_i (tensional force is taken as positive), is designed on the basis of the theoretical result derived above. By replacing $\partial u(s,t)/\partial s$ with $u_{i-1}-u_i$, where u_i is the ratio of expansion to contraction of the ith link, f_i is designed as

$$
f_i = -k(u_{i-1}-u_i), \quad (7)
$$

where k is a positive constant. By employing this design scheme, efficient locomotion can be realized on the basis of autonomous decentralized control.

3. SIMULATION RESULTS

We performed simulations on the basis of the autonomous decentralized control scheme proposed in the previous section. We designed u_1 of the first link from the head end as follows:

$$
u_1 = A\sin\omega t + B, \quad (8)
$$
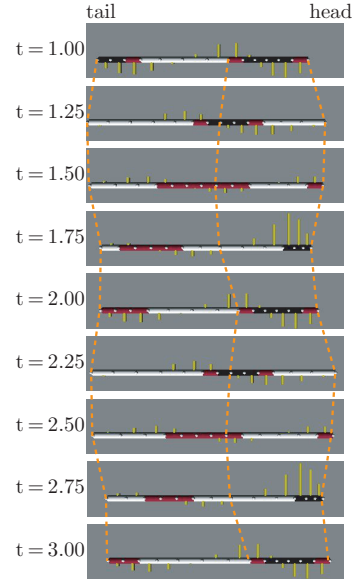
Fig. 2 Snapshots of simulation results. The color of the body is black, red, and white when $u_i < 0.9$, $0.9 \leq u_i \leq 1.1$, and $u_i > 1.1$, respectively. The yellow bars indicate the value of f_i (upper bars indicate positive values). The dotted lines track the 1st, 7th, and 14th body segments.

where A and B are positive constants, and ω is the angular frequency. Fig. 2 shows the snapshots of simulation results. We find that the robot locomotes by propagating waves of bodily contractions from the head to the tail. This result is qualitatively in good agreement with the locomotion of real earthworms.

4. CONCLUSION

To clarify the mechanism of mechanical interaction between individual components of the body, which contributes to the emergence of adaptive behavior, we focused on the locomotion of an earthworm. We theoretically analyzed the locomotion of earthworms on the basis of a continuum model, and we derived an optimal force distribution that enables efficient locomotion. On the basis of this result, we proposed an autonomous decentralized control scheme for the efficient locomotion of an earthworm-like robot, whereby a force proportional to the derivative of the ratio of expansion to contraction is generated. The results showed that the robot locomoted efficiently.

REFERENCES

[1] G. Taga, Y. Yamaguehi, and H. Shimizu, "Self-organized Control of Bipedal Locomotion by Neural Oscillators", *Biol. Cybern.*, Vol. 65, pp. 147-159, 1991.

[2] R. Pfeifer and C. Scheier,"Understanding Intelligence", *MIT Press*, Cambridge, MA, 1999.

[3] H. Date and Y. Takita, "Adaptive Locomotion of a Snake Like Robot Based on Curvature Derivatives", *in Proc. of the IEEE/RSJ International Conference on Intelligent Robots and Systems*, pp. 3554-3559, 2007.

Efficient Undulating Locomotion Driven by a Decentralized Control That Fully Exploits Multi-articular Muscles

Takeshi Kano[1], Takahide Sato[1], Ryo Kobayashi[2,3], and Akio Ishiguro[1,3]

[1]Research Institute of Electrical Communication, Tohoku University, Sendai, Japan
(Tel: +81-22-217-5465; E-mail: tkano@riec.tohoku.ac.jp)
[2]Department of Mathematical and Life Sciences, Hiroshima University, Higashi Hiroshima, Japan
(Tel: +81-82-424-7335; E-mail: ryo@math.sci.hiroshima-u.ac.jp)
[3]Japan Science and Technology Agency, CREST, Tokyo, Japan

Abstract: To clarify the mechanism of multi-articular muscles that contributes to the emergence of animal behavior, we focus on the locomotion of a snake. Analyses on the basis of the continuum model show that the body propels efficiently as the number of segments spanned by each muscle increases. On the basis of this result, we propose a decentralized control scheme for the efficient locomotion of a multi-articular serpentine robot, and we confirm its validity by simulations.

Keywords: Autonomous decentralized control, Multi-articular muscles, Serpentine robot

1. INTRODUCTION

Animals exhibit adaptive and efficient locomotion in real time under unpredictable real world constraints. A key mechanism underlying such functionality of animals is an autonomous decentralized control, whereby non-trivial macroscopic behavior or functionality emerges through the coordination of simple individual components. In particular, the design of the mechanical system (*i.e.*, body) in autonomous decentralized control systems is of significant importance, because highly intelligent behavior emerges through interactions between the body and the environment [1].

Although numerous biologically inspired robots was developed on the basis of the decentralized control, they could not fully reproduce the innate behavior of animals; one of its reasons is that the actuators in most robots act on single joints, whereas animals generally have multi-articular muscles that enable long-distant physical interaction. It was suggested that multi-articular muscles play a role in generating smooth, fine, and precise motions [2]; however, theoretical understanding of their functional role is currently at a rudimentary stage.

To address this issue, we focus on the locomotion of a snake that exploits its long muscle-tendon structures. Date and Takita showed using a continuum model that a snake propels efficiently when a bending moment proportional to the curvature derivative of the body curve is applied [3]. In this study, we extend their theory to investigate the effect of multi-articular muscles, and we show that the body propels efficiently as the number of segments spanned by each muscle increases. On the basis of this result, we propose a decentralized control scheme for the efficient locomotion of a multi-articular serpentine robot, and we confirm its validity by simulations.

2. CONTROL SCHEME BASED ON THEORETICAL ANALYSES

The adopted model is shown in Fig. 1. We consider two-dimensional motion. The body consists of a non-stretchable continuous backbone curve of length L and zero thickness. The backbone curve is parameterized by the arclength $s \in [0, L]$ from the head to tail. N rectilinear links of length $2r$ are aligned such that they are perpendicularly bisected by the backbone curve. The ith link intersects the backbone curve at $s = (i - 0.5)\Delta s [\equiv X_i]$, where $\Delta s = L/N$. n-articular muscles connect the tips of the links at $s = X_i$ and $s = X_{i+n}$ on the ipsilateral side. We disregard the viscoelastic property of muscles. We assume that the line density of the backbone curve ρ is uniform along the body, and that the weights of the links and muscles are negligible. The frictional coefficients in the longitudinal and latitudinal directions are assumed to be 0 and ∞, respectively. Furthermore, $n\Delta s \ll 1/\kappa(s)$ and $n\Delta s \ll L$ are assumed, where $\kappa(s)$ is the curvature of the backbone curve; owing to the former assumption, the angles between the longitudinal direction of the backbone curve at $s = X_i$ and the directions of the muscles attached on the ith link are found to be sufficiently smaller than unity, although the proof is not shown because of the page restriction.

Thus, the equations for the longitudinal force balance and momentum balance of a section of the backbone curve within the range of $[X_{i-\frac{1}{2}}, X_{i+\frac{1}{2}}]$, where $X_{i\pm\frac{1}{2}} \equiv X_i \pm \Delta s/2$, are expressed as

$$
\begin{aligned}
\rho\Delta s\alpha = \quad & f_s(X_{i+\frac{1}{2}}) - f_s(X_{i-\frac{1}{2}}) \\
& -[q(X_{i+\frac{1}{2}}) + q(X_{i-\frac{1}{2}})]\kappa(X_i)\Delta s/2 \\
& +F_r(X_{i-n}) + F_l(X_{i-n}) \\
& -F_r(X_i) - F_l(X_i),
\end{aligned} \tag{1}
$$

and

$$
\begin{aligned}
0 = \quad & [q(X_{i+\frac{1}{2}}) + q(X_{i-\frac{1}{2}})]\Delta s/2 \\
& -r[F_r(X_{i-n}) - F_l(X_{i-n})] \\
& +r[F_r(X_i) - F_l(X_i)],
\end{aligned} \tag{2}
$$

respectively. Here, α is the longitudinal acceleration, $f_s(s)$ is the internal force along the backbone curve, and $q(s)$ is the shear stress. $F_r(X_i)$ and $F_l(X_i)$ are the forces
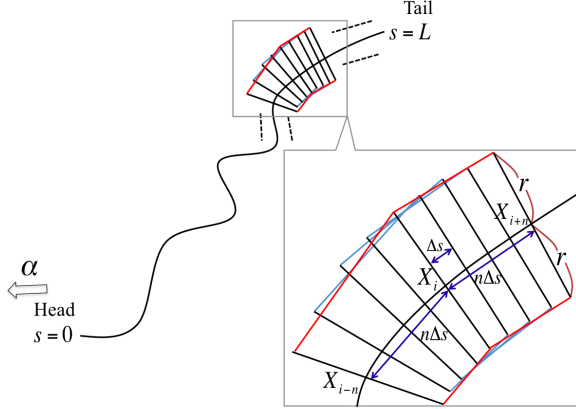
Fig. 1 The adopted continuum model. The red and blue lines denote multi-articular muscles.

generated by the muscles that connect the links at $s = X_i$ and $s = X_{i+n}$ on the right and left side, respectively. $q(X_{i\pm\frac{1}{2}})$ is eliminated from Eqs. (1) and (2), and the obtained equations are summed from $i = 1$ to N under the assumption of $f_s(0) = f_s(L) = 0$; furthermore, the summation is represented integrally. Then, we obtain

$$\rho L \alpha = \int_0^L ds \cdot nr[F_l(s) - F_r(s)]\kappa'(s). \qquad (3)$$

For a given α, the optimal force distribution of muscles that minimizes the quadratic cost function $N^{-1}\sum_{i=1}^{N-n}(F_l^2(X_i) + F_r^2(X_i))$ can be derived using the Lagrange multiplier method with continuum approximation as

$$
\begin{aligned}
F_l^*(s) &= \text{Max}[K\kappa'(s), 0], \\
F_r^*(s) &= \text{Max}[-K\kappa'(s), 0], \qquad (4)
\end{aligned}
$$

where $K = \rho L \alpha [\int_0^L ds \cdot rn\kappa'^2(s)]^{-1}$. Thus, $F_l^*(s)$ and $F_r^*(s)$ decrease as n increases, which implies that the body can locomote via small actuation forces when n is large.

On the basis of this result, we design a decentralized control scheme of a multi-articular serpentine robot in which rigid links of length Δs are concatenated one dimensionally. As $\Delta s \to 0$, $(\phi_{i+n} - \phi_i)/n\Delta s$ corresponds to the curvature derivative $\kappa'(X_i)$ in the continuum model, where ϕ_i is the ith joint angle; hence, from (4), we design the force generated by the muscle that connects the ith and $i + n$th link on the right and left side, $F_{r,i}$ and $F_{l,i}$, respectively, as follows:

$$
\begin{aligned}
F_{l,i} &= \text{Max}[-k(v_d - v)(\phi_i - \phi_{i+n}), 0], \\
F_{r,i} &= \text{Max}[k(v_d - v)(\phi_i - \phi_{i+n}), 0] \qquad (5)
\end{aligned}
$$

for $2 \leq i \leq N - n$, where k is the control gain and v_d is the desired longitudinal velocity. Note that $F_{r,1}$ and $F_{l,1}$ are arbitrarily manipulated by the robot controller.

3. SIMULATION RESULTS

We conducted simulations to investigate the validity of the control scheme described above. We designed a simu-
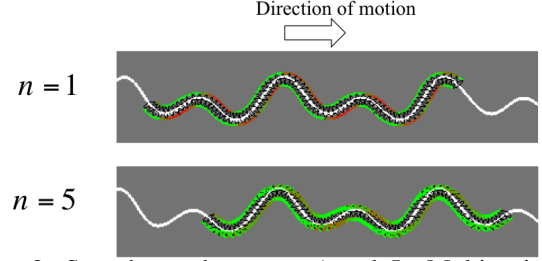

Fig. 2 Snapshots when $n = 1$ and 5. Multi-articular muscles are denoted by red color when they generate forces and by green color otherwise. White curve denotes a sulcus along which the robot locomotes.
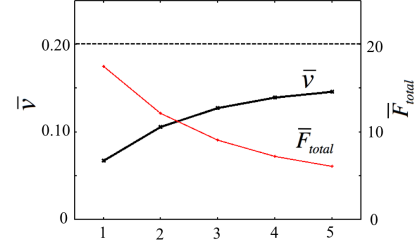

Fig. 3 $\bar{v}$ and $\bar{F}_{total}$ when n is varied. Black and red lines denote $\bar{v}$ and $\bar{F}_{total}$, respectively. The dashed line denotes the desired velocity v_d.

lation course with a curved sulcus, along which the robot locomoted. Fig. 2 shows the snapshots at $t = 400$ when $n = 1$ and 5. It is clear that the forces generated by the muscles when $n = 1$ are larger than those when $n = 5$. Fig. 3 shows the plots of the time averages of the velocity and the total force generated, $\bar{v}$ and $\bar{F}_{total}$, respectively, when n is varied. We find that $\bar{v}$ approaches v_d while $\bar{F}_{total}$ decreases as n increases. This result strongly suggests that multi-articular muscles play a pivotal role for enhancing locomotion efficiency.

ACKNOWLEDGMENTS

REFERENCES

[1] R. Pfeifer and C. Scheier, *Understanding Intelligence*, MIT Press, 1999.

[2] M. Kumamoto, T. Oshima, and T. Yamamoto, "Control Properties Induced by the Existence of Antagonistic Pairs of Bi-articular Muscles - Mechanial Engineering Model Analyses", *Human Movement Science*, Vol. 13, pp. 611-634, 1994.

[3] H. Date and Y. Takita, "Adaptive Locomotion of a Snake Like Robot Based on Curvature Derivatives", *in Proc. of the IEEE/RSJ International Conference on Intelligent Robots and Systems*, pp. 3554-3559, 2007.

Development of Multi-legged Passive Dynamic Walking Robot

Yasuhiro Sugimoto[1], Hidetaka Yoshioka[2] and Koichi Osuka[1]

[1]Department of Mechanical Engineering, Osaka University, Japan
(Tel: +81-6-6879-4084 ; E-mail: {yas, osuka}@mech.eng.osaka-u.ac.jp)
[2]Department of Mechanical Engineering, Kobe University, Japan
(Tel: +81-6-6879-4084; E-mail: h-yoshioka@stu.kobe-u.ac.jp)

Abstract: This research realizes and analyze Multi-legged Passive Dynamic Walking(PDW). Although various PDW studies have been conducted based on its interesting features, most of them dealt with bipedal robots. There are many kinds of multi-legged creatures, not only quadrupedal animals but also creatures with more than six legs. In this paper, we focus on a "Multi-legged PDW," which is a PDW with more than four legs. We develop multi-legged Passive Dynamic Walking robots, Jenkka-I, II and III, and discuss whether these robots can be realized and whether they can change its locomotion depending on such factors slope angle or their structure through simulations and experiments.

Keywords: Passive Dynamic Walking, multi-legged, locomotion transition

1. INTRODUCTION

Recently, Passive Dynamic Walking (PDW), which was first studied by McGeer[1], has been focused on in the research of walking robots. It is well known that PDW shows various interesting features. Although various studies of PDW have been conducted based on the PDW's interesting features[2], most previous studies dealt with bipedal robots. However, many walking creatures have more than four legs in nature and the animal that routinely travels bipedaly are humans only. And it is also well known that many multi-legged animal shows various locomotions depending on variety factors, such as a size of the animal or a locomotion speed. To reveal the walking principle, it is important to determine whether a PDW robot with four legs or more can be realized.

As for a quadrupedal PDW, some research has already been carried out, but they were only simulation-base studies [3, 4]. So, the research of multi-legged (more than four legs) PDW remains inadequate. In this paper, we focus on multi-legged PDW, which have more than four legs or more and verify the capability using real walking robots. And we dealt not only quadrupedal PDW but also Super-multi-legged[1] PDW that had more than six legs. There are many other kinds that have more than six legs exist. The realization and investigation of Super-multi-legged PDW will also provide significant insights into their interesting locomotion.

2. JENKKA

We developed a multi-legged PDW robots named "Jenkka." The concept of Jenkka series is as follows: (1) its fundamental structural component is a bipedal Passive Dynamic Walker, (2) by connecting each component to a **body**, it can become a Multi-legged Passive Dynamic Walker with more than four legs, (3) there is no direct leg-synchronizing mechanism, and (4) Only through the body, each component interacts indirectly. Based on this
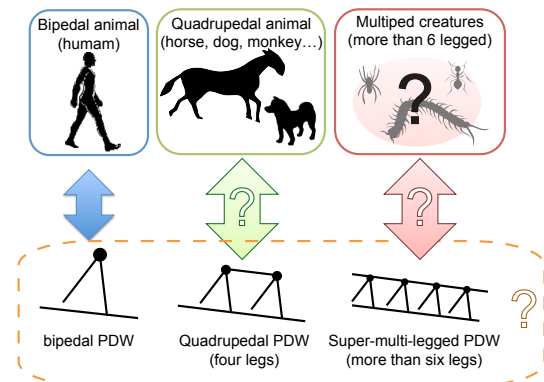
Fig. 1 Concept of Multi-legged PDW

concept, three types of Jenkka have been made. Jenkka-I is q quadrupedal PDW robot, that is, the multi-legged PDW robot with four legs (Fig. 2(a))[5]. The second type "Jenkka-II" has six legs. It was redesigned to be downsized and the size of Jenkka-II is about 50% of Jenkka-I. The latest is Jenkka-III (Fig. 2(b)). At present, it has up to 20 legs, that is, 10 bipedal elements. However, the number of legs on these robots is not fixed and can be increased based on the concept of Jenkka.

In our previous simulation study, it was shown that the degrees of freedom of the body element, which corresponds to the spine of Jenkka, played a crucial role in the realization of stable walking or locomotion transition. Then, we designed a few types of bodies and these bodies

---

[1]To distinguish from Quadrupedal, we use the word "Super-multi-legged" as a more than 6-legged.
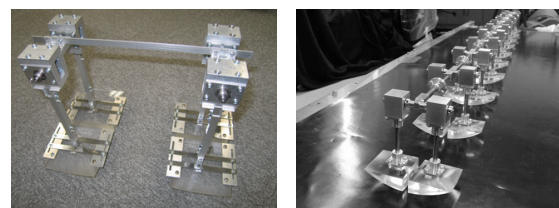
(a) Jenkka-I   (b) Jenkka-III

Fig. 2 Multi-legged PDW robot "Jenkka"

(a) Pace gait(with rigit body)   (b) Trot gait(with rollable body)
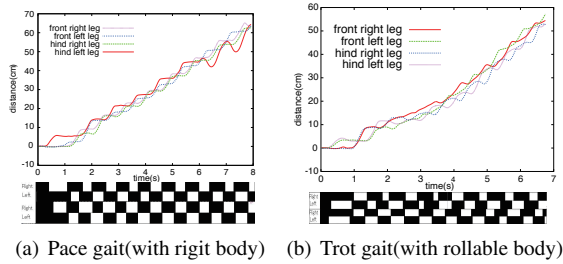
Fig. 3 Experimental Results of Jenkka-I
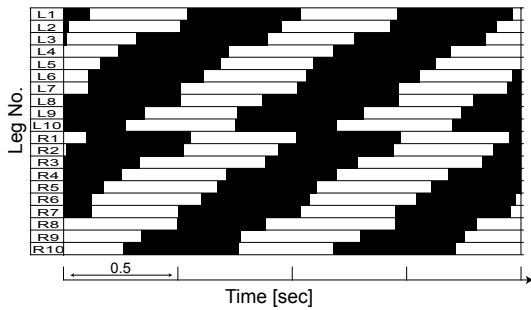
(a) with the pitch rollable body
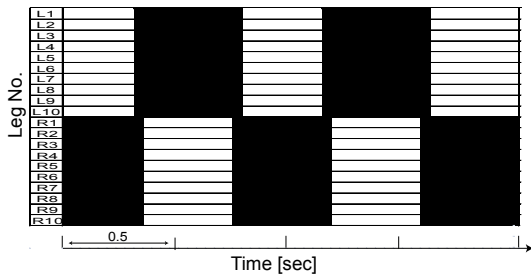
(b) with the pitch and roll rollable body

Fig. 4 Experimental Results of Jenkka-III

were tested in the follwing walking experiments.

3. EXPERIMENT RESULTS

3.1 Jenkka-I

Fig. 3 shows the experimental result of Jenkka-I. In the case of Fig. 3(a), a flat rigit body was used and Jenkka-I showed a pace gait. On the other hand, in the case of Fig. 3(b), a rollable body was used and Jenkka-I showed a trot gait. From these experimental result, it can verified that not only q quadrupedal PDW can be realizable but also it can show some different locomotions depending on the degree of freedom of the body.

3.2 Jenkka-III

Figure 4 show the experiments result of Jenkka-III.Figs. 4(a) and 4(b) show a gait chart of Jenkka-III with a pitch rollable body and with a pitch and roll rollable body, respectively. As it can be easily seen, these gait are clearly different. Fig. 5 shows a snapshot of the locomotion with the pitch and roll rollable body. In this case, ipsilateral legs touched down on the ground in sequence (from hind leg to front leg). This walking corresponds to a walk gait of a 4 legged creature.
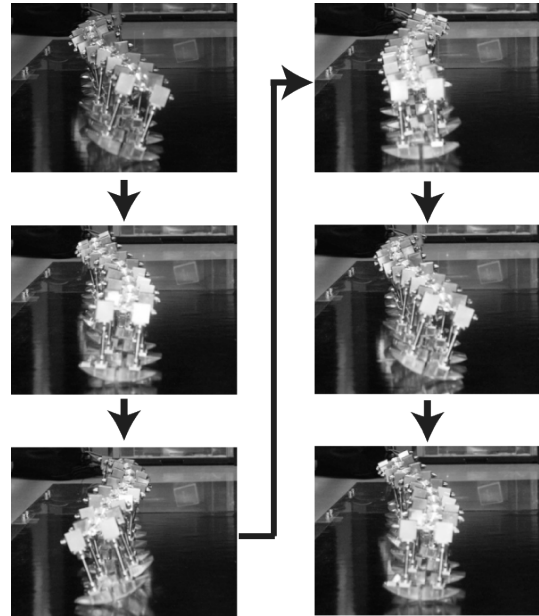
Fig. 5 Snapshot of Jenkka-III Gait

4. CONCLUSION

In this paper, we investigated the multi-legged PDW. Through experiments with multi-legged PDW robots Jenkka-I, II and III, we verified that the quadrupedal PDW and Super-multi-legged PDW can be realizable. We also showed that a multi-legged PDW robot could exhibit various locomotions depending on its structure or parameters. It is quite interesting that the locomotion and locomotion transition were induced absolutely passively based on the structure of the robot and the interaction between the robot and the environment and these results are very significant for the follow-on research of multi-legged PDW.

REFERENCES

[1] T. McGeer, "Passive Dynamic Walking," *The International Journal of Robotics Research*, vol. 9, no. 2, pp. 62–82, Apr. 1990.

[2] S. Collins, A. Ruina, R. Tedrake, and M. Wisse, "Efficient bipedal robots based on passive-dynamic walkers," *Science*, vol. 307, no. 5712, pp. 1082–1085.

[3] M. Smith, A.C. and Berkemeier, "Passive dynamic quadrupedal walking," in *Proc., of IEEE International Conference on Robotics and Automation 1997*, 1997, pp. 34–39.

[4] C. D. Remy, K. Buffinton, and R. Siegwart, "Stability Analysis of Passive Dynamic Walking of Quadrupeds," *The International Journal of Robotics Research*, vol. 29, no. 9, pp. 1173–1185, 2009.

[5] K. Nakatani, Y. Sugimoto, and K. Osuka, "Demonstration and Analysis of Quadrupedal Passive Dynamic Walking," *Advanced Robotics*, vol. 23, no. 5, pp. 483–501, Mar. 2009.

Development of 3D Quadruped Robot with Animal-like Trunk and Leg Mechanisms

Takashi TAKUMA[1], Masahiro IKEDA[1], and Tatsuya MASUDA[1]

[1]Dept. of Electrical and Electronic Systems Engineering, Osaka Institute of Technology
5-16-1 Asahi-ku, Osaka city, Japan
(Tel: +81-6-6954-4323; E-mail: takuma@ee.oit.ac.jp)

Abstract: One major challenge in the development of quadruped robots is achieving animal-like energy efficient locomotion at low computational cost. In this regard, joint viscoelasticity such as that found in animals has been attracting considerable attention. In the present paper, based on animal body designs, we introduce a quadruped robot that has (i) a trunk mechanism with multiple passive joints with tunable viscoelasticity and (ii) legs driven by viscoelastic pneumatic actuators. We carry out an experiment to determine the effect of the viscoelasticity of the truck joints on dynamic locomotion of the robot.

Keywords: trunk structure, quadruped locomotion, joint viscoelasticity

1. INTRODUCTION

One highly promising approach to achieving energy efficient dynamic locomotion at low computational cost is adopting animal body designs, especially passive joint mechanisms. Some research has already been reported on viscoelastic joints [1]. In the present study we focus on a robot trunk design that has redundant joints, similar to an animal's spine. The joints have tunable viscoelasticity, similar to living muscles. We also consider a leg structure driven by antagonistic muscles. We have previously reported that such a trunk mechanism facilitated locomotion constrained to a 2D plane with simple leg actuation [2]. In the present paper, we describe the results of an experiment carried out on a 3D quadruped robot that has a trunk with redundant viscoelastic joints and legs driven by pneumatic actuators. The results demonstrate that the robot achieves dynamic trotting locomotion with a simple gait pattern. We determine the appropriate combination of joint viscoelasticity and walking cycle that provides the most energy efficient locomotion.

2. DEVELOPED QUADRUPED ROBOT

Figure 1 shows the developed quadruped robot. It is 0.35 m high, 0.32 m wide, 0.53 m long, and weighs 4.8 kg. The robot has an animal-like trunk structure that has redundant joints with tunable viscoelasticity. It also has four legs driven by antagonistic pneumatic actuators. The actuators are operated by simple ON/OFF air valves. The leg joints are viscoelastic, and passively bend when the robot is placed on the ground.

Figure 2(a) shows the design of the trunk. We adopt an animal-like spinal structure with redundant joints. The trunk has vertebrae made of chemical wood, as shown in Figure 2(b) and intervertebral discs made of rubber, as shown in Figure 2(c). Both the vertebrae and the intervertebral discs have circular cross sections so that the trunk can bend and stretch in arbitrary directions. The vertebrae and intervertebral discs have holes, through which non-extensible wires are passed. One end of each wire is
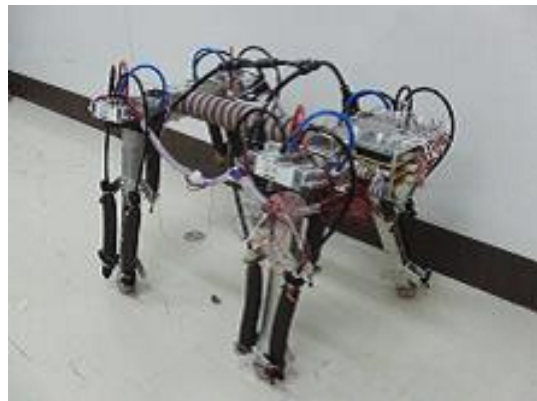
Fig. 1 Developed quadruped robot

fixed to the head of the trunk, while the other is wound by a winch. The tensile force exerted on the wires, which corresponds to the compressive force on the trunk, can then be varied by rotating the winch. A force sensor is attached to the head of the trunk as shown in Figure 2(a) to measure the tensile force on the wires. Because the tensile force is correlated to the viscoelasticity of the trunk, we use this force as the viscoelasticity parameter.

Figure 3 shows the configuration of the pneumatic actuators to drive the legs. In this study, we use McKibben pneumatic actuators and, as shown in the figure, each leg has two joints and four actuators. Joint $i (i = 1, 2, 3, 4)$ is driven by two actuators ei and fi.

3. EXPERIMENT

3.1 Setup

In the experiment, the trotting pattern shown in Figure 4(a) was adopted. In order to investigate the most appropriate trunk viscoelasticity for different walking cycles, we systematically recorded the walking velocity for walking cycles of 0.50, 0.68, 0.83, and 1.00 s, and tensile forces of 291, 318, 373.0, 403.7, and 449.4 N. The walking velocities with the trunk made rigid by immobilizing its joints using a lightweight metal plate were also

(a) trunk design

(b) vertebra   (c) intervertebral disc
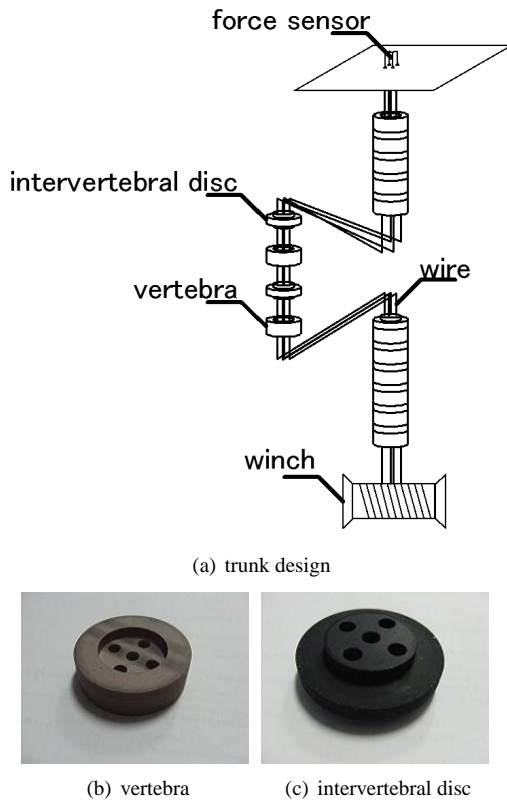
Fig. 2 Trunk design including redundant joints and tunable viscoelasticity
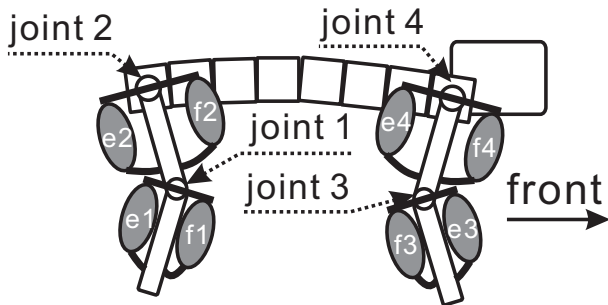
Fig. 3 muscle configuration

(a) swing / support phase chart for trotting


(b) supply / exhaust timing chart

Fig. 4 leg operation for trotting

recorded. The timing chart for each pair of air valves (supply / exhaust / close) is shown in Figure 4(b). Since the trunk has passive viscoelastic joints, it is not necessary to plan the trajectory of each joint, so that the robot walks at very low computational cost.

3.2 Results

Table 1 shows the experimental results. The values indicate the walking velocity (cm/s), and "*" means that the robot could not walk for a distance of 1 m within 120 s. The dark and light shading indicates the 1st and 2nd highest velocity for each walking cycle, respectively. These results lead to the following conclusions. First, the robot can achieve successful trotting locomotion by an appropriate choice of viscoelasticity for each walking cycle. Second, the robot cannot achieve locomotion when its trunk is a single rigid body. Finally, since the amount of energy expended (air consumption) was almost the

same for each trial, velocity can be directly equated to energy efficiency. Therefore, Table 1 indicates that the robot can achieve energy efficient locomotion by tuning the viscoelasticity of the trunk structure depending on the walking cycle.

Table 1 Experimental results : average velocity for different walking cycles and tensile forces (unit : cm/s)

		walking cycle [s]			
		0.50	0.68	0.83	1.00
tensile force [N]	291.0	*	*	*	*
	318.0	*	*	*	3.16
	373.0	*	*	2.65	3.76
	403.7	*	*	4.73	3.37
	449.4	*	1.96	5.88	2.84
	rigid body	*	*	*	*

REFERENCES

[1] Y.Fukuoka and H.Kimura and A.H.Cohen, "Adaptive Dynamic Walking of a Quadruped Robot on Irregular Terrain Based on Biological Concepts", International Journal of Robotics Research,vol. 22, No. 3-4, pp.187-202, 2003

[2] T.Takuma and M.Ikeda and T.Masuda, "Facilitating Multi-modal Locomotion in a Quadruped Robot utilizing Passive Oscillation of the Spine Structure", Proceedings of the 2010 IEEE/RSJ International Conference on Robotics and Automation (IROS), pp.4940-4945, 2010

Pitch Angle Control using Flapping Frequency for a Flapping-Wing Robot

Yoshiyuki Higashi[1], Tatsuya Miyazaki and Hiroshi Kimura[2]

[1]Department of Mechanical and System Engineering, Kyoto Institute of Technology, Kyoto, Japan
(Tel: +81-75-724-7364; E-mail: higashi@kit.ac.jp)
[2]Department of Mechanical and System Engineering, Kyoto Institute of Technology, Kyoto, Japan
(Tel: +81-75-724-7352; E-mail: kimura61@kit.ac.jp)

Abstract: This paper presents methods of estimating and controlling the pitch angle for a flapping-wing robot. Measured values by the rate gyro sensor and the acceleration sensor mounted on a flapping-wing robot include high frequency noises and the drift caused by accumulating the error. For controlling a flapping-wing robot using values of internal sensors, we estimate the pitch angle of a flapping-wing robot based on the value combined the low-pass filtered output of the rate gyro sensor with the high-pass filtered output of the acceleration sensor. And a flapping-wing robot is controlled using the estimated pitch angle and the robot's characteristics which the pitch angular velocity changes in response to the flapping frequency.

Keywords: flapping-wing robot, attitude estimation, control

1. INTRODUCTION

Recently, a lot of researchers have been studying on several types of MAVs (Micro Aerial Vehicles)[1]. Flapping-wing robots, one of the MAVs, shaped like dragonflies[2] and birds are considered to have superior flying ability as well as such animals. However the autonomous control of a flapping-wing robot with the on-board computer has never realized, because of the limit of the payload and the noise in sensors caused by flapping the wing for flying. In this paper, we present the estimation method of the pitch angle of the flapping-wing robot using internal sensors include such noises, and validate its method through the experiment. Moreover, the flapping-wing robot is controlled using the estimated pitch angle and the robot's characteristic, flies autonomously with the on-board computer.

2. FLAPPING-WING ROBOT

Fig.1 shows our flapping-wing robot and mounted devices. This robot has the 2D rate gyro sensor, the 3D acceleration sensor for measuring the robot's attitude angles and the controller unit composed of the microcomputer and the 2D motor driver. A 2-cell lithium polymer battery supplies the power to the motor for flapping the wing, sensors and the controller unit. Parameters of the flapping-wing robot are shown in Table1.
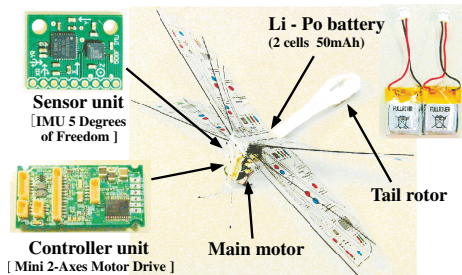

Fig. 1 The sensor unit (the 2D rate gyro and the 3D acceleration sensor), the controller unit (the microcomputer and the 2D motor driver), our flapping-wing robot, and Li-Po battery.

Table 1 Physical parameters of the flapping-wing robot.

Parameter	Value
Mass	28.5g
Length	280mm
Wing Span	410mm
Chord (Average)	80mm
Flapping Frequency	15.0Hz(Max)

3. PITCH ANGLE ESTIMATION

3.1 Estimation Method

In theory, the pitch angle is able to be calculated by integrating outputs of the rate gyro sensor and the relation between outputs of the acceleration sensor and the gravitational acceleration. However the pitch angle calculated from outputs of the rate gyro sensor drifts because of accumulating the error in flight. The acceleration sensor measures the robot's acceleration include inertia noises caused by flapping the wing. Thus the pitch angle calculated from the acceleration is also incorrect for controlling the robot.

For getting more accurate pitch angle using these sensors, we estimate the pitch angle from eq.(1) using high-frequency component of measured values by the rate gyro sensor $\mathrm{HPF}(\theta_\mathrm{n}^\mathrm{gyr})$ and low-frequensy component of measured values by the acceleration sensor $\mathrm{LPF}(\theta_\mathrm{n}^\mathrm{acc})$[3].

$$\theta_n^\mathrm{est} = \mathrm{HPF}(\theta_\mathrm{n}^\mathrm{gyr}) + \mathrm{LPF}(\theta_\mathrm{n}^\mathrm{acc}) \tag{1}$$

In eq.(1), the drift of the rate gyro sensor's values is removed by passing the high-pass filter (HPF), inertia noises caused by flapping are removed by passing the low-pass filter (LPF). Where HPF and LPF in eq.(1) are first-order IIR (Infinite Impulse Response) filters. However, because a power unit composed 2-cell lithium polymer battery supplies the power to the motor, the controller unit and all sensors by reason of the robot's payload, the pitch angle calcurated by the rate gyro sensor $\mathrm{HPF}(\theta_\mathrm{n}^\mathrm{gyr})$ has the offset caused by change of the input voltage to the rate gyro sensor response to the duty ratio of the motor,

viz. the wing's flapping frequency. This problem solving, we use the correct method which changes the zero point of the rate gyro sensor response to the duty ratio. And the estimated pitch angle is represented by eq.(2) using the corrected output of the rate gyro sensor $\mathrm{HPF}(\theta_n^{\mathrm{gyr}*})$. The detail of the estiomation and the correction is shown in [4].

$$\theta_n^{\mathrm{est}*} = \mathrm{HPF}(\theta_n^{\mathrm{gyr}*}) + \mathrm{LPF}(\theta_n^{\mathrm{acc}}) \qquad (2)$$

3.2 Validation of Estimation Method

Fig.2 shows experimental results with the flapping wing robot (Fig.1) for validating above estimation method. In the upper figure, the estimated pitch angle θ^{est} calculated from eq.(1) has the error to the given reference θ^{msr} along with the change of the flapping frequency f^{flap}. On the other hand, the pitch angle $\theta_n^{\mathrm{est}*}$ estimated using the corrected value $\mathrm{HPF}(\theta_n^{\mathrm{gyr}*})$ approximately corresponds to the reference θ^{msr} though the flapping frequency f^{flap} changes.
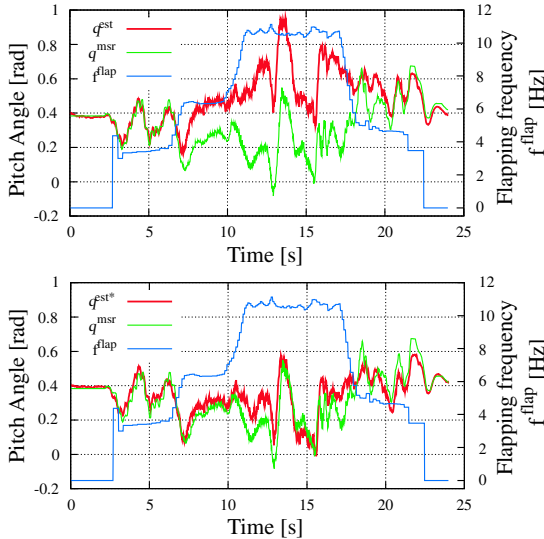

Fig. 2 Experimental results of the estimation. The θ^{msr} is a reference angle of the pitch. The f^{flap} is the flapping frequency. **Upper:** The pitch angle θ^{est} calculated from eq.(1). **Lower:** The pitch angle $\theta^{\mathrm{est}*}$ calculated from eq.(2).

4. PITCH ANGLE CONTROL

The flapping-wing robot has the characteristic that its pitching moment depends on both the flapping frequency and the airspeed. Causing this characteristic the fluctuation in flight without the pitch angle control, the robot gradually descends and cannot fly for a long time.

For stabilizing the pitch angle, the flapping frequency is controlled by PD controller considering the robot's characteristic and using the estimated angle $\theta_n^{\mathrm{est}*}$.

Fig.3 shows experimental results of the pitch angle control in autonomous flight. Where the flapping frequency is constant for the level flight in the experiment without the pitch angle control. In another experiment, the flapping frequency is controlled based on this constant value. In the controlled flight, the desired pitch
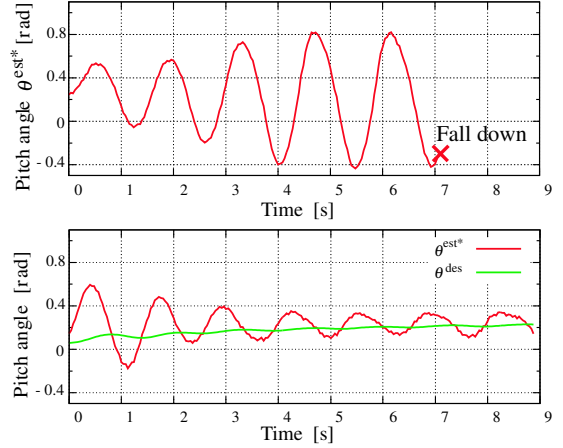

Fig. 3 Experimental results of self-contained flight. **Upper:** The estimated pitch angle $\theta^{\mathrm{est}*}$ in flight without the control. **Lower:** The estimated pitch angle $\theta^{\mathrm{est}*}$ and the desired pitch angle θ^{des} in controlled flight.

angle θ^{des} is the estimated angle passed low-pass filter $\mathrm{LPF}(\theta^{\mathrm{est}*})$.

The upper figure shows the result that the amplitude of the pitch angle increases as time passes, as a result, the robot falls down at 7th second. When the robot flies with the pitch angle control, the experimental results, bottom figure, shows tendency to converge on the desired pitch angle θ^{des}.

5. CONCLUSIONS

This paper has presented the estimation method the pitch angle for the flapping-wing robot using the rate gyro sensor and the acceleration sensor. The validation experiment has shown the pitch angle was able to be calculated from the measured value by internal sensors include the several noises. In addition, we have controlled the flapping frequency using the estimated pitch angle based on the robot's characteristic, have succeeded in autonomous flight of the flapping-wing robot by the on-board computer.

REFERENCES

[1] J. M. Grasmeyer and M. T. Keennon, "Development of the black widow micro air vehicle", *AIAA-2001-0127*, pp.1-9, 2001.

[2] C. DiLeo and X. Deng, "Experimental Testbed and Prototype Development for a Dragonfly-Inspired Robot", *Proceedings of IEEE/RSJ IROS'07*, pp. 1594-1599, 2007.

[3] A. Baerveldt and R. Klang, "A Low-cost and Low-weight Attitude Estimation System for an Autonomous Helicopter", *Proceedings of IEEE INES'97*, pp. 391-395, 1997.

[4] T. Miyazaki, Y. Higashi and H. Kimura "Pitching angle estimation for a flapping-wing robot using a rate gyro sensor and an acceleration sensor." *Proceedings of 38th SICE Symposium on Intelligent Systems*, 2011.

Study for Emergence of Implicit Control Law in Swiss Robot Phenomena

Yuichiro Sueoka[1], Yasuhiro Sugimoto[1], Koichi Osuka[1], Masato Ishikawa[1], Teruyo Wada[1]
and Akio Ishiguro[2]

[1]Department of Mechanical Engineering, Osaka University, Osaka, Japan
(Tel: +81-6-6879-4084; E-mail: s.yuichiro@dsc.mech.eng.osaka-u.ac.jp,
{yas, osuka, ishikawa, wada}@mech.eng.osaka-u.ac.jp,
[2]Department of Electrical and Communication Engineering, Tohoku University, Sendai, Japan
(Tel: +81-22-795-3781; E-mail: ishiguro@ecei.tohoku.ac.jp)

Abstract: Living things exhibit adaptive and supple locomotion under the real world characterized by rapid changes, high uncertainty, and limited availability of information. We propose that Implicit Control Law is a key concept to understand the adaptive locomotion of the living things. In this paper, the Swiss Robot is picked up. The experimental results show this robot utilizes the Implicit Control Law for the realization of its interesting behavior. Then, this element is investigated using the molecular dynamics.

Keywords: Swiss Robot, Implicit Control Law, embodiment

1. INTRODUCTION

Living things can move adaptively even if they are placed in an unknown environment. To understand these adaptive locomotion, we focus on the element that appears by interaction among the brain (*e.g.* control law), the body (*e.g.* plant), and the environment. This element is recognized as an another control law called Implicit Control Law (Implicit C.L.). The remainder element is the element which stayed after substract the Implicit Control Law from the control law as the Explicit Control Law (Explicit C.L.) [1].

In this study, we focused on a Swiss Robot that shows interesting behavior even if the Exlicit C.L. is very simple [2]. Our experimental result verified that the Swiss Robot can cluster the cubes using the Implicit C.L.. In this paper, we proposed how to formulte the collecting mechanism and show the way to collect more cubes.

2. SWISS ROBOT

2.1 Experiment

Fig. 1 shows an overview of the Swiss Robot. The Swiss Robot is equipped with two motors and two infrared sensors, mounted symmetrically on its right and left sides. This robot is programmed with the following algorithm that provides a simple Explicit C.L..

if Left sensor stimulation **then**
  (left motor, right motor)=(forward, inverse)
else if Right sensor stimulation **then**
  (left motor, right motor)=(inverse, forward)
else
  (left motor, right motor)=(forward, forward)
end if

We set one Swiss Robot and 15 cubes in a closed area (Fig. 2(a)). The length of one side of the cubes is 0.09 [m] and that of the field is 1.8 [m]. We set the sensor reference distance (l) at 0.15[m] and the sensor angle (ϕ) at 30° and the distance between two sensors (d) at 0.12[m]. Fig. 2 shows the experiment result. Fig. 2 indicates that


Fig. 1 Swiss Robot

(a) Initial State   (b) Final State
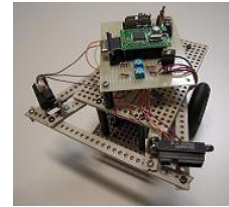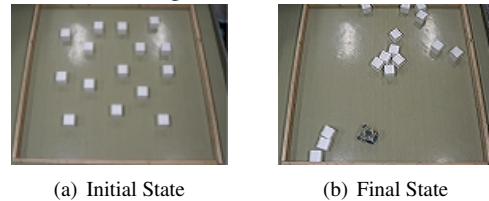
Fig. 2 The Experiment Result

the Swiss Robot can cluster the cubes even if the Explicit C.L. is very simple. This implies that the robot clusters them using Implicit C.L. that appears by the interaction between itself and its environment.

2.2 Formulation of this robot phenomena

In this section, we do not focus on the movement of the robot but that of the cubes and formulate as the state equation by using the kinetic theory of the molecules. In this process, we consider the attraction field as follows.

(a) When one cube is out of the attraction field (the attraction field is a part of a circle in a vertical direction to the cube movement), this cube moves with the velocity $\boldsymbol{u}$ caused by the random force $\boldsymbol{F}$ from the Swiss Robot (Fig. 3(a)).

(b) When one cube is inside the attraction field, the attraction force $\boldsymbol{F}_I$ and viscous force $\boldsymbol{F}_C$ is applied to this cube (Fig. 3(b)). This attraction potential can be decided by using Lennard-Jones potential $\phi(r)$ written by the equation [4].

$$\phi(r) = \epsilon_0\{(\frac{r_0}{r})^{12} - 2(\frac{r_0}{r})^6\}$$

(a) Out of the attracton field

(b) Inside the attraction field

(c) Influence of the repulsive force
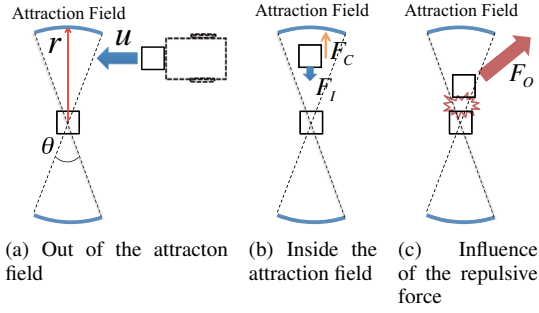
Fig. 3 Formulation with the attraction field


(a) Swiss Robot

(b) Attraction Field
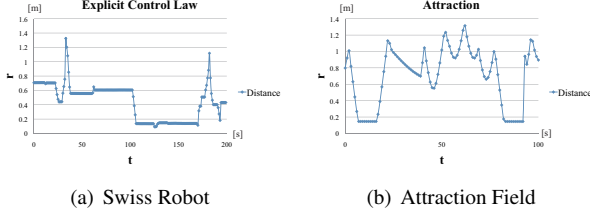
Fig. 4 Comparision with the Swiss Robot model and attracion field model

Where ϵ_0 is the potential coefficient, r is the distance between the cubes and r_0 is the distance which cut off the force. Moreover the viscous force $\boldsymbol{F}_C$ is stronger than the attraction force $\boldsymbol{F}_I$. That is, the cube inside the attraction field do not move so much.

(c) The cube existed in the attraction field, the random repulsive force $\boldsymbol{F}_O$ is applied to this cube under the small probability (Fig. 3(c)).

Moreove, the radius of the circle r is approximately equal to the sensor reference distance l of the Swiss Robot. And the angle θ is decided by the sensor angle ϕ.

From the above consideration, the Swiss Robot phenomena is written by the equation.

$$\xi \frac{d\boldsymbol{x}}{dt} = \boldsymbol{F}_a \tag{1}$$

$$m \frac{d^2\boldsymbol{x}}{dt^2} = \nabla \phi(r) - c\frac{d\boldsymbol{x}}{dt} \tag{2}$$

$$m \frac{d^2\boldsymbol{x}}{dt^2} = \boldsymbol{F}_c \tag{3}$$

Where ξ is the resistance coefficient, m is the mass of the cubes, $\boldsymbol{F}_a$ is the random force, r is the distance between cubes, c is the viscosity coefficient and $\boldsymbol{F}_c$ is the random repulsive force.

Then, we set the simulation environment as follows:
1. We use two cubes and five robots to simplify the cubes phenomena.
2. We set the field as equal probability condition $-1 \leq x \leq 1, -1 \leq y \leq 1$.

Fig. 4(a) shows the result of the above Swiss Robot model and the Fig. 4(b) shows that of the above the model with the equation (1)-(3). From Fig. 4, we consider that attraction force $\boldsymbol{F}_I$ express the clustering and repulsive force $\boldsymbol{F}_O$ also express the cubes are devided by Swiss Robot accidentaly. That is, the Swiss Robot phenomena can be


(a) l=0.10m

(b) l=0.25m
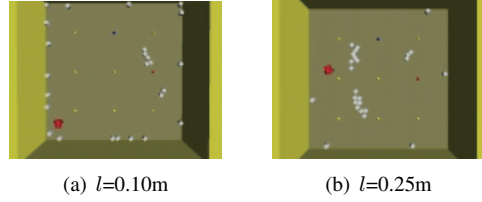
Fig. 5 The influence of the short and long sensor reference distance
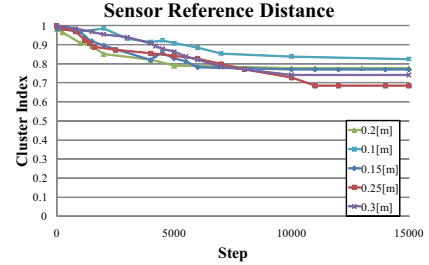
Fig. 6 The influence of the sensor reference distance

expressed as the another simulation model which consists of the attraction and repulsive force that will be expected to be equivalent to the Implicit Control Law.

2.3 Influence of the radius of the attraction field

In the real Swiss Robot model, we have to consider the influence from the walls. If the cubes is pushed near the walls at once, the cubes near the walls should not move. From the reason in order to collect more cubes, the size of the attraction field will be important.

Then, the simulation is carried out with the sensor reference distance $l = 0.10, 0.15, 0.20, 0.25, 0.30[m]$. Moreover, using the statistical approach, the Cluster Index that is able to examine the collecting ability is introduced. Fig. 5 shows the worst and best collected results and the change of the Cluster Index is shown in Fig. 6. From Fig. 6, we verified that the cubes is more collected when the sensor reference distance is large.

3. CONCLUSION

In this paper, we formulated the Swiss Robot model using the kinetic theory if the molecules and shows the attraction force and viscous force is equivalent to the Implicit C.L. element.

ACKNOWLEDGMENTS

REFERENCES

[1] K. Osuka et.al., "Dual Structure of mobiligence -implicit control and explicit control," *IROS2010*, pp. 2407-2412, 2010.

[2] R. Pfeifer and J. Bongard, *How the body shapes the way we think*, The MIT Press, 2006.

[3] Y. Sueoka et.al., "Analysis of Implicit Control Law in Swiss Robot phenomena" *16th Robotics Symposia*, pp. 373-378, 2011 (in Japanese).

[4] Abraham Nitzan, "Chemical Dynamics in Condensed Phases", Oxford University Press, pp. 175-189, 2006.

A CPG-based Control of Bipedal Locomotion by Exploiting Deformable Feet

Dai Owaki[1], Shota Kubo[1], and Akio Ishiguro[1,2]

[1]Research Institute of Electrical Communication, Tohoku University, Japan
(Tel: +81-22-217-5465; E-mail: owaki@riec.togoku.ac.jp)
[2]Japan Science and Technology Agency, CREST, Japan
(Tel: +81-22-217-5464; E-mail: ishiguro@riec.tohoku.ac.jp)

Abstract: In this paper, we investigate adaptive bipedal walking that exploits sensory information stemming from a "soft deformable" body. To this end, we modeled soft deformable feet for a bipedal robot and a CPG-based control of bipedal locomotion that exploits local sensory feedback generated from the deformation of these feet. Through numerical simulations, we have found that a bipedal robot controlled by the proposed controller exhibits remarkably adaptive walking in response to experimental perturbations. This result supports the conclusion that the "deformation" of a robot's body plays a pivotal role in the emergence of "sensor-motor coordination", which is the key to generating adaptive locomotion in a robotic system.

Keywords: Deformable feet, CPG, Adaptive bipedal walking

1. INTRODUCTION

Animals exhibit astoundingly adaptive, supple and versatile locomotion under real world constraints by orchestrating large degrees of bodily freedom. Recent studies have clarified that this amazing capability is controlled in part by an intraspinal neural network called *central pattern generators* (CPGs) [1].

Based on this biological finding, various studies have been conducted so far to incorporate artificial CPGs into legged robots with the aim of generating highly adaptive locomotion [2], [3]. A key concept underlying these studies is to generate a limit cycle in the state space, which is composed of brain-nervous system (*i.e.*, control system), musculoskeletal system (*i.e.*, mechanical system) and environment. Once a limit cycle is established, its intrinsic structural stability allows the robot to exhibit resilience against environmental perturbations. However, the design principle that can assuredly establish a limit cycle with a large basin of attraction have not yet been devised.

This paper aims to generate a more stable limit cycle by exploiting the spatiotemporal sensory information stemming from the *deformability* of a robot's body, leading to a close interaction between motion and perception (*i.e.*, sensor-motor coordination [4]), which will in turn accomplish adaptive locomotion. To this end, we give attention to the deformability of soft human feet during bipedal walking. A soft body enables a robot to not only stabilize its motion but also gain *rich* sensory information, which stems from the deformation in ways favorable to the motion underway. In this paper, we propose a novel CPG-based control method for bipedal locomotion, in which local sensory information stemming from the deformability is fed back to a coupled oscillator system. Simulation results indicate that the proposed model enhances the adaptability in response to environmental perturbations by exploiting the sensory information stemming from soft deformable feet. We expect these findings to prove the useful in the development of a methodology that allows robots to generate adaptive locomotion.
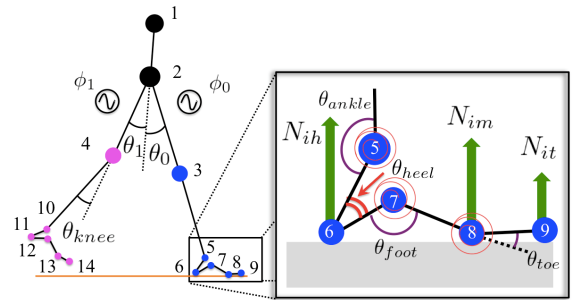

Fig. 1 Schematic representation of musculoskeletal system.

2. MODEL

Figure 1 shows the musculoskeletal system employed in this study. The model we adopted was inspired by the deformation of human feet during walking [5]. The closeup in this figure shows the skeletal system of the feet in detail. Here, the key point of the present model is that the torsion springs are purposefully put into the joints: ankle, foot, and toe. Because such elastic materials can deform in ways favorable to the motion underway, the deformation of the feet provides rich information about how the robot interacts with the environment as well as stabilizing motion (*e.g.*, shock absorption). In this paper, we model a control scheme for a bipedal robot by using local feedback of the sensory information stemming from these deformable feet. The actuators at the hip joints drive the legs back and forth using PD (proportional and differential) control such that the hip angles $\theta_i (i = 0, 1)$ correspond to the target angles $\theta_{di} (i = 0, 1)$. We implemented a stopper into the knee joint, which prevents hyperextension.

The phase oscillators described in (1) are implemented for the hip joints in our model:

$$\dot{\phi}_i = \omega + \epsilon \sin(\phi_j - \phi_i - \pi) + f_i, \tag{1}$$

where ω represents the intrinsic frequency of the ith oscillator (left: $i = 0$, right: $i = 1$). The second term on the right hand side denotes the interaction between the
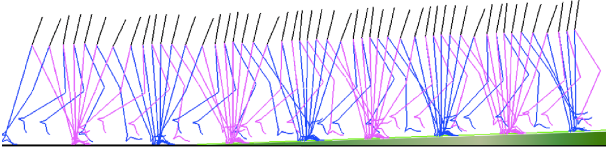
Fig. 2 Stick diagram showing environmental change from level ground to sloping ground (2.0 deg.) during 9 periods.

oscillators. ϵ represents the magnitude of the interaction. The third term denotes the local sensory feedback from the musculoskeletal system to this control system. In this paper, we model the local sensory feedback as follows:

$$f_i = (aN_{ih} + bN_{im} + cN_{it}) \cos \phi_i. \qquad (2)$$

As shown in Fig. 1, N_{ih}, N_{im}, and N_{it} represent GRFs (ground reaction forces) perpendicular to the ground at the heel (6 and 11), metatarsal (8 and 13), and toe (9 and 14), respectively. The parameters a, b, and c represent the magnitudes of the sensitivities to these GRFs. These parameters play a crucial role in modulating the phases based on the sensory information from the superficial senses (N_{ih}, N_{im}, N_{it}).

3. SIMULATION RESULT

We show the simulation results in terms of the adaptability in response to environmental changes. Here, we set the control parameters in our model as follows: $\omega = 4.4$ rad/s, $\epsilon = 0.30$, $a = 0.011$, $b = 0.008$, $c = 0.008$, $C_1 = 0.384$ rad, and $C_2 = 0.454$ rad. Fig. 2 shows a stick diagram of the transition from walking on level ground to walking on sloping ground (2.0 deg). As this figure shows, the proposed model generates a phase modification based on the situation encountered. This result indicates that the local sensory feedback stemming from the sensory information of the deformable feet allows the spontaneous modification of the step length during walking, leading to the convergence to steady-walking on sloping ground. Fig. 3 shows the oscillator phases, $\sin \phi_i$, and gait diagram used in the verification. In these figures, the light green area represents the walking on the sloping ground. As this figure shows, the period of the stance phase is spontaneously modified from 0.877 s (level ground) to 1.032 s (sloping ground) by the local sensory feedback in response to the environment.

4. SUMMARY

In this study, we proposed a control scheme that exploits the local sensory feedback stemming from deformable soft feet. Simulation results indicate that the proposed model enhances the adaptability in response to environmental perturbations. The key in our model is the exploitation of a reasonable degree of physical deformation in soft feet, reflecting the interaction between the robot and environment. In future, we will discuss the detailed model of the musculoskeletal system in human
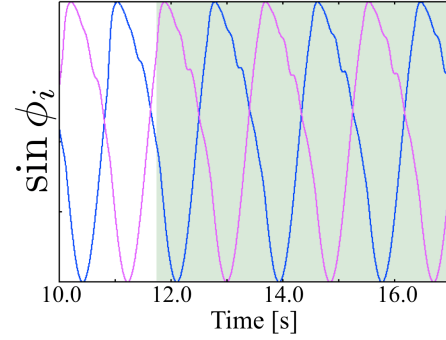

(a)
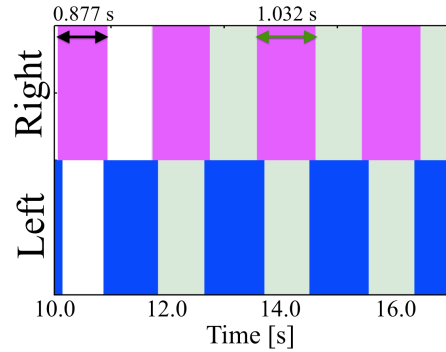
(b)

Fig. 3 Simulation results for transition during environmental change from level ground to sloping ground (2.0 deg) (10.0–17.0 s): (a) oscillator phases and (b) gait diagram.

feet, which deform in ways favorable to the motion underway. And we aim to develop a real bipedal robot to further verify the validity of this design scheme.

AKNOWLEDGEMENT

REFERENCES

[1] S. Grillner, "Neurobiological Bases of Rhythmic Motor Acts in Vertebrates", *Science*, Vol. 228, pp. 143–149, 1985.

[2] G. Taga, Y. Yamaguchi, and H. Shimizu, "Self-organized Control of Bipedal Locomotion by Neural Oscillators", *Biological Cybernetics*, Vol. 65, pp. 147–159, 1991.

[3] H. Kimura, S. Akiyama, and K. Sakurama, "Realization of Dynamic Walking and Running of the Quadruped Using Neural Oscillator", *Autonomous Robots*, Vol. 7, No. 3, pp. 247-258, 1999.

[4] R. Pfeifer and J. Bongard, *How the Body Shapes the Way We Think: A New View of Intelligence*, The MIT Press; 2006.

[5] T. Takashima, H. Fujimoto, and A. Takanishi, "Analysis of the Human Foot Arch Viscoelasticity using the Simple Model of the Arch Support Elements", *Transactions of the Japan Society of Mechanical Engineers. C*, Vol. 69, No. 685, pp. 173–178, 2003.

Mode Analyses on the Kinematical Structure of Basic Movements and Residual Patterns in Human Locomotion using Motion Capture Data

Nanase Takata, Sadahiro Senda, Kazutaka Nakai and Katsuyoshi Tsujita

Department of Biomedical Engineering, Osaka Institute of Technology, Osaka, Japan

(Tel : +81-6-6954-4243; E-mail: m1m11h15@st.oit.ac.jp)

Abstract: This article treats mode analysis of kinematic structure of human locomotion. We investigated human locomotion using singular value decomposition. From motion-captured data of human locomotion, we extracted common basic movements and residual modes, and analyzed kinematical structures. The results show that there are basic movements commonly observed for all participants in usual walk. On the other hand, higher modes in knee-constrained walk represent different control strategies depending on the physical property of the legs. These residual modes involve personal peculiarities or symptoms of motor dysfunction in locomotion.

Keywords: Human locomotion, Mode analysis, Motion patterns

1. INTRODUCTION

Human locomotion control is typical of a multi-body system control that may be specific for periodic and stable motion patterns of locomotion[1]-[4]. During rhythmic and steady motion such as straight walking, many joints and muscles are organized into a collective unit that is controlled as though it has fewer degrees of freedom (DOFs), even though it still needs to retain the necessary flexibility for adapting to changes in the environment[5]. In this study, we investigated human locomotion by mode analyses using singular value decomposition[6]-[8]. From motion-captured data of human locomotion, we extracted common basic movements and residual modes, and analyzed kinematical structures. The results show that there are basic movements whose proportion of variance is significant, and those are common to all the test participants. The residual modes involve personal peculiarities or symptoms of motor dysfunction in locomotion. We can note that by utilizing the results, we may expect to identify personal traits and run diagnostic check systems for applications.

2. METHOD

Human locomotion on a treadmill is measured with an optical motion capture system. The motion capture system in this study is composed of six cameras with a frame rate at 100[Hz] and 34 markers attached to the human body. Nine healthy participants (4 men and 5 women, 1.47-1.77 m) volunteered for the experiments. Two types locomotion conditions are given for all participants: One is usual walk; the other is constrained walk that the knee on the left side is physically constrained (Figure 1). Measured data on participants' motions are transformed to joint angle vectors of the 18 DOF skeleton models (Figure 2). The motion pattern matrix consists of the obtained time series of joint angle vectors as follows:

$$A = \begin{bmatrix} \theta_1(t_1) & \theta_2(t_1) & \cdots & \cdots \\ \theta_1(t_2) & \theta_2(t_2) & \cdots & \cdots \\ \vdots & \vdots & \ddots & \\ \vdots & \vdots & & \theta_N(t_M) \end{bmatrix} \quad (1)$$

The motion pattern matrix is decomposed to motion components with the SVD (Singular Value Decomposition) method as follows:

$$A = U \Sigma V^*　\quad (2)$$

where Σ consists of singular values. U and V^* are composed of temporal basis vectors relating time-dependent motion patterns and spatial basis vectors relating inter-joint coordination, respectively. We first defined correlation coefficient S in equation (3). We evaluated the correlation between mode basis vectors for all participants, and extracted commonly observed modes between participants. The modes are named common basic modes, in this study.

$$S = \frac{|Trace(A_A{}^T A_B)|}{\sqrt{Trace(A_A{}^T A_A)}\sqrt{Trace(A_B{}^T A_B)}} \quad \begin{array}{l} A_A = u_A \\ A_B = u_B \end{array} \text{ or } \begin{array}{l} A_A = v_A \\ A_B = v_B \end{array} \quad (3)$$

From the decomposed motion components, we investigated the kinematical structure and discrepancy of the basic movements and the residual motion patterns in human locomotion.
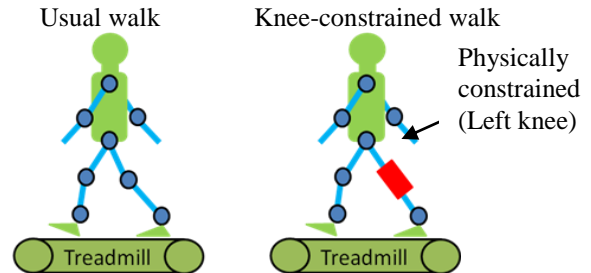

Fig. 1 Experimental conditions
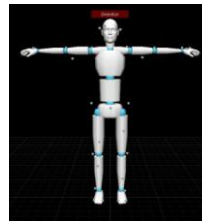
Fig. 2 Human skeleton model with 18 joints and 34 markers

3. RESULTS AND DISCUSSION

The results show that there are three modes whose numbers of high correlation (S>0.75). (Figure 3). These modes are common to all the participants in

experiments. On the other hand, we investigated the locomotion of participants whose knees on the left side were physically constrained with knee supporters. In those cases, the two significant higher modes (modes 3 and 4) also observed. Correlation coefficients between the spatial modes for different participants in knee-constrained walk are around 0.79-0.95. In mode 3, knee's motion on the opposite side became larger. The motion pattern is considered as compensation of posture balance due to the left-knee constraints (Figure 4). In mode 4, on the other hand, situations are completely different from mode 3. There are two types of spatial vectors in mode 4 in knee-constrained walk. One is the activation of the opposite side of ankle; this motion pattern is standing on tiptoe. The other is activation of the same side of ankle; this motion pattern is posture swaying. And interestingly, these two types of inter-joint coordination does not depend on gender, age, and so on, but on physical structure of legs, such as X legs, bandy legs, and so on.

We can note that the results show the common basic modes are essential movements in human locomotion. As well, higher-order modes, in this study, modes 3 and 4 whose correlation coefficients are high between the participants in knee-constrained walk are the residual modes that involve personal peculiarities or symptoms of motor dysfunction in locomotion. It is expected that by utilizing the results, we will be able to identify personal traits and run diagnostic check systems for applications.


(a)

(b)
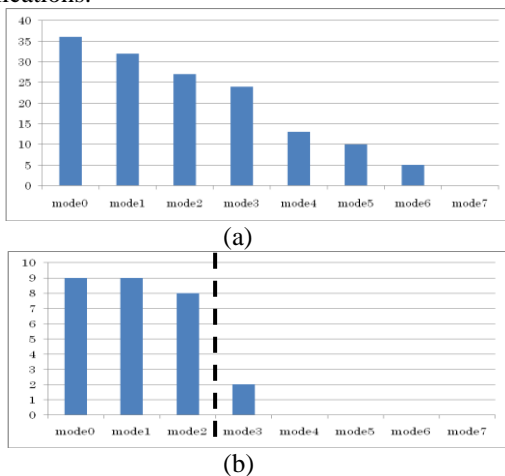
Fig. 3 (a) Histogram of mode numbers with high correlation (>0.75) (a) in usual walk: Primary 4 modes are commonly observed between participants (b) between usual walk and constrained walk: Primary 3 modes are commonly observed. But mode 3 has a difference between usual walk and knee-constrained walk.
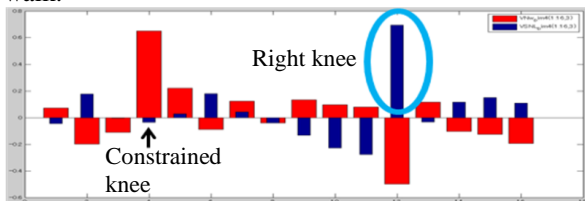

Fig. 4 Spatial basis vector in mode 3
(Red bar: usual walk, Blue bar: knee-constrained walk)


(a)

(b)
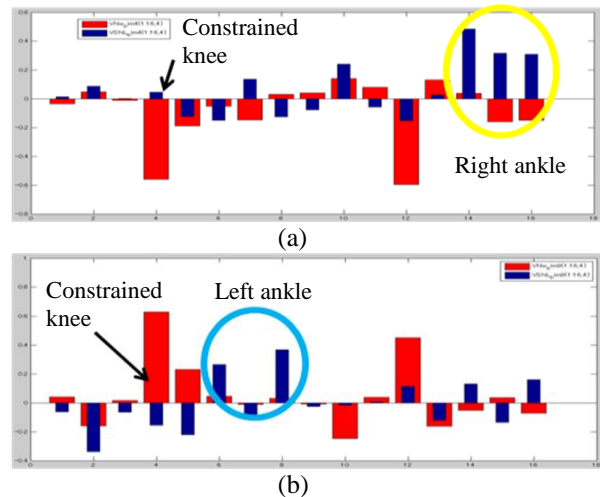
Fig. 5 Spatial basis vector in mode 4 in usual walk and in knee-constrained walk (Red bar: usual walk, Blue bar: knee-constrained walk) There are two types of control strategies: (a) Standing on tiptoe (b) Posture swaying

Acknowledgements

REFERENCES

[1] S.Grillner,"Neurobiological bases of rhythmic motor acts in vertebrates," *Science,* 228, pp.143-149, 1985.
[2] J.A.S.Kelso, *Dynamic patterns: The Self-Organization of Brain and Behavior (Complex Adaptive Systems)*, MIT Press, 1997.
[3] G.Taga, Y.Yamaguchi and H.Shimizu, "Self-organized control of Bipedal locomotion by neural oscillators in unpredictable environment," *Biological Cybernetics,* 65, pp.147-159, 1991.
[4] G.Taga, "Emergence of bipedal locomotion through entrainment among the neuro-musculo-skeletal system and the environment," *Physica D,* 75, pp.190-208, 1994.
[5] N.Bernstein, *The co-ordination and regulation of movements.* Oxford:Pergamon, 1967.
[6] K.Mishima, S.Kanata, H.Nakanishi, T.Sawaragi and Y.Horiguchi, "Extraction of Similarities and Differences in Human Behavior using Singular Value Decomposition," *Proc. of The 11th IFAC/IFIP/ IFORS/IEA Symp. on Analysis, Design and Evaluation of Human-Machine Systems,* 2010.
[7] Y.P.Ivanenko, G.Cappellini, N.Dominici, R.E.Poppele and F. Lacquaniti, "Coordination of locomotion with voluntary movements in humans," *J. Neuroscience* 25, pp.7238 –7253. 2005.
[8] Y.P.Ivanenko, N.Dominici, G.Cappellini and F.Lacquaniti, "Kinematics in newly walking toddlers does not depend upon postural stability," *J Neurophysiology* 94, pp.754 –763, 2005.

A Study on Trunk Stiffness and Gait Stability in Quadrupedal Locomotion Using Musculoskeletal Robot

Katsuyoshi Tsujita and Kenji Miki

Department of Robotics, Osaka Institute of Technology, Osaka, Japan
(Tel: +81-6-6954-4243; E-mail: tsujita@bme.oit.ac.jp)

Abstract: In this study, a feasibility study on the stability of gait patterns with changeable body stiffness is reported. The periodic motions of the legs are generated as a rhthmic motion. The stability of locomotion strongly depends on the mechanical properties of the body mechanism, especially the joint stiffness. In this report, the muscle tone of the robot motion at the trunk is changeable by using the changeable elasticity of the pneumatic actuators. The stability of quadruped locomotion in crawl, trot and pace patterns with changeable body stiffness was evaluated with hardware experiments.

Keywords: Quadruped locomotion, Musculoskeletal robot, Body stiffness, Stability

1. INTRODUCTION

Locomotion is one of the basic functions of a mobile robot and the important topic to develop a new control strategy for nonlinear multi-modal system. Therefore, a considerable amount of research has focused on controlling the motion of legged locomotion robots[1],[2]. This article discusses the relation between stability of gait patterns and body's dynamic properties in quadruped locomotion using musculoskeletal quadruped robot.

In this study, the first topic is development of musculoskeletal structure of the robot's trunk to imitate the animal's kinematical structure and physical properties in terms of stiffness(visco-elasticity). We can change the stiffness of the trunk through the balanced adjustment of the elasticity in coordiations of pneumatic actuators[3],[4]. The robot has artificial spinal structure with many segments of vertebra and interspinal disk in line. The articifial spine plays a role of structural member of the system and also becomes a passive device to be a dynamic damper with its visco-elasticity property[5],[6].

In this article, we focused on the point that the stability of quadruped locomotion in crawl, trot and pace patterns with changeable body stiffness through artificial musculoskeletal mechanism was evaluated with hardware experiments. We evaluated the relation between body stiffness and stable gait patterns. In hardware experiments, the stability is checked by evaluating the deviations of body motions in angular velocities. The results show there is appropriate parameter set of body stiffness and locomotion speed for each gait pattern in terms of stability.

2. MODEL

2.1 schematic model

Consider the quadruped robot shown in Figure 1; it has four legs and a main body. The main body is composed of two parts, a fore body and a hind body, that are connected through a multi-segmented spinal structure. Leg's joints are driven by geared DC motors. The spine, on the other hand, has no acturator to actuate directly its motion, but the robot has pneumatic actuators to change the trunk's stiffness through tendon mechanism.
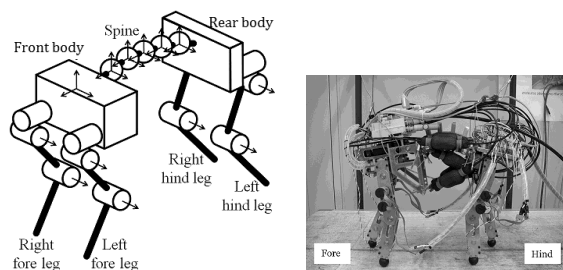
Fig. 1 Models of the musculoskeletal robot

2.2 Spine model

The schematic design of the trunk structure is summarized in Figure 2. This structure consists of artificial spine and eight pneumatic actuators. The spine is composed of ten vertebras and nine interspinal disks assembled in line. The tensile force of the steel wire in the spine is adjusted by a winch. The alignment of the actuators and geometrical scale of structure is designed to imitate usual size of living cats. The pneumatic actuators to change the trunk stiffness are enumerated as shown in the figure. Robot's total length and height are 0.41[m] and 0.35[m], respectively.
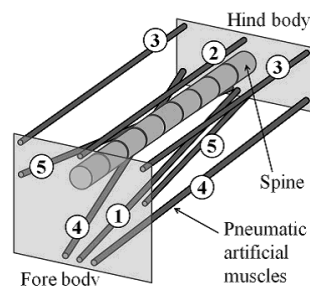

Fig. 2 Musculoskeletal structure of the trunk (1)Rectus abdominis. (2)Spinalis. (3)Iliocostalis. (4)External oblique. (5)Internal oblique.

3. HARDWARE EXPERIMENTS

The pneumatic actuators are controlled to change the stiffness of the trunk. The stiffness of each actuators are controlled in two states; 0.40 [MPa] and 0.15 [MPa]. The combination of the actuators' determines the trunk stiffness. The trunk stiffness is experimentally measuerd for each combination. The value of trunk stiffness changes from 0.1[Nm/rad] to 2.9 [Nm/rad].

First we investigated the motion of the robot selecting three parameters changeable: one is combination of pneumatic actuators' pressure modes to control trunk stiffness; Another is gait pattern and the other is time period of walking cycle T_f. Figures 3∼ 6 show the difference between roll and pitch angular velocities of main body. The locomotions were stable in both the trot and pace patterns (Figures 3 and 5). On the other hand, the robot's locomotion becomes unstable in the case that the trunk's stiffness becomes lower. When the time period of walking cycle could not match the natural mode of posture motion, the locomotion also becomes unstable(Figures 4 and 6). In figure 4 and 6, the rolling motion of the body became unstable. The difference between the motion of the fore and the hind bodies oscillated by the spinal mechanism. The excitation or convergence of periodic rolling motion of the main body depends on the stiffness of the spinal mechanism and muscles of the trunk.

Next, the stiffness of the trunk is changed in the crawl, trot and pace patterns, and the locomotion stability is investigated. Figure 7 shows the results. In the figure, gait patterns are expressed as phase difference, 0.00 for pace, 1.57 for crawl and 3.14 for trot. Trunk stiffness is expressed as multiple number of the stiffness of the spinal mechanism. In terms of the trunk stiffness, in the case of trot pattern, if the stiffness is too small, locomotion itself becomes unstable. However, if we choose appropriate stiffness at the trunk, the robot can continue stable trotting pattern. In terms of the time period of walking cycle, fast locomotion is suitable for trotting pattern, but to the contrary slow locomotion matches the crawl pattern.

These results show that there are different conditions for stable locomotion in each gait pattern, in terms of trunk stiffness and time period of walking cycle. We can note that periodic leg's motion causes excitation of oscillatory motion of the spinal mechanism. The the appropriate trunk stiffness makes effective damping factor to reduce the spine's oscillation excited by periodic leg's motion in the given gait pattern.

REFERENCES

[1] Y. Fukuoka, H. Kimura, and A. Cohen, Adaptive Dynamic Walking of a Quadruped Robot on Irregular Terrain Based on Biological Concepts, *The International Journal of Robotics Research* 22, No. 3, pp. 187-202, 2003.

[2] A. J. Ijspeert, A connectionist central pattern generator for the aquatic and terrestrial gaits of a simulated salamander, *Biological Cybernetics*, Vol. 84, pp. 331-348, 2001.
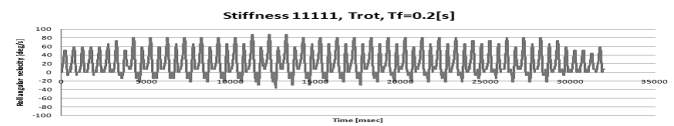
Fig. 3 Trunk stiffness:2.9 [Nm/rad], Trot, Tf=0.20[sec]
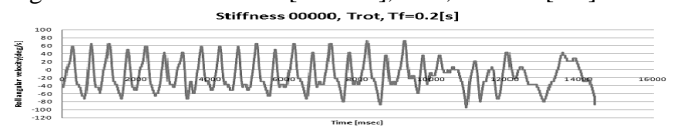
Fig. 4 Trunk stiffness:0.1 [Nm/rad], Trot, Tf=0.20[sec]
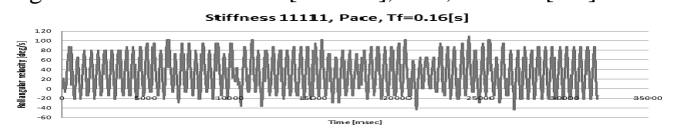
Fig. 5 Trunk stiffness:2.9 [Nm/rad], Pace, Tf=0.16[sec]
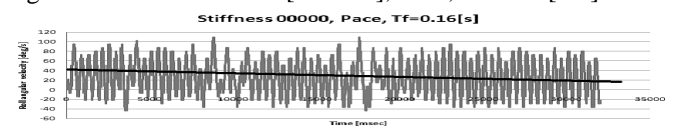
Fig. 6 Trunk stiffness:0.1 [Nm/rad], Pace, Tf=0.16[sec]
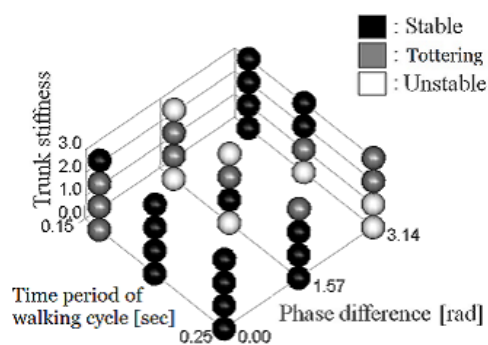
Fig. 7   Stability map: Black point=Stable, Gray point=Tottering, White point=Unstable

[3] D. G. Caldwell, G. A. Medrano-Cerda, and M. J. Goodwin, Control of pneumatic muscle actuators, *IEEE Control Systems Magazine*, Vol. 15(1), pp. 40-48, 1995.

[4] K.Tsujita, T.Kobayashi, T.Inoura and T.Masuda, "Feasibility Study on Stability of Gait Patterns with Changable Body Stiffness using Pneumatic Actuators in Quadruped Robot," *Advanced Robotics*, Vol.23, pp.503-520, 2009.

[5] I.Mizuuchi, R.Tajima, T.Yoshikai, D.Sato, K.Nagashima, M.Inaba, Y.Kuniyoshi, and H.Inoue, "The design and control of the flexible spine of a fully tendon-driven humanoid 'kenta'," Proc. of the 2002 IEEE/RSJ International Conference on Intelligent Robots and Systems (IROS2002), pp. 2527-2532, 2002.

[6] T.Takuma, M.Ikeda, and T.Masuda, "Facilitating Multi-modal Locomotion in a Quadruped Robot utilizing Passive Oscillation of the Spine Structure," Proc. of the 2010 IEEE/RSJ International Conference on Intelligent Robots and Systems (IROS2010), ThBT5.4, 2010.

Development of a Monopedal Robot with a Biarticular Muscle and Its Hopping Motion

Yoshihiro Nakata[1], Atsuhiro Ide[1], Katsuhiro Hirata[2] and Hiroshi Ishiguro[1]

[1]Department of Systems Innovation, Graduate School of Engineering Science, Osaka University, Osaka, Japan
(Tel : +81-6-6850-6360; E-mail: {nakata.yoshihiro, ide.atsuhiro, ishiguro}@is.sys.es.osaka-u.ac.jp)
[2]Department of Adaptive Machine Systems, Graduate School of Engineering, Osaka University, Osaka, Japan
(Tel : +81-6-6879-7533; E-mail: k-hirata@ams.eng.osaka-u.ac.jp)

Abstract: An electromagnetic linear actuator which we developed can emulate the spring-damper characteristics of a human muscle by quick control of the output force (i.e. impedance control) and it is expected to be used as an artificial muscle. We have been developing the electromagnetic linear actuator which has long stroke, quick response and large thrust by effective use of interior permanent magnets. In this paper, we develop a monopedal robot possessing bi- and mono-articular muscles implemented by the linear actuators. Thanks to the biarticular muscle, the bouncing direction of the robot can be controlled by changing the stiffness ellipse at the endpoint (i.e. foot) of the robot. We confirm that the bouncing direction of the robot and realize hopping by changing the stiffness ellipse.

Keywords: Compliance control, Electromagnetic linear actuator, Hopping, Monopedal robot, Stiffness ellipse.

1. INTRODUCTION

Animals perform dynamic whole body motions such as running and hopping in various environments. To realize these motions, compliance of muscles against external force and structural stability contributed by biarticular muscles are crucial. [1].

Biarticular muscles improve the stability of their body motion by changing the direction of the force output and the compliance characteristics at the endpoint. The latter property can be represented by the stiffness ellipse [1]. We focus on a control of a monopedal robot with a biarticular muscle to realize the hopping motion, as a first step for dynamic motions.

An electromagnetic linear actuator which we developed is advantageous in its response compared to pneumatic actuator which is widely used for various robots [2, 3]. Pneumatic actuator has compliance due to its physical property. A legged robot "Athlete Robot" driven by pneumatic actuators [2] can change the direction of the long axis of the stiffness ellipse. Though a control of the bouncing direction can be achieved by presetting the stiffness ellipse, a quick change of stiffness during the robot moving is difficult due to the slow response of the pneumatic actuator.

For compliance control, direct drive rotary electric motor is suitable thanks to its quick response. However, linear actuator is advantageous for adopting biarticular muscle since rotary motor requires complex wire drive system for it.

In this research, we develop a monopedal robot which

has bi- and mono-articular muscles implemented by electromagnetic linear actuators [3]. The stiffness ellipse at the endpoint (i.e. foot) of the robot is easily controllable thanks to the biarticular muscle. The robot can control its bouncing direction when it touches down to the ground. We confirm the bouncing direction and realize hopping by changing the stiffness ellipse.

2. STIFFNESS ELLIPSE

The model of human leg is shown in Fig. 1. f_n and e_n are the flexor and extensor muscles respectively. M_n is antagonistic pair of muscles. M_1 and M_2 are the monoarticular muscles at the hip and knee joint respectively. M_3 is the biarticular muscles which can constrain the motion of two joints. The compliance characteristic at the foot is expressed as an ellipse (stiffness ellipse) defined by three parameters; the length of the long axis, short axis and the direction of the long axis. They are determined uniquely according to elastic coefficients of M_1, M_2 and M_3

3. MONOPEDAL ROBOT AND RESULTS

The monopedal robot which we developed is shown in Fig. 2. The height from the foot to the hip is about 210mm (θ_1=20° and θ_2=40°). Three antagonistic pairs of muscles (i.e. six) are replaced by three actuators.

Since the current actuator cannot output sufficient thrust for the robot to jump under the environment with the gravity acceleration, a counter weight is used in the experiment. The movement of the trunk is restricted to the translation (i.e. no rotation) in horizontal and


Fig. 1 Simple model of human leg
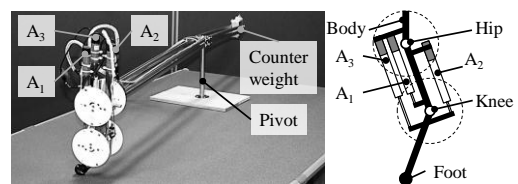
Fig. 2 The monopedal robot. A_1, A_2 and A_3 are actuators correspond to M_1, M_2 and M_3 respectively.
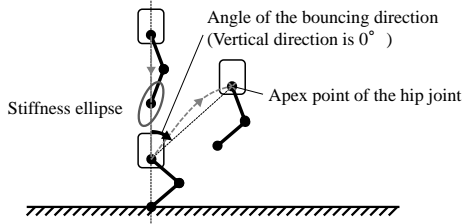
Fig. 3 Bouncing direction
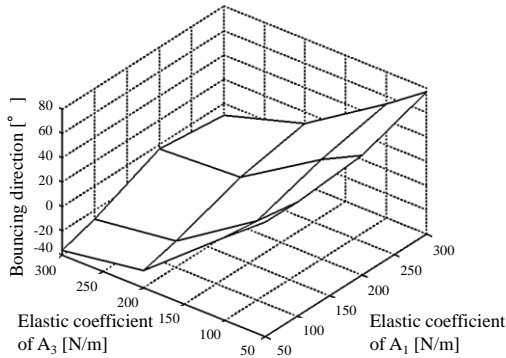
Fig. 4 Relationship between the elastic coefficients and the bouncing direction. A_1 and A_3 are actuators as mono- and bi-articualr muscles respectively.

vertical directions (sagittal plain).

The bouncing direction defined by the angle between the vertical direction and the moving direction is shown in Fig. 3. The bouncing direction can be controlled by changing the elastic coefficients of the linear actuators; i.e. stiffness ellipse. Fig. 4 shows the relationships between these parameters and the bouncing direction. The bouncing direction becomes larger as the elastic coefficient of A_1 increases and vice versa.

The above discussion on the stiffness ellipse is about the passive behavior of the robot. During each hopping cycle, energy loss occurs for each unloading. In order to continue the hopping, we employ a new control method for the knee joint; i.e. the monoarticular muscle A_2. Since this actuator does not affect to the direction of the stiffness ellipse, it is able to change the output force of the actuator at the knee joint without changing hopping direction. Therefore, bouncing direction and thrust force can be controlled independently. In the landing duration, the elastic coefficient is set to be small. In the unloading duration, on the other hand the elastic coefficient is set to be large. Fig. 5 shows motion sequences of hopping of the monopedal robot. The robot jumped twice.

It is important to note that use of biarticular muscle reduces computational cost. Even if there is no biarticular muscle, the stiffness ellipse can be controlled by calculating output force depending on posture of the robot with rapid control cycle. However, in our robot, it can be controlled by making each actuator emulate a spring, i.e. each actuator is controlled by a simple P control with fixed target. The robot only changes stiffness of actuators around hip joint (A_1, A_3) in each cycle and does not consider the motion on the ground. As the result, the robot with compliant actuator and biarticular muscle can realize stable hopping by using simple controller.

4. CONCLUSIONS

In this research, we developed a monopedal robot with the electromagnetic linear actuators. To realizing hopping of the monopedal robot, the monoarticular muscle around the hip joint and biarticular muscle are used to determine the bouncing direction of the robot. The monoarticular muscle around the knee joint is used to provide energy loss during each step. As the result, the hopping of the robot is achieved.

ACKNOWLEDGEMENT

REFERENCES

[1] M. Kumamoto, T. Oshima and T. Yamamoto, "Control properties induced by the existence of antagonistic pairs of bi-articular muscles — Mechanical engineering model analyses", *Human Movement Science*, Vol.13, No.5, pp.611-634, 1994.
[2] R. Niiyama and Y. Kuniyoshi, "Design principle based on maximum output force profile for a musculoskeletal robot", *Industrial Robot: An International Journal*, Vol.37, No.3, pp.250-255, 2010.
[3] Y. Nakata, H. Ishiguro, K. Hirata, "Dynamic Analysis Method for Electromagnetic Artificial Muscle Actuator under PID Control", *IEEJ Transactions on Industry Applications*, Vol.131, No.2, pp.166-170, 2011.
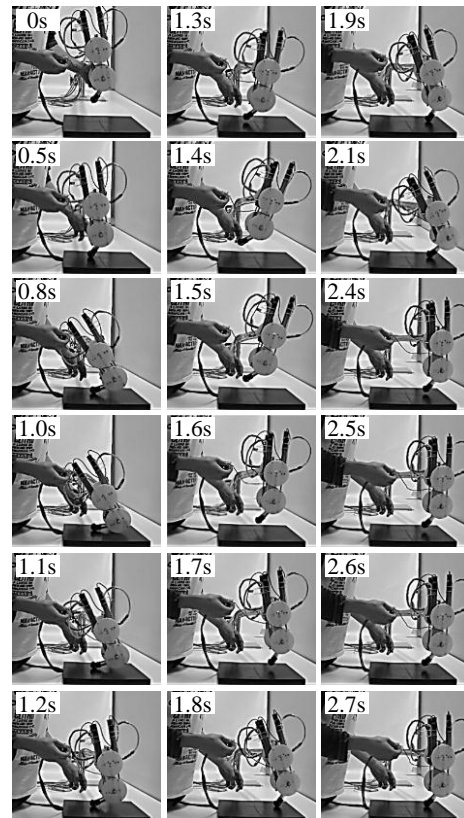

Fig. 5 Hopping of the monopedal robot. The black board under it is hard rubber board as slip-proof mat.

Toward Biorobotic Systems with Muscle Cell Actuators

Masahiro Shimizu[1], Shintaro Yawata[2], Koichiro Miyamoto[3], Kota Miyasaka[4], Toshifumi Asano[5],

Tatsuo Yoshinobu[3], Hiromu Yawo[5], Toshihiko Ogura[4], and Akio Ishiguro[2]

[1]Department of Multimedia Engineering, Osaka University, Osaka, Japan
(Tel: +81-6-6879-7752; E-mail: m-shimizu@ist.osaka-u.ac.jp)
[2]Research Institute of Electrical Communication, Tohoku University, Sendai, Japan
(Tel: +81-22-217-5464; E-mail: yawata@cmplx.riec.tohoku.ac.jp, ishiguro@riec.tohoku.ac.jp)
[3]Department of Electronic Engineering, Tohoku University, Sendai, Japan
(Tel: +81-22-795-7076; E-mail: k-miya@ecei.tohoku.ac.jp, nov@ecei.tohoku.ac.jp)
[4]Institute of Development, Aging and Cancer (IDAC), Tohoku University, Sendai, Japan
(Tel: +81-22-717-8596; E-mail: k.miyasako@idac.tohoku.ac.jp, ogura@idac.tohoku.ac.jp)
[5]Department of Developmental Biology and Neuroscience, Tohoku University, Sendai, Japan
(Tel: +81-22-217-6210; E-mail: asano@ige.tohoku.ac.jp, yawo@mail.tains.tohoku.ac.jp)

Abstract: The authors aim to develop muscle cell actuators driven by a photostimulation. Recently, bioactuators that exhibit self-organization have been attracting a lot of attention, because biological devices are expected to have significant abilities such as self-reproduction, self-repair, self-assembly. Based on this consideration, we have developed a myofilament-actuator, where we have utilized effects of a mechanical stimulation to construct the mechanical structure of such a bio-actuator. More specifically, we found that induction of differentiation into myofilament-like cells from a cultured myoblasts C2C12 is promoted under the mechanical stimulation. Under above circumstances, the next step is to find an appropriate method for driving the bio-actuators. To do so, we introduce channelrhodopsin-2(ChR2) which works as both a photoreceptor and an ion channel. Based on the above, we cultured muscle cells embedded with the gene of this protein. Then, we observed that the muscle cell actuator is contracted by a blue light stimulation.

Keywords: Biorobotic system, Muscle cell actuator, Mechanical stimulation, Channelrhodopsin-2.

1. INTRODUCTION

Living organisms change their bones, muscles and neurons by self-organization in order to adapt to their environment[1]. This process occurs not only at the level of the individual, but also on a cellular level, as prominent functions such as self-reproduction, self-repair and self-assembly. In Cell Biology, Engler *et al.*[2] found that ES cells recognize the mechanical strength of the substrate to which they adhere and in response to the stiffness of the scaffolding, differentiate into bones, muscles or neurons.

However, most state-of-the-art robots are made of metals and semiconductors which are unable to dynamically change physical and chemical characteristics during operation so it is not possible to show the adaptive functionality of structural changes in the body itself. Because of this, to implement a robot with the adaptive functionality of a living organism derived from a mechanical system, robotics and control system technologies need to be combined to achieve a flexible intelligent mechanical system like that of a living organism[3][4][5].

Hence, this study will attempt the creation of a bio-robot which expresses the inherent superior characteristics of a living organism with less invasive control method. To do so, we resulted in creation of the structure of muscle cell actuators as an initial stage of development of a biological device for a bio-robot. Using mechanical stimulations that promotes cell differentiation, the design and construction of muscle actuators through self-organization became possible. Then, as the next step, we dealt with

how to make the constructed actuators perform movements. In this study, by introducing "photostimulation" and "genetic engineering technology", the construction of muscle cell actuators that allow the drive control at a specific site and with specific timing is attempted in such a way that cell damage is minimized. Specifically, the method of driving the actuators is the protein ChR2, which functions as light-gated ion channel[6] and is introduced into cultured myoblasts so cells can be synchronized to the stimulus pulse of blue light. Thus, unlike the existing technique for creating an electric field, this method drives more than just one particular region and it is expected that the continued operation of the minimally invasive actuator does less damage to cells.

The purpose of this study is development of a muscle cell actuator toward biorobotic systems driven by photostimulations. More specifically, we here report on the deeply interesting experimental results as follows: (1) Creating the muscle actuator; (2) Driving the muscle actuator. The former of which is done by utilizing self-organization induced by mechanical stimulations. In the latter of which, the movement of the channelrhodopsin-2 gene-induced cultured muscle cells were synchronized to the light pulse.

2. CREATING THE MUSCLE ACTUATOR

This study intend to deal with a muscle cell actuator, which is made from cultured myoblasts by culturing and differentiating by exploiting mechanical stimulus re-
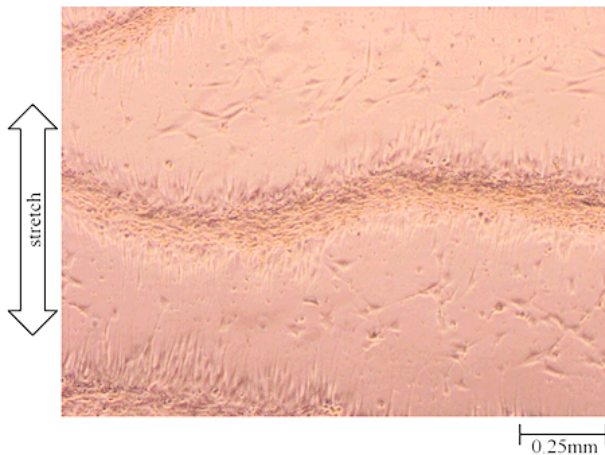
Fig. 1 : Photo of the C2C12 visualized by the microscope. As in the photo, large myofilament-like cells are indicated. This cells are cultured with mechanical stimulations.

sponse of muscle cells. In Cell Biology, recently, it is found that induction of differentiation into myofilament cells from a cultured myoblasts cells(*i.e.*, C2C12). Based on this knowledge, we create the muscle actuator by fully exploiting self-organization induced by mechanical stimulations(see Fig.1).

3. DRIVING THE MUSCLE ACTUATOR

Here, the next step is how to drive the muscle cell actuator. To do so, here, we investigated a photostimulation as a driving method. The results of the muscle cell photostimulation application experiment are shown in Fig 2. The distance between two points is shown with time development. The blue band represents when photostimulation was performed. This result indicates that muscle contraction occurred at the times corresponding to the light pulses. In addition, it was confirmed from the chart that around 7% contraction occurred.

4. CONCLUSIONS

The main contribution of this paper is development of a muscle cell actuator toward biorobotic systems driven by photostimulations. Utilizing biological devices in real-world situations remains challenging. For example, cells are only capable of surviving in cell culture medium, hence it is necessary to maintain this state by changing the cell culture medium regularly. Also, the current cell culture is 2 dimensional, therefore, for 3 dimensions it is still necessary to consider how to blanket the cells with nutrients and to consider how the individual parts can move in 3D space. For future works, it will be necessary to combine the current actuators with gel or PDMS in 3 dimensions and to also use optical fiber to create a device that can be controlled by pinpoint photostimulation. In the future, not only muscle cells as well as neurons will be used as circuits in biological devices and interaction between muscle cell actuaors and neurons can be verified.
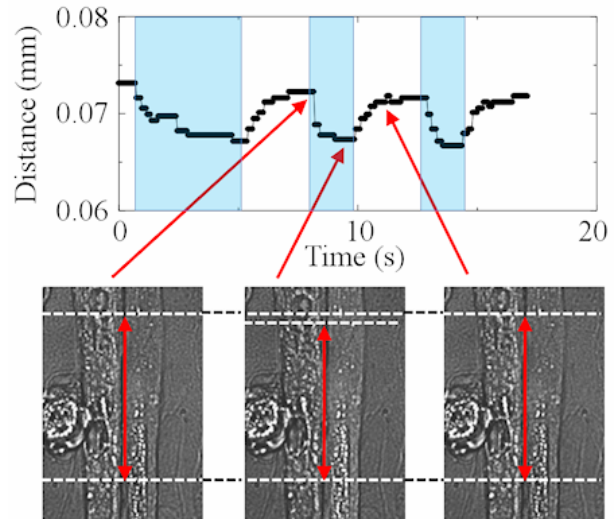
Fig. 2 Time course of a typical contraction of a muscle cell during the photostimulation. The muscle cell is contracting in the vertical direction.

5. ACKNOWLEDGMENTS

REFERENCES

[1] H. Asama, et al., "System Principle on Emergence of Mobiligence and Its Engineering Realization", *in Proc. of 2003 IEEE/RSJ IROS*, pp.1715–1720, 2003.

[2] Engler, J. A., Sen, S., Sweeney, L. H., Discher, E. D., "Matrix Elasticity Directs Stem Cell Lineage Specification," *Cell*, vol.126, issue 4, pp.677-689, 2006.

[3] A. Takashima, R. Minegishi, D. Kurabayashi and R. Kanzaki"Construction of a Brain-machine Hybrid System to Analyze Adaptive Behavior of Silkworm Moth", *in Proc. of 2010 IEEE/RSJ IROS*, pp.2389-2394, 2010.

[4] K. Morishima, K. Imagawa, T. Hoshino, S. Maruo, "DEMONSTRATION OF MUSCLE-POWERED AUTONOMOUS MICRO MOBILE GEL", *in Proc. of 2010 IEEE/RSJ IROS*, pp.4005-4010, 2010.

[5] Kim, J., Yang, S., Baek, J., Park, S., Kim, C. H., Yoon ,E ., "CARDIOMYOCYTES SELF-POWERED POLYMERMICROROBOT", *Proc. of The 14th International Conference on Solid-State Sensors, Actuators and Microsystems*, pp.1405-1408, 2007.

[6] Ishizuka T., Kakuda, M., Araki, R. and Yawo, H., "Kinetic evaluation of photosensitivity in genetically engineered neurons expressing green algae light-gated channels", Neurosci, Res 54, pp.85-94, 2006.

Unilateral Odor Input Activates Bilateral Premotor Areas in the Moth Brain

Shigehiro Namiki[1] and Ryohei Kanzaki[1]

[1]Research Center for Advanced Science and Technology, University of Tokyo
(Tel : +81-3-5452-5197; E-mail: namiki@brain.imi.i.u-tokyo.ac.jp)

Abstract: Bilateral integration of olfactory inputs from the left and right olfactory organs facilitates odor source localization in humans, rodents, fish, and insects. We investigated representation of bilateral odor input by a population of neurons in the lateral accessory lobe, a premotor area in the brain of the moth. The circuit generates the locomotor command for pheromone-source orientation behavior. We analyzed the physiological changes in response to stimulation on the left or right antennae by using intracellular recording and staining techniques with sharp glass microelectrode. Most of the interneurons showed similar patterns of excitatory activity in response to both left and right side stimulations. These results suggest that the LAL integrates bilateral odor information. We will discuss the command signal for moth walking behavior.

Keywords: command signal, insect, premotor area, central pattern generation, reticulospinal cell

1. INTRODUCTION

Animals have a pair of olfactory organs. The bilateral integration of olfactory inputs from the left and right olfactory organs facilitates odor source localization. Analysis of neural mechanisms for bilateral odor integration is important for understanding odor localization strategy of animals. In this context, moths are one of the model systems used for odor source localization.

Male moths show mating behavior in response to the sex pheromones emitted by conspecific females. Silkmoths

Fig. 1. Neuronal structures in the moth brain.

Bombyx mori show sustained walking behavior called the mating dance in response to transient pheromone exposure, and the walking direction is dependent on the stimulation: moths show straight walking to the right side to pheromone stimulation on the right antenna, and vice versa [1]. A series of electrophysiological, anatomical, and behavioral studies in *B. mori* has identified a neuronal circuit called the lateral accessory lobe (LAL) as the brain center of walking behavior [2,3]. A group of descending neurons that commands walking behavior has dendrites in the LAL.

Herein, we investigate the neural representation of pheromone input in the LAL. We recorded the physiology of the LAL interneurons in response to stimulation on either side of antennae and systematically analyzed their response properties as the first step to understanding the neural mechanisms underlying bilateral odor integration.

2. METHODS

Bombyx mori (Lepidoptera: Bombycidae) were reared under a long-day photoperiod regime (16/8-h L/D). Electrodes prepared from thin-walled glass capillaries by using a puller. The electrodes were filled with 5% Lucifer yellow solution in order to stain the neurons. The electrodes were inserted using a micromanipulator. The acquired signals were stored in a computer by using an A/D converter. Spike analysis was done by custom made programs written in MATLAB.

The odorant was applied to a piece of filter paper and inserted into a glass stimulant cartridge. We applied 10 ng of bombykol (the major pheromone component of *B. mori*) to the filter paper. Stimulus was applied to either side of the antenna. Compressed pure air was passed through a charcoal filter, and each stimulus was applied at approximately 35 cm/s. The moths were exposed to the odor for 200 ms, after which an exhaust tube was placed on the opposite side and the odor was removed (exit cartridge, ø~4.5 cm; 15 cm from the antennae; ~55 cm/s).

We stained each neuron by iontophoreticd dye injection with constant hyperpolarizing current. The brain was fixed, dehydrated and cleared. Each stained neuron was frontally imaged using a confocal imaging system. Serial optical sections were acquired throughout the entire depth of the neuron, and 3-D reconstructions of the labeled neurons were generated from these sections. Neuron and neuropil tracing was carried out using a image processing software AVIZO 6.0.

3. RESULTS

The LAL consists of 2 major interneuron types: unilateral neurons (UNs) and bilateral interneruons (BNs). Both UNs and BNs had dendrtic branches in single LAL. BNs also had axonal processes in the contralateral LAL.

In this study, we examined the odor response properties of the LAL
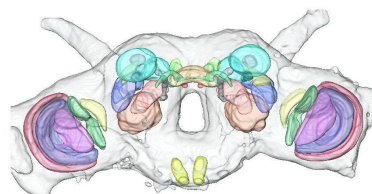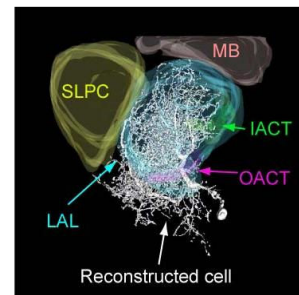
Fig. 2. Morphology of the LAL interneuron.

interneurons to unilateral pheromone inputs. Our results are based on physiologically and morphologically identified neurons (*n* = 26).

We characterized the morphology and physiology of 10 LAL UNs that innervated the LAL on one side. We performed pheromone stimulation on left or right antenna and arranged the data by ipsi- and contralateral stimulations,

Fig. 3. Three examples of the odor response of the LAL unilateral interneurons. Response to ipsilateral antenna (ipsi, gray) evoked stronger activity than that to contralateral one (contra, black) in each case.

according to the soma position. All UNs showed firing rate change in response to pheromone stimulation (Fig. 3). One UN showed an inhibitory response and the other 9 UNs showed an excitatory response. Hence in most cases, unilateral pheromone stimulation triggers the excitatory activity of the neurons in bilateral LALs.

We characterized the morphology and physiology of 16 LAL BNs that innervated LALs in both the left and right hemispheres. All BNs had smooth processes in the LAL, which is the same side of the soma and the blebby processes in contralateral LAL. Ten BNs had branches in the ventral protocerebrum. In most cases, responses to the unilateral and contralateral stimulations were similar but a difference was observed in the response intensity in some cases. Three BNs showed persistent firing activity that lasted over 30 s, but did not show flip-flop activity, which was observed in several types of descending neurons [2]. One BN showed an inhibitory response to unilateral pheromone stimulation and an excitatory response to contralateral stimulation.

We compared neuronal responses to the ipsi- and contralateral stimulations. We calculated the firing rate change of UNs and BNs (Fig. 4). In both types, the time course of the population responses were similar, but the response to ipsilateral stimulation showed slightly higher amplitude than that to contralateral stimulation.

Finally, we examined the cell-type specific feature. We compared 3 parameters: response intensity, response duration, and response latency. When we compared the firing rate for each time window, there was a difference during the early phase of the response (Fig.4A, B). There were no significant differences in response duration and latency between the populations, suggesting that the importance of the total neuronal activity for command generation of the waling behavior.

4. DISCUSSION

We revealed bilateral activation of the LAL for unilateral odor input in moth, and also reported the reliability of response, which have not been examined [3]. When moths receive pheromone input on one side, they show initial surge activity (unidirectional turn) toward the input side [1]. The present study suggests that both sides of the premotor areas are active during the initial phase of behavior. There is a possibility that the slight difference among the activities of LALs on both sides might be important for determining the walking direction. We will discuss the process how the neural activity is transmitted to the pattern generating circuit.

REFERENCES

[1] R. Kanzaki, N. Sugi, T. Shibuya, "Self-generated zigzag turning of *Bombyx mori* males during pheromone-mediated upwind walking" *Zool Sci*, Vol. 9, No. 3, 515-257, 1992.

[2] R. Kanzaki, A. Ikeda, T. Shibuya, "Mophological and physiological properties of pheromone-triggered flipflopping descending interneurons of the male silkworm moth, *Bombyx mori*", *J Comp Physiol A*, Vol. 175, No. 1, pp. 1-14, 1994.

[3] M. Iwano, E.S. Hill, A. Mori, T. Mishima, T. Mishima, K. Ito, R. Kanzaki, "Neurons associated with the flip-flop activity in the lateral accessory lobe and ventral protocerebrum of the silkworm moth brain", *J Comp Neurol*, Vol. 518, No. 3, 366-388, 2010.

Fig. 4. Population activity in response to the odor stimulation of the LAL unilateral interneurons (A) and bilatreral interneurons (B).

Planar Law of Intersegmental Coordination during Bipedal Walking in Japanese Macaques and Humans

Naomichi Ogihara[1], Takeo Kikuchi[1], Yutaro Ishiguro[1], Haruyuki Makishima[2], Masato Nakatsukasa[2]

[1]Department of Mechanical Engineering, Keio University, Yokohama, Japan
(Tel : +81-45-566-1423; E-mail: ogihara@mech.keio.ac.jp)
[2]Laboratory of Physical Anthropology, Department of Zoology, Kyoto University, Kyoto, Japan

Abstract: We investigated covariation of the elevation angles of the lower limb segments during bipedal walking in bipedally-trained Japanese macaques and humans with a view to understand the mechanism underlying the origin and evolution of the planar law in human bipedal walking. Two highly trained Japanese macaques and two adult humans walking on a treadmill were recorded, and the time course of the elevation angles at the thigh, shank and foot segments relative to the vertical axis were calculated. Our analyses indicated that this planar law also holds true for macaque bipedal walking. However, the orientations of the plane are largely apart in the two species, indicating that the way the limb segments are kinematically coordinated is variable according to species, possibly due to the difference in the anatomy and mechanics of the foot segment.

Keywords: locomotion, kinematics, elevation angle, foot, *macaca fuscata*

1. INTRODUCTION

In human walking, the elevation angles of the thigh, shank, and foot segments, i.e., the orientations of the segments with respect to the vertical axis, are known to be stereotyped across subjects, and the temporal changes of these angles covary such as to form a regular loops lying close to a plane in a three-dimensional (3D) space [1,2]. This planar covariation of the elevation angle is suggested to be indicative of the coordinated neural control of bipedal locomotion, by reducing the degrees of freedom of variables to be controlled. However, it is also postulated that biomechanical factors such as strong correlation between the foot and shank elevation angles also play a part in emergence of the planar law [3].

In this study, we investigated the planar covariation of the elevation angles during bipedal walking in Japanese macaques to clarify if the same planar law holds true for bipedal walking in an inherently-quadrupedal primate. Differences in the planar covariations of the elevation angles in Japanese macaques, whose musculoskeletal system is not as adapted to bipedalism as that of humans, may hopefully provide valuable insight about the mechanism underlying the origin and evolution of the planar law in human bipedalism.

2. METHOD

Two highly-trained, adult Japanese macaques (KA, 12.3 kg; KU, 9.2 kg) walking bipedally on a treadmill at 3, 4, and 5 km/h were filmed using synchronized high-speed cameras at 125 frames/s and locomotor kinematics were analyzed [4]. Five landmarks on the right side of the body at 1) head of the fifth metatarsal, 2) lateral malleolus of the fibula, 3) lateral epicondyle of the femur, 4) greater trochanter, 5) acromion were manually digitized frame-by-frame. The coordinates of markers were calculated using 3D motion analysis software. The change in position of each coordinate over time was low-pass filtered at 12 Hz. For comparisons, two adult humans (K, 57 kg; M, 68 kg) walking on a treadmill at 3, 4, and 5 km/h were also recorded using a 3D optical motion capture system.

The elevation angles of the thigh, shank and foot segments were then calculated as the sagittally projected angles of the corresponding limbs with respect to the vertical axis. The calculated angle profiles were interpolated over cycle duration to fit a 100-points time base for normalization of the time.

To evaluate the inter-segmental coordination, the time courses of the elevation angles were plotted in a three-dimensional space and the trajectories were fitted by a plane using a least-square method. For this, principal component analysis of the covariance matrix of the elevation angles was performed and three eigenvectors were calculated. The first two eigenvectors describe the best-fitting plane and the third vector is the normal to the plane, representing the orientation of the plane. See literature for more details about the calculation method [1,2].

3. RESULTS

Figure 1 illustrates the 3D plot of the mean time-courses of the elevation angles of one human (M) and one macaque (KU) subjects walking at 3, 4, and 5 km/h, and the best-fitted planes of the corresponding loop trajectories. The % variance accounted for the first two eigenvectors was ~99% for all speeds and subjects in human bipedal walking, while that of macaque bipedal walking was <99%, indicating that the 3D trajectories of the elevation angles are essentially planar for both humans and macaques but the degree of planarity was comparatively low in macaques. The first eigenvector was very similar between the two species across and in all speeds. However, the second eigenvector was substantially different between humans

and macaques. Therefore, the orientations of the best-fitted plane of angular covariation were substantially different between the two species. The mean % variance accounted for the first and second eigenvectors was 93.1% and 5.0%, respectively, in macaques and 87.4% and 11.5%, respectively, in humans. Figure 1 also shows that the orientation of the plane was more or less consistent with speed in human bipedal walking, but it was dependent of speed in macaque bipedal walking because the range of movement of the thigh elevation angle increased with speed in macaques.

4. DISCUSSIONS

This study demonstrated that the planar low of the intersegmental coordination holds true for bipedal walking in Japanese macaques. However, the way the planar law is achieved during bipedal walking was found to be different between humans and macaques. In both species, the first eigenvector was headed in almost the same direction, but the % variance accounted for the first and second eigenvectors were much higher and lower, respectively, in Japanese macaques, indicating that the planarity of the 3D trajectory of the elevation angle is higher in humans but the leg movements in macaques seems to be relatively more confined to one component axis along the first eigenvector.

What distinguished human bipedal walking from that of macaques was the large component of the second eigenvectors. This difference may be attributed the time course of the elevation angle during the stance phase of bipedal walking. In human walking, the foot elevation angle remained almost constant in early to mid stance phase and the change in the elevation angle occurred mainly in the thigh segment. Therefore, the 3D trajectory of the elevation angle moved along the second eigenvectors to form the plane. On the other hand, in macaque bipedal walking, the foot elevation angle continued to decrease soon after the initial contact of the foot until the push-off, and hence the fluctuations of the elevation angle of the three segments resembled each other, resulting in the larger and smaller % variance accounted for the first and second eigenvectors, respectively. Therefore, the difference in the foot motion with respect to the ground between humans and macaques was considered to make a difference in the planar low of intersegmental coordination during bipedal walking in the two species.

This is possibly resulted from the difference in the anatomy and mechanics of the foot segment between human and macaque. The human foot is rigidly structured to form a longitudinal arch acting as an effective lever for push-off. However, the macaque's prehensile foot is a more flexible structure and bends at the midtarsal region in the stance phase (midtarsal break) [5]. As a result, the heel is gradually raised from the early stance phase, resulting in the continuous decrease in the foot elevation angle in the macaque bipedal walking. Consequently, the human foot segment

specialized for terrestrial bipedalism seems to largely contribute to the emergence of the planar law in human walking.
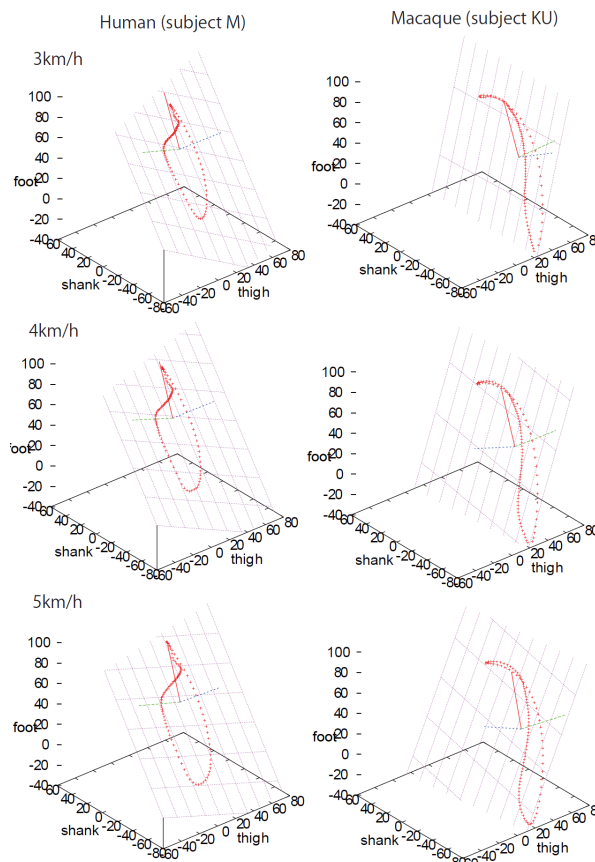
Fig. 1. 3D plot of the mean time courses of the elevation angles and the best-fitted planes of the corresponding loop trajectories. Trajectories progress counterclockwise. Foot-ground contact corresponds to the top of the loop.

REFERENCES

[1] Borghese NA, Bianchi L, Lacquaniti F, "Kinematic determinants of human locomotion", *J Physiol*, 494(3): 863-879, 1996.

[2] Ivanenko YP, d'Avella A, Poppele RE, Lacquaniti F, "On the origin of planar covariation of elevation angles during human locomotion", *J Neurophysiol*, 99(4): 1890-1898, 2008.

[3] Hicheur H, Terekhov AV, Berthoz A, "Intersegmental coordination during human locomotion: does planar covariation of elevation angles reflect central constraints?", *J Neurophysiol*, 96(3): 1406-1419, 2006.

[4] Ogihara N, Makishima H, Nakatsukasa M, "Three-dimensional musculoskeletal kinematics during bipedal locomotion in the Japanese macaque, reconstructed based on an anatomical model-matching method", *J Hum Evol*, 58(3): 252-261, 2010.

[5] DeSilva JM, "Revisiting the "midtarsal break"", *Am J Phys Anthropol*, 141(2): 245-258, 2010.

Adaptive Motion of a Musculoskeletal Robot Arm utilizing Physical Constraint

Shuhei Ikemoto[1], Yoichi Nishigori[2] and Koh Hosoda[1,2]

[1]Graduate School of Information Science and Technology, Osaka University, Osaka, Japan
(Tel: +81-06-6879-7739; E-mail: {ikemoto, koh.hosoda}@ist.osaka-u.ac.jp)
[2]Graduate School of Engineering, Osaka University, Osaka, Japan
(E-mail: {yoichi.nishigori, hosoda}@ams.eng.osaka-u.ac.jp)

Abstract: Musculoskeletal robots have been developed to investigate how musculoskeletal systems contribute to intelligent behaviors in living things. In this research, we develop a musculoskeletal robot arm, which has a skeleton similar to human's arm and pneumatic muscles to drive the skeleton, in order to investigate how the design contributes to adaptive behavior under physical constraint. As an example of a physical constraint, we focus on a door-opening task in which the robot arm reaches and grasps a doorknob to open the door. In this paper, we show that the musculoskeletal robot arm can accomplish the door-opening task by using its characteristics even if the door slightly moves and rotates.

Keywords: Musculoskeletal robot arm, Adaptive behavior, Constrained environment

1. INTRODUCTION

Design of a robot bears a central role for the attainment of a given task because it determines how the given task is difficult for the robot. So far, in terms of engineering, it has been mentioned that the most important characteristic of the robot's design is how easily and accurately it can be modeled analytically. In contrast with this common sense of control engineering, in recent years, it is known that well-designed robot's body can make a huge contribution for task accomplishment even if the robot cannot be modeled sufficiently. The information processing, which provided by the well-designed robot's body, is called morphological computation[1]. In this research, we focus on the morphological computation of a musculoskeletal robot arm designed by referring human's musculoskeletal system.

So far, many researhes have focused on musculoskeletal system as a driving system for robot arms. However, these designs are not similar to human's nor other living organism's musculoskeletal system. In contrast with these researches, there are several researches which strongly focus and mimic a human's musculoskeletal system. Holland and Knight developed a humanoid robot called CRONOS[2], and Mizuuchi et al. also developed a humanoid robot called Kojiro[3]. These robots have a structure similar to human's one and they are not limited to an arm. However, the concrete advantage of their structure is still not quantitatively shown in these researches.

In this research, we develop a musculoskeletal robot arm based on a human's upper limb musculoskeleton in order to investigate how the design contributes adaptive behavior of human beings. As one of tasks which a human naturally does, we focus on a task in which the developed robot arm reaches and grasps a doorknob and opens the door. This door-opening task, where the robot arm has to physically contact with the doorknob, is known as one of most difficult task for traditional robots[4]. In this paper, we realize the door-opening task by using very simple control and evaluate how the design of the robot arm contributes for the task accomplishment quantitatively.
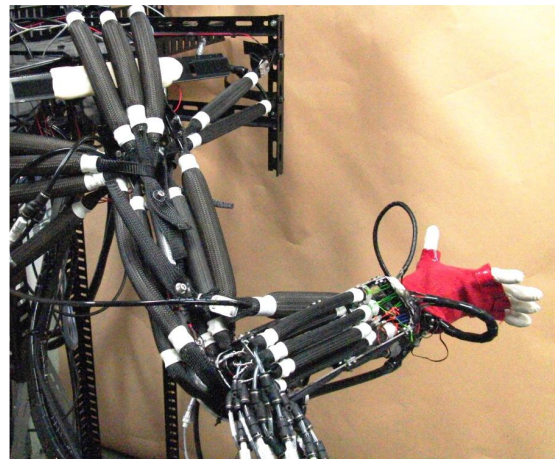
Fig. 1 The developed musculoskeletal robot arm.

2. MUSCULOSKELETAL ROBOT ARM

Fig.1 shows the overview of the developed musculoskeletal robot arm. In this design, there are several similarities with humans' structure. For example, the forearm consists in a radioulnar joint (two bones called ulna and radius set in a parallel configuration that allows for twisting) and the wrist joint employs an ellipsoidal joint[5]. In order to drive this structure, 17 McKibben pneumatic muscles are attached to the bones. The muscle's layout is also inspired by that of humans. For instance, there are not only monoarticular muscles but also biarticular muscles and almost of them are part of antagonistic pairs[5]. Additionally the robot hand mounted on the developed robot is also driven by pneumatic muscles. Each pneumatic muscle has a pressure sensor and its internal pressure is controlled by a PID control system.

Fig.2 shows the sequential snapshots of the realized door-opening task. The motions were generated by a very simple control which switches several desired pressures of each muscles because the flexibility of the muscles and the humanlike skeleton can allow physical interactions with the door in a careless way. At the same time,
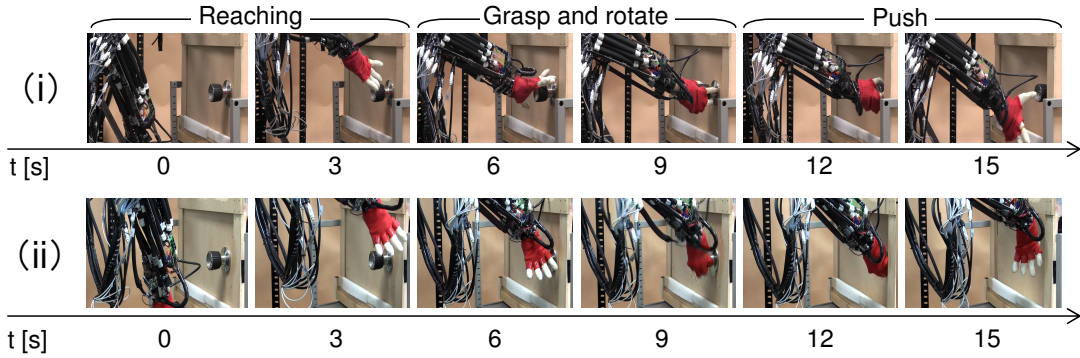
Fig. 2 Door opening movements by the developed robot arm. (i)Precision grip, and (ii)power grip were executed.

the muscle flexibility and humanlike skeleton would provide high robustness when the relative attitude between the door and the arm is changed. The desired pressures were configured by a trial-and-error process and it was not very difficult. In fact, if the robot can keep grasping the doorknob, randomly generated motions are still sufficient to rotate the doorknob and open the door.

3. EXPERIMENT AND RESULT

In this section, we evaluate the robustness of the both motions employing precision grip and power grip which require different postures of the forearm to grasp the doorknob. Fig.3 shows the result of the evaluation of the door-opening robustness. In this experiment, the same sets of desired pressure were used for different relative attitude between the door and the arm. Note that, however, the reaching phase was skipped by fixing the robot hand on the doorknob. In this figure, the blue and red arrows indicate successful and failed directions of the door-opening, respectively, obtained for different attitudes In this result, it is shown that both kinds of motions can open the door by using same sets of desired pressure even if the relative attitude between the door and the arm was changed. This would show the advantage of the flexibility of the developed robot arm because the flexible muscles can store and emit elastic energy to adapt the environmental change. Additionally, difference of the grip can be seen as difference in the directions for which the robot can successfully open the door. This indicates that the flexibility of the arm robot can adapt the changing of the external physical constraints.

Table.1 shows the result of quantitative evaluation of the robustness. From this table, it can be seen that the design of the developed robot arm contribute to improve the robustness of attainment of the door-opening task quantitatively. Additionally, it is also clarified that the difference in the grip provides different property of robustness. In order to increase the success rate, adopting sensory feedback control or machine learning technique will be an important future work.

REFERENCES

[1] R.Pfeifer and J.Bongard. *how the body shapes the way we think. a new view of intelligence*. MIT Press,

(i) Precision grip   (ii) Power grip
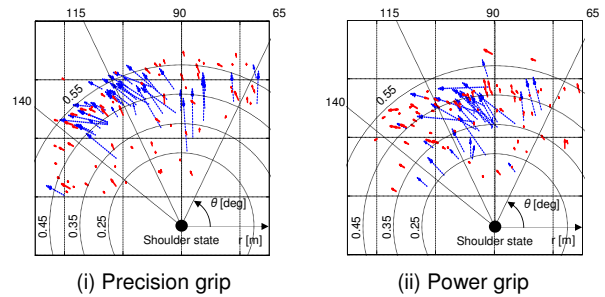
Fig. 3 Result of the robustness analysis.

Table 1 Success rates of door opening

r[m]	Success rate[%](trials)	
	(i) Precision grip	(ii) Power grip
$r < 0.25$	0 (5)	60.0 (10)
$0.25 \leq r < 0.35$	26.7 (15)	57.1 (21)
$0.35 \leq r < 0.45$	64.5 (31)	43.2 (44)
$0.45 \leq r < 0.55$	40.0 (50)	24.2 (33)
$0.55 \leq r$	7.1 (14)	0 (2)

θ[deg]	Success rate[%](trials)	
	(i) Precision grip	(ii) Power grip
$\theta < 65$	33.3 (6)	14.3 (7)
$65 \leq \theta < 90$	26.9 (26)	42.9 (28)
$90 \leq \theta < 115$	53.1 (32)	52.4 (42)
$115 \leq \theta < 140$	50.0 (36)	27.6 (29)
$140 \leq \theta$	6.7 (15)	50.0 (4)

2006.

[2] O.Holland and R.Knight. The anthropomimetic principle. *Proceedings of the AISB06 Symposium on Biologically Inspired Robotics*, 2006.

[3] I. Mizuuchi, Y. Nakanishi, Y. Sodeyama, Y. Namiki, T. Nishino, N. Muramatsu, J. Urata, K. Hongo, T. Yoshikai, and M. Inaba. An advanced musculoskeletal humanoid kojiro. pages 294 –299, nov. 2007.

[4] W. Chung, C. Rhee, Y. Shim, H. Lee, and S. Park. Door-opening control of a service robot using the multifingered robot hand. *Industrial Electronics, IEEE Transactions on*, 56(10):3975 –3984, oct. 2009.

[5] D.A. Neumann and D.L. Wong. *Kinesiology of the musculoskeletal system: foundations for physical rehabilitation*. Mosby St Louis, MO, 2002.

Tactile Sensitivity Modulation of Elastic Skin by Change of Grasping Force

Shouhei Shirafuji[1], Shuhei Ikemoto[2] and Koh Hosoda[2]

[1]Department of Adaptive Machine Systems, Graduate School of Engineering, Osaka University, Osaka, Japan
(E-mail: shouhei.shirafuji@ams.eng.osaka-u.ac.jp)
[2]Department of Multimedia Engineering,Graduate School of Information Science and Technology, Osaka University, Osaka, Japan
(E-mail: ikemoto@ise.eng.osaka-u.ac.jp, koh.hosoda@ist.osaka-u.ac.jp)

Abstract: This paper reports the variation of the outputs of the sensors embedded in the elastic skin in incremental steps of the grasping force. The instantaneous changes of the strain gauges outputs at the moment of inpact force were recorded. Initially, the amount of the output decreased along with the increase of the grasping force. It begun to rise again, and reached the second peak.

Keywords: Grasp force, Sensing,

1. INTRODUCTION

The tactile sense plays important roles when people manipulate objects. Similarly, the tactile sense is a key for advanced robot manipulation, and it has been investigated in recent years[1]. At the same time, how robots get these information effectively from a wide variety of sensors with which they are equipped and make these tactile information available are crucial for adaptive robotic manipulation systems. In this study, we investigated the relationship between the grasping force exerted by the robot hand and the amount of information obtained from strain gauges randomly embedded in the elastic skin of the robot hand finger.

There are some studies which suggest the method that controls grasping force with sensors embedded in elastic artificial skin, in order to protect the objects from excessive grasp force and to prevent slips[6][3][5]. They described the purpose of preventing excessive force as saving energy and reducing damages. We hypothesize that minimizing grasp force is necessary to get information of events effectively in object manipulation. We examined this using the developed robot hand with sensors embedded in elastic skin randomly. In this paper, we report that the instantaneous changes of the outputs of sensors embedded in the artificial elastic skin caused by increase of the grasping force. We have proposed the method to learn optimal gasping force on the basis of previous experiences. If there are differences in the amount of information, appropriate grasping force can be learned using these variation.

2. SYSTEM DESCRIPTION

2.1 Artificial Skin and Sensors

Fig. 1 shows the artificial skin and a finger of the robot hand which were used for the experiments described in this paper. The artificial skin is a modification of the anthropomorphic robotic soft fingertip which was proposed by Hosoda et al.[5]. The skin is composed of two layers. The inner skin layer is made of soft urethane resin (Hitohada gel Hardness 0, Exseal Co., Japan). This ure-
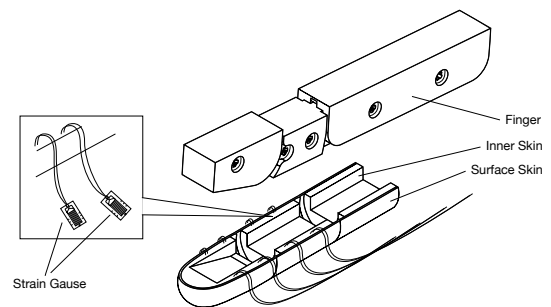
Fig. 1 A finger of the anthropomorphic robot hand and the artificial skin in which sensors are randomly embedded.

thane has softness similar to the one of human skin and its compressive elastic modulus is $11.8N/cm^2$. The softness of the skin not only provides increase in stability of grasping but also transmits events which occur between the hand and an object to the sensors. The inner skin is wrapped in a thin outer skin which is made of relatively stiff non-foamed polyurethane (Pro-350, Temcofine Co., Japan) to prevent damages to the inner skin and sticking between the inner skin and objects, since Hitohada gel is fragile and has strong stickiness.

The eight strain gauges (KFG-1-350-C1-11, Kyowa Electronic Co., Japan) are embedded in the skin randomly. The sensors were inserted into a mold and Hitohada gel was cast into the mold of an adult finger. The strain gauges are used to measure skin strain. In this experiment, these sensors are embedded only in the index finger

2.2 Anthropomorphic Robot Hand

Fig.2 shows the anthropomorphic human scale robot hand that we designed. The robot hand feature human-like form and structure, and has five fingers which are driven by pneumatic muscle actuators through tendons. We use pneumatic muscle actuator of McKibben type. When the actuator is filled with compressed air, it contracts and force is generated. The robot hand has 16 joints which provide 16 DOF; the thumb has four joints and the
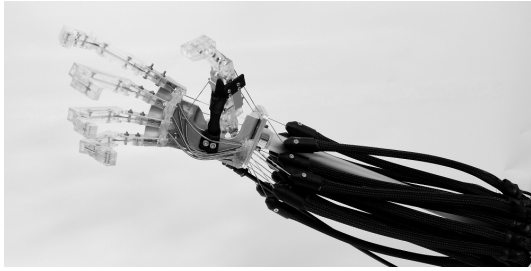
Fig. 2 Robot hand used in this experiment.

(a)   (b)
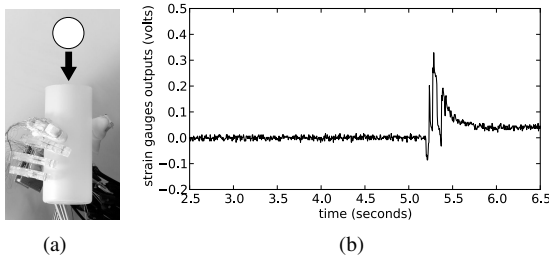
Fig. 3 (a)A ball was dropped in the cup holded by the robot hand. (b)Exsample of the output of a strain gauge when the ball collided with the cup.

other fingers have three joints. The fingers and the palm are equipped with the artificial skins that we described above.

3. EXPERIMENT AND RESULT

The cylinder cup was hold by the robot hand using the index finger and the thumb with constant force (Fig. 3a). In that condition, we dropped a 50 grams ball in the cup. An example of output of one of the strain gauges is shown in Fig. 3b. We recorded the average increase of the strain gauges outputs at the moment of the collision. We repeated it in incremental steps of the grasping force. Fig. 4 shows the relationship between the average output increase in ten trials and the pressure of the pneumatic muscle attached to the index finger considered as the grasping force. Initially, the output gradually decreased along with the increase of the grasping force. The amount of the output begun to rise after the pressure reached about 0.43 MPa. Afterward, it begun to decrease again.

4. DISCUSSION

The elastic tissue in the skin of human finger has a property similar to rubber. The behavior of polymer materials is so complex that it is difficult to express its constitutive equation. Nakazawa et al.[4] has represented the dynamics of a fingertip by the Kelvin model, which is composed of a spring and a damper placed in parallel, and investigated the characteristics of the human fingertips while the shear force is being applied. They reported that the shearing stiffness increases proportionally with the contact force, while the viscosity is almost constant.

Assuming the skin of the robot hand has characteristics similar to the human skin, the reaction of the sensors embedded in elastic skin should be reduced in strength
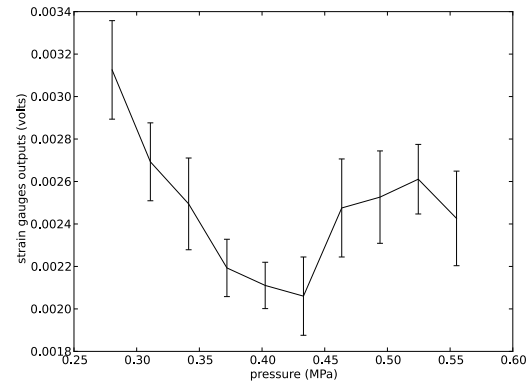

Fig. 4 Relationship between the instantaneous response of the sensors and the grasping force.

along with the skin stiffness increasing caused by the increase of the grasping force. The initial decrease of the output in Fig. 4 is believed to be due to this increase of the stiffness.

Han et al.[2] reported that the Heltz model can be used to approximate the relationship between the contact area and the load in the human skin. The increase of the outputs is suspected to be caused by the increase of the contact area between the finger skin and the object. As future work, we plan to investigate the results analytically with these models and to use this variation of information to the learning of adaptive manipulation.

REFERENCES

[1] R.S. Dahiya, G. Metta, M. Valle, and G. Sandini. Tactile sensing: from humans to humanoids. *IEEE Transactions on Robotics*, 26(1):1–20, 2010.

[2] H.Y. Han, A. Shimada, and S. Kawamura. Analysis of friction on human fingers and design of artificial fingers. In *Robotics and Automation, 1996. Proceedings., 1996 IEEE International Conference on*, volume 4, pages 3061–3066. IEEE, 1996.

[3] T. Maeno and S. Hiromitsu T. Kawai. Control of grasping force by detecting stick/slip distribution atthe curved surface of an elastic finger. In *Proceedings of IEEE International Conference onRobotics and Automation*, volume 4, pages 3895–3900, 2000.

[4] N. Nakazawa, R. Ikeura, and H. Inooka. Characteristics of human fingertips in the shearing direction. *Biological Cybernetics*, 82(3):207–214, 2000.

[5] Y. Tada and K. Hosoda. Acquisition of multi-modal expression of slip through pick-up experiences. In *Intelligent Robots and Systems, 2006 IEEE/RSJ International Conference on*, pages 5810–5815. IEEE, 2007.

[6] MR Tremblay, WJ Packard, and Cutkosky. Utilizing sensed incipient slip signals for grasp force control. In *Proceedings of the 1992 Japan-USA Symposium on Flexible Automation*, pages 1237–1243, 1992.

Three-Dimensional Muscle Arrangement and Dynamic Walking of Musculoskeletal Humanoid

Keita Ogawa[1] and Kenich Narioka[2] and Koh Hosoda[2]

[1]Department of Adaptive Machine Systems, Osaka University, Osaka, Japan
(Tel: +81-6-6879-7752; E-mail: keita.ogawa@ams.eng.osaka-u.ac.jp)
[2]Department of Multimedia Engineering, Osaka University, Osaka, Japan
(Tel: +81-6-6879-7752; E-mail: narioka@ist.osaka-u.ac.jp, koh.hosoda@ist.osaka-u.ac.jp)

Abstract: Humans have the highly-complicated musculoskeletal body structure and perform adaptive behavior. To investigate the advantages of this structure, we built a whole-body musculoskeletal humanoid with pneumatic artificial muscles. The skeletal structure and muscle arrangement of the robot are three-dimensionally designed to be similar to those of humans, especially in the lower body. Taking advantage of the human-like structure of the robot, we conducted a walking experiment. To make muscle activation patterns, we use a human EMG patterns. As a result, if the structure of the robot is close to that of humans, we found the motion of the robot can be easily created and realized dynamic walking.

Keywords: Biomechanics, Musculoskeletal system, Humanoid robot, Pneumatic artificial muscle, Dynamic Walking

1. INTRODUCTION

Humans have the highly-complicated musculoskeletal body structure with the many joints and muscles. Humans are able to utilize the complicated body and to perform adaptive behavior such as walking. The complex human body structure might have some reasons, because "Nature creates nothing without a purpose"(Aristotle, 350 B.C.E). One of the advantages of the musculoskeletal system, bi-articular muscles have the function that dissolve contact tasks with open loop control [1]. If we understand advantages of the musculoskeletal structure and apply them to robots correctly, we can enhance the performance of the robot.

In biomechanics, some human body structures have been mimicked and some musculoskeletal humanoid robots have been developed in recent years. The musculoskeletal robots with pneumatic artificial muscle realized various dynamic tasks [2, 3]. However, these robots have only basic muscles in the lower body or these muscles are attached only for pitch, roll, or yaw movements. The contraction forces of most of the human muscles exert influences on pitch, roll and yaw movements simultaneously. In addition, for humans, even the single movement such as the hip flexion is realized in coordination of several muscles around the hip joint. Since human musculoskeletal structure has redundant muscles attached three-dimensionally, we should take it into account in designing musculoskeletal robots.

In this study, under the assumption that musculoskeletal robot performing three dimensional movements should have three dimensional muscle arrangement, we built a musculoskeletal humanoid robot driven by pneumatic artificial muscles attached three dimensionally. The robot's musculoskeletal structure is highly similar to that of humans, especially in the lower body. In this paper, we introduce the design of the robot and its three-dimensional muscle arrangement. In addition, we make a walking motion taking advantage of human-like musculoskeletal body and conduct a walking experiment.

2. PNEUMATIC ARTIFICIAL MUSCULOSKELETAL HUMANOID "PNEUMAT-BS"

We developed a musculoskeletal humanoid robot "Pneumat-BS" actuated by pneumatic artificial muscles. Fig. 1 shows the appearance of the robot, its DOF and the arrangement of the artificial muscles. The overall height

No.	Muscle Name
#1	Soleus
#2	Tibialis anterior
#3	Peroneus
#4	Ankle adductor
#5	Gastrocnemius
#6	Popliteus
#7	Vastus lateralis
#8	Hamstring muscle
#9	Rectus femoris
#10	Sartorius
#11	Gracilis
#12	Gluteus medius
#13	Adductor magnus
#14	Iliacus
#15	Gluteus maximus
#16	Obturator externus
#17	Rectus abdominis
#18	Erector spinae
#19	Arm abductor
#20	Arm adductor
#21	Arm flexor
#22	Arm extensor

(a)Front View   (b)Side View

■ : Hinge joint (1 DOF)   ⬭ : Mono-articular muscle
● : Ball joint (3 DOFs)   ⬭ : Bi-articular muscle

Fig. 1 A musculoskeletal humanoid robot "Pneumat-BS". Left: Photograph. Right: DOF and muscle arrangement.

of the robot is 1181 [mm] and the weight is 10.1 [kg]. The link length and the center of gravity of the robot are designed to be the same ratio as that of humans. This robot has 21 DOFs, and 44 pneumatic artificial muscles are attached to the robot in total. Supplying and exhausting compressed air from an air compressor is controlled by on-off electric valves. As the sensor configuration, there are two acceleration sensors (3-axes) on the head and waist, two gyro sensors on the head (pitch, roll) and 8 force sensing resistors on the four corners of both feet.

The robot has complex body structure, including not

only mono-articular muscles but also bi-articular muscles. In particular, the hip joint of the robot is driven by 9 muscles (♯8∼♯16). Using PE braided lines, we arrange these muscles three dimensionally (Fig. 2). The three-dimensional arrangement of muscles is important in dealing with three-dimensional movements. For example, sartorius (♯10) is a bi-articular muscle which has the function of knee flexion, hip flexion, hip external rotation, and hip abduction. This muscle generate pelvic rotation at the beginning of the swing phase. Pelvic rotation make the step width narrow and make stride long (Fig. 3). It makes the walking more stable and efficient.
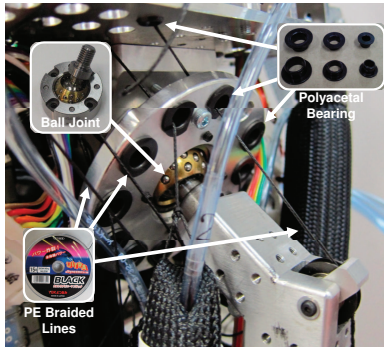

Fig. 2 Around hip joint of Pneumat-BS.
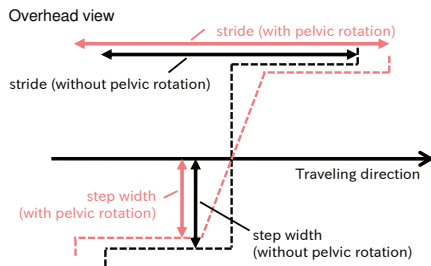
Fig. 3 Effect of the pelvic rotation.

3. WALKING EXPERIMENT WITH HUMAN MUSCLE ACTIVATION PATTERNS

We conduct walking experiments to confirm that the robot is able to perform dynamic tasks by using the complicated muscles. To realize dynamic walking, we used human muscle activation patterns (EMG data) for driving the pneumatic muscles. The human muscle activation patterns can be utilized in driving musculoskeletal robots because the structures are close to those of humans. Since pneumatic muscles can hold a given power by closing the valves, we decided how to drive the muscles by trial-and-error (Fig. 4). Fig. 5 shows the experimental sequence of the walking experiment. We realized a few steps without feedback and confirmed that the robot had enough power to perform dynamic walking. However, a stable periodic gait could not be achieved.

4. CONCLUSIONS AND FUTURE WORKS

In this study, we presented the musculoskeletal humanoid "Pneumat-BS" driven by pneumatic artificial
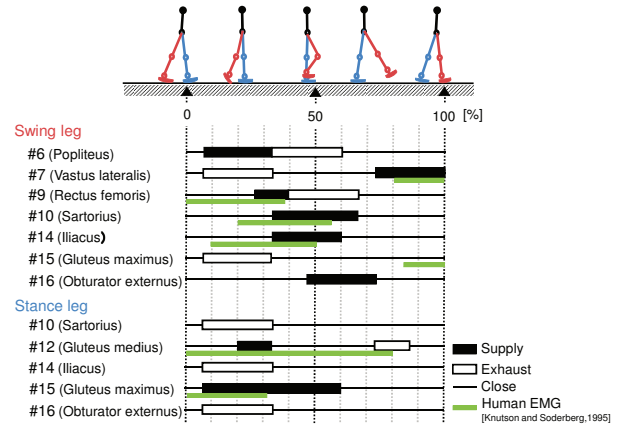

Fig. 4 Muscle actuation patterns with EMG (using [4]).
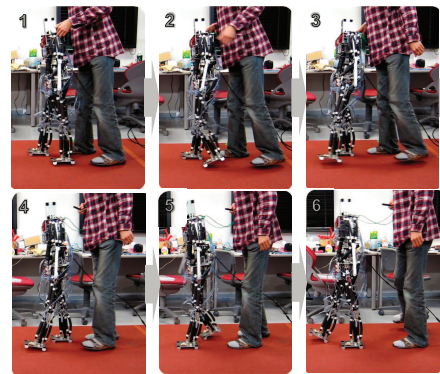
Fig. 5 Experimental sequence of walking experiment.

muscles, and we introduced that method to make muscle activation patterns for musculoskeletal humanoid using human EMG data and results of walking experiments. For future work, we have to develop a control method for the musculoskeletal robot and realize stable behaviors.

REFERENCES

[1] M. Kumamoto. Animal inspired motion control mechanism. In *Advanced Motion Control, 2004 8th IEEE International Workshop on. AMC*, pages 11–19. IEEE, 2004.

[2] Ryuma Niiyama, Satoshi Nishikawa, and Yasuo Kuniyoshi. Athlete robot with applied human muscle activation patterns for bipedal running. In *Proc. IEEE-RAS Int. Conf. on Humanoid Robots (Humanoids 2010)*, pages 498–503. Nashville, Tennessee USA, Dec. 2010.

[3] T. Takuma, S. Hayashi, and K. Hosoda. 3d bipedal robot with tunable leg compliance mechanism for multi-modal locomotion. In *Intelligent Robots and Systems, 2008. IROS 2008. IEEE/RSJ International Conference on*, pages 1097–1102. IEEE, 2008.

[4] Donald A. Neumann PhD PT FAPTA. *Kinesiology of the Musculoskeletal System: Foundations for Physical Rehabilitation*. Mosby, 1 edition, 3 2002.

Manipulation of aggressive behavior of the cricket using a small robot

Hitoshi Aonuma[1], Rodrigo da Silva Guerra[2], Minoru Asada[3,4] and Koh Hosoda[3,5]

[1]Research Institute for Electronic Science, Hokkaido University, Sapporo, Hokkaido 060-0812, Japan (Tel : +81-11-706-3832; E-mail: aon@es.hokudai.ac.jp), [2]Dept. of Electrical Engineering, UFRGS, Osvaldo Aranha Aranha, 103, Porto Alegre, RS 90035-190, Brazil (Tel : +55-51-3308-3515; E-mail: rsguerra@ece.ufrgs.br), [3]JST Erato Asada Project, Osaka University, Suita, Osaka 565-0871, Japan, [4]Department of Adaptive Machine Systems, Osaka University, Suita, Osaka 565-0871, Japan (Tel : +81-6-6879-7347; E-mail: asada@ams.eng.osaka-u.ac.jp), [5]Dept. of Adaptive Machine Systems, Grad. Sch. of Inf. Science and Tech., Osaka Univ., Suita, Osaka 565-0871, Japan (Tel : +81- 6-6879-7750; E-mail: koh.hosoda@ist.osaka-u.ac.jp)

Abstract: Male crickets *Gryllus bimaculatus* are known to exhibit intensive aggressive behavior towards other males. These crickets are often used as an experimental model in aggression researches. We establish a real-time recording system and behavior manipulation system using a small robot that can elicit aggressive behavior in a test cricket.

Keywords: insect, aggressive behavior, biogenic amine, social interaction.

1. INTRODUCTION

It is widely observed in animals that dominant hierarchy is established by agonistic behavior, through the complex interaction among physiological, motivational, and behavioral systems. Social and physical environment must be two of the most important factors to understand agonistic behavior in animals, which makes it difficult to fully understand it.

The cricket provides one of the greatest model systems to investigate neuronal mechanisms underlying aggressive behavior. Aggressive behavior in crickets is released by antennal contact detecting cuticular substances between two conspecific males [1]. When a male cricket encounters another male by chance, it exhibits intensive aggressive behavior. The battle starts out slowly and escalates into a fierce struggle [2]. Once the fighting is settled, the loser (subordinate) will refuse to fight again for a while [3]. It has been demonstrated that biogenic amine system is closely linked with agonistic behavior [5, 6]. Octopamine level of the hemolymph might mediate aggression level. Biogenic amines in the insect brain work as neurotransmitters, neuromodulators and as neurohormones. However, it remains unclear how the biogenic amine system in the central nervous system is mediated during a fight. In this study, we attempt to manipulate aggressive behavior of a male cricket using a small robot that is a kind of decoy of a conspecific male cricket so that we can record neuronal activities in the cricket brain.

2. MATERIALS AND METHODS

2.1 Animals

Cricket *Gryllus bimaculatus* used were raised in our laboratory colony. They were reared at 25-30°C under L/D 14:10 (lights on at 6:00 h) and fed a diet of insect pellets, carrots and water *ad libitum*. We used sexually mature male crickets for all experiments. To reduce the influence of prior fighting experience and to motivate fighting, each cricket was individually separated in a 100 ml glass beaker lined with filter paper for 2 days before the experiments.

2.2 Robot

The robot has dimensions of 18x18x22mm and is driven by two differential wheels. It has a size comparable to that of a typical cricket. It has no sensors except for an infrared receiver used for receiving commands encoded into pulses of infrared light. Movements can be controlled both in open or closed-loop with or without real-time feedback from insects' position [7]. In order to elicit aggressive behavior in a male cricket, another male cricket body parts that has head and thorax parts were attached on the robot or extraction of cuticular carbons were painted in the surface of the robot.

2.3 Electrophysiological recording from a free moving animal

Electromyograms (EMG) of mandible muscles were obtained using two varnish-coated copper wires (17 μm diameter) inserted proximally into the mandible muscle. Large amplitude mandible muscle potentials were recorded in free moving male crickets. The cricket recorded EMGs were placed in an experimental arena (12x12x10cm). Other male cricket or a robot was placed at the arena to observe the behavior and to record the activities of mandible muscles.

2.4 Measurement of biogenic amines using a micro-dialysis system

Animals were anaesthetized by rapid cooling on crushed ice. Microdialysis probe (0.22mm outer diameter, 2.0 mm total length) was implanted in the head. After implanted, crickets can walk around freely. Then another cricket or a robot was placed in the arena to elicit aggressive behavior to the cricket with the probe implanted. Probes were perfused at a rate of 2.0μl/min with cricket saline (85.55mM NaCl, 5.63mM KCl, 2.25mM $CaCl_2$). Probes were perfused 30min prior to the experiment. For all microdialysis experiments, samples were collected every 10 min. The samples collected were injected directly onto the HPLC column for qualitative and quantitative analyzing [8].

3. RESULTS AND DISCUSSION

3.1 Aggressive behavior of the cricket

Male crickets show intensive aggressive behavior when they encounter another male (Fig.1). The previous

agonistic interaction between males had influence over the following behavior in subordinates. We focused on the subordinate behavior to understand how animals alter their behavior dependent on previous experience. Pharmacological experiments demonstrated that nitric oxide (NO) signaling and biogenic amine octopamine (OA) play a crucial role in the behavioral decision making in fighting. We found that NO has an inhibitory effect on aggressive motivation whereas OA has a facilitating effect on aggressive motivation. We hypothesize that NO and OA signals mediate internal state of the cricket to introduce aggressive behavior. We also designed dynamic behavior models and neurophysiology model to understand how cricket develop internal state for aggressive motivation. We then understand that social interactions constantly improve internal state of animals.

Fig. 1. Fighting between male crickets.

3.2 Real time analysis of the cricket internal state

In order to investigate how animals realize real time adaptation, we established a real time recording system from a free moving animal. In male cricket, aggressive behavior is elicited by cuticular pheromone from conspecific male. We have developed a behavior manipulation system using a small robot that can easily introduce aggression behavior from a male cricket (Fig. 2). Cricket showed intensive aggressive behavior toward the robot. During aggressive behavior, we succeeded in recording EMG from mandible opener muscle using a fine copper wire electrode. Cricket attacked the robot again and again although it stopped attacking another male cricket once the fighting was settled. Therefore we can elicit aggressive behavior any time in a test animal.
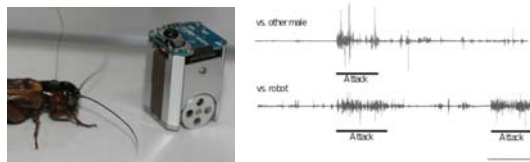

Fig. 2 Cricket and robot. EMG was recorded from a test animal that elicit attacking toward another male or the robot.

Aggressive motivation in animals is thought to be mediated by biogenic amines. In cricket, octopamine and serotonin are thought to play important role in releasing aggressive behavior [4]. Then we also established a microdialysis system to analyze dynamical change in the contents of biogenic amines in the test animals (Fig. 3). The samples of the microdialysis were collected every 10 min. The samples collected were quantitatively and qualitatively analyzed using a high-

performance liquid chromatography (HPLC) with electrochemical detection (ECD) system [8]. Using this system we can evaluate our multi-feedback model that was designed to describe dynamical change of internal state of the cricket [9].
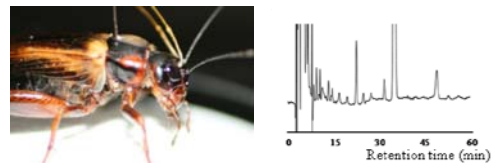

Fig. 3. Microdialysis system for a cricket.

4. CONCLUSION

We hypothesize that important mechanism underlying behavior adaptability is a multiple feedback structure that is composed of feedback loop in the nervous systems and feedback loop through the social environment [9]. In order to evaluate this hypothesis, we tried to establish a real-time recording system and behavior manipulation system using a small robot that can elicit aggressive behavior in a test cricket.

5. REFERENCES

[1] Nagamoto, J., Aonuma, H., and Hisada, M. (2005) Discrimination of conspecific individuals via cuticular pheromones by males of the cricket *Gryllus bimaculatus*. Zool. Sci. 26(11):1079-1088.

[2] Alexander, R. D. (1961) Aggressiveness, territoriality, and sexual behaviour in field crickets (Orthoptera: Gryllidae). *Behaviour* 17: 130-223.

[3] Hoffmann, H. A. and Stevenson, P. A. (2000) Flight restores fight in crickets. *Nature* 403, 613.

[4] Adamo, S. A. and Hoy, R. R. (1995) Agonistic behaviour in male and female field crickets, *Gryllus bimaculatus*, and how behavioural context influences its expression. *Anim. Behav.* 49, 1491-1501.

[5] Stevenson, P. A., Hoffmann, H. A., Schoch, K. and Schildberger, K. (2000) The fight and flight responses of crickets depleted of biogenic amines. *J. Neurobiol.* 43, 107-120.

[6] Stevenson, P. A., Dyakonova, V., Rillich, J. and Schildberger, K. (2005) Octopamine and experience-dependent modulation of aggression in crickets. *J. Neurosci.* 25, 1431-1441.

[7] Guerra R.D., Aonuma H., Hosoda K. and Asada M. (2010) Semi-automatic behavior analysis using robot/insect mixed society and video tracking. *J. Neurosci. Methods*. 191: 138-144.

[8] Katsumata A., Yamaoka R. and Aonuma H. (2011) Social interactions influence dopamine and octopamine homeostasis in the brain of the ant, *Formica japonica*. *J. Exp. Biol.* 214: 1707-1713.

[9] Kawabata K., Fujii T., Aonuma H., Suzuki T., Ashikaga M., Ota J. and Asama H. (2011 *accepted*) A neuro-modulation model of behavior selection in the fighting behavior of male crickets. *Robot. Auton. Syst.*

Automatic estimation of neural properties for Hodgkin-Huxley type models

Daisuke Miyamoto[1], Tomoki Kazawa[1], Stephan Shuichi Haupt[1], Hidehito Sato[1], Masashi Tabuchi[1],

Kei Nakatani[2], Ryohei Kanzaki[1]

[1] Graduate School of Information Science and Technology, University of Tokyo, Tokyo, Japan
(Tel: +81-3-5452-5195; E-mail: miyamoto@brain.imi.i.u-tokyo.ac.jp, kazawa@brain.imi.i.u-tokyo.ac.jp)
[2]Graduate School of Life and Environmental Science, Tsukuba University, Ibaraki, Japan

Abstract: Detailed neuron models based on measured ionic currents are still exceptional when considering the bewildering variety of cell types investigated because determining ionic currents requires very favorable experimental conditions. The situation is still worse for multi-compartment models, but such models are required for detailed simulations of complex neural networks. To alleviate these difficulties, we propose a method that allows estimating ionic currents and passive properties based on simple electrophysiological responses and assumptions concerning the types of currents involved.

Keywords: Genetic algorithm, Parallel computing, NEURON, Compartmental modeling, Electrophysiology simulation

1. INTRODUCTION

Nervous systems are capable of solving problems that pose considerable difficulties to conventional computing methods. An example of such a problem is the chemical plume tracking problem, solved by male silkmoths (*Bombyx mori*) displaying odor-source orientation behaviour[1]. We use various approaches to elucidate the solution of this problem are followed using a combination of robotics, models, silkmoths, and their brains[2, 3].

In particular, the use of neural network models as robot controllers is promising as behavior at different levels can be directly compared to the biological system. However, a suitable level of detail is required for the implementation of such neural network models because much of the properties of the neurons reside in their complex morphological and electrical properties. Generally, it is not feasible to obtain complete biophysical characterisations of all the neurons of interest. Therefore, it is highly desirable to obtain at reasonable estimates of the actual biophysical properties from more restricted experimental data. The number of parameters to be estimated is a drawback in this strategy: an automated fitting scheme is required, notably when expanding estimations to allow for multi-compartment models including neural morphology.

To address this problem, we have developed a system in which parameter estimates can be carried out automatically by including the simulation of the neurons in the fitting process. Due to the computational demands, we implemented our system on the RIKEN integrated Cluster of Clusters (RICC) and KEI facilities.

2. MATERIALS AND METHODS

2.1 Neuron Model Construction

We adopted silkmoths antennal lobe (AL) projection neuron model as example (Fig. 1). This model is composed of four parts: dendrite, soma, spike generator and axon. Dendrite and soma compartments have passive membrane potentials. Spike generator and axon compartments have Hodgkin-Huxley (HH) type membrane potentials[4] with three types of channels: Na$^+$, K$^+$ and Ca^{2+}
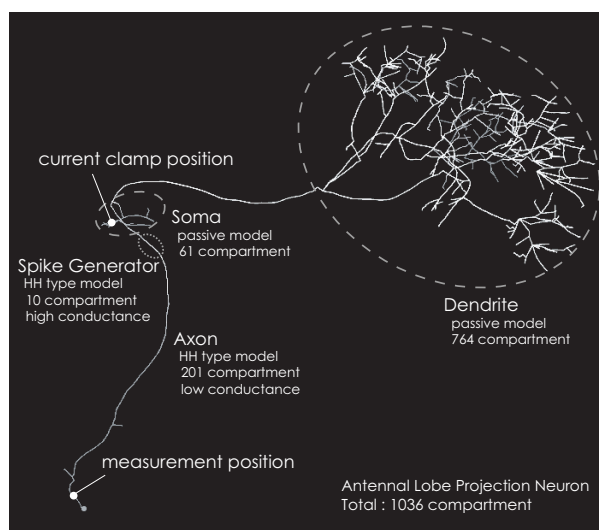

Fig. 1 The model of antennal lobe projection neuron of the silkmoth, using in the simulation.

transit. Spike generator compartments have higher ionic conductance than axon compartments.

This model neuron was simulated by "NEURON"[6], an empirically-based neuron simulator. At the simulation, neuron was subjected to a simulated experimental current clamp, injecting a depolarizing ramp or ramp + sin wave current. The voltage responses of the model neurons to this stimulus were used as target data for re-estimating the parameters used to construct the model neurons.

2.2 Parameter Estimation

We adopted the real-coded genetic algorithm (RCGA)[5] for parameter estimation because of its good parallel efficiency. Parameters to estimate were property of spike generator: position on axon, number of compartments, a K$^+$ conductance (G_K), a Na$^+$ conductance (G_{Na}), and a Ca^{2+} conductance (G_{Ca}).

During parameter estimation, we simulated the model neuron with the parameters of each gene, determining voltage responses to the current injections.Based on

these potential changes $P(t)$ and the target data potential changes $T(t)$, we defined fitness (F) as:

$$F = \frac{1}{\int_0^{t_{\max}} [\int_0^a (P(t) - T(t)) dt]^2 da}$$

Reproduction on the GA, we apply uniform mutation as mutation algorithm and BLX-α as crossover algorithm. Additionally, some genes were mutated normal random value for local searching.

Parameter estimates were done under the following conditions:

- **Processor:** 256 cores
- **Number of genes:** 2048
- **Number of generations:** 200
- **Simulation time step:** 0.025 msec
- **Simulation time range:** 0 - 400 msec
- **Estimation range:**
  - position of spike generator on axon: 0 - 200
  - compartment number of spike generator: 1 - 50
  - $\overline{G_K}$ of spike generator: 0.0001 - 1.0000 S/cm^2
  - $\overline{G_{Na}}$ of spike generator: 0.0001 - 10.000 S/cm^2
  - $\overline{G_{Ca}}$ of spike generator: 0.00001 - 0.10000 S/cm^2

3. RESULT

We estimated parameters by using three types of current clamp. Results of the estimations are shown in Fig.2.

4. DISCUSSION

Genetic algorithm in conjunction with the simulation of neuron models allows parameter estimates for model neurons. However, comparing each results of estimation, case of ramp stimulation was not accurate as others (Fig.2). It probably suggests that stimulation optimizing is very important for estimation.

In the present study, we used model neurons and simulations both for target data and for determining the fitness. In the next step, we will employ complete electrophysiological data from real neurons. To avoid overfitting due to

errors (and noise) in the experimental data, an error evaluation function may be implemented or the fitness function may have to be modified, for example by using spike timing and number.

Our approach can easily be extended for application to more detailed multi-compartment models. However, such systems need very large computational resource. To tackle this problem, we will use more CPUs (ex. 8192 cores on RICC or >10000 cores on KEI) and extend GA like the island model GA.

REFERENCES

[1] R. Kanzaki, N. Sugiand and Shibuya T, "Self-generated zigzag turning of Bombyx mori males during pheromone-mediated upwind walking", *Zoological Science* Vol. 9, pp. 515–527, 1992.

[2] S. Emoto, N. Ando, H. Takahashi and R. Kanzaki, "Insect-controlled robot - evaluation of adaptation ability -", *The Journal of Robotics and Mechatronics* Vol. 19, pp. 436–443, 2007.

[3] A. Takashima, R. Minegishi, D. Kurabayashi and R. Kanzaki, "Estimation of Feedback System during Programmed Behavior Exhibited by Silkworm Moth", 2010 Second World Congress on Nature and Biologically Inspired Computing (Fukuoka), pp. 92–97, 2010.

[4] AL. Hodgkin and AF. Huxley, "A quantitative description of membrane current and its application to conduction and excitation in nerve", *The Journal of Physiology*, Vol. 117, No. 4, pp. 500–544, 1952.

[5] AH. Wright, "Genetic algorithms for real parameter optimization", *Foundations of Genetic Algorithms*, pp. 205–218, 1991.

[6] NEURON web, "http://www.neuron.yale.edu/neuron/".
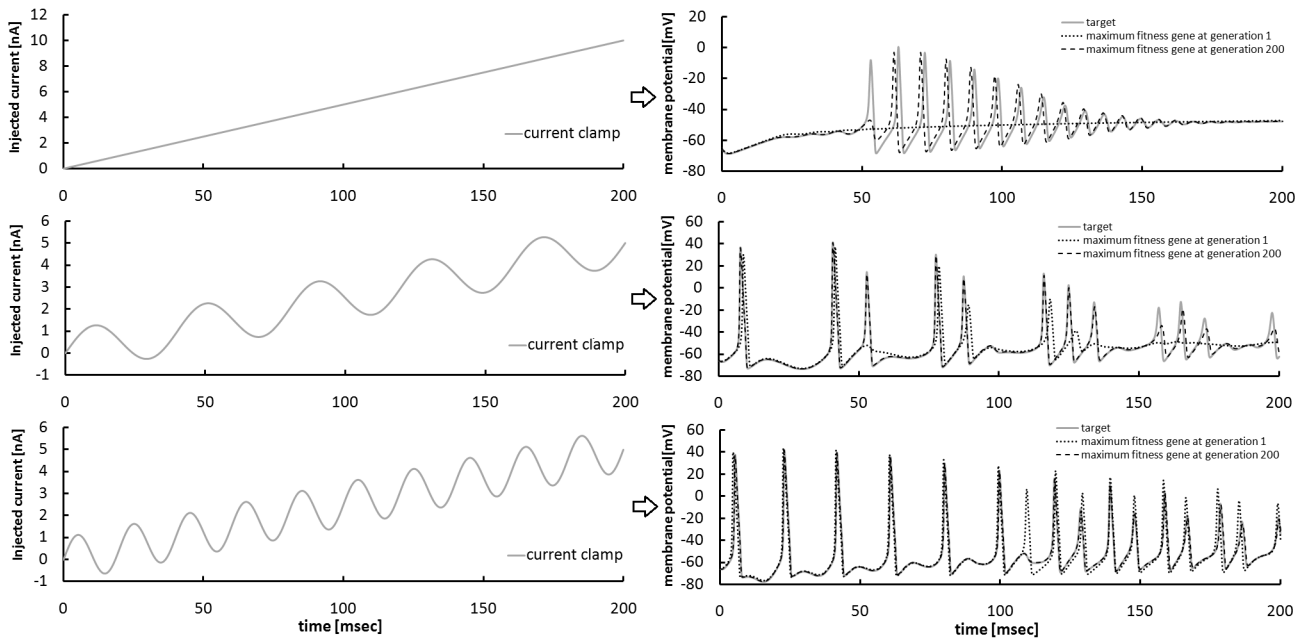
Fig. 2 **Result of estimation** Top: ramp stimulus current, Middle: ramp + sin wave (low frequency) stimulus current, Bottom: ramp + sin wave (high freqency) stimulus current.

Minimalistic Behavioral Rule for Reflecting Robot's Morphology

Fabio Dalla Libera[1], Shuhei Ikemoto[2], Koh Hosoda[2] and Hiroshi Ishiguro[3]

[1]Research Fellow of the Japan Society for the Promotion of Science (E-mail: fabiodl@gmail.com)

[2]Graduate School of Information Science and Technology, Osaka University, Osaka, Japan
(Tel: +81-06-6879-7739; E-mail: {ikemoto, koh.hosoda}@ist.osaka-u.ac.jp)

[3]Department of Systems Innovation, Graduate School of Engineering Science, Osaka University, Osaka, Japan
(Tel: +81-06-6850-6360; E-mail: ishiguro@sys.es.osaka-u.ac.jp)

Abstract: In a previos work, we proposed a very simple stochastic model, termed Minimalistic Behavioral Rule, in order to show how small bacteria such as *Escherichia coli* can robustly reach high concentrations of nutrient despite the noise in the sensory information. In particular, we showed that when this simple behavioral rule is employed, environmental or internally generated noise can be beneficial to the resultant behaviors of the living being, a phenomenon that can be explained by Stochastic Resonance. In this paper, we apply such behavioral rule to a real world complex robot, whose behavior is strongly influenced by its morphology and its surroning environment. Through the experiments, in particular, we show that the sensory information used for the task achievement greatly influences the resultant behavior.

Keywords: Minimalistic Behavioral Rule, Musculoskeletal robot arm, Adaptive behavior

1. INTRODUCTION

Living things can survive in complex and dynamical environments by taking full advantage of their body dynamics, sensing and interaction with the surrounding environments. Small bacteria such as *Escherichia coli* (E. coli) are no exception. In a previous work, we proposed a Minimalistic Behavioral Rule (MBR) in order to explain how E. coli can effectively reach high concentrations of nutrients and avoid high concentrations of repellent substance despite highly noisy sensory information[1]. Since MBR is extremely simple and makes very limited assumptions, it can be easily applied without knowing the robot's body structure or its actuators properties. Experiments showed that MBR can control simple mobile robots with no information on its actuators and sensors [2]. However, to date, MBR was not tested on complex, multi-DOFs robots.

The idea of applying a very simple control to highly complex robots is not new. So far, many researchers have developed biologically inspired robots [3] that can operate with simple control laws. Usually, the exploitation of the morphological computation[4], emergent from a well-designed robot's body, allows the achievement of a specific task with very simple control laws.

However, the identification of such simple control laws requires the developer's inspiration, knowledge and experience. In other words, even if the control laws are very simple, it is not easy to find them.

The ultimate goal of this research is to build a simple but general control law which can exploit the characteristics of the robot's morphology automatically. We propose MBR as a possible solution for controlling a robot when no previous knowledge on the robot's actuators and sensory data is available. If specific knowledge is available, clearly, task and robot specific controllers can be designed to improve the system efficiency. Actually, MBR can be used for collecting the data necessary to this development process.
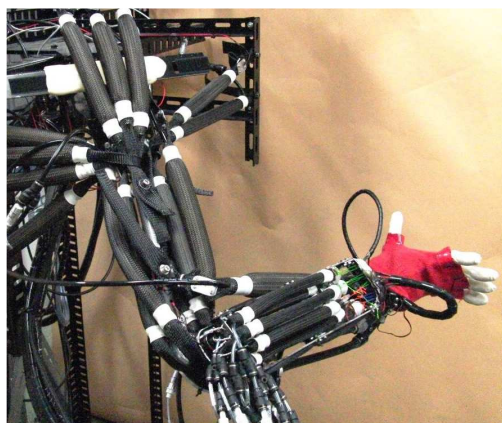
Fig. 1 The complex musculoskeletal robot arm used in the experiment.

In this paper, we show that MBR is applicable even when the robot has a very complex structure. In detail, MBR was used to control the pneumatic musculoskeletal robot arm shown in Fig. 1. This robot has a 7 DOFs driven by 17 McKibben pneumatic muscles. Each muscle is equipped with a pressure sensor, used for closed loop pressure control. In other terms, the robot is controlled by setting the variation of the pressure in each of the 17 pneumatic actuators. The task chosen consists in reaching three points in sequence. In the experiments, the sensory information available to the robot was changed in the experiments, to observe differences in the behavior.

2. MINIMALISTIC BEHAVIORAL RULE

In [2] we proposed the Minimalistic Behavioral Rule:

$$u_{t+1}^i = \begin{cases} u_t^i + \eta^i R & if\ \Delta A_t \geq 0 \\ random\ selection & otherwise \end{cases}. \quad (1)$$

Where the u_t^i indicates the i-th component of an m-dimensional motor command $u_t^i \in \mathbb{R}^{>}$ given at time t

and $R \sim \mathcal{N}(0,1)$ is a random variable and ΔA_t expresses how much the robot improved its conditions during time the t-th timestep. For instance, in a goal reaching task, ΔA_t could express how much a robot got closer to its target. The term $\eta^i R$ indicates internal noise, that could be generated intentionally [2] or not.

If no perturbations are introduced ($\eta^i = 0$), the binary evaluation ($\Delta A_t \geq 0$) can only correspond directly to "keeping" or "changing" the motor command. Conversely, if the perturbations are very strong, the motor command corresponds to a random walk in the motor command space. Intuitively, there is a specific noise intensity that maximizes the performances. This stochastic resonance phenomenonwas reported in [1], where we showed that an optimal level of noise is able to maximize the mutual information between the function that determines ΔA_t and the robot behavior.

MBR is very general, in fact only the sign of ΔA_t, and no precise "state value" is required. Furthermore, the behavior generated by the rule implicitly reflects the robot's characteristics. In fact, since the commands are chosen by random selection, commands that do not require a precise tuning, intuitively commands that are "simpler for the robot", are executed with high frequency.

3. EXPERIMENT AND RESULTS

We conducted an experiment in which the robot arm continuously and repeatedly reaches three targets in the robot reachable space. These targets are located at the robot's right, left and bottom part of the reachable space, and have coordinates, in m, $t_1 = (0.34, 0.21, 0.66)$, $t_2 = (0.24, 0.02, 0.62)$ and $t_3 = (0.46, -0.10, 0.46)$, respectively. In order to calculate ΔA_t, it is necessary to measure the position of the end-effector. We tested the following three ways to measure and express the end-effector position:

1. A four dimensional vector composed by the end-effector centroid in the images of the two cameras mounted on the head.
2. The three dimensional position of the end effector, obtained using stereo computation.
3. A three dimensional position of the end-effector observed by a motion capture system.

The task could be achieved with all the three types of the information. This result confirms the generality of MBR, that can be applied successfully with a variety of input information and without requiring a model of the robot's dynamics. In particular, the directions taken by the end effector when each muscle is contracted are unknown, and the mapping between the control signal u and the resulting ΔA_t is very complex, depending both on the robot structure and on the sensory information employed.

We analyzed the differences in the robot behavior when the sensory information varies. Fig.2 shows the reaching time for each of the three targets using each of the sensory information. For simplicity, the robot reaches the targets in the order $1, 2, 3, 1, 2, \ldots$. Analysis of the effect of the reaching order will be provided in future
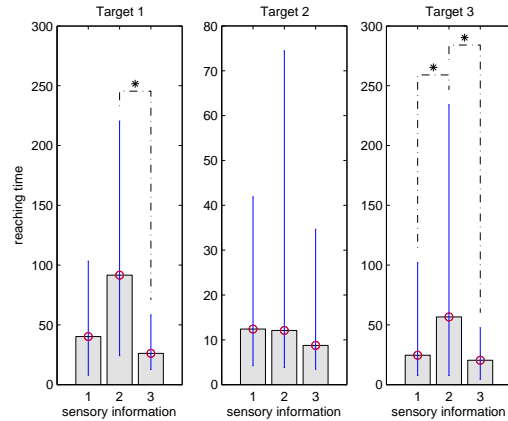

Fig. 2 The reaching time [sec] for each of the targets. The x axis indicates the sensory information type.

works. The figure reports the median values, with the 90% confidence intervals, and highlights the length distributions that are statistically different by the KruskalWallis analysis. We note that the task sensory information 1 and 3 lead better results than the sensory information 2. This is interesting, because the sensory information 2 and 3 are intuitively closer. In fact, for the three targets the normalized mutual information between the sensory information 1 and 3 is 0.73, 0.76 and 0.77, respectively, while the mutual information between the sensory information 2 and 3 is 0.81, 0.81, 0.83 and 0.80.

This result probably comes from the fact that the noise on the depth information has more influence on ΔA_t using the stereo computation than directly using the raw centroid information data. More detailed analysis will be presented in future works. Additionally, it is interesting to investigate whether the Stochastic Resonance effect, observed for simple 2D reaching, can be observed using complex robots like the one presented here.

ACKNOWLEDGMENT

REFERENCES

[1] S. Ikemoto, F. DallaLibera, and H. Ishiguro. Stochastic resonance emergence from a minimalistic behavioral rule. *Journal of Theoretical Biology*, 2011.

[2] F. DallaLibera, S. Ikemoto, T. Minato, H. Ishiguro, E. Menegatti, and E. Pagello. Biologically inspired mobile robot control robust to hardware failures and sensor noise. *RoboCup 2010*, pages 218–229, 2011.

[3] T. Takuma and K. Hosoda. Controlling the walking period of a pneumatic muscle walker. *The International Journal of Robotics Research*, 25(9):861, 2006.

[4] R.Pfeifer and J.Bongard. *how the body shapes the way we think. a new view of intelligence*. MIT Press, 2006.